+

The University Of Sheffield.

Maximising Long Chain Polyunsaturated Fatty Acids Eicosapentaenoic Acid Biosynthesis of Marine Microalgae Species *Nannochloropsis oculata*

Wan Aizuddin bin Wan Razali

A thesis submitted in partial fulfilment of the requirements for the degree of Doctor of Philosophy

The University of Sheffield
Faculty of Engineering
Department of Chemical and Biological Engineering

June 2022

Abstract

Nannochloropsis oculata is a microalga species known to produce a significant amount of eicosapentaenoic acid (EPA). However, a commercially feasible approach is needed to produce a pure EPA. It is clear from the literature review that EPA is located within complex membrane lipids during the exponential growth phase, but these membrane lipids are degraded to neutral lipids when transitioning to the stationary growth phase, and hence EPA is translocated to the neutral lipids. In addition, the rigid cell wall of the *Nannochloropsis* genus is an obstruction to simplifying the downstream process of pure EPA extractions. Thus, this study developed a mutation-selection method to increase EPA production and accessibility for a pure EPA extraction. Ethyl methane sulfonate (EMS) was used as a mutagenised agent and followed by two screening steps. The first step was to culture the wild-type *Nannochloropsis oculata* on f/2 agar medium containing 50 µM fatty acid synthase inhibitor, cerulenin. The fatty acid synthase inhibitor is expected to inhibit fatty acid biosynthesis. Therefore, mutants that can grow with cerulenin are expected to produce a significant EPA amount. More than 1000, 82, and no colonies were observed on *Nannochloropsis oculata* treated with 100, 200, and 300 mM of EMS, respectively. 82 colonies were isolated and cultured with f/2 medium containing 50 and 60 µM cerulenin, and 3 mutants named M1, M18, and M45 that grew fastest were selected. The mutant was then cultivated on f/2 agar medium containing 10 µM MGDG synthase inhibitor, galvestine-1. Galvestine-1 is expected to inhibit the formation of the membrane lipids, MGDG. Therefore, mutants that can grow in the inhibitor's presence are expected to have fewer membrane lipids; hence, the EPA is channelling and synthesising in other cell compartments. M1 mutant had the fastest growth rate of 0.156/day, followed by M18, M45, and wild-type *Nannochloropsis oculata* with 0.147/day, 0.131/day, and 0.121/day, respectively. The highest percentage of EPA was found in M1, M18, and M45 with 29.20 %, 26.42 %, and 25.08 %, while 18.57 % of EPA was found in wild-type *Nannochloropsis oculata*. Label-free quantitative (LFQ) proteomics analysis was conducted to discover the protein changes at the molecular level. Label-free quantitative proteomics for differential protein expression analysis revealed that the wild-type and mutant strains might have alternative channelling routes for EPA synthesis. The mutant strain showed potentially improved photosynthetic efficiency, thus synthesizing

a higher quantity of membrane lipids and EPA. The EPA synthesis pathways could also have deviated in the mutant, where fatty acid desaturase type 2 (13.7-fold upregulated) and lipid droplet surface protein (LDSP) (34.8-fold upregulated) were expressed significantly higher than in the wild-type strain. This study increases the understanding of EPA trafficking in *Nannochloropsis oculata*, leading to further strategies that can be implemented to enhance EPA synthesis in marine microalgae. The M1 mutant *Nannochloropsis oculata* was tested in an outdoor 300 L pilot-scale photobioreactor located at Arthur Willis Environmental Centre, University of Sheffield (53.38241, -1.49883). The results showed that M1 mutant *Nannochloropsis oculata* recorded the highest EPA percentage with 47.52 % EPA of total lipids, while 22.33 % was recorded for wild-type *Nannochloropsis oculata* that were supplied with standard aeration. In the experiments supplied with CO_2, the highest amount of 129.87 mg/g DCW (on day 7) and 75.43 (on day 10) mg/g DCW EPA quantities were recorded in M1 mutant and wild-type *Nannochloropsis oculata*, respectively. A techno-economic assessment (TEA) was then conducted to evaluate the feasibility of the study. Combined scenarios: M1 mutant grew 28.30 % faster than wild-type *Nannochloropsis oculata*; a longer culturing period; the development of the process microalga plant in tropical countries has resulted in a positive NPV and ROI at £49,051,303.49 and 712.11 % after 10 years, respectively. The combined scenario is expected to gain profits starting after year 4 investments. TEA of the improved EPA quantity by M1 *Nannochloropsis oculata* showed that the high processing cost could be overcome by high yields and the right operational strategy, such as continuous harvesting systems.

Acknowledgement

Thank God, the most gracious and merciful, for granting me time and good health conditions to complete this PhD journey. Studying at one of the prestigious universities is one of my biggest dreams. Firstly, I would like to thank the University of Sheffield for giving me a brilliant opportunity to fulfil my dream. I would also like to thank the Ministry of Higher Education Malaysia, the Malaysian government, and the University of Malaysia Terengganu (UMT) for financial support throughout the PhD journey.

Four years and ten months to wrap everything up for the PhD journey. It was a long and challenging journey to pursue knowledge and enhance my research skills and personal growth. Despite the challenges, I'm very grateful that I decided to jump into the microalgae world for my PhD study. Microalgae research was a new field to me, and I would not have gotten through this without the help and support of so many wonderful people around me. An enormous thank you to my supervisor, Dr. Jagroop Pandhal, for taking me in, giving me an excellent scientific opportunity, and always encouraging me from the start until the end of the PhD. I also enjoyed his methods of guiding me in organising my thoughts and ideas in order to achieve the PhD project's goal. I would also like to thank Katarzyna Okurowska for her enthusiastic support in guiding me in culturing and maintaining the microalgae in the most practical and correct ways and for assisting me in doing biochemical assays for analysing microalgae growth. A great thank you also goes to Dr. Caroline Evans for valuable and helpful input and for guiding me from scratch in preparing protein samples, running, and analysing the proteomics data. A special thank you to Dr. Eric Maréchal for generously sharing galvestine-1 for this project and Dr. Josselin Noirel for assisting me in combining and filtering all the *Nannochloropsis* proteomes for LFQ proteomics analysis. A special thanks also to my second supervisor, Dr. Seetharaman Vaidyanathan, for his kindness in sharing his laboratory space and lending me the chemicals at the early stage of the project. A big thank you to Dr. Rahul Kapoore, Duncan Schofield, and Muhammad Firdaus bin Hashim for guiding me to extract the microalgae oils, prepare and run the FAME in GC-FID, and interpret the GC-FID results. Many thanks to the technical staff, James Grinham, Adrian Lumby, Andy Patrick, Usman Younis, Josie May Whitnear, Maggi Killion, and Tanya C Berresford, for their help and

technical support. Thank you to all my postgraduate friends, Officemate in D72, and my colleagues in the Pandhal Research group for help, advice, cheerful time, and support.

Many love to all my family, especially my parent, Wan Razali bin Wan Awang and Hamatilah Binti Wan Ab. Rahman for their prayer, blessings, and support throughout my PhD journey. Thanks a million to my lovely wife, Nurulhuda Mohamed Ariff, for unwavering support, encouragement, and giving birth to our children, Wan Naurah Rayyana and Wan Aydan, and for taking great care of them when I was battling my PhD research. Special thanks to the Center for Talent Development & Innovation of University Malaysia Terengganu for motivational support, especially Mrs. Azunaidah Deraman, Mr. Mohd Zameri Othman, and Mrs. Zakiah Mohamed.

I want to thank all members of the Algal Biotechnology Sheffield network for their support. I would also like to thank the Scottish Association for Marine Science (SAMS) for organising the Algaculture Course in 2018, where I learned and improved the microalgae isolating, culturing, and maintaining techniques. Last but not least, thanks to all our friends and neighbours in Sheffield for the great hospitality that made us feel at home.

Table of Contents

Abstract 2
Acknowledgement 4
List of Tables 10
List of Figures 12
Declaration 18
Abbreviations 19
1. Eicosapentaenoic acid from microalgae species of *Nannochloropsis*: strategies, synthesis, and trafficking pathways in enhancing the production. 22
1.1. Introduction 22
1.2. Photosynthesis process of microalgae cells 24
1.3. Lipid and Fatty acids synthesis of *Nannochloropsis* genus 28
1.4. The effect of environmental conditions on EPA and TAG production in the species of *Nannochloropsis* 34
1.4.1. Light intensities 35
1.4.2. Temperature 36
1.4.3. Salinity 39
1.4.4. Nitrate, phosphate, and pH 41
1.5. Current research and development for species of *Nannochloropsis* to increase EPA and fatty acids synthesis 43
1.6. Genomics, transcriptomics, metabolomics, and proteomics analyses in revealing fatty acids and EPA synthesis pathways 49
1.7. Microalgae growth systems 54
1.8. Objectives and hypothesis 62
1.9. Thesis outline 62
2. Characterisations of wild-type *Nannochloropsis oculata* culturing subjected to different salinities and light intensities 66

2.1. Introduction....66
2.2. Materials and Methods....67
2.2.1. Microalga strain....67
2.2.2. Experimental setup....67
2.2.3. Analytical Methods....70
2.2.4. Determination of Fatty Acids Methyl Ester....71
2.2.5. Statistical analysis....72
2.3. Results....73
2.4. Discussions....85
2.4.1. Growth, physiological and biochemical analyses....85
2.4.2. Wild-type *Nannochloropsis oculata* fatty acids....88
2.5. Conclusion....89
3. Enhancement of Eicosapentaenoic Acid Synthesis in The *Nannochloropsis Oculata* Mutant by an Ethyl Methanesulfonate Random Mutagenesis-Screening Procedure....91
3.1. Introduction....91
3.2. Materials and Methods....93
3.2.1. Microalga strain....93
3.2.2. Mutagenesis and selection of EPA-overproducing mutant strains....93
3.2.3. Lab Scale experiment for Selecting Two-Time Points for Label-Free Quantitative Proteomics....94
3.3. Results....95
3.3.1. Sensitivity of *Nannochloropsis oculata* to cerulenin and galvestine-1....95
3.3.2. Fatty acids content....98
3.3.3. Growth profiles of wild-type and M1 mutant *Nannochloropsis oculata*....101
3.4. Discussion....106
3.4.1. *Nannochloropsis oculata* mutants screening procedure....106

3.4.2. Growth profiles of wild-type and M1 mutant *Nannochloropsis oculata* 107
3.4.3. Fatty acid methyl ester (FAME) profiles 108
3.5. Conclusion 109
4. Comparative proteomics reveals proteins involved in eicosapentaenoic acid trafficking of wild-type and mutant *Nannochloropsis oculata* 111
4.1. Introduction 111
4.2. Materials and Methods 113
4.2.1. Protein extraction and quantification 113
4.2.2. 1D SDS-PAGE protein visualisation 114
4.2.3. In solution digestion 115
4.2.4. LC-MS/MS for proteomics 116
4.2.5. Data analysis 116
4.2.6. Quantifications of fatty acid profiles in TAG and polar lipids 117
4.3. Results 118
4.3.1. Protein profiles 118
4.3.2. Photosynthetic system 120
4.3.3. FA, TAG, and EPA Synthesis 121
4.3.4. Membrane Lipid Remodelling 121
4.3.5. Cellular Location of EPA 123
4.4. Discussion 125
4.4.1. Protein profiles 125
4.4.2. Photosynthetic system 125
4.4.3. FA, TAG, and EPA Synthesis 126
4.4.4. Membrane Lipid Remodelling 128
4.4.5. Cellular Location of EPA 129
4.5. Conclusion 129

5. Feasibility Study of Eicosapentaenoic Acid Production from wild-type and Mutant *Nannochloropsis oculata* using a Pilot-Scale 300 L PhycoFlow® photobioreactor 132
5.1. Introduction 132
5.2. Materials and methods 133
5.2.1. Microalgae strains 133
5.2.2. Description of Pilot-scale photobioreactor 133
5.2.3. Techno-economics assessment 136
5.3. Results 138
5.3.1. Physiological and biochemical analysis of wild-type *Nannochloropsis oculata* supplied with standard aeration 138
5.3.2. Physiological and biochemical analysis of M1 mutant *Nannochloropsis oculata* supplied with standard aeration 143
5.3.3. Physiological and biochemical analysis of M1 mutant Nannochloropsis oculata supplied with CO2 147
5.3.4. Physiological and biochemical analysis of wild-type *Nannochloropsis oculata* supplied with CO_2 152
5.3.5. Techno-economic assessment results 155
5.4. Discussion 157
5.4.1. Wild-Type Versus M1 Mutant *Nannochloropsis oculata* in Standard Aeration Experiments 157
5.4.2. Wild-Type Versus M1 Mutant *Nannochloropsis oculata* in supplied CO_2 Experiments 159
5.4.3. Techno-economic assessment 161
5.5. Conclusion 163
6. Future Directions 165
6.1. Future perspectives 165
7. References 167

List of Tables

Table 1.1: Effect of temperature, light intensity, and light regime cycle on EPA content and ratio of EPA to triacylglycerol (TAG) content. All standard mediums and salinity (25-35 g/L) are used without additional nutrients. 37
Table 1.2: Effect of salinity, light intensity and light regime cycle on EPA content and ratio of EPA to triacylglycerol (TAG) content. All standard mediums without additional nutrients and optimum temperature (20-25 °C) are employed. E, exponential phase; S, stationary phase.40
Table 1.3: Effect of growth medium and nutrients addition, light intensity and light regime cycle to EPA content and ratio of EPA to triacylglycerol (TAG) content. Standard salinity level (25-35 g/L) and optimum temperature (20-28 °C) is applied. E, exponential phase; S, stationary phase.....41
Table 1.4: Advantages and disadvantages of different photobioreactors for microalgae culturing adapted from previous studies. 57
Table 1.5: *Nannochloropsis* species biomass productions produced by photobioreactors. The temperature is ranged from 20-28 °C, standard salinity and medium are used, light intensity 50-300 µmol m^{-2} s^{-1} (except for *Nannochloropsis oculata* in bubble column (Valdés et al., 2012) and *Nannochloropsis gaditana* in a tubular photobioreactor (Moraes et al., 2019) that used sunlight).....60
Table 2.1: Tested environment conditions experiments subjected to different salinity, light intensity, and photoperiod cycles that were cultured at 20 °C.....69
Table 4.1: All proteomics analysis articles published for species of *Nannochloropsis* were based on google scholar and StarPlus - University Library Discovery searched in April 2022. 112
Table 5.1: Parameters and input of microalga biomass, lipid, and EPA production comparisons for baseline *Nannochloropsis* sp., wild-type, and M1 mutant *Nannochloropsis oculata*. All other parameters and input are considered as constant variables and similar to the baseline *Nannochloropsis* sp. 137
Table 5.2: Average daily temperature and hours of daylight comparison between Halle, Germany and Sheffield, United Kingdom, referring to a forecast website (https://weatherspark.com/). The website uses the NASA climate model, Modern Era

Retrospective-analysis for Research and Applications (MERRA-2, https://gmao.gsfc.nasa.gov/reanalysis/MERRA-2/). 137
Table 5.3: TFA profiles (mg/g DCW) for wild-type and M1 mutant *Nannochloropsis oculata*. The data show the mean value of three technical replicate samples. The data for M1 mutant (standard) was not available (N/A). 155
Table 5.4: Parameters and input for four possible scenarios to be applied to M1 mutant *Nannochloropsis oculata* to increase microalga oil production productivity. All other parameters and information are considered constant variables similar to the baseline *Nannochloropsis* sp. (Schade and Meier, 2021). 156
Table 5.5: Net present value (NPV) and return of investment (ROI) comparisons for 10 years timeline. 157

List of Figures

Figure 1.1 : Schematic structure of monogalactosyldiacylglycerol, digalactosyldiacylglycerol, sulfoquinovosyldiacylglycerol, phosphatidylcholine, triacylglycerol (TAG) and diacylglyceryl-N,N,N-trimethylhomoserine. Adapted from previous studies (Boudière et al., 2014; Kong et al., 2018). 26

Figure 1.2: General fatty acids synthesis in green microalgae for long-chain polyunsaturated fatty acids (LC-PUFA), TAG, and glycolipids synthesis. LC-PUFA are blue-coloured text. Desaturases and elongases steps are red and orange colour text, respectively. PEP, phosphoenolpyruvate; PK, pyruvate kinase; ME, malic enzyme; PDC, pyruvate dehydrogenase complex; ACCase, acetyl-CoA carboxylase; MCAT, malonyl-CoA:ACP transacylase; FAS-KS,β-ketoacyl-ACP synthase; FAS-KR, β-ketoacyl-ACP reductase; FAS-HD, β-hydroxyacyl-ACP dehydrase; FAS-ER, enoyl-ACP reductase; TE, acyl-ACP thioesterases; FAS, fatty acid synthase; PEPC, phosphoenolpyruvate carboxylase; G, glycolipids; PDAT, phospholipid:diacylglycerol acyltransferase; GPAT, glycerol-3-phosphate acyltransferase; LPAAT, lysophosphatidic acid acyltransferase; PAP, phosphatidic acid phosphatase; DGAT, diacylglycerol acyltransferase; LDSP, lipid droplet surface protein. This figure is adapted from (Khozin-Goldberg and Cohen, 2011; Martins et al., 2013; Mühlroth et al., 2013; Ma et al., 2016b; Dolch et al., 2017; Janssen et al., 2020; Blasio and Balzano, 2021). 29

Figure 1.3: Adaptive laboratory evolution (ALE) methods with modification (Dragosits and Mattanovich, 2013), where the evolution is monitored for an extended period of time (500 to 5000 generations) in order to develop a new phenotype of microalgae.....48

Figure 2.1: Schematic diagram of experimental cultivation system for cultivating *Nannochloropsis oculata* at a laboratory scale. All experiments were conducted at room temperature at 20 °C. The cultures were subjected to continuously filtered aeration and bubbled at 2 L/minute. 68

Figure 2.2: 800 mL volume culture in 1 L flasks of *Nannochloropsis oculata* experimental setup in triplicates. 69

Figure 2.3: *Nannochloropsis oculata* image during mid-exponential phase at 1000 × magnifications. The overall measuring bar represents 50 µm, and one bar segment represents 10 µm. 73

Figure 2.4: The average cell sizes (six cells) of *Nannochloropsis oculata* cells at exponential growth phase (day 5) and stationary phase (day 15) that were measured under 1000 × magnifications microscope image. 74
Figure 2.5: a) Growth profiles represented by optical density at 595 nm, b) Growth rates, and c) Nitrate and Phosphate uptake concentrations for environmental conditions (E1-E8). E1-E4 were cultivated under 24 hours photoperiod, while E5-E8 were cultivated under 12:12 (h:h) photoperiod . Mean ± standard deviation is shown (n = 3) and t-tests determine statistical significance ($p < 0.05$ [*]; $p < 0.01$ [**]; $p < 0.001$ [***]). The statistical significance of days 3, 6, 9 and 12 was calculated by referring to the standard condition E7. The statistical significance of days 5, 10, 15 and 20 was calculated by referring to the standard condition E3. 76
Figure 2.6: a) Dry cell weight profiles. b) Chlorophyll a profiles and c) Protein profiles for eight tested environmental conditions. Mean ± standard deviation is shown (n = 3) and t-tests determine statistical significance ($p < 0.05$ [*]; $p < 0.01$ [**]; $p < 0.001$ [***]). The statistical significance of days 3, 6, 9 and 12 was calculated by referring to the standard E7. The statistical significance of days 5, 10, 15 and 20 was calculated by referring to the standard E3.....77
Figure 2.7: Percentage of fatty acids for wild-type *Nannochloropsis oculata* for experimental conditions: a) E1, b) E2, c) E3, d) E4, e) E5, f) E6, g) E7, and h) E8. Mean ± standard deviation is shown (n = 3) and t-tests determine statistical significance ($p < 0.05$ [*]; $p < 0.01$ [**]; $p < 0.001$ [***]).....81
Figure 2.8: Quantification of fatty acids for wild-type *Nannochloropsis oculata* for experimental conditions: a) E1, b) E2, c) E3, d) E4, e) E5, f) E6, g) E7, and h) E8. Mean ± standard deviation is shown (n = 3) and t-tests determine statistical significance ($p < 0.05$ [*]; $p < 0.01$ [**]; $p < 0.001$ [***]).....84
Figure 3.1: Fatty acid synthesis acid in the species of *Nannochloropsis*—modified from a previous study (Beacham et al., 2015). Blue boxes and purple boxes indicate omega-6 and omega-3 pathways, respectively. The light green line indicates the chloroplast. 92
Figure 3.2: *Nannochloropsis oculata* mutant colonies of (a) 100 mM, (b) 200 mM, and (c) 300 mM EMS were grown on the f/2 medium agar containing 50 µM cerulenin after 3 weeks of incubation at 130 µmol m^{-2} s^{-1}, 20 °C, and 12-h (light/dark) cycles. Approximately more than 1000, 82, and no colonies were presented on the plate (a), (b), and (c), respectively, after 3 weeks of incubation.....96

Figure 3.3: a) Growth of 82 *Nannochloropsis oculata* mutants b) Growth of 20 *Nannochloropsis oculata* mutants, cultured in f/2 medium containing 60 µM cerulenin, incubated at 130 µmol m^{-2} s^{-1}, 20 °C, and 12-h light/dark cycles for 8 days. 9 mutants were grown faster than wild-type *Nannochloropsis oculata* (represented by green rectangular). 97
Figure 3.4: Growth rate comparisons of mutants M1, M18, M45, and wild-type *Nannochloropsis oculata*, incubated at 130 µmol m^{-2} s^{-1}, 20 °C, and 12-h light/dark cycles, 160 RPM shaking for 10 days. Mean ± standard deviation is shown (n = 3) and t-tests determine statistical significance ($p < 0.05$ [*]; $p < 0.01$ [**]; $p < 0.001$ [***]). 98
Figure 3.5: Comparative analysis of percentage (%) changes in the fatty acid composition of TFA in wild-type (WT), M1 mutant (treated with 60 µM cerulenin), M1, M18, and M45 (treated with 10 µM galvestine-1) *Nannochloropsis oculata* at exponential growth phase cells having $OD_{595\ nm}$ 0.8. Mean ± standard deviation is shown (n = 3) and t-tests determine statistical significance ($p < 0.05$ [*]; $p < 0.01$ [**]; $p < 0.001$ [***]) 99
Figure 3.6: Quantities (mg EPA/g DCW) comparison for wild type, wild-type *Nannochloropsis oculata*, M1 mutant (treated with 60 µM cerulenin), M1, M18, and M45 (treated with 10 µM galvestine-1) at exponential growth phase cells having 0.8 OD at *595 nm*. Mean ± standard deviation is shown (n = 3) and t-tests determine statistical significance ($p < 0.05$ [*]; $p < 0.01$ [**]; $p < 0.001$ [***]).....100
Figure 3.7: Percentage of primary fatty acids of TFA comparison for M1, M18, and M45 *Nannochloropsis oculata* mutants over 3 cycles adaptation in f/2 medium containing 10 µM galvestine-1. The experiments were carried out in sterile cell culture flasks (Nunc™) at 130 µmol m^{-2} s^{-1}, 20 °C, and 12-h light/dark cycles, 160 RPM shaking for 24 days (8 days for 1 cycle). 100
Figure 3.8: Growth profiles for wild-type and M1 mutant *Nannochloropsis oculata* cultivated in 1 L flasks under 150 µmol m^{-2} s^{-1}, 20 °C, and aerated bubbling for mixing and carbon source for 12 days. a) Growth curves illustrated by optical density at 595 nm and b) Dry cell weight. Comparison of wild-type and M1 mutant *Nannochloropsis oculata* over 12 days of culturing for c) chlorophyll concentration and d) phosphate (P) and nitrate (N) uptake profiles. Mean ± standard deviation is shown (n = 3) and t-tests determine the statistical significance ($p < 0.05$ [*]; $p < 0.01$ [**]; and $p < 0.001$ [***]) of the M1 mutant strain compared to the wild-type strain. 102

Figure 3.9: Percentages (%) of fatty acids at day 12. a) Wild-type and b) M1 mutant *Nannochloropsis oculata*. Quantification (mg/g) of fatty acids at day 12. c) Wild-type and d) M1 mutant *Nannochloropsis oculata*. Mean ± standard deviation is shown (n = 3) and t-tests determine the statistical significance ($p < 0.05$ [*]; $p < 0.01$ [**]; $p < 0.001$ [***]) for EPA content in the M1 mutant strain compared to the wild-type strain. 104
Figure 4.1: Protein quantifications comparison for M1 mutant and wild-type *Nannochloropsis oculata* by Microbiuret method (Itzhaki and Gill, 1964) and Nanodrop 2000 method (Thermo Fisher Scientific, United Kingdom). The protein was quantified for all samples using the microbiuret method, while two-time proteins were determined using the Nanodrop 2000 method and compared with the microbiuret method. 118
Figure 4.2: PCA plots show 12 samples clustered by biological replicates: Figure 7.8 (a) wild-type *Nannochloropsis oculata* samples day 3 (light blue) and day 12 (pink), Figure 7.8 (b) M1 *Nannochloropsis oculata* samples day 2 (light blue), and day 12 (pink). Volcano plots show the significant protein distributions in wild-type (Figure 7.8 (c)) and M1 mutant (Figure 7.8 (d)) *Nannochloropsis oculata.* 120
Figure 4.3: Diagram of enzyme regulations from day 3 to day 12 for carbon fixation toward TAG biosynthesis pathways for wild-type *Nannochloropsis oculata*. The diagram shows the pathways and their relation to fatty acid synthesis pathways. Upregulated proteins are shown in the green boxes (Wan Razali et al., 2022). 122
Figure 4.4: Diagram of enzyme regulations from day 2 to day 12 for carbon fixation toward TAG biosynthesis pathways for M1 mutant *Nannochloropsis oculata*. The diagram shows the pathways and their relation to fatty acid synthesis pathways. Upregulated proteins are shown in the green boxes (Wan Razali et al., 2022). 123
Figure 4.5: Fatty acid content. a) EPA percentages (%) of TFA in polar lipids and TAG at day 2 (M1 mutant), day 3 (wild-type), and day 12 (wild-type and M1 mutant) *Nannochloropsis oculata*. b) Polar lipid (PL):TAG quantity ratio (mg/g) at day 2 (M1 mutant), day 3 (wild-type), and day 12 (wild-type and M1 mutant) *Nannochloropsis oculata*. Mean ± standard deviation is shown (n = 3) and t-tests determine the statistical significance ($p < 0.05$ [*]; $p < 0.01$ [**]; $p < 0.001$ [***]) for EPA content in the M1 mutant strain compared to the wild-type strain.124
Figure 5.1: An outdoor 300 L PhycoFlow® Photobioreactor that was installed at Arthur Willis Environmental Centre *(53.3832000157627° North, -1.4995194567741421° West)*, Department of Animal and Plant Sciences, University of Sheffield. 135

Figure 5.2: Growth profiles for wild-type and M1 mutant *Nannochloropsis oculata* cultivated in an outdoor 300 L Photobioreactor supplied with standard aeration. a) Optical density at 595 nm and pH profiles, b) and c) dry cell weight and optical density correlation. Mean ± standard deviation is shown (n = 3) for each day. 140
Figure 5.3: Temperature and weather profiles throughout 15 days experimental period: a) wild-type supplied with standard aeration, b) M1 mutant *Nannochloropsis oculata* supplied with standard aeration. 141
Figure 5.4: Profiles for wild-type and M1 mutant *Nannochloropsis oculata* cultivated in an outdoor 300 L pilot-scale photobioreactor supplied with standard aeration. a) Chlorophyll-*a*, b) nitrate uptake, c) phosphate uptake, and d) protein quantity profiles. Mean ± standard deviation is shown (n = 3) for each day. 142
Figure 5.5: Percentage of primary fatty acids profiles: a) wild-type, and b) M1 mutant *Nannochloropsis oculata* (standard aeration). The data show the mean value and standard deviation of three technical replicate samples. Asterisks indicate the significant differences that were determined by Student's t-test (*p<0.05, **p<0.01, ***p<0.001). 145
Figure 5.6: Quantification of main fatty acids profiles: a) wild-type, and b) M1 mutant *Nannochloropsis oculata* (standard aeration). The data show the mean value and standard deviation of three technical replicate samples. Asterisks indicate the significant differences that determined by Student's t-test (*p<0.05, **p<0.01, ***p<0.001). 146
Figure 5.7: Growth profiles for wild-type and M1 mutant *Nannochloropsis oculata* cultivated in an outdoor 300 L Photobioreactor supplied with CO_2. a) Optical density at 595 nm and pH profiles, b) and c) dry cell weight and optical density at 595 nm correlation. 148
Figure 5.8: Temperature and weather profiles throughout 15 days experimental period: a) wild-type supplied with CO_2, b) M1 mutant *Nannochloropsis oculata* supplied with CO_2. ..149
Figure 5.9: Profiles for wild-type and M1 mutant *Nannochloropsis oculata* cultivated in an outdoor 300 L pilot-scale photobioreactor supplied with CO_2. a) Chlorophyll-*a*, b) nitrate uptake, c) phosphate uptake, and d) protein quantity profiles. Mean ± standard deviation is shown (n = 3) for each day.....151
Figure 5.10: Percentages of main fatty acid profiles: a) wild-type, and b) M1 mutant *Nannochloropsis oculata* supplied with 4.5 and 4 % CO_2, respectively. The data show the mean value and standard deviation of three technical replicate samples. The significant differences,

that determined by Student's t-test, are indicated by asterisks (*p<0.05, **p<0.01, ***p<0.001). 153
Figure 5.11: Quantification of main fatty acid profiles. a) wild-type and b) M1 mutant *Nannochloropsis oculata* supplied with 4.5 and 4 % CO_2, respectively. The data show the mean value and standard deviation of three technical replicate samples. Asterisks indicate the significant differences determined by Student's t-test (*p<0.05, **p<0.01, ***p<0.001). .154

Declaration

I, the author, confirm that the Thesis is my own work. I am aware of the University's Guidance on the Use of Unfair Means (www.sheffield.ac.uk/ssid/unfair-means). This work has not been previously been presented for an award at this, or any other, university.

Publications

1) Wan Razali, W. A., Evans, C. A., and Pandhal, J. (2022). Comparative Proteomics Reveals Evidence of Enhanced EPA Trafficking in a Mutant Strain of *Nannochloropsis oculata*. *Frontiers in Bioengineering and Biotechnology* 10, 1–16.
2) Feasibility Study of Eicosapentaenoic Acid Production from Wild-type and Mutant *Nannochloropsis oculata* using an outdoor pilot-scale 300 L photobioreactor (Draft).

Conference

1) 'Development of *Nannochloropsis oculata* strain for Eicosapentaenoic acid (EPA) production via mutagenesis approaches' Presented at 9th International Conference on Algal Biomass, Biofuels & Bioproducts, Boulder, USA, 17-19th June 2019. (Oral presentation).

Abbreviations

1D-SDS PAGE	1 dimensional sodium dodecyl sulphate polyacrylamide gel electrophoresis
ACCase	Acetyl CoA carboxylase
ACN	Acetonitrile
ALA	α-linoleic acid
ALE	Adaptive laboratory evolution
ASW	Artificial seawater
ARA	Arachidonic acid
ARTP	Atmospheric and room temperature plasma
ATP	Adenosine 5'-triphosphate
BMR	Basal metabolic rate
BODIPY	Boron-dipyrromethene
BSA	Bovine serum albumin
CCAP	Culture Centre of Algae and Protozoa
DAG	Diacylglyceride
DCW	Dry cell weight
DGDG	Digalactosyldiacylglycerol
DGCC	Diacylglycerylcarboxyhydroxymethylcholine
DGTS	Diacylglyceryl-N,N,N-trimethylhomoserine
DHA	Docosahexaenoic acid
DMSO	Dimethyl sulfoxide
DNA	Deoxyribonucleic acid
DPBS	Dulbecco's phosphate buffer saline
EDTA	Ethylene diamine tetra acetic acid
EMS	Ethyl methane sulfonate
EPA	Eicosapentaenoic acid
ER	Endoplasmic reticulum
FA	Fatty acid
FAME	Fatty acids methyl esters
FAS	Fatty acid synthase

FDR	False discovery rate
FFA	Free fatty acids
GC-FID	Gas chromatography flame ionisation detector
HCl	Hydrochloric acid
KAS	3-ketoacyl-ACP synthase
LA	Linoleic acid
LC-PUFA	Long chain polyunsaturated fatty acids
LDSP	Lipid droplet surface protein
LFQ	Label free quantification
M	molarity
mL	Millilitre
MGDG	Monogalactosyldiacylglycerol
MUFA	Monounsaturated fatty acids
MS/MS	Tandem mass spectrometry
NEM	N-ethylmaleimide
NPV	Net present value
OD	Optical density
PCA	Principle component analysis
PS I	Photosystem I
PS II	Photosystem II
ROI	Return on investment
SQDG	sulphoquinovosyldiacylglycerol
TAG	Triacylglycerol
TCA	tricarboxylic acid cycle
TEA	Techno-economic assessment
TFA	Total fatty acids
TTC	Triphenyltetrazolium chloride
UDP	Uridine 5’ diphosphate

CHAPTER 1: LITERATURE REVIEW

1. Eicosapentaenoic acid from microalgae species of *Nannochloropsis*: strategies, synthesis, and trafficking pathways in enhancing the production.

1.1. Introduction

Long-chain polyunsaturated fatty acids (LC-PUFA) such as Eicosapentaenoic acid (EPA) and Docosahexaenoic acid (DHA) are derived from α-linoleic acid (ALA) and linoleic acid (LA), offering a great benefit, especially to humans. Consumption of the EPA and DHA are proven scientifically to have a wide range of health benefits due to their functions as an essential part of the body's defence mechanism. In addition, they have a crucial role in reducing inflammation and counteracting reactive oxygen species (ROS) at the cellular level (Winwood, 2013).

DHA and EPA are the two primary omega-3 fatty acids (FAs) that are often consumed as health supplements (Adarme-Vega et al., 2014). The omega-3 primary sources are fish oil, and it is a growing industry with a global market. The global market of omega-3 value was estimated at 2.49 billion USD in 2019 (Nichols et al., 2014; Oliver et al., 2020) and is estimated to grow at a compound annual growth rate of 7.7 % by 2027 (Jakhwal et al., 2022). A techno-economic assessment (TEA) based on the generated model for a commercial microalga plant shows pure EPA production produced by *Nannochloropsis* sp. at 42 mg/g DCW can reduce the production cost by around 50 % compared to the pure EPA extracted from the edible salmon (Schade et al., 2020). In addition, EPA production from microalgae can support the market for vegan products and create a safe product in a fully controlled photobioreactor. Toxicity from contaminated seawater was identified as one of the most significant consumer concerns affecting the LC-PUFA produced from fish oil (Yaakob et al., 2014). Therefore, researchers have been exploring microalgae as a sustainable source that might support the growing LC-PUFA industry in the future.

Omega-3 is essential for humans, as humans cannot produce the lipids required for the body’s basal metabolism. Basal metabolic rate (BMR) is an individual's energy metabolism to sustain essential, life-sustaining functions such as circulation, breathing, cell creation, nutrition processing, protein synthesis, and ion transport (Henry, 2005). From a medical standpoint,

eating foods and diets containing omega-3 helps to minimise the incidence of different chronic diseases, such as diabetes, arthritis, cardiovascular disease, obesity, the nervous system, and inflammatory conditions (Adarme-Vega et al., 2012; Levasseur et al., 2020). The most common omega-3 supplements are EPA and DHA. EPA and DHA are significant biological regulators of human health and disease. They play various roles in cellular function, such as changing the structure and function of the cell membrane by increasing fluidity and lipid-lipid proteoglycan interactions and cell uptake (Dunbar et al., 2014). EPA has essential health benefits for humans, especially reducing heart problems, including arrhythmia, stroke, and high blood pressure (Bajpai and Bajpai, 1993). Also, regular intake of DHA by a pregnant woman is vital for fetal brain development (Devarshi et al., 2019). Further health benefits are described in a previous study (Adarme-Vega et al., 2012).

Terrestrial plants and microalgae contain LA (C18:2) and ALA (C18:3) and share similar routes for triacylglycerol (TAG) synthesis (Ruiz-Lopez et al., 2013; Wang et al., 2021). However, in terrestrial plants, the EPA accumulates in phospholipid rather than seed oil, and the EPA level is substantially lower (Norambuena et al., 2015), favouring microalgae as a replacement for fish oil, particularly *Nannochloropsis* species (Qi et al., 2004; Napier et al., 2015).

In light of the above, microalgae are thought to be potential sources and have vast advantages over terrestrial plants. Firstly, microalgae grow faster than terrestrial plants due to the simple cellular structure and submerge in an aqueous environment, making them a leading producer of 40-50 % of the photosynthesis on Earth (Grant et al., 2014; Wang et al., 2015). Secondly, rapid microalgae growth is efficiently utilised carbon dioxide (CO_2) for photosynthesis (Tongprawhan et al., 2014). The oceans and algae naturally absorb CO_2 in the atmosphere, and marine aquatics plants, including algae, utilise the soluble CO_2 to produce biomass and contribute to 50-71 % carbon fixation globally (Chung et al., 2011; Moreira and Pires, 2016). Thirdly, microalgae cultivation does not require arable land or specific conditions for water (Bleakley and Hayes, 2017). In addition, microalgae can grow in brackish and seawater, depending on the purpose of the culturing. However, a sterile culture medium is preferred for LC-PUFA production for human consumption (Santos-Sánchez et al., 2016). Despite the fact that microalgae may be a more promising source of EPA than terrestrial plants, the present challenge is developing an economically viable method for producing pure EPA

(Peltomaa et al., 2018). Maximizing EPA synthesis in a well-known microalga EPA producer, such as the species of *Nannochloropsis*, is one of the most viable techniques. However, the extraction of EPA at the optimum point is challenging due to the incorporation of EPA in membrane lipids, while a lower EPA content is translocated to TAG towards the end of the culturing period (Ma et al., 2016a). In *Nannochloropsis* sp., only 37 % of EPA is translocated from polar lipid to neutral lipid during nitrogen starvation that usually occurs at the latter stage of culturing period (Hulatt et al., 2017). The microalga oil or TAG is easier to extract compared to membrane lipids for the *Nannochloropsis* genus. During nutrient-depleted conditions, cell division slows, and the main components in TAGs are dominated by saturated and monounsaturated FA (Pal et al., 2011). A few microalgae species have been reported to synthesize high content of LC-PUFA in TAGs, such as *Phaeodactylum tricornutum* and *Thraustochytrium aureum,* which accumulated EPA and DHA, respectively (Mühlroth et al., 2013). Microalgae can be cultivated to store LC-PUFA in TAG by manipulating the environmental conditions, as well as altering EPA and TAG synthesis cellular pathways (Khozin-Goldberg et al., 2005). However, the EPA synthesis and trafficking mechanisms to TAG are not yet fully understood.

This chapter reviews the strategies that can be implemented to maximise EPA production, primarily in *Nannochloropsis* species, without impeding the microalga growth, the pathways that contributed to the EPA translocation in microalgae cells, and the factors affecting EPA synthesis at molecular levels.

1.2. Photosynthesis process of microalgae cells

Plants and microalgae experience photosynthesis to convert CO_2 and water to chemical energy through a series of complex reactions. The light and dark reactions are the two primary types of photosynthetic processes. Solar energy is harvested by the pigments of the photosynthetic antennae and used to divide water into protons, electrons, and oxygen in light reactions. The electrons and protons are then employed to produce energy carriers (NADPH and ATP), which support the organism's metabolic needs. In the dark reaction in the stroma, the Calvin cycle uses the energy derived from NADPH and ATP to convert CO_2 to carbohydrates (Markou et al., 2012). In photosynthesis, CO_2 is used to carboxylate ribulose

1,5-bisphosphate to 3-phosphoglycerate. Ribulose-1,5-bisphosphate and 3-phosphoglycerate involve in carbon fixation and function as a substrate for carbohydrate synthesis, respectively (Markou et al., 2012). The biochemical compositions of microalgae cells consist of carbohydrates, proteins, lipids and pigments. Therefore, knowledge of the microalgae's physiological and metabolic conditions is crucial in determining the changes in carbohydrates, proteins, lipids and pigments (Chen and Vaidyanathan, 2013).

Carbohydrate production has two objectives for microalgae: they serve as structural components in cell walls and storage components within the cell. Carbohydrates, as storage molecules, supply energy for microalgae metabolic processes and, if necessary, allow for temporary survival in dark environments (Markou et al., 2012). Starch and chrysolaminarin synthesized by ADP- and UDP-glucose pyrophosphorylase enzymes, respectively, are primary carbon and energy storage compounds in microalgae (Choix et al., 2014; Santin et al., 2021). Besides carbohydrates, lipids are major energy stores in microalga cells, whereas total proteins in actively growing microalga cells indicate the pace of metabolic activities (Chen and Vaidyanathan, 2013). One possible way to increase lipid accumulation is to block the pathways that lead to the accumulation of energy-rich storage compounds like starch and chrysolaminarin (Vogler et al., 2018). Starch, chrysolaminarin and lipid synthesis share common carbon precursors in green microalgae (Li et al., 2010; Santin et al., 2021). Hence, the inhibition of carbohydrate synthesis could increase the metabolic flux going to the synthesis of lipids and FAs.

In the species of *Nannochloropsis,* the primary lipids are membrane lipids and neutral lipids. Membrane lipids consist of monogalactosyldiacylglycerol (MGDG), digalactosyldiacylglycerol (DGDG), sulfoquinovosyldiacylglycerol (SQDG), phosphatidylcholine (PC), phosphatidylethanolamine (PE), phosphatidylglycerol (PG), phosphatidylinositol (PI), and diacylglyceryl-N,N,N-trimethylhomoserine (DGTS). Under standard growth conditions, MGDG (30 %) is the highest composition, followed by DGDG (17 %), SQDG (14 %) and PG (12 %) that part of membrane lipids in the chloroplast (Murakami et al., 2020). TAG is the primary component of neutral lipids (Ma et al., 2016b). The structure of the lipids is shown in Figure 1.2. MGDG, DGDG, SQDG and PG are in the chloroplast, DGTS is in ER, and TAG is in lipid bodies (Kong et al., 2018). EPA synthesis is closely related to the MGDG and DGTS (Poliner et

al., 2018). Hence, modifying carbohydrate pathways could indirectly affect the lipids and FA pathways, including EPA.

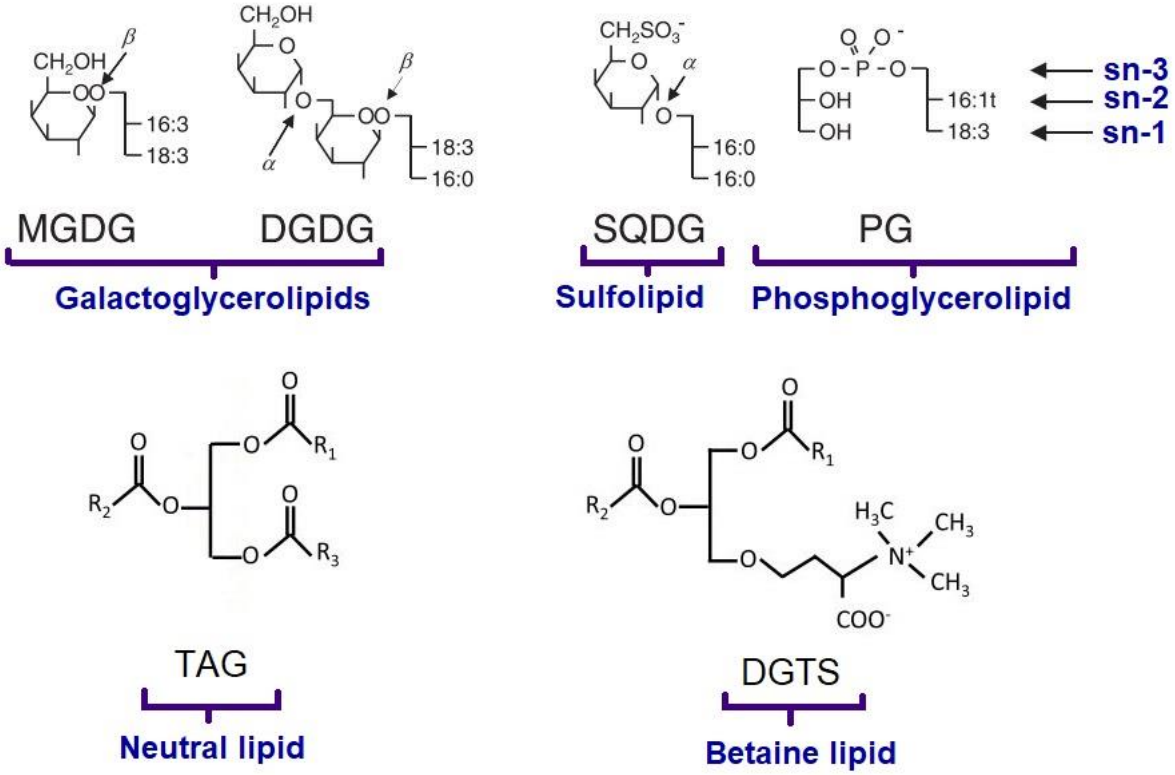

Figure 1.1 : Schematic structure of monogalactosyldiacylglycerol, digalactosyldiacylglycerol, sulfoquinovosyldiacylglycerol, phosphatidylcholine, triacylglycerol (TAG) and diacylglyceryl-N,N,N-trimethylhomoserine. Adapted from previous studies (Boudière et al., 2014; Kong et al., 2018).

Monitoring the changes in biochemical components could reveal the microalgae's responses to various environmental conditions such as light, temperature, salinity, nutrient deprivations, and pH. In general, storage compounds, including proteins, lipids, and carbohydrates, allow microalgae to adjust their growth to changing environmental conditions. All species of *Nannochloropsis* contain chlorophyll-*a* only, and any environmental stress conditions could reduce the chlorophyll-*a* and affect the PSI. Changes in chlorophyll levels indicate the photosynthetic efficiency and could be related to carbon fixation and biogenesis of the thylakoid membrane (Lafarga-De la Cruz et al., 2006; Wietrzynski and Engel, 2021). In *Nannochloropsis* sp., high salinity causes a reduction in chlorophyll-*a* quantity and indicates a substantial decrease in photosystem II (PS II) levels (Martínez-Roldán et al., 2014).

However, in another study, chlorophyll-*a* and *b* are rich in photosystem I (PS I) and PS II, respectively (Caffarri et al., 2014).

Nitrogen and phosphorus are primary nutrients for microalgae growth. Nitrogen is required for the development and biogenesis of microalgae cells. Nitrogen deprivation affects photosynthetic systems, particularly PS II, and has a deleterious impact on the production of proteins involved in photosystems (PS I and PS II) and chlorophylls (Markou et al., 2012). In addition, the flow of photosynthetically fixed carbon is diverted from the protein synthesis metabolic pathway to the lipid or carbohydrate synthesis pathways when nitrogen is scarce (Markou et al., 2012). In all species of *Nannochloropsis*, nitrogen deprivation causes the accumulation of neutral lipids (Ma et al., 2016a, 2016b), while nitrogen repleted condition favours the formation of membrane lipids (Hulatt et al., 2017; Janssen et al., 2019).

Phosphorus is a necessary component of organic compounds like RNA, nucleic acid, phospholipids, DNA, and ATP (Markou et al., 2012). Phosphorus deprivation caused a decrease in protein content and increased TAG content in *Nannochloropsis* species (Rodolfi et al., 2009; Shi et al., 2020). The carbohydrate is increased under high salinity or nitrogen depletion to protect the microalgae from osmotic pressure (Chiu et al., 2017; Wang et al., 2022). Shutting down the ADP glucose pyrophosphorylase enzyme has led to the increase of TAG in starchless mutant *Chlamydomonas reinhardtii* (Li et al., 2010). Phosphorus stress decreases starch synthesis while increasing lipid synthesis (Yaakob et al., 2021). Hence, the ADP glucose pyrophosphorylase enzyme could indirectly be related to phosphorus availability in the culture medium. Similar trends are demonstrated when silencing the UDP-glucose pyrophosphorylase enzyme. Knocking down the UDP-glucose pyrophosphorylase enzyme increased the TAG accumulation (45-fold) in *Phaeodactylum tricornutum* (Daboussi et al., 2014), indicating the close relationship between carbohydrate and TAG synthesis. The knockdown enzyme responsible for the chrysolaminarin synthesis in *Nannochloropsis gaditana* by CRISPR/Cas9 method shows a ~5-fold decrease in the carbohydrate content (Vogler et al., 2021). However, there are no results demonstrated on lipid and EPA contents. The changes in biochemical compositions could affect the EPA synthesis and trafficking in the microalgae cells.

1.3. Lipid and Fatty acids synthesis of *Nannochloropsis* genus

Over two decades, there has been sustained research activity in improving the species of *Nannochloropsis* as a biomanufacturing host. Microalgae-derived LC-PUFAs have been extensively studied as nutraceuticals and sustainable alternatives to petroleum-based diesel. FAs distributions are varied across microalgae species (Mühlroth et al., 2013) due to the different pathways involved. C14:0, C16:0, C16:1, C18:0, C18:1, C18:2, C18:3, C20:4, and C20:5 are the primary FAs present in all species of *Nannochloropsis*. Initially, the pathways for FA synthesis in the species of *Nannochloropsis* were predicted from all the discovered lipid pathways in microalgae and plants as green microalgae share the ancestry with higher plants (Minhas et al., 2016). Over the last decade, a lot of research has been conducted to manipulate the FA pathways in the species of *Nannochloropsis* to enhance TAG and EPA contents.

In chloroplast, de novo FA synthesis occurs when acetyl-CoA is carboxylated and then converted to malonyl-CoA (Adarme-Vega et al., 2012). Then, the malonyl-CoA is catalysed by malonyl-CoA:ACP transacylase (MCAT) to produce malonyl-ACP (Khozin-Goldberg and Cohen, 2011). Khozin-Goldberg and Cohen, (2011) stated that fatty acids synthase (FAS) is produced by an unidentified process from malonyl-ACP. The synthesis of acetyl-CoA to malonyl-ACP is found in all unicellular microalgae including in the species of *Nannochloropsis* (Minhas et al., 2016). A recent review by Blasio and Balzano (2021) described that malonyl-ACP is further condensed by ketoacyl synthase to produce ketoacyl intermediate. The de novo FAS is continuous with three reactions: KR reduces ketoacyl intermediate to hydroxyacyl ACP, HD converts β-hydroxyacyl ACP to enoyl-ACP, and ER saturates enoyl-ACP to acyl-ACP (Figure 1.1) (Blasio and Balzano, 2021). Ketoacyl synthase (KAS) functions for FA elongations where C2:0-ACP to C16:0-ACP act as the substrates (Chaturvedi and Fujita, 2006). Recently, 3-ketoacyl ACP synthase (KAS) I, II, and III are also found in *Nannochloropsis oceanica* and potentially contributed to medium chain length FA synthesis (Sugihara et al., 2019).

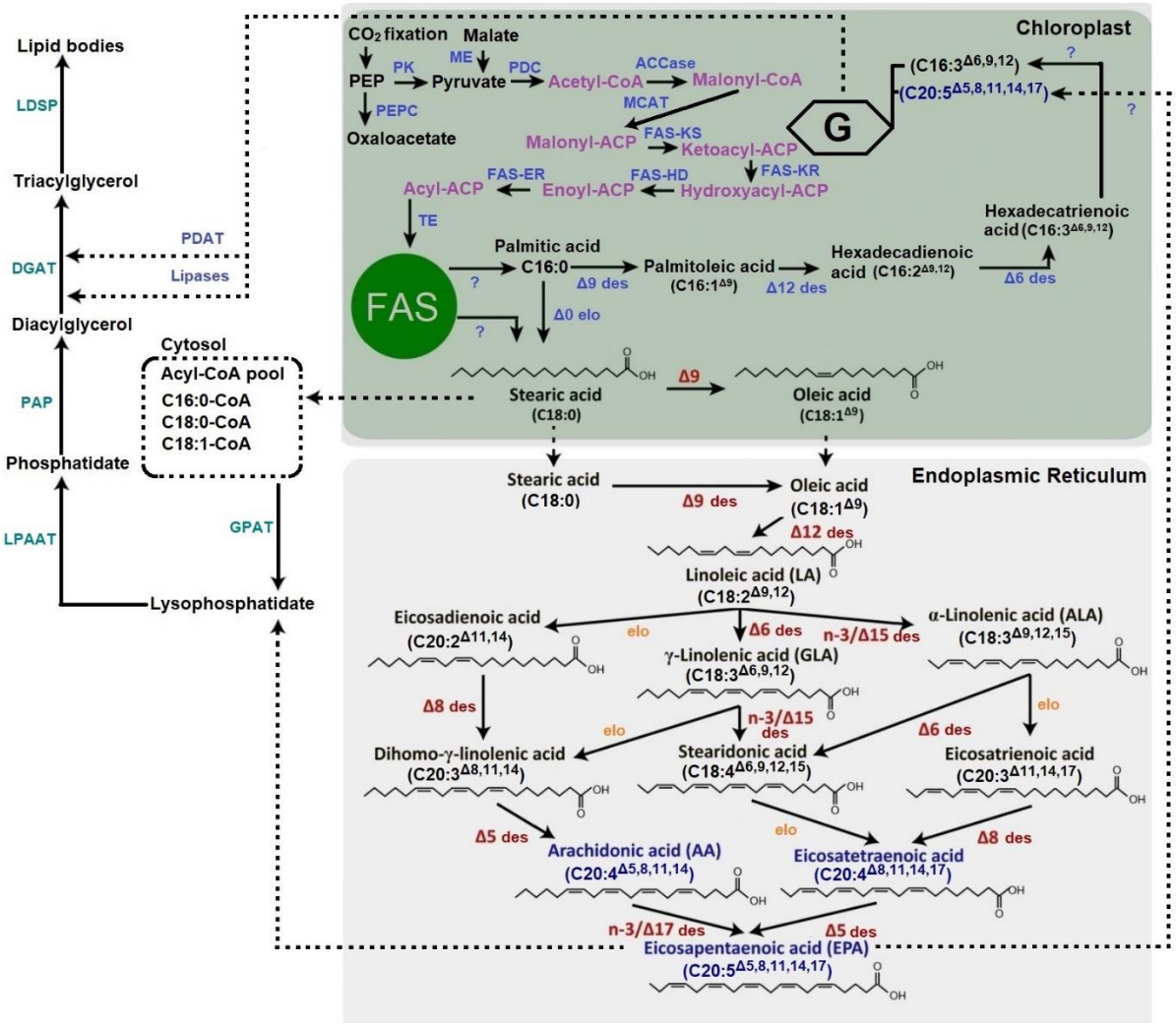

Figure 1.2: General fatty acids synthesis in green microalgae for long-chain polyunsaturated fatty acids (LC-PUFA), TAG, and glycolipids synthesis. LC-PUFA are blue-coloured text. Desaturases and elongases steps are red and orange colour text, respectively. PEP, phosphoenolpyruvate; PK, pyruvate kinase; ME, malic enzyme; PDC, pyruvate dehydrogenase complex; ACCase, acetyl-CoA carboxylase; MCAT, malonyl-CoA:ACP transacylase; FAS-KS, β-ketoacyl-ACP synthase; FAS-KR, β-ketoacyl-ACP reductase; FAS-HD, β-hydroxyacyl-ACP dehydrase; FAS-ER, enoyl-ACP reductase; TE, acyl-ACP thioesterases; FAS, fatty acid synthase; PEPC, phosphoenolpyruvate carboxylase; G, glycolipids; PDAT, phospholipid:diacylglycerol acyltransferase; GPAT, glycerol-3-phosphate acyltransferase; LPAAT, lysophosphatidic acid acyltransferase; PAP, phosphatidic acid phosphatase; DGAT, diacylglycerol acyltransferase; LDSP, lipid droplet surface protein. This figure is adapted from (Khozin-Goldberg and Cohen, 2011; Martins et al., 2013; Mühlroth et al., 2013; Ma et al., 2016b; Dolch et al., 2017; Janssen et al., 2020; Blasio and Balzano, 2021).

LC-PUFA synthesis starts at the intersection of C16:0 in the chloroplast. From C16:0, the FA is elongated by Δ0 elongase (Dolch et al., 2017), and the synthesis of C18 FAs in the ER may follow five routes by utilising desaturase and elongase enzymes to produce the end product EPA as reviewed in an article (Martins et al., 2013) (Figure 1.1). A recent study discovered that *Nannochloropsis gaditana* takes the omega-6 pathway (C16:0 → C18:0 → C18:1(Δ9) → C18:2 (Δ9,12) → C18:3 (Δ6,9,12) → C20:3 (Δ8,11,14) → C20:4 (Δ5,8,11,14) → C20:5 (Δ5,8,11,14,17)) (Janssen et al., 2020). *Porphyridium cruentum* takes the omega-6 pathway, similar to *Nannochloropsis*, while other microalgae species such as *Phaeodactylum tricornutum*, *Isochrysis galbana* and *Pavlova salina* follow two other routes for EPA synthesis (Khozin-Goldberg et al., 2011). Reverse genetic techniques are used to study the overexpression in *Nannochloropsis oceanica,* including targeting Δ12 desaturase (Kaye et al., 2015), Δ6 desaturase (Yang et al., 2019a), Δ6 elongase (Shi et al., 2021), and combined Δ5, Δ9 and 12Δ desaturase (Poliner et al., 2018). Overexpression of Δ6 desaturase lowered the EPA percentage of total fatty acid (TFA) in total lipids compared to the wild-type strain (Yang et al., 2019a), while most of these genetically modified strains showed a minor increase in EPA content compared to the wild-type strain. No previous research has investigated the overexpression of $\Delta 17$ desaturase in any *Nannochloropsis* or microalgae species. Overexpressing $\Delta 17$ desaturase investigated in oleaginous fungus, *Mortierella alpina* shows 26 % EPA in TFA in the transformant, while no EPA is presented in the wild-type strain (Okuda et al., 2015).

In the chloroplast, photosynthesis includes carbon fixation, hence increasing the carbon flux prepared for FA synthesis. Pyruvate kinase (PK) and NADP-malic enzyme (ME) catalyse the carbon flux to produce pyruvate, releasing CO_2 and NADPH in the chloroplast (Khozin-Goldberg and Cohen, 2011; Jeon et al., 2021). Pyruvate dehydrogenase complex (PDC) catalyses pyruvate to acetyl-CoA, the first substrate for FA synthesis. The increase of carbon flux, increased by overexpressing ME in *Nannochloropsis salina*, has increased NADPH, dry cell weight (DCW) and total lipids in the engineered strain compared to the wild-type strain (Jeon et al., 2021). However, EPA levels are lower in the engineered strain than in the wild-type (Jeon et al., 2021), suggesting that the engineered strain grows and utilises the nutrients in the medium faster than the wild-type strain. Hence, TAG synthesis takes place quicker in

the engineered strain, and the membrane lipids become carbon substrates for TAG synthesis. Therefore, when comparing EPA levels in an engineered and wild-type strain, it's crucial to compare the same growth phase when the number of cells and nutrient quantities are comparable. Unfortunately, there is no report yet on the overexpressing PK and PDC in any species of *Nannochloropsis*.

Generally, a few routes have been previously suggested for EPA synthesis, as reviewed in the previous study (Mühlroth et al., 2013). In *Nannochloropsis*, EPA synthesis occurs in the endoplasmic reticulum and is exported to the membrane lipids in the chloroplast (Murakami et al., 2018). DGTS and MGDG are two primary lipids that are suggested to acquire the EPA component for development (Murakami et al., 2018). The membrane lipids synthesis in microalgae might be different from terrestrial plants as no EPA is presented in the terrestrial plant, and it requires engineering tools to synthesize the EPA in plants (Napier et al., 2015).

During nutrient deprivation, the membrane lipids and cell walls are remodelled to preserve the microalga functions inside the cell (Janssen et al., 2020; Roncaglia et al., 2021). The EPA translocates to aid the synthesis of MGDG in the chloroplast, and the reason why EPA is needed is unknown and requires further research. The synthesis of membrane lipids starts at C16:0 and is involved with the elongation via C16:1$^{\Delta 9}$, C16:2 $^{\Delta 9,12}$, and C16:3 $^{\Delta 6,9,12}$ (Figure 1.1) (Mühlroth et al., 2013). In *Arabidopsis thaliana*, MGDG synthase is responsible for forming MGDG membrane lipids (Botté et al., 2011). In *Chlamydomonas*, only single-copy genes *MGD* and *DGD* are involved in synthesising the galactolipids monogalactosyldiacylglycerol (MGDG) and digalactosyldiacylglycerol (DGDG), respectively. In contrast, several genes are involved in *Arabidopsis thaliana* for similar functions (Liu and Benning, 2013). *MGD* gene in the *Nannochloropsis* is comparable to *Chlamydomonas reinhardtii* (Wang et al., 2014), suggesting that similar membrane lipids synthesis occurs in the species of *Nannochloropsis*.

Nannochloropsis possess plastids bounded by four membranes, where the two innermost membranes contain plastid-specific lipids, such as MGDG, DGDG, and SQDG, whereas the two outermost membranes may be related to ER lipid composition, such as phosphatidylcholine (PC) and betaine lipids (Guéguen et al., 2021). MGDG, DGDG, SQDG, PC, and betaine lipids

support normal cell functions, while PUFA's role is to scavenge reactive oxygen species (ROS) (Ma et al., 2016b). There is minimal information on details of membrane lipids biogenesis in *Nannochloropsis* species found in the literature. In *Arabidopsis thaliana*, the synthesis of glycerolipids has been extensively explored. The common knowledge on the formation of membrane glycerolipids indicates phosphatides could be used as a substrate to produce phosphatidylglycerol (PG) via a cytidine diphosphate diacylglycerol intermediate, while DAG could be used as a substrate to produce SQDG and MGDG synthesis in the plastid, and PC, PE, and betaine lipids synthesis in ER (Guéguen et al., 2021). The synthesis of MGDG involves a one-step process from DAG by using the UDP-gal enzyme, while the enzymatic reaction of UDP-gal and MGDG as a substrate produces DGDG (Kobayashi, 2016). Another mechanism for DGDG production is catalysed by SENSITIVE TO FREEZING 2 (SFR2), which removes the headgroup from MGDG and transfers it to DGDG during cold weather adaptation (Roston et al., 2014).

SQDG synthesis pathway involves three steps. The first step starts with UDP-glucose-1-phosphate, and UTP is catalysed by UDP-glucose pyrophosphorylase (UGP3) to produce UDP-glucose. Secondly, SQD1 converts UDP-glucose to UDP-sulfoquinovose (SQ) with sulphite, and finally, SQDG synthase (SQD2) transfers the SQ moiety of UDP-SQ to the diacylglycerol to form SQDG. PG is synthesized in plastids. The first step is CDP-diacylglycerol synthase converts phosphatidic acid (PA) and CTP to CDP-diacylglycerol. The second step is PGP synthase converts CDP-diacylglycerol to PG phosphate (PGP) with glycerol 3-phosphate. The last step for PG synthesis is the dephosphorylation of PGP by PGP phosphatase (Kobayashi, 2016).

DGTS is the only betaine lipid that has been found to have a synthesis path, precursors, and enzymes. The synthesis of DGTS is accomplished in two steps: attaching a C4 homo-Ser moiety to a DAG backbone, followed by adding three methyl groups to its amino group (Murakami et al., 2018). A recent study about the adaptation of *Nannochloropsis oceanica* to low temperatures (Murakami et al., 2018) suggests that betaine lipids, especially DGTS and MGDG, may partially compete to acquire EPA for their synthesis. In contrast, PE and DGTS are discovered to act as a carrier for EPA synthesis and translocates the EPA to MGDG (Meng et al., 2017).

TAGs are packed into lipid droplets in microalgae and plants and act as a reservoir for polyunsaturated carbon recycling, allowing for fast recovery. In *Phaeodactylum tricornutum*, the composition of lipid droplets (LD) is 99 % TAG and 1 % membrane lipids to build a lipid droplet bounding membrane, while *Nannochloropsis* lipid droplet composition has yet to be characterised (Guéguen et al., 2021). In addition, pigments such as fucoxanthin and β-carotene are also identified in lipid droplet fractions (Guéguen et al., 2021). In *Nannochloropsis,* the translocation of EPA to TAG has yet to be discovered. Three pathways are identified for TAG synthesis (Zienkiewicz et al., 2020). The de novo synthesized FA from the chloroplast is incorporated into diacylglycerol (DAG), a precursor for TAG production; alternatively, the de novo synthesized FA from chloroplast is exported directly to TAG by a series of acylation steps in the Kennedy pathway in ER. Lastly, TAG is produced by acyl-chain recycled from the degradation of membrane lipids. The Kennedy pathway is partially involved in glycolipids synthesis (Guéguen et al., 2021). The common pathway of TAG starts with the esterification of acyl-CoA to lysophosphatidate by GPAT enzyme, followed by the formation of phosphatides by LPAAT enzyme. Then, diacylglycerol (DAG) and TAG are produced by phosphatidic acid phosphatase (PAP) and diacylglycerol acyltransferase (DGAT) enzymes, respectively.

In green microalga *Chlamydomonas reinhardtii*, the chloroplast and the ER is involved in lipid droplet synthesis (Guéguen et al., 2021). TAG production in microalgae is substantially more active when growth rates are lowered due to poor environmental or stress conditions (Meng et al., 2017). On the contrary, resupplying the medium with excess nitrogen degrades the TAG reserves, resulting in energy generation through released carbon and synthesis of a new plastid membrane by polyunsaturated carbon recycling, allowing for a quick microalga cells recovery (Zienkiewicz et al., 2020). In addition, the microalga cell numbers increase when the nutrient is replenished in the medium. The higher number of cells could possess light inhibition; hence, the light exposure per cell is decreased, resulting in increased EPA synthesis. In *Phaeodactylum tricornutum*, DGAT activities are found in EPA during nitrogen repleted condition, suggesting that EPA could be translocated to TAG or TAG degrades to form membrane lipids and EPA (Guéguen et al., 2021). A study to uncover the relationship between EPA and TAG in *Nannochloropsis oceanica* reveals NoDGAT2K enzyme is responsible for the formation of EPA in TAG (Xin et al., 2019).

A recent finding stated that LD is involved in a variety of functions, including energy supply, membrane structure and function, trafficking, and signal transduction (Zienkiewicz and Zienkiewicz, 2020). LD is initiated in ER and translocated to cytosol when the synthesis is completed. Lipid droplet surface protein (LDSP) is the main protein found in LD of *Nannochloropsis oceanica,* while MLDP is the main protein in LD of green microalgae such as *Chlamydomonas reinhardtii*, *Dunaliella salina*, *Scenedesmus quadricauda*, *Chromochloris zofingiensi* and *Lobosphaera incisa* (Zienkiewicz and Zienkiewicz, 2020). Modifying the enzyme related to FA synthesis demonstrates changes in FA profiles, especially EPA and TAG. As a result, strategies could be developed to untangle EPA and TAG synthesis, with the goal of redirecting the EPA synthesis into TAG. In addition, the relationship between EPA trafficking across lipid and carbohydrate pathways is novel research that currently lacks understanding.

1.4. The effect of environmental conditions on EPA and TAG production in the species of *Nannochloropsis*

Conventionally, different microalgae species are utilised depending on the purposes and characteristics of microalgae, such as fast-growing microalgae species being used for biomass production, while others are used for the high value of bioactive compounds (Hlavova et al., 2015). The wild-type microalgae species refer to genetically unmodified species that can grow fast, accumulate a high amount of biomass, and have a high amount of valuable bioactive compounds that might have existed in nature. However, finding these characteristics among millions of microalgae species is very difficult. Alternatively, bioactive compounds can be increased by manipulating the environmental parameters such as nutrient starvation, light intensity, salinity, and temperature, yet the strain development has been further improved by emerging technologies in the field (Fu et al., 2016).

EPA and DHA components are naturally produced by microalgae cells. The quantity of EPA and DHA are varied among microalgae species. Furthermore, several microalgae species can only synthesise EPA and DHA, while others generate both. The microalgae culturing phases consist of four-phase; lag phase, exponential phase, declining relative growth phase, and death phase (Farag, I., & Price, 2013). In general, EPA percentages of overall FAs for most microalgae species are higher in the exponential phase than in the stationary phase. When

the nutrients became limited during the stationary phase, the microalgae cells induced TAG accumulations, and the membrane lipids were converted to TAG. During this conversion, EPA is translocated to TAG (Janssen et al., 2019). The level of EPA presented in TAG at the stationary phase was lower than the predetermined exponential growth phase (Roncarati et al., 2004). The incorporation of the EPA in membrane lipids suggests that the EPA is synthesised together with cell growth, and the EPA is channelled from membrane lipids to neutral lipids when the inorganic carbon has become limited (Spilling et al., 2021). Varying growth conditions can adjust both total lipids and omega-3 FA production. The main environmental factors that have been extensively studied to express the synthesis of FAs are light intensity, including variations of light colours, temperature, salinity, nitrate phosphate, pH, CO_2, and dissolved-oxygen level (Ma et al., 2016b) (Ma et al., 2016a). Tables 1.1, 1.2, and 1.3 show the EPA quantity subjected to the environmental conditions in the species of *Nannochloropsis*.

1.4.1. Light intensities

Light quantity and quality are crucial for photosynthesis and metabolic activities in microalgae. Changes in light intensities influence the pigments, unsaturated FAs, carbohydrates and protein content (Khoeyi et al., 2012). The literature shows light intensity by Watts per square metre (W/m^2) and µmol m^{-2} s^{-1}. Conversion of the units from photons to energy and vice versa could be made by multiplying the conversion values for a specific light source (Sager and Farlane, 2003). In *Nannochloropsis salina*, low light intensity, 50 µmol m^{-2} s^{-1}, showed a 10 % higher EPA compared to 100 µmol m^{-2} s^{-1} at the exponential phase, while the EPA percentage decreased (10-15 % EPA of TFA) at higher light intensities (Van Wagenen et al., 2012). On the contrary, neutral lipid, C16:0 profile showed an opposite trend compared to EPA. In general, the growth under 100 µmol m^{-2} s^{-1} slows the growth of *Nannochloropsis* species. No investigations are known to have been performed on the effect of low and high light intensities on EPA synthesis in any *Nannochloropsis* species at molecular levels.

From the literature search, light settings such as the exposure of light to dark ratio might also contribute to EPA synthesis. Several studies have light and dark cycles, for example, 12:12, 14:10, and 16:8 hours light to dark ratio, and several studies prefer continuous light exposure.

It was found that saturated and monounsaturated FAs were decreased from 8-16 % at night, whereas polyunsaturated FAs (C18) and the EPA were increased by 24 and 7 % (Chini Zittelli et al., 1999). A recent study showed that red light could increase the biomass and lipids in *Phaeodactylum tricornutum* at the stationary phase (Sharma et al., 2020). Another light colour usage could induce EPA synthesis. Different microalgae species have different responses to light colours (Sharmila et al., 2018) due to the diverse preference associated with light antennae and different pigments presented in microalgae species. Blue light-emitting diode (465 nm) could increase the growth rate of *Nannochloropsis oceanica* (Sirisuk et al., 2018), but no report on the EPA quantity during the exponential growth phase.

In *Nannochloropsis oceanica*, blue light increases the EPA quantity (50-56 mg/g DCW) (Chen et al., 2013), possibly due to the blue light having a suitable wavelength for absorption by microalgae cells. A combination of blue and other colour light could increase the EPA content in microalgae cells. A sequential study by Chen et al. (2015) indicates the EPA contents are comparable for single blue light and combined blue light with other colours. *Nannochloropsis oceanica* has a slower growth rate under blue light compared to white light (Chen et al., 2013), indicating lower photosynthesis efficiency in blue light. In contrast, blue light promotes the growth of *Nannochloropsis oceanica* on day 10 of culturing period (Wei et al., 2020). The different growth rate implies that the light wavelength change at low light intensity could easily be adapted by microalga cells.

1.4.2. Temperature

Climate conditions change the microalgae metabolism, hence could enhance the production of total lipids and EPA in microalgae cells (Aussant et al., 2018). Different countries or regions might have wild-type strains adapting to the weather conditions, especially in high and cold temperatures. The species of *Nannochloropsis* that originated from the European countries' weather climates have an optimum temperature range of 20-25 (°C). This optimum temperature range might be expanded to suit the temperatures of other countries, with the added benefit of additional sunshine for photosynthesis to boost microalgae cell production. The effect of temperature on EPA content in the species of *Nannochloropsis* is compared in Table 1.1.

Table 1.1: Effect of temperature, light intensity, and light regime cycle on EPA content and ratio of EPA to triacylglycerol (TAG) content. All standard mediums and salinity (25-35 g/L) are used without additional nutrients.

Species	**Light intensity (µmol m^{-2} s^{-1}) (Light:dark)(h:h)**	**Temp. (°C)**	**(Growth phase)**	**EPA content (%)**	**C20:5 to C16:0 ratio**	**References**
N. oculata CCMP 529	100 (24:0)	25	22 (S)	5.41 ± 0.32	0.19	(Ma et al., 2014)
N. oceanica IMET 1	100 (24:0)	25	22 (S)	7.45 ± 0.25	0.27	(Ma et al., 2014)
N. gaditana CCMP 527	100 (24:0)	25	22 (S)	7.63 ± 1.20	0.19	(Ma et al., 2014)
N. granulata CCMP 525	100 (24:0)	25	22 (S)	4.74 ± 0.17	0.18	(Ma et al., 2014)
N. salina CCMP 537	100 (24:0)	25	22 (S)	10.93 ± 0.14	0.34	(Ma et al., 2014)
Nannochloropsis sp.	170 (24:0)	25	2 (E) 7 (E)	24.7 17.8	0.99 0.53	(Pal et al., 2011)
Nannochloropsis sp.	700 (24:0)	25	2 (E) 7 (E)	18.4 10.8	0.54 0.27	(Pal et al., 2011)
N. oceanica IMET	Day 1-3= 80 Day 4-5= 100 Day 6-7= 180 (14:10)	25	7 (E)	33	1.02	(Meng et al., 2015)
Nannochloropsis sp. CCNM 1081	100 (18:6) 30 (18:6)	25 10	18 (S) 22 (E)	6.96 ± 0.38 26.17 ± 0.71	0.15 1.12	(Mitra et al., 2015b)
N. gaditana CCNM1032	40 (24:0) 40 (18:6) 40 (12:12) 40 (6:18)	25	18 (E)	22.0 ± 0.01 32.2 ± 0.40 30.9 ± 0.02 21.3 ± 0.19	0.85 1.35 1.38 0.88	(Mitra et al., 2015a)
N. gaditana CCNM1032	60 (12:12) 150 (12:12)	25	18 (E)	37.8 ± 0.37 28.5 ± 0.52	2.14 1.60	(Mitra et al., 2015a)
Nannochloropsis sp.	50 (24:0)	22	10 (E)	25.3 ± 1	1.00	(Hu and Gao, 2003)
Nannochloropsis sp.	50 (24:0)	14 22 30	10 (E)	31.7 ± 1.8 25.3 ± 1.0 16.4 ± 0.4	1.36 1.00 0.41	(Hu and Gao, 2006)
Species	**Light intensity (µmol m^{-2} s^{-1}) (Light:dark)(h:h)**	**Temp. (°C)**	**Days (Growth phase)**	**EPA content (mg/g) DCW**	**C20:5 to C16:0 ratio**	**References**
N. salina CCMP 1776	250 (16:8)	25	4 (E)	31.7 ± 6.28	0.89	(Willette et al., 2018)
N. salina CCMP 1776	250 (16:8)	20	4 (E)	59.4 ± 10.4	1.73	(Willette et al., 2018)
N. salina CCMP 1776	250 (16:8)	15	4 (E)	49.1 ± 7.05	1.74	(Willette et al., 2018)

N. salina CCMP 1776	250 (16:8)	10	4 (E)	46.4 ± 8.77	1.21	(Willette et al., 2018)
N. salina CCMP 1776	250 (16:8)	5	4 (E)	30.0 ± 8.74	0.93	(Willette et al., 2018)
N. oceanica IMET	Day 1-3= 80 Day 4-5= 100 Day 6-7= 180 (14:10)	25	7 (E)	52.3 ± 2.9	1.77	(Meng et al., 2015)

In *Nannochloropsis salina*, 20 °C had the highest EPA, recorded at 59.38 mg/g DCW and 29 % EPA of TFA, compared to other temperature conditions (25, 15, 10, and 5 °C), at the exponential growth phase (Willette et al., 2018), while the EPA decreased from 15 to 5 % of TFA when the temperature increased from 13 to 30 °C, at the stationary phase (Van Wagenen et al., 2012). In *Nannochloropsis oculata*, EPA reported an increase of 11 % EPA of TFA when the temperature was lowered from 20 to 10 °C at the early stationary phase (Roleda et al., 2013). Generally, the growth rate decreases when the culturing in a lower temperature. In *Nannochloropsis* sp., photoautotrophic growth at a standard temperature of 14 °C records EPA percentage of TFAs in total lipids (25.3 %) and biomass yield (633 ± 27.1 mg/L) (Hu and Gao, 2003). Low temperature at 14 °C indicates the highest EPA percentage of TFAs in total lipids (31.7 %), while the biomass decreases to 388 ± 17.8 mg/L (Hu and Gao, 2006). Hu and Gao (2006) tuned the environment conditions at low light intensity (50 µmol m^{-2} s^{-1}) possibly to monitor the effect of temperature on EPA synthesis at a lower photosynthetic rate. The optimum EPA synthesis occurs at the exponential growth phase; hence, the EPA content could be closely monitored at a low photosynthetic rate. Interestingly, comparable cell growth was observed when *Nannochloropsis oceanica* was cultured at 15 and 30 °C in nutrient repleted conditions (Chua et al., 2020). The lower temperature had around 35 % EPA of TFA, which was 10 % higher than its counterpart (Chua et al., 2020). The ratio of saturated FA to unsaturated FA varies throughout the culturing periods in the species of *Nannochloropsis*. Under low light intensity, microalga cells could be considered as an exponential phase when the EPA to TAG ratio is higher than 0.5 (Table 1.1). The cells' growth progress determines the ratio of unsaturation and saturation level (Pal et al., 2011). 20 and 15 °C produce the comparable EPA to C16:0 ratio (Willette et al., 2018), suggesting the microalga cells are in the optimum growth range for EPA synthesis. While at a very low temperature of 5 °C, the microalga cells cannot grow at standard functions, hence, triggering TAG production.

C20:5 to C16:0 ratio greater than 1 at the exponential phase indicates a high EPA content in the *Nannochloropsis* cells. EPA decreases while C16:0, which represents TAG, increases at the stationary phase in all species of *Nannochloropsis* (Ma et al., 2014). Low temperatures cause slower cell development, which prevents TAG synthesis from overtaking FA production. Hence, evaluating the quantity of EPA should be correlated with cell growth, cell conditions, and the ratio of saturated FA to unsaturated FA (Ma et al., 2014). The exponential growth phase had a higher EPA percentage of TFA compared to the stationary growth phase. In *Nannochloropsis oceanica*, EPA had reported an approximately 2 % increase when the cells that reached the stationary phase were incubated at a cold temperature, reduced from 20 to 5 °C (Sirisuk et al., 2018). The increase of EPA in the stationary growth phase at a lower temperature could be due to the increase of chloroplast size to protect the cell from high oxidative stress (Chua et al., 2020). A rise in PUFAs is expected because these FAs have good flow properties and are primarily used in the cell membrane to retain fluidity at low temperatures (Adarme-Vega et al., 2012).

1.4.3. Salinity

All species of *Nannochloropsis* are identified as marine microalgae except *Nannochloropsis limnetica*. FAs comparisons at stationary phase for biofuel industry show all marine *Nannochloropsis* species contain a low level of EPA while C18:1, C18:2 and C18:3 are the main FA in freshwater species, *Nannochloropsis limnetica* (Ma et al., 2016b). In contrast, the *Nannochloropsis limnetica* recorded similar FA profiles to *Nannochloropsis gaditana* at the exponential phase, with around 25 % EPA of TFAs in the microalgae cells (Freire et al., 2016). Based on these findings, salinity might alter the FA synthesis in *Nannochloropsis* species. The effect of different salinity levels is compared in Table 1.2. The optimum temperature (20-25 °C) and standard growth medium recipe for *Nannochloropsis* species are selected as constant parameters. The EPA content is compared with the palmitic acid (C16:0) component as the primary counterpart for EPA synthesis. The ratio of C20:5 to C16:0 could indicate the FA changes, where the ratio is reduced when the neutral lipids are dominating the microalga cells at the end of the exponential and stationary phase.

The data can be divided into two parts, the effect of salinity at low light intensity (< 100 µmol m^{-2} s^{-1}) and standard and higher light intensity (≥ 100 µmol m^{-2} s^{-1}). Low light intensity and

lower salinity (less than 30 g/L) show the highest EPA percentage at 27 %, compared to standard salinity levels (30-35 g/L), having around 20-24 % of EPA of TFA in microalga cells (Table 1.2). In contrast, low light intensity and high salinity (higher than 35 g/L) shows a comparable EPA content compared to standard salinity levels, except an extremely higher salinity (64 g/L) indicates a reduction in EPA percentage (Table 1.2).

Table 1.2: Effect of salinity, light intensity and light regime cycle on EPA content and ratio of EPA to triacylglycerol (TAG) content. All standard mediums without additional nutrients and optimum temperature (20-25 °C) are employed. E, exponential phase; S, stationary phase.

Species	**Light intensity (µmol m^{-2} s^{-1}) (Light:dark) (h:h)**	**Salinity (g/L)**	**Days (Growth phase)**	**EPA content (%)**	**C20:5 to C16:0 ratio**	**References**
N. gaditana CCNM1032	40 (12:12)	20 30 35 40	18 (E)	20.5 ± 0.14 21.1 ± 0.07 22.0 ± 0.07 19.1 ± 0.08	0.78 0.72 0.94 0.78	(Mitra et al., 2015a)
Nannochloropsis sp.	50 (24:0)	22 31 49 64	10 (E)	27.0 ± 0.5 23.6 ± 0.9 23.7 ± 1.1 8.4 ± 0.4	1.07 0.95 1.07 0.28	(Hu and Gao, 2006)
Nannochloropsis sp. UTEX2379	170 (24:0)	13 27 40	2 (E)	26.7 24.7 17.5	1.08 0.99 0.53	(Pal et al., 2011)
		13 27 40	7 (E)	19.2 17.8 13.1	0.60 0.55 0.36	
N. salina 1776	700 (24:0)	0 27 40	7 (E)	18 15 15	NA NA NA	(Solovchenko et al., 2014)
N. oculata CS 179	160 ± 5 (24:0)	25 35 45	19 (E)	25.4 ± 4.31 20.2 ± 2.55 22.6 ± 0.94	0.86 0.75 0.84	(Gu et al., 2012)
Species	**Light intensity (µmol m^{-2} s^{-1}) (Light:dark)(h:h)**	**Salinity (g/L)**	**Days (Growth phase)**	**EPA content (mg/g) DCW**	**C20:5 to C16:0 ratio**	**References**
N. oceanica CY2	150 (24:0)	15 30 45	10 (E)	19 31 28	NA NA NA	(Chen et al., 2018a)

Under standard or high light intensity, low salinity shows a slightly higher EPA percentage compared to standard salinity levels, while high salinity shows the lowest EPA percentage (Pal

et al., 2011). In *Nannochloropsis oculata*, low and high salinity show a higher EPA percentage compared to standard salinity (Gu et al., 2012). Low salinity has the potential to increase EPA content, but low biomass due to slow growth is impeding the potential. In *Nannochloropsis oceanica*, low salinity shows the lowest EPA quantity (19 mg/g DCW) (Chen et al., 2018a). In *Nannochloropsis gaditana* cultured, salinity at 35 g/L shows the highest EPA percentage compared to other salinity concentrations (Mitra et al., 2015a).

Based on the findings shown in table 1.2, the salinity range of 15-35 g/L seems to be the optimum level for EPA synthesis. However, other strategies could be implemented, such as two stages cultivations, growing the species of *Nannochloropsis* at the optimum cells in the first stage and replenishing in low or high salinity culture medium in the second stage. High salinity stressor in the second stage could translocate the EPA from membrane lipids to TAG. In *Nannochloropsis salina*, high salinity level (58 g/L) shows the highest TAG production and a lower cell density compared to the optimum salinity levels (22 and 34 g/L) (Bartley et al., 2013).

1.4.4. Nitrate, phosphate, and pH

Nutrient availability in the culture medium influences lipid synthesis in microalgae cells; hence, it's essential to identify any changes in FA composition over time in order to tune abiotic parameters to boost EPA levels (Mitra et al., 2015b).

A high level of $NaNO_3$ (3000 μM) shows the highest EPA percentage of TFAs in total lipids (29.9 %) compared to other $NaNO_3$, NaH_2PO_4 and salinity levels (Hu and Gao, 2006). Conceptually similar work has also been carried out by Hoffmann et al. (2010), discovering that the increase of $NANO_3$ (1800 μM) in the f/2 medium has a higher EPA percentage than the standard medium at the stationary growth phase. The increase of nitrate could trigger the EPA synthesis, while nitrate limitation triggers the TAG synthesis. However, the EPA quantity remains at the highest level (40-50 mg/g DCW) and has low TAG content as long as the nitrate is available in the culture (Hulatt et al., 2017). On the contrary, a low level of nitrate induces TAG synthesis (Table 1.3).

Table 1.3: Effect of growth medium and nutrients addition, light intensity and light regime cycle to EPA content and ratio of EPA to triacylglycerol (TAG) content. Standard salinity level

(25-35 g/L) and optimum temperature (20-28 °C) is applied. E, exponential phase; S, stationary phase.

Species	**Light intensity (µmol m^{-2} s^{-1}) (Light:dark)(h:h)**	**Growth medium/ nutrients**	**Days (Growth phase)**	**EPA content (%)**	**C20:5 to C16:0 ratio**	**References**
Nannochloropsis sp. (PP983)	50 (24:0)	$NaNO_3$ 150 (µM) 600 (µM) 3000 (µM)	10 (E)	 7.9 ± 0.3 15.7 ± 0.8 29.9 ± 0.9	 0.21 0.46 1.32	(Hu and Gao, 2006)
Nannochloropsis sp. (PP983)	50 (24:0)	NaH_2PO_4 6 (µM) 25 (µM) 120 (µM)	10 (E)	 12.8 ± 1.0 27.9 ± 1.3 27.4 ± 0.5	 0.43 1.10 1.19	(Hu and Gao, 2006)
N. salina	200 (24:0)	$NaNO_3$ 150 (µM) 600 (µM) 1800 (µM)	14 (S)	 2.9 ± 0.14 8.8 ± 0.3 16.3 ± 0.5	 0.06 0.22 0.47	(Hoffmann et al., 2010)
Species	**Light intensity (µmol m^{-2} s^{-1}) (Light:dark)(h:h)**	**Growth medium**	**Days (Growth phase)**	**EPA content (mg/g) DCW**	**C20:5 to C16:0 ratio**	**References**
N. gaditana strain B-3	100 (24:0)	Continuous recycled fertilizer at 8mM KNO_3	Winter Spring Summer	42.7±0.15 42.0±0.09 42.5±0.05	1.67 2.41 1.75	(Camacho-Rodríguez et al., 2014)
Nannochloropsis sp. (strain CCAP 211/78)	180 (16:8)	**Low (g/L)** $NaNO_3$ -1.5 NaH_2PO_4-0.1 **High (g/L)** $NaNO_3$ -3 NaH_2PO_4-0.2	8 (E) 12 (S) 16 (S) 8 (E) 12 (S) 16 (S)	41.5 ± 2.7 43.9 ± 3.6 49.3 ± 3.9 43.2 ± 1.1 45.0 ± 5.1 46.8 ± 2.4	2.13 2.03 1.59 1.83 0.72 0.45	(Hulatt et al., 2017)
N. oceanica CY2	150	BG-11 $NaNO_3$ (g/L) 0.375 0.750 1.50 2.250	8 (S)	 23.8 ± 0.2 40.9 ± 0.4 43.1 ± 0.2 34.2 ± 0.3	 - - ≈0.25 -	(Chen et al., 2013)
N. oceanica CY2	150 (NA) -White TL5 -white LED -Blue LED -red LED -yellow LED	BG-11 $NaNO_3$ (g/L) 1.50	5 (E)	 43.1 ± 3.5 35.6 ± 3.5 55.7 ± 3.3 54.1 ± 4.1 37.8 ± 2.8	 - - - - -	(Chen et al., 2013)
N. oceanica CY2	150 (NA) -Blue-red LED Blue-yellow LED Blue-white LED	BG-11 $NaNO_3$ (g/L) 1.50	5 (E)	 51.3 ± 3.2 48.6 ± 3.5 48.7 ± 3.5	 - - -	(Chen et al., 2015)

	red-yellow LED yellow-white LED			43.8 ± 3.9 48.6 ± 4.2	- -	

A combination of two phases has optimised cell growth and nutrient depletion to induce TAG (Su et al., 2011). In contrast, lipids trafficking involves EPA and TAG from neutral lipids to glycolipids and phospholipids when nutrients are replenished at phase two (Mitra et al., 2015b). The EPA to TAG ratio increases from 0.15 to 1.12 from day 18 to day 22, indicating the percentage of EPA increases while TAG decreases (Table 1.1). Nitrogen deprivation has been proved to accumulate a lot of lipids in oleaginous microalgae described in many studies (Yaakob et al., 2021). However, no evidence found that the nitrogen limitation could induce EPA synthesis. Recent studies have discovered that repleted culture medium is crucial for enhancing EPA content within cells (Wang and Jia, 2020).

1.5. Current research and development for species of *Nannochloropsis* to increase EPA and fatty acids synthesis

Microalgae strain development has been carried out to establish fast-growing microalgae and enhance bioactive compound production, such as EPA, using emerging technology in the field (Fu et al., 2016). In addition, strain improvements are necessary to make EPA industrial production becomes feasible. Three strategies can be implemented to improve the EPA synthesis in microalgae cells: first, by exploiting the cultivation conditions to trigger the EPA synthesis; secondly, by mutagenesis and selected breeding; and thirdly, by improving the EPA synthesis through genetic modifications (Chauton et al., 2015). Mutagenesis, genetic engineering, and adaptive laboratory evolution (ALE) are three areas that have been investigated for microalgae strain improvements (Fu et al., 2016). Metabolic engineering strategies have been intensively studied to improve the microalgae strains and benefit LC-PUFA and carotenoids (Gimpel et al., 2015).

Genes are transferred from parents to progeny in all living organisms and create the basis of heredity traits (Hlavova et al., 2015). Genes also might change to form mutants by natural environmental interactions such as UV radiation (Hlavova et al., 2015). These mutants are the main source of genetic variability and have the potential for evolution; however, the natural

processes are too slow for breeding and evolution study. Physical and chemical mutagens can increase the mutagenesis development; this leads to the production of mutant populations (Hlavova et al., 2015). Mutagenesis is a process of bringing out a higher frequency of mutation than the natural rate of an organism by using physical (ultraviolet light, gamma and X-rays) or chemical (N'-nitro-N-nitrosoguanidine and Ethyl methanesulfonate) mutagen (Fu et al., 2016). Ultraviolet (UV) light can be employed without knowing the genetic information of microalgae species and can be handled flexibly to avoid contaminations (Fu et al., 2016). There are three advantages of UV mutagenesis in microalgae breeding: 1) genetic information is not required to initiate the mutagenesis, 2) it can be easily manipulated compared to gene expression, and 3) it can be controlled conveniently to avoid secondary contamination (Liu et al., 2015). Usually, the wavelength of UV is 253.7 nm with a distance of 15 to 20 cm to the culture cells of microalgae can be used to induce mutagenesis. The challenge of the mutagenesis technique is to identify the mutated genes in the mutant strains, especially for the microalgae species that do not have complete genomes (Hlavova et al., 2015). In addition, screening the mutants that enhance EPA content could be challenging as, at present, no chemical stressors specifically develop to inhibit desaturase and elongase steps for LC-PUFA synthesis.

Microalgae could evolve by interactions between environmental factors such as UV irradiation, different geographical locations and genetic materials (Hlavova et al., 2015). Improved phenotype or mutant populations can be developed by imitating and increasing the mutagen levels, leading to the development of ideal-type microalgae species. Chemical and physical mutagens are among the most commonly employed in both basic and applied science, owing to the fact that most of them are simple to use at various doses and have well-defined mutagenic potentials (Hlavova et al., 2015). Chemical mutagens, N-methyl-N-nitrosourea (MNU) and ethyl methanesulfonate (EMS) are alkylating agents and show an increase in EPA (5-7 mg/g DCW) and total lipids (6-14 mg/g DCW) in mutants compared to wild-type *Nannochloropsis oculata* (Chaturvedi et al., 2004; Chaturvedi and Fujita, 2006). In addition, mutagenesis of *Nannochloropsis oceanica* by methylnitronitrosoguanidine (MNNG) shows a faster growth rate compared to the wild-type strain (Liang et al., 2017). The increase of EPA indicates the effectiveness of cerulenin (FAS inhibitor) and quizalofop (ACCase inhibitor) in screening the enhanced FAs mutant's producer.

UV, gamma or heavy ion beams are examples of physical mutagens that are widely applied to microalgae. The UV light causes a photochemical reaction leading to a cyclobutane ring, while gamma-ray and heavy-ion irradiation cause the ionisation reaction leading to a stranded break in microalga cells (Hlavova et al., 2015). On the contrary, the use of UV in *Nannochloropsis* species is effective in increasing TAG and total lipids that benefit biofuel production. In *Nannochloropsis oculata*, microalga cells exposed to UV-A irradiance show a decrease in chlorophyll content and an increase in TAG (Srinivas and Ochs, 2012). In *Nannochloropsis salina*, a combination of EMS and UV mutagenesis show the mutant increases in total lipids while the EPA has decreased (Beacham et al., 2015). Fluorescence-activated cell sorting (FACS) is used for screening the mutant with high neutral lipids content. On the contrary, a mutant *Nannochloropsis oceanica* induced by heavy ion irradiation mutagenesis shows a 19 % increase in biomass accumulation, a 6 % increase in lipid productivity and a 28 % increase in total lipids productivity (Ma et al., 2013). The chlorophyll-*a* in the mutant is increased, while the EPA content is comparable between the mutant and the wild-type (Ma et al., 2013). However, the screening methods are not described in detail in the report.

There is no report on using gamma-ray and Cs– γ nuclear radiation to increase total lipids and EPA in *Nannochloropsis* species. However, the gamma-ray is successfully applied to increase violaxanthin yield in *Nannochloropsis oceanica* without impeding cell growth and biomass production (Park et al., 2021). The mutant induced by Cs– γ nuclear radiation can maximise light-use efficiency and increase biomass productivity (Lu et al., 2020), potentially increasing EPA production. The screening for gamma-ray and Cs– γ nuclear radiation is based on the selection of the faster growth mutants compared to the wild-type strain.

In *Nannochloropsis oceanica*, MGDG is one of the key components, accounting for roughly 40-50 % of membrane lipids and around 60 % of the EPA of TFA in MGDG (Junpeng et al., 2020). In another study, MGDG and DGTS reported may comprise two major EPA pools in membrane lipids (Murakami et al., 2018). During the exponential phase, the primary membrane polar lipids discovered in the *Nannochloropsis* oceanica are MGDG, PC, and PG

(Han et al., 2017). Therefore, exploiting the EPA and MGDG relationship in the chloroplast could be the key to modifying the EPA trafficking in the *Nannochloropsis* cells. Changing DGTS pathways could also affect the EPA synthesis pathways. Therefore, membrane lipids inhibitors could be used to screen the mutants and enhance the EPA synthesis in the species of *Nannochloropsis*. A previous study stated that several compounds had been used as an inhibitor for MGDG synthase, but none are suitable as a tool for chemical genetic strategy (Boudière et al., 2012). Galvestine-1, a chemical probe specifically developed for plant chemical genetics, has successfully applied to *Arabidopsis thaliana* to inhibit MGDG synthase, reducing the MGDG content. Up to this review point, there are no reports on this compound applied to microalgae and increasing the bioactive compounds in microalgae cells. In addition, the combination of mutagenesis and enzyme inhibitors might induce a new phenotype of microalgae cells; that has an excellent ability to grow fast and produce high bioactive compounds. Meanwhile, there is no chemical inhibitor that specifically develop to inhibit DGTS. In *Nannochloropsis oceanica*, DGTS content shows $\sim$50 % lower compared to PC (Han et al., 2017), while *Chlamydomonas reinhardtii* and *Chlamydomonas moewusii* possess DGTS with no PC (Oishi et al., 2022). The overexpressed *BTA1* gene responsible for DGTS synthesis shows an increase in DGTS content (Oishi et al., 2022). Hence, the inhibition of the *BTA1* gene could decrease the synthesis of DGTS. In the species of *Nannochloropsis*, inhibiting DGTS, MGDG, or both lipids could translocate the EPA synthesis to other lipids. In addition, *Nannochloropsis* have a complex cell wall that could operate as a barrier to any cell's metamorphosis or engineering. An investigation into the relationship between EPA and the membrane polar lipid MGDG reveals that $\Delta 0$ elongase could play a key role in EPA translocation from MGDG to TAG (Dolch et al., 2017).

Synthetic biology approaches have gained popularity in recent years to engineer the downstream production pathways in several microalgae strains. However, the resources and tools needed for nuclear manipulation, synthetic gene network construction, and algal genome-scale restoration are limited (Jagadevan et al., 2018). Advances in molecular biology techniques such as; clustered regularly interspaced short palindromic repeats (CRISPR), transcription activator-like effectors (TALEs), and zinc-finger nucleases (ZFN) have paved the way for unravelling novel metabolic pathways occurring within algal cells or designing and synthesising new biological systems (Jagadevan et al., 2018). In *Nannochloropsis salina*,

overexpressing Δ12 desaturase by CRISPR/Cas9 method shows a 4-fold and 1.5-fold increase in LA and EPA, respectively (Ryu et al., 2021). The sufficient increase of LA substrate has led to the increase of EPA synthesis without impeding the growth of the cells. Applying platinum transcription activator-like effector nucleases (TALENs) to target nitrate reductase and acyltransferase genes simultaneously in *Nannochloropsis oceanica*, indicates a higher efficiency in editing the microalga cells compared to CRISPR-Cas9 method (Kurita et al., 2020). There is a lack of information on the usage of the ZFN method to enhance the EPA in the species of *Nannochloropsis*.

Besides, the upstream pathways could also be engineered by focusing on photosynthetic and carbon fixation metabolism to enhance microalgae growth (Naduthodi et al., 2021). In brief, the synthetic biology approaches to engineering the upstream pathways are divided into three. Firstly, improving photosynthetic efficiency by replacing with different D1 subunit in PS II; introducing a new chlorophyll type, for example, chlorophyll *b* in the species of *Nannochloropsis*; and overexpressing ribulose-1,5-bisphosphate carboxylase-oxygenase (RuBisCO) enzyme to improve carbon fixation (Naduthodi et al., 2021). In *Nannochloropsis oceanica*, overexpressed gene 1248 (possibly responsible for carbon fixation) by CRISPR/dCas9 method shows an increase in growth rate and PS II photosynthetic parameter (Fv/Fm) in engineered strains M4 and M6 (Wei et al., 2022). The EPA synthesis could be enhanced with the increase in photosynthetic efficiency. Engineered light-harvesting complex (LHC) could increase photo-damage resistivity and light penetration in microalgae cells (Fajardo et al., 2020). The main challenge of synthetic biology is limited bioinformatics resources and tools to manipulate endogenous and synthetic gene networks (Ng et al., 2020), and more experiments are needed to engineer the upstream pathways. In addition, more investigations are required in order to demonstrate the engineered strains on a bigger scale (Hlavova et al., 2015).

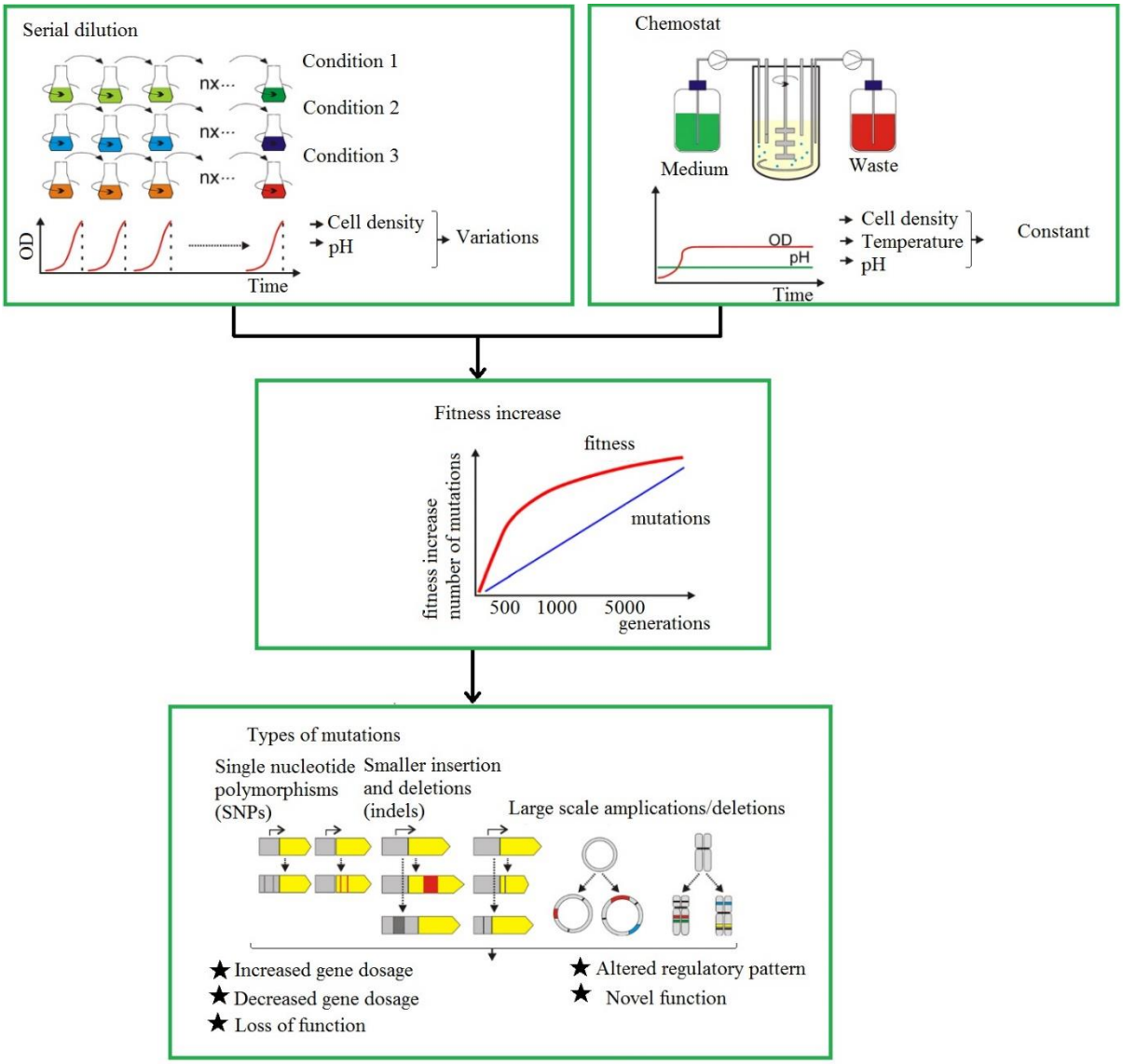

Figure 1.3: Adaptive laboratory evolution (ALE) methods with modification (Dragosits and Mattanovich, 2013), where the evolution is monitored for an extended period of time (500 to 5000 generations) in order to develop a new phenotype of microalgae.

Insertional mutagenesis is another method to improve the microalgae phenotype. The difference is this method inserts a foreign DNA fragment into the genome. An established method of DNA transformation is necessary to undertake insertional mutagenesis in microalgae cells (Hlavova et al., 2015). This method is like a combination of synthetic biology approach and mutagenesis in order to find an ideal type of microalga cells. In a recent study, *Nannochloropsis oceanica* mutant developed by insertional mutagenesis shows a 55 % increase in PUFA compared to the wild-type strain (Südfeld et al., 2021). Interestingly, FACS use for screening the mutants with enhanced neutral lipids content. In another study,

Nannochloropsis salina mutant screened by insertional mutagenesis exhibited a 53 % faster growth rate and 34 % higher TFAs compared to wild-type strain after 8 days of cultivation (Ryu et al., 2020).

ALE is a standard method in biological studies to understand the fundamental mechanisms of molecular evolution; it is further related to the microorganism adaptation throughout the culturing under specific growth conditions (Figure 1.2) (Dragosits and Mattanovich, 2013). ALE can be conducted for strain optimisation by determining the environmental parameters that affect the growth and targeting metabolic pathways (Fu et al., 2016). ALE is a long-term serial transfer procedure and is repeatedly conducted in a 24 h cycle, runs for 40 cycles, and the evolutions were measured by taking a few points such as cycles 10, 20, 30, and 40 (Sun et al., 2016). Hence, the new mutant strain can be studied in ALE and investigate whether photo repairs occur in the developed mutants (Meireles et al., 2003a).

The strain characteristics could be changed by ALE (Sun et al., 2016), hence, triggering the synthesis of EPA. ALE is conducted by selecting valuable parameters such as illumination, salinity, nutrient starvation, and temperature, depending on the metabolic pathway for the targeted product. The ALE can be further comprehended by applying genetic engineering and synthetic biology approaches for specific phenotype consequence determination (Fu et al., 2016). ALE experiments have been implemented to study microalgae development and strain improvement, followed by genome resequencing to study the basic genetic behind adaptation to different environmental conditions (Fu et al., 2016). ALE can be conducted to investigate strain development to improve the production of bioactive compounds. There are no previous reports in the literature on ALE experiments conducted for enhancing EPA in the species of *Nannochloropsis*.

1.6. Genomics, transcriptomics, metabolomics, and proteomics analyses in revealing fatty acids and EPA synthesis pathways

This section reviews the investigation conducted to find the cause of omega-3 synthesis. The past decade has seen genomics, transcriptomics, metabolomics, and proteomics have been used to entangle the regulation and network integration for FAs synthesis pathways in

microalgae. The term "omics" has been used in any biological study that needs to characterise and quantify large datasets of an organism's structure, function, and dynamics, while bioinformatics tools are needed to archive and interpret high-resolution molecular maps (Arora et al., 2018). Genomics has been a crucial tool in harnessing microalgae's biocatalytic potential. The genomic analysis makes it easier to examine an organism's whole gene complement's primary sequencing and structural assembly. As a result, genomics identifies an organism's innate biosynthetic and metabolic capacity as a potential microbial cell factory and gives a blueprint for maximising productivity. Traditional static genomic applications have been supplemented with transcriptomic, proteomic, and metabolomic profiling, which is beginning to bridge the gap between an alga's genotype and observed phenotype (Guarnieri and Pienkos, 2015). Lipidomics is part of metabolomic profiling that focus on evaluating as many as possible lipid compounds in a sample (Arif et al., 2020). Combining two analyses (e.g., transcriptomics and proteomics) has been effectively implemented to facilitate the understanding of biological processes, making genetic manipulation for targeting the specific compound of interest possible (Anand et al., 2017). The emergence of the omics age and the advancement of related technologies to acquire and analyse the massive amounts of available data have transformed biological science (Lauritano et al., 2019). This proactive approach promises to investigate and understand the biochemical processes in microalgae cells, and it has a wide range of biotechnology applications. This study focuses on EPA synthesis; however, DHA is also included in this section since DHA shares the same pathways with the EPA.

Omics analysis could be implemented to discover the effect of environmental conditions on microalgae cells at molecular levels. In the species of *Nannochloropsis*, regulatory mechanisms on the impact of temperature on the EPA synthesis and trafficking in membrane lipids, especially MGDG, DGDG, and DGTS, are little explored in the literature. In a metabolomic study, Willette et al. (2018) discovered that membrane lipids could be associated with the citrate cycle under low temperatures. In another study, proteomics analysis shows FAS and polyketide synthase pathways are responsible for DHA and FAs synthesis in *Schizochytrium* sp. (Hu et al., 2020). At low temperatures, the amount of acetyl-CoA and NADPH are upregulated, indicating that low temperature promotes the substrates into PKS pathways, increasing the DHA percentage of TFAs (Hu et al., 2020).

In a combination of the transcriptomic and metabolomic study of adaptation *Nannochloropsis gaditana* in a different colour of light; red colour involves in amino acids metabolism, blue elevates EPA content and decreases the carbohydrate, while green shows the lowest response to metabolite and gene transcripts level (Patelou et al., 2020). The increase in EPA could be contributed by the upregulation of ER Δ5 desaturase, ER Δ6 desaturase, ER Δ12 desaturase, and ER omega-3 desaturase. In addition, transcriptomic and proteomics study in response to light quality variation reveals the *Nannochloropsis oceanica* cells exposed to blue light (80 µmol m^{-2} s^{-1}) could increase the chlorophyll content (Wei et al., 2020), hence potentially increasing membrane lipids and EPA. In addition, the increase of NADPH-dependent glyceraldehyde-3-phosphate dehydrogenase (GAPDH) enzyme in microalga cells exposed to red and blue light indicates more energy is produced compared to white light (Wei et al., 2020). In *Haematococcus pluvialis*, blue light enhances the germination efficiency and accumulates a higher level of astaxanthin compared to light and white LED lights (Ma et al., 2018).

Incubation of *Phaeodactylum tricornutum* in the dark at the end of the exponential phase period showed that the cellular distributions of carbon, nitrogen and energy were shifted to lipid synthesis, increasing lipid production (Bai et al., 2016). Hence, this finding may suggest that light: dark cycle is beneficial in converting carbohydrates to lipids, decreasing the membrane lipids, and increasing the EPA in other compartments such as TAG. Ultraviolet radiation and high temperature could cause the photodamage to microalga *Isochrysis galbana* cells and decrease the photosynthetic efficiency. Depriving ultraviolet radiation in *Isochrysis galbana* has resulted in increasing photosynthetic efficiency, hence accumulating more polar lipids, MGDG, DGDG, SQDG, diacylglycerylcarboxyhydroxymethylcholine (DGCC), DGTS, and lysolipids, while TAG was decreased (Cao et al., 2019). The enzymes involved with MGDG and SQDG synthesis were analysed (Riccio et al., 2020), where MGDG synthase, UDP-sulfoquinovose synthase (SQD1), and sulfoquinovosyltransferase (SQD2) are distributed across different taxonomy. MGD genes found are also similar to MGD genes found in terrestrial plants (Riccio et al., 2020).

The effect of different salinity levels on EPA synthesis were reported in several studies. In *Nannochloropsis gaditana* cultured at hypersaline conditions, lipid oxidation pathways are

upregulated, while the proteins related to photosynthesis, carbon fixation, and chlorophyll are downregulated (Karthikaichamy et al., 2021). Adapting freshwater microalga to salinity indicates the thylakoid membrane lipids, MGDG, DGDG, SQDG and PG, are decreased (Mao et al., 2020). Interestingly, the salt stress and nitrogen deprivation conditions in *Chromochloris zofingiensis* show comparable upregulated genes, indicating the microalgae may have similar response to salt and nitrogen stress conditions (Mao et al., 2020). Salinity range 13-30 g/L indicates the highest percentage of EPA, as discussed in the previous section 1.4.3. To date, no assessment at the molecular level on the effect of low salinity on EPA synthesis in *Nannochloropsis* species. In *Schizochytrium* sp., high salinity levels have decreased the DHA percentage of TFAs, and downregulated the enzymes related to FA synthesis in microalga cells (Jiang et al., 2019).

A few studies are conducted at the molecular level in *Nannochloropsis* species to uncover the mechanism of nitrogen-depleted conditions in producing high lipid content. In general, from the review in the previous section, nitrogen depletion or starvation shows a lower EPA content than the nitrogen-repleted conditions. Hence, the overexpressed omics data caused by the nitrogen-repleted conditions could be useful for identifying any genes, metabolites, and protein changes related to FAs and EPA synthesis pathways. In *Nannochloropsis oceanica*, nitrogen deprivations cause the cells to enter a quiescence state in order to survive unfavourable environmental conditions (Zienkiewicz et al., 2020). However, when the nitrogen is resupplied, the microalga cells reinitiate the cell cycle gene and continue the growth. In addition, gene encoding proteins involved in chlorophyll-*a* are upregulated after nitrogen is resupplied in the culture medium. Besides, the level of PSI and PSII, cytochrome b6f, ATP synthase and glyceraldehyde-3P dehydrogenase are also increased in nitrogen repleted conditions. The increase of energy levels compared to the initial phase of culturing (standard nitrogen levels) could increase the biogenesis of membrane lipids and EPA in nitrogen resupplied conditions. It is crucial to fully understand the lipid bodies' conversion to other cell compartments, especially in chloroplast and ER, where the EPA was originally initiated.

ACCase, FAS, 3-ketoacyl-ACP synthase, 3-ketoacyl-ACP reductase, hydroxyacyl-ACP dehydrogenase, and enoyl-ACP reductase enzymes related to FAs synthesis are also

upregulated in nitrogen repleted conditions (Zienkiewicz et al., 2020), indicating higher FAs synthesis activities in the chloroplast. This finding indicates the initial steps of FAs synthesis is important in preparing the substrate for LC-PUFA synthesis in the ER. In a previous study, overexpressed ME has increased the carbon flux and NADPH hence increasing the overall TFAs in *Nannochloropsis salina* cells (Jeon et al., 2021). Another study on the effect of nitrogen repleted and depleted conditions on *Nannochloropsis oculata* discovers that breakdown proteins and pigments are channelled to FA synthesis (Tran et al., 2016). The upregulated of LDSP indicates the TAG and lipid droplet accumulation in the microalga cells, while ACCase is downregulated in nitrogen-depleted conditions (Tran et al., 2016). Interestingly, the LDSP is 2-fold upregulated, and 5-fold downregulated in *Nannochloropsis oceanica* population heterogeneity under nitrogen repleted and deprived conditions, respectively (Chen et al., 2019). Early investigation of the combination of low nitrogen and phosphorus in *Nannochloropsis* sp. shows an increase in neutral lipids, and EPA content remains at similar levels throughout the culturing (Hulatt et al., 2017). The biochemical analysis of TAG shows the percentage of EPA in TAG is decreased at the stationary phase, indicating that the EPA might be preserved in the microalga cells in other lipids such as MGDG and DGTS. The detailed proteomics and transcriptomic analysis of the effect of low phosphorus and nitrogen on *Nannochloropsis* sp. reveal the degrading of polar membrane lipids may contribute to the partially translocated EPA to TAG (Hulatt et al., 2020). Δ5 desaturase, one of the key enzymes for EPA synthesis is downregulated, suggesting EPA synthesis is decreased in low nitrogen and phosphorus medium.

Cadmium is one of the toxic pollutants commonly found in the environment that inhibit microalgae growth and biomass accumulation (Kim et al., 2005). Exposing the *Nannochloropsis oculata* cells to cadmium suppresses glyceraldehydes 3-phosphate dehydrogenase A protein that could be related to glycolysis in microalga cells (Kim et al., 2005). However, there are no direct biochemical quantifications described in the study to show the relation between the suppressed protein with carbohydrate and FAs contents.

In *Aurantiochytrium sp.*, microalga cells treated with phytohormone 6-benzylaminopurine (6-BAP) increase lipid and DHA content by 48.7 % and 55.3 %, respectively, compared to untreated microalga cells (Yu et al., 2019). 6-BAP increases cellular membrane fluidity while

decreasing the amount of saturated FAs (Yu et al., 2019). In addition, 6-BAP is capable of reinforcing the key enzymes for FAs syntheses, such as acetyl-CoA, malonyl-CoA, and NADPH (Yu et al., 2019). Transcriptomic analysis of *Aurantiochytrium* sp. discovers very-long-chain (3R)-3-hydroxyacyl-CoA dehydratase (PH) and dehydrase/isomerase (DH) in FA synthesis and PKS pathways, respectively, that are responsible for DHA synthesis under various salinity levels (Liang et al., 2018). In addition, PH and DH could be related to the *Aurantiochytrium* sp. cell growth. The growth of *Aurantiochytrium* sp. was decreased when the PH and DH genes were knockout from the culture (Liang et al., 2018). In another study, *Crypthecodinium cohnii* mutant showed 24.32 % faster and accumulated 7.05 % more lipids than the wild-type strain (Liu et al., 2017). *Crypthecodinium cohnii* mutant transcriptomic analysis discovered a higher ACCase enzymatic activity and ACCase-encoding gene compared to wild-type strain (Liu et al., 2017), indicating the success of screening strategies in random mutagenesis experiments to enhance the lipid production.

In the species of *Nannochloropsis*, no known work exists for a detailed study on EPA translocation using proteomics approaches. Most of the proteomics study covers lipid synthesis for producing a higher quantity of TAG. This is a novel area of research, and little is currently known regarding the mechanism of translocating EPA to TAG.

1.7. Microalgae growth systems

Sustainability is one of the essential principles in managing natural resources, and it includes operational efficiency, minimising environmental impact, and social and economic considerations (Singh and Sharma, 2012). Hence, selecting a suitable microalgae cultivation system is crucial in achieving sustainability in the EPA production industry. The type, design, and advantages of photobioreactors are well-reviewed in a recent article (Legrand et al., 2021). Conical flasks and vertical columns photobioreactors are usually used for a small laboratory scale photobioreactor (Pal et al., 2011; Meng et al., 2015; Sforza et al., 2015), while flat plats and tubular photobioreactors are usually used at a bigger scale (Chini Zittelli et al., 1999; Pereira et al., 2018).

Closed photobioreactors are classified into five types; stirred-tank, bubbled-column, air-lift, flat-plate and tubular design (Kwon and Yeom, 2017). Table 1.4 compares the advantages and disadvantages of close photobioreactors, adapted from previous studies. A few criteria must be considered for finding a suitable type of photobioreactors. The suitability of a photobioreactor depends on the physiological and growth characteristics of selected microalgae species. For example, *Nannochloropsis* is a unicellular species with a small cell size (3-4 μm) average (Iwai et al., 2015). These characteristics make the *Nannochloropsis* suitable for all types of photobioreactors. Furthermore, no biofouling is expected in *Nannochloropsis* cells sticking to the photobioreactor wall since EPA synthesis mainly involves the exponential phase. Different microalgae species vary in morphological characteristics that could contribute to biofouling in the photobioreactor. Biofouling is described as biofilm formation at the photobioreactor illuminate surface, especially when the excess light is absorbed by the microalgae cells. The biofilm causes less solar radiation received by the microalgae cells, reducing the biomass productivity and photosynthetic efficiency of the cultivation system. *Nannochloropsis gaditana* showed a formation of biofilm during long-term cultivations (Soriano-Jerez et al., 2021), indicating the tendency of biofouling towards the stationary growth phase.

Photobioreactor design could also contribute to biofouling. Poor mixing and lack of microalgae cell circulations on the light site for photosynthesis could contribute to biofouling. Even though the helical-tubular photobioreactor could overcome the necessity for space limitation, biofouling occurred (Briassoulis et al., 2010). *Nannochloropsis* sp. showed the maximum productivity under continuous culturing in the helical-tubular photobioreactor (Briassoulis et al., 2010), indicating that *Nannochloropsis* sp. is unfavourable for biofouling under healthy conditions. In contrast, *Nannochloropsis gaditana* showed a formation of biofilm during long-term cultivations (Soriano-Jerez et al., 2021), indicating the tendency of biofouling towards the stationary growth phase.

The microalgae culture mixing is crucial for gas-liquid mass transfer, nutrient uptake and exposing all cells to light for photosynthesis. Vertical column photobioreactors offer adequate gas-liquid mass transfer via bubble mixing (Egbo et al., 2018). Optimum mixing could effectively decrease dissolved oxygen in the culture, especially in the vertical column, and

enhance the photosynthetic process by exposing all microalgae cells to light (Chai and Zhao, 2012). Mechanical stirring offers the most efficient mixing in microalgae culture. However, high capital cost and processing cost by stirred tank photobioreactor and the decrease of light-harvesting efficiency due to low surface area to volume ratio are the significant challenges that need to be addressed for an enhanced microalgae growth performance. In stirred tank photobioreactor, the hydrodynamic stress is also produced by the mechanical stirrer mixing. 75-150 rpm is determined as the suitable rotation speed that produces around 1.97-3.96 Pa shear stress (Verma et al., 2019). The shear stress values cause different shear stress effects depending on the microalgae cell's morphology.

Besides, shear stress could occur if a higher frequency or speed is applied. The gas flow rate and velocity are critical for photobioreactors to avoid hydrodynamic stress. A suitable turbulence flow rate could alleviate the dissolved oxygen, while a higher rate could cause shear stress. Shear stress causes impaired cell growth, cell damage and cell death (Barbosa et al., 2004). In a bubble column photobioreactor, a small nozzle (0.4 mm diameter) size causes a detrimental effect on microalgae cells compared to a bigger nozzle size (0.8-1.2 mm diameter) (Barbosa et al., 2004). The small nozzle size contributes to a smaller bubble size that influences the gas flow rate and increases the gas velocity, changes the aeration flow pattern, and causes higher hydrodynamic stress to microalgae cells. Choosing the suitable aeration rate is crucial to achieving aeration velocity and optimising photosynthetic activity, microalgae cell mixing, and growth. *Phaeodactylum tricornutum* is sensitive to hydrodynamic stress in bubble columns, and the breakup of tiny bubbles on the liquid surface seems to cause cell damage (Barbosa et al., 2004). Hence, bubble column and airlift are less suitable as a bigger scale photobioreactor requires a higher bubbling rate for fast liquid-circulation times for cell mixing.

Microalgae utilise CO_2 and produce oxygen during phototrophic development in microalgal culture systems. High dissolved oxygen concentrations in photobioreactors can hinder photosynthesis and microalgae growth (Kazbar et al., 2019). The geometric design of the photobioreactors plays a crucial role in releasing the trapped dissolve oxygen to encourage microalgae growth. Vertical column, stirred-tank, and flat plat photobioreactors are more efficient in removing dissolved oxygen than the tubular photobioreactor (Mirón et al., 1999)

(Table 1.4). The geometric design of the tubular photobioreactor contains a high concentration of dissolved oxygen. Hence, strategies must be developed to overcome this problem. The design of the tubular photobioreactor could be improved by having a degassing system for discharging the trapped dissolved oxygen into the atmosphere (Egbo et al., 2018). A combination of vertical columns equipped with a bubble tank and tubular system could help alleviate the dissolved oxygen in the tubular system. In a previous study, the application of a bubble tank instead of a plain bubble in the vertical column photobioreactor demonstrated the alleviation of dissolved oxygen in the microalgae culture medium (Chai and Zhao, 2012). Besides the photobioreactor design, fluorochemicals such as perfluorooctyl bromide, perfluorodecalin, methoxynonafluorobutane, and ethoxynonafluorobuta can remove dissolved oxygen in the photobioreactor and enhance the biomass for *Nannochloropsis oculata* (Lee et al., 2013). In addition, close photobioreactors provide higher biomass productivity resulting from a higher efficiency of light supplied (Sforza et al., 2012).

Light-harvesting in a vertical column depends on the diameter of the column. A bigger diameter could inhibit the light from reaching the column's centre, hence making the vertical column less suitable at a bigger scale.

Table 1.4: Advantages and disadvantages of different photobioreactors for microalgae culturing adapted from previous studies.

Photobioreactor	**Advantages**	**Disadvantages**	**References**
1) Bubbled-column	1) High surface area to volume ratio 2) Lowest capital and operating cost	1) Less efficient at pilot or commercial scale compared to tubular and flat plat photobioreactor	(Xu et al., 2009)
	3) Satisfactory heat and mass transfer 4) Homogenous culture environment 5) Efficient release of oxygen and residual gas mixture 6) No moving parts, low power consumption		(Singh and Sharma, 2012)
2) Air-lift	1) Can be modified into many shapes like putting sparger into annular tube	1) Complex and difficult in scale-up	(Singh and Sharma, 2012)
	2) Create circular and uniform mixing pattern		(Xu et al., 2009)

	3) No moving parts, low power consumption 4) high mass transfer rate & good solids suspension 5) homogeneous shear & rapid mixing 6) Less space required		
	7) Rectangular shaped have better mixing characteristic with high photosynthetic efficiency		(Janssen et al., 2003)
	8) Uniform exposure of the microalgae to light		(Kwon and Yeom, 2017)
3) Stirred-tank	1) Excellent mechanical mixing	1) Light harvesting efficiency decreases due to low surface area to volume ratio 2) The use of optical fibres for illumination cause disturbance in mixing pattern	(Singh and Sharma, 2012)
		3) Impeller requires high energy consumption	(Egbo et al., 2018)
4) Flat-plate	1) The highest light harvesting efficiency due to large illumination surface area to volume ratio 2) Volumetric mass productivity is 1.7 times higher than bubble column	1) 4.8 % less photosynthetic efficiency to inclined tubular reactor 2) Light saturation effect reduced at midday due to the curved surface	(Singh and Sharma, 2012)
	3) Low accumulation of dissolved oxygen compared to horizontal tubular photobioreactors		(Xu et al., 2009)
	4) Can be positioned to have maximum exposure to an external light source	3) Fouling and gas hold-ups	(Egbo et al., 2018)
	5) Excellent bubble mixing		(Kwon and Yeom, 2017)
5) Horizontal tubular	1) High light harvesting efficiency due to their orientation towards light. 2) Higher volumetric productivity	1) High energy consumption 2) Lower dissolve oxygen removal compared to bubble column	(Mirón et al., 1999; Singh and Sharma, 2012; Egbo et al., 2018)

	3) Excellent choice for outdoor mass microalgae culture		(Xu et al., 2009)
6) Helical type	1) Low land requirement. 2) Better CO_2 transfer from gas phase to liquid phase. 3) Excellent photosynthetic efficiency.	1) Fouling 2) Very high energy consumption	(Singh and Sharma, 2012)
7) Hybrid type: **a) Helical tubular**	1) Optimised light penetration depth. 2) Easy control of temperature and contaminants 3) Effective spatial distribution of fresh air and CO_2 4) Better CO_2 transfer through extensive interface surface between fresh air and culture liquid medium		(Singh and Sharma, 2012)
b) Flat panel-airlift	1) Hydrodynamic and mass transfer are more efficient than tubular and other flat plate photobioreactors		(Singh and Sharma, 2012)
c) Tubular-airlift	1) It allows CO_2 and oxygen to be exchanged between the liquid medium and the aeration gas 2) Potential cell damage associated with mechanical pumping may be minimized 3) Circulation is achieved without moving parts		(Xu et al., 2009)

The bubble column and airlift use a sparger to produce bubbling for mixing, while stirred tank uses a stirrer for mixing the microalgae culture. The microalgae culture in an air-lift photobioreactor is continuously mixed in circular mixing patterns through dark and light phases, while there is no flow pattern in a bubbled column (Singh and Sharma, 2012). Culturing *Nannochloropsis* sp. in an airlift photobioreactor records a higher cell growth (375 × 10^5 cells/mL), efficient light distributions, and better mixing compared to bubbled column (Roncallo et al., 2013). Combining the bubbling and mixer has increased the cell growth up to 42.9 % in a flat-plate panel compared to a bubbled mixing only (Huang et al., 2014). Modifying flat panel airlift photobioreactor shows 1.7 times higher volumetric mass productivity than bubble column photobioreactor. In addition, the helical tubular photobioreactor shows an efficient liquid-gas mass transfer and has a smaller space requirement compared to the tubular photobioreactor (Singh and Sharma, 2012).

Besides, a more sophisticated photobioreactor is designed to enhance microalgae growth. Algem (Algenuity, UK) is a rotary flask photobioreactor equipped with a device that can simulate any environmental conditions or choose any place on Earth (Pereira et al., 2018). All the growth parameters, such as optical density (OD), light variations and intensities, pH, and temperature, can be monitored for the best experimental controls. The only limitation is that chlorophyll could interfere with the OD reading when the microalgae cell culture gets denser at the later stage of the culturing. The OD or turbidity refers to the amount of light absorbed by a suspension of cells that is proportional to the cell mass or the number of cells, and at some point, the measurement is less accurate due to the interference by the increase of chlorophyll content (Griffiths et al., 2011).

Table 1.5 shows several examples of *Nannochloropsis* species culturing in all types of photobioreactors. The *Nannochloropsis* species are suitable to grow on all kinds of photobioreactors. However, there are very few published results about a head-to-head comparison of the growth of species of *Nannochloropsis* in a different types of photobioreactors. Table 1.5 compares the biomass productivity of the species of *Nannochloropsis* in all photobioreactors. Light intensity and regime, type of medium used, CO_2 percentage, and photobioreactor are compared to investigate the growth of *Nannochloropsis* in different photobioreactor systems.

Table 1.5: *Nannochloropsis* species biomass productions produced by photobioreactors. The temperature is ranged from 20-28 °C, standard salinity and medium are used, light intensity 50-300 μmol m^{-2} s^{-1} (except for *Nannochloropsis oculata* in bubble column (Valdés et al., 2012) and *Nannochloropsis gaditana* in a tubular photobioreactor (Moraes et al., 2019) that used sunlight).

Photo-bioreactor Type	**Species (Medium used)**	**Volume (cycle) (h,h)**	**(V/V) CO_2, (aeration flow rate, L/minute)**	**Day**	**Initial conc. (g/L)**	**Final conc. (g/L)**	**References**
Bubble column	*Nannochloropsis* sp. UTEX2379 (f/2 medium)	1 L (internal (24:0)	2 %	7	0.8	5	(Pal et al., 2011)
	N. oceanica IMET1 (f/2 medium)	500 mL (14:10)	2 % (0.16)	7	0.03	1.14	(Meng et al., 2015)

	N. *oculata* (f/2 medium)	25 L (12:12)	Regular air (1.5)	7	0.07	0.36	(Valdés et al., 2012)
Stirred tank	*N. oceanica* CY2 (BG-11)	1 L	2 %	7	0.07	1.0	(Chen et al., 2015)
	Nannochloropsis sp. CCNM 1081	6 L (18:6)	0.05 % (2)	18	∼0.1	1.6	(Mitra et al., 2015b)
Flat-plate	*N. salina* (f/2 medium)	0.3 L (24:0 h)	5 % (0.017)	10	0.1	1.09	(Sforza et al., 2015)
	Nannochloropsis sp. KMMCC 290 (Conway medium)	5 L (24:0)	Regular air (2.5)	10	0.03	0.55	(Kwon and Yeom, 2017)
Air-lift	*Nannochloropsis* sp. KMMCC 290 (Conway medium)	5 L (24:0)	Regular air (2.5)	10	0.03	0.51	(Kwon and Yeom, 2017)
Tubular	*N. gaditana* (Commercial seawater culture medium Algal, Bionova, Spain)	2600 L (∼14:10) sunlight	∼0.11 % (1.9 mL CO_2/L/minute)	NA	NA	0.24 g/L/day	(Moraes et al., 2019)

The final concentrations are ranged from 1.0 to 5 g/L biomass when at least 2 % CO_2 is supplied to the *Nannochloropsis* culture. In contrast, 0.3 to 0.6 g/L biomass is recorded when the regular air is provided to the *Nannochloropsis* culture. The biomass is usually represented by DCW samples measured either by freeze or oven dry. Providing at least 2 % CO_2 could enhance biomass production in *Nannochloropsis* species cultured in any photobioreactors. Therefore, there is no issue in selecting suitable photobioreactors for species of *Nannochloropsis* when the biomass concentration is comparable to each other (Table 1.5).

In conclusion, vertical columns photobioreactors are the lowest capital cost photobioreactor with a bigger surface area to volume ratio than stirred tank photobioreactors and provide an adequate performance at a small laboratory scale. A similar setup, such as using a conical flask instead of bubble columns, can be used for a low-cost lab scale experiment. In addition, a conical flask size could be more suitable for steam sterilised than a column. Flat plat and tubular photobioreactors are the most efficient in light harvesting due to the high surface area to volume ratio and orientation for harvesting light compared to other types of photobioreactors. Furthermore, hybrid-type photobioreactors have an edge to overcome the disadvantages of other photobioreactors. However, fundamental technological and economic

obstacles continue to obstruct the commercialization of an ideal photobioreactor type (Sforza et al., 2012).

1.8. Objectives and hypothesis

The main aim of this thesis was to investigate a strategic approach to maximise EPA synthesis in marine microalga, *Nannochloropsis oculata*. Increasing the EPA yield in microalga cells will support the industry in producing omega-3 oil from microalgae, thus, reducing the dependency on fish oil. This goal has led to the following key objectives:

1) to assess the fundamental techniques in culturing microalgae subjected to different environmental conditions; have complete characteristics and FAs profiles for wild-type *Nannochloropsis oculata* species;

2) to develop a mutant strain that grows fast, has ease of harvesting and cell disruptions, and has a high EPA content per gram DCW;

3) to access the performance of wild-type and M1 mutant *Nannochloropsis oculata* in an outdoor 300 L pilot-scale PhycoFlow® photobioreactor;

4) to reveal significant metabolic pathways contributing to the EPA synthesis in wild-type and mutant *Nannochloropsis oculata*.

1.9. Thesis outline

The thesis was divided into six chapters. The study's introduction and literature review were discussed in chapter 1. Chapters 2 through 5 covered the four objectives mentioned in the previous section. The final chapter 6 summarises how the work in the thesis has proceeded and what further research could be done to improve the developed microalga strains further, and the potential for industrial exploitation.

In chapter 1, the literature review focused on the strategies to enhance the EPA content in species of *Nannochloropsis*; however additional microalgae species were included in the review when information on the species of *Nannochloropsis* species was lacking. The review was conducted on photosynthesis, FA synthesis pathways, the effects of environmental conditions on EPA content, current research and development to improve microalga cells, omics analysis, and the photobioreactor systems.

In chapter 2, the wild-type *Nannochloropsis oculata* was cultured under different environmental conditions. The characterisations of the growth and FAs profiles were needed to act as a benchmark, even though a lot of studies have been reported on the culturing of all *Nannochloropsis* species subjected to various environmental conditions. Furthermore, the standard is essential for the developed microalga strain later in this study.

Chapter 3 provided *Nannochloropsis oculata* strain development strategies by the chemical mutagen ethyl methanesulfonate (EMS). FAS inhibitor cerulenin was used to screen the mutants, and monogalactosyldiacylglycerol (MGDG) synthase inhibitor was used as a selective pressure. It was hypothesised that the mutants have a standard growth rate with the presence of FAS inhibitor, cerulenin and MGDG synthase inhibitor, galvestine-1, which could be able to synthesise a higher content of FAs and maximise the EPA synthesis. This chapter demonstrates the improved mutants *Nannochloropsis oculata* enhanced the EPA synthesis compared to the wild-type strain.

Chapter 4 shows the wild-type and M1 mutant *Nannochloropsis oculata* were compared by LFQ proteomics analysis. The early exponential and late exponential phases were selected as two-time points for the LFQ proteomics analysis. It was hypothesised that wild-type and M1 mutant *Nannochloropsis oculata* would have a different EPA synthesis pathway; hence, the protein expressed differently and involved in EPA and FAs synthesis pathways will be shortlisted as having potential roles in the trigger for EPA synthesis.

In chapter 5, wild-type and M1 mutant *Nannochloropsis oculata* were scale-up and cultured in an outdoor 300 L PhycoFlow® photobioreactor. The experiments were conducted in the summer of 2018 and 2019, where wild-type and M1 mutant *Nannochloropsis oculata* were cultured twice, with standard aeration and CO_2 as carbon sources. It was hypothesised that M1 mutant *Nannochloropsis oculata* could produce the FAs profiles similar to lab-scale experiments, hence will become suitable for commercialisation purposes. TEA was also conducted, where net present value (NPV) and return on investment (ROI) were used to evaluate the impact of M1 mutant *Nannochloropsis oculata* compared to wild-type *Nannochloropsis oculata*. It was hypothesised that M1 mutant *Nannochloropsis oculata*

would have a higher NPV and ROI value which means a shorter payback period and more profits can be achieved.

CHAPTER 2: CHARACTERISATIONS OF WILD-TYPE *NANNOCHLOROPSIS OCULATA*

2. Characterisations of wild-type *Nannochloropsis oculata* culturing subjected to different salinities and light intensities

2.1. Introduction

Species of *Nannochloropsis* have been investigated to enhance EPA production further. At present, there are many experimental designs and various methods for analysing microalgae growth, physiological and biochemical changes, and lipids analyses. One of the feasible approaches is testing the species of *Nannochloropsis* subjected to various environmental conditions that were previously reviewed in chapter 1 of this thesis.

Microalgae cells are susceptible to changes in environmental conditions, affecting the physiological and biochemical microalgae cells. Enhancing microalgae's environmental tolerance prior to experiments is crucial for physiological responses to be at equilibrium under optimal growing conditions (Zhang et al., 2021). Therefore, quantifying physiological and biochemical changes is essential to discover the effect of environmental changes on EPA synthesis. Besides, methods that can quickly process and produce high-quality data, low cost, and are reproducible using a small sample volume are the preferred option for assessing the conditions of microalgae cells. The quickest way to observe the species of *Nannochloropsis* growth is by quantifying chlorophyll-*a*, counting the cell numbers and measuring the cell density (Rocha et al., 2003). Dissolved oxygen, pH, nitrate, phosphate, and heavy metals are physicochemical parameters that can be quantified from the culture medium (Miranda and Krishnakumar, 2015), while FAs and lipids, protein and carbohydrates require cell extraction (Guedes et al., 2010). In addition, pigments (chlorophyll and carotenoids), carbohydrates and protein can be measured simultaneously by the biochemical assays method (Chen and Vaidyanathan, 2013), hence providing a practical option for small-volume lab-scale experiments.

On the contrary, the quantification of EPA can only be done by gas and high-performance liquid chromatography. Several extraction methods are demonstrated to extract FAs from microalgae cells. In a previous study, potassium hydroxide (KOH) two-step transesterification

and Griffith's methods produce the highest FA quantity for *Nannochloropsis oculata* (Cavonius et al., 2014).

Regardless of the established methodologies for examining physiological and biochemical changes in microalga cells, the suitability and availability of equipment in the University of Sheffield's Chemical and Biological Engineering laboratory must be evaluated before beginning the studies. Hence, this chapter aimed to establish baseline data for cultivating wild-type *Nannochloropsis oculata* in eight environmental (E1 to E8) experiments by choosing the suitable methods tested for physiological, biochemical, and FAs analyses. Then, the effect of environmental changes on EPA percentage and quantity were investigated.

2.2. Materials and Methods

2.2.1. Microalga strain

Wild-type strain *Nannochloropsis oculata* (849/1) was provided by the Culture Centre of Algae and Protozoa (CCAP, UK). The strain was cultured in modified f/2 medium (CCAP, Scotland) composed of the following: 33.5 g/L artificial seawater salt (Ultramarine Synthetic Sea Salt, Waterlife, United Kingdom), 75 mg/L $NaNO_3$, 4.35 mg/L $NaH_2PO_4.2H_2O$, enriched with trace elements (4.16 mg/L Na_2EDTA, 3.16 mg/L $FeCl_3.6H_2O$, 0.01 mg/L $CuSO_4.5H_2O$, 0.022 mg/L $ZnSO_4.7H_2O$, 0.01 mg/L $CoCl_2.6H_2O$, 0.18 mg/L $MnCl_2.4H_2O$, and 0.006 mg/L $Na_2MoO_4.2H_2O$) and vitamins (0.1 mg/L thiamine HCl (B1), 0.005 mg/L cyanocobalamin (B12), and 0.0005 mg/L biotin). All the chemicals used in this project were purchased from Sigma–Aldrich, United Kingdom unless otherwise specified. The stock culture was maintained in a 500 mL conical flask and bubbled with 2 L/minute of 0.22 µm filtered-air for aeration and mixing. The incubation temperature was 20 °C, and the culture was illuminated by artificial lighting, using Lumilux cool white fluorescent bulbs (Osram, England); the emitting light intensity was 100 to 130 µmol m^{-2} s^{-1} range for 12-h light/dark cycles. The stock culture is refreshed every 5 days to keep the microalga culture in the mid-exponential growth phase.

2.2.2. Experimental setup

Figure 2.1 shows the schematic diagram lab-scale experiment setup for this study, which was adapted from the vertical column photobioreactor design. Borosilicate conical flasks were

used for this study due to glass is an ideal material for photobioreactor design (Huang et al., 2017). In addition, the glass is easily clean, has high transparency and light penetration for photosynthesis, and is suitable for autoclaving.

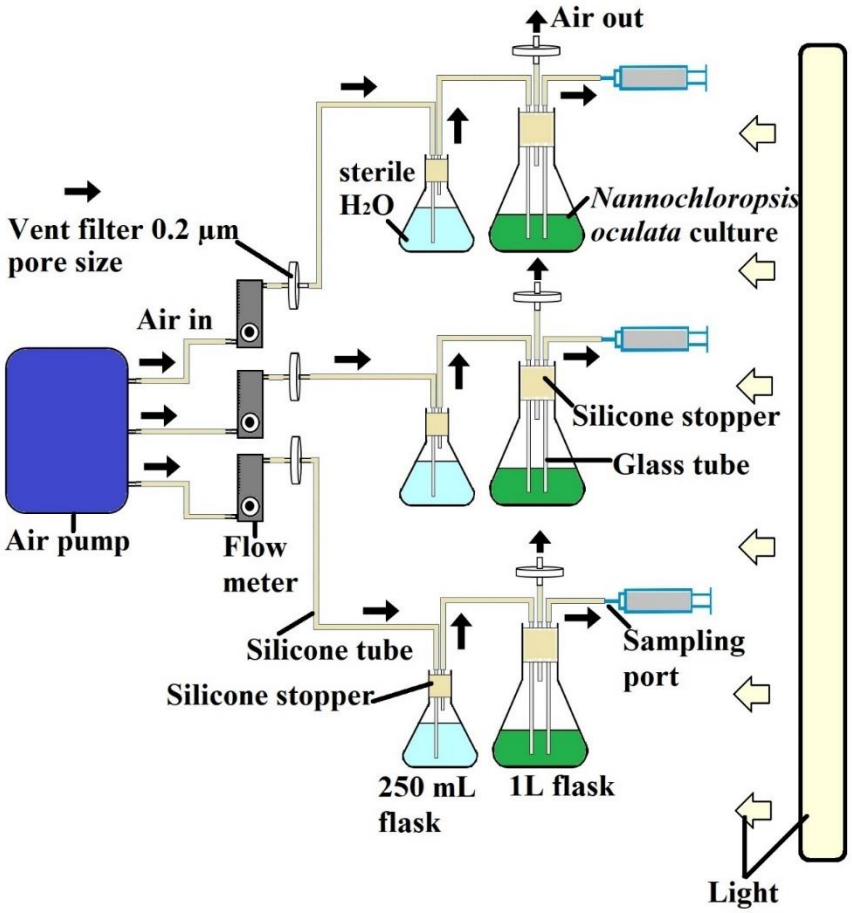

Figure 2.1: Schematic diagram of experimental cultivation system for cultivating *Nannochloropsis oculata* at a laboratory scale. All experiments were conducted at room temperature at 20 °C. The cultures were subjected to continuously filtered aeration and bubbled at 2 L/minute.

Nannochloropsis oculata cultures were set up in triplicates of the 1 L flasks photobioreactor system, as shown in Figures 2.1 and 2.2. The starting OD at 595 nm was 0.15. All flasks were maintained at a room temperature of 20 °C. E1 to E8 were conducted to get baseline physiological and biochemical content data. The baseline data were correlated with the EPA percentage and quantity in the *Nannochloropsis oculata* cells. Table 2.1 shows the details of environmental parameters for E1 to E8.

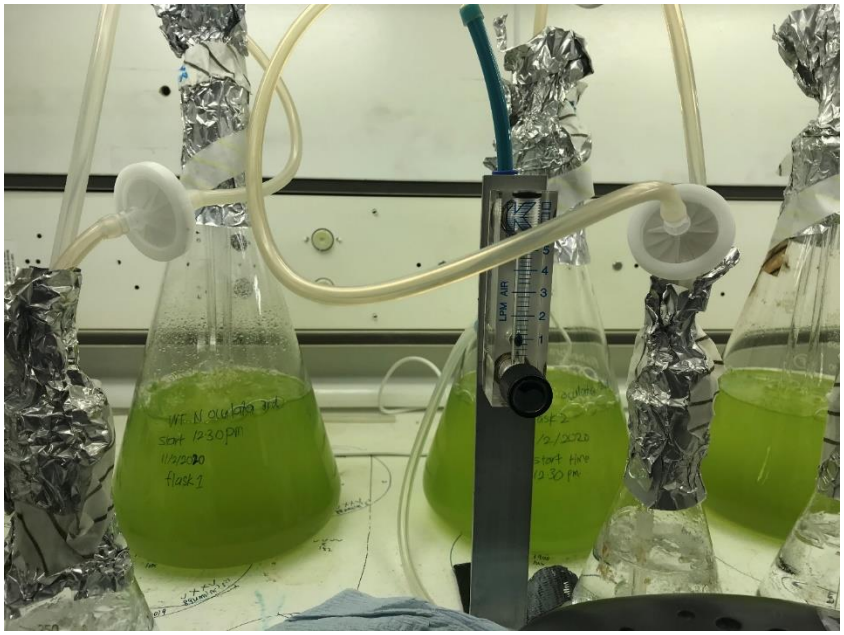

Figure 2.2: 800 mL volume culture in 1 L flasks of *Nannochloropsis oculata* experimental setup in triplicates.

Table 2.1: Tested environment conditions experiments subjected to different salinity, light intensity, and photoperiod cycles that were cultured at 20 °C.

Environmental Conditions	**Salinity (g/L)**	**Light Intensity (µmol m^{-2} s^{-1})**	**Photoperiods (light:dark) (h: h)**
E1	40	200	(24:0)
E2	15	200	(24:0)
E3	33.5	200	(24:0)
E4	33.5	400	(24:0)
E5	40	400	(12:12)
E6	55.5	200	(12:12)
E7	33.5	200	(12:12)
E8	15	200	(12:12)

The inoculum stock for E6, E7 and E8 were adapted for 12 cycles prior to starting the experiments. The stock of E6, E7, and E8 were refreshed with f/2 medium containing 55.5, 33.5, and 15 g/L salinity, respectively, every 5 days to maintain the culture at the early exponential growth phase. After 12 cycles, the E6, E7 and E8 stock inoculum were used for the experiments. All the experiments were conducted in triplicates.

The starting OD at 595 nm was 0.15 for all experiments. The OD was measured using a spectrophotometer (SPECTRONIC™ 200, Thermo Fisher Scientific, United Kingdom). OD at 595 nm and 750 nm were suggested for measuring the wild-type *Nannochloropsis oculata* growth of microalga cells (Chiu et al., 2009; Nielsen and Hansen, 2019). Figure and table supplementary S2.1 show the standard OD curve. A calibration curve of cell number versus OD and DCW is beneficial for practical application (Rocha et al., 2003). The specific growth rate (μ/day) was calculated as follows:

$$\mu = \frac{\ln\left(Wf/Wi\right)}{\Delta t},$$

where *Wf* and *Wi* were the final, and initial OD at 595 nm, respectively and Δt was the cultivation time in day (Chiu et al., 2009; Converti et al., 2009). The pH was monitored and maintained at 7 to 9 for all E1 to E8 experiments using a portable pH meter LAQUA B-712 (Horiba, Moulton Park, United Kingdom). Experiments were performed over a period of 20 days for E1 to E5 and 15 days for E6 to E8. The samples were taken at 9 a.m. for all experiments E1 to E8. The sampling for E1 to E5 was on days 5, 10, 15, and 20. Adapted experiments sampling for E6 to E8 was on days 3, 6, 9, 12, and 15. 5 ml culture was taken for each analysis of DCW, proteins and chlorophylls, lipids, and EPA.

2.2.3. Analytical Methods

Methods for quantification of nitrate (Collos et al., 1999) and phosphate (Strickland, J.D.H and Parsons, 1972) in an f/2 medium were adapted from previous studies. The supernatants from the harvested samples were kept after filtration through a 0.22 μm syringe filter (Millex, United Kingdom). The nitrate and phosphate concentrations were determined for each sampling day by measuring the absorbance values at 220 and 885 nm, respectively. Supplementary Figure S2.2 showed the standard curve for nitrate and phosphate.

Cell pellets were freeze-dried for 24-h by using a freeze drier (LyoQuest, Telstar, United Kingdom), and the DCW was measured using a microbalance (CPA2P, Sartorius, OH, United States). Chlorophylls and proteins were extracted using the spectrophotometric method in triplicate (Chen and Vaidyanathan, 2013). In brief, cell pellets were lysed by glass bead-beating using a cell disruptor (DISRUPTOR GENIE®, United States). The samples were

saponified by heating at 100 °C for 30 minutes (Digital Drybath, Thermo Fisher Scientific, United Kingdom). An aliquot was used for protein assay, and the remaining sample was mixed with chloroform and methanol (ratio 2:1,v/v), vortexed (2 minutes), centrifuged (12,000 × g, 2 minutes), and the top aqueous phase was used for chlorophyll assays. 500 µL samples were aliquoted to 1 mL (2 mm) quartz cuvette and measured by spectrophotometer at 416, 453, and 750 nm for chlorophyll. The blank for chlorophyll was methanol. Chlorophyll *a* (µg/mL) was calculated using the equation (6.4 × A416 - 0.79 × A453).

The proteins were quantified using the microbiuret method and bovine serum albumin (BSA) as a standard curve (Itzhaki and Gill, 1964). The BSA standards were plotted in two standard curves due to the difficulty in weighing the same amount for BSA. 2 mg/L of BSA in 25 % methanol in 1N NaOH was prepared as a stock standard (Supplementary Figure S2.3). The stock standard then used to prepare other concentrations (1, 0.8, 0.6, 0.4, 0.2, 0 mg/mL). 100 µL of copper sulphate (0.21 % $CuSO_4*5H_2O$ in 30 % NaOH) was added to 200 µL standards. 100 µL of 30 % NaOH was added to the other 200 µL standards for blank reference. The samples were vortexed for 5 minutes, and a spectrophotometer recorded the colour formation at 310 nm.

2.2.4. Determination of Fatty Acids Methyl Ester

The method for measuring fatty acid methyl ester (FAME) was adapted from a previous study with slight modifications (Griffiths et al., 2010). First, 300 µL toluene was added to the 2 mL Eppendorf tube containing a wet microalga sample. The Eppendorf tube then vortexed for 2 minutes and continued by adding 300 µL of sodium methoxide. Then, the mixture was then transferred into the 2 mL glass vial and then incubated at 80 °C for 20 minutes. The vials were kept at room temperature to cool them down. Next, 300 µL boron trifluoride was added to the vial and incubated at 80 °C for 20 minutes. In the meantime, 300 µL HPLC grade water and 600 µL hexane were added to other prepared empty 2 mL Eppendorf tubes. Next, the mixture in the vial was transferred to the prepared Eppendorf tube containing water and hexane and then centrifuged at 7,916 × *g* for 10 minutes. Then, the 750 µL organic phase (upper hexane-toluene layer) was transferred to a new labelled Eppendorf tube. The extract was then dried using inert nitrogen gas and stored at -20 °C until further analysis.

80 µL of toluene was added to the extracted sample and vortexed to ensure all the extracts were well-mixed. The mixture was then centrifuged at 11,337 × *g* for 2 minutes. 35 µL FAME was transferred into a GC vial and was identified and quantified using a Thermo Finnigan TRACE 1300 GC-FID System (Thermo Fisher Scientific, United Kingdom) onto a TR-FAME capillary column (25 m × 0.32 mm × 0.25 µm). 1 µL of Supelco 37 Component FAME Mix standard was injected as a reference. Next, 1 µL of sample volume was injected in split injection mode at 250 °C. The split flow was 75 mL/ minute. The GC was operated at a constant flow of 1.5 mL/ minute helium. The temperature program was started at 150 °C for 1 minute, followed by temperature ramping at 10 °C / minute to a final temperature of 250 °C and held constant at 250 °C for 1 minute. The total running time for one sample was 15 minutes, and the standard 37 FAME was injected for every 24 samples to ensure the system was working correctly.

The peak identities were determined for data interpretation and analysis using external Supelco 37 Component FAME Mix standard, C16, C18, and C20:5 standards. The peak areas were integrated using a chromatography data system, Chromeleon 7 software (Thermo Fisher Scientific, United Kingdom). A ratio was developed between the area and the quantity based on the known amount value of 37 FAME components, C16, C18, and C20:5 standards (supplementary Figure S2.4). The amount of unknown components in the microalgal extract was then calculated using their peak regions in mg/g DCW.

2.2.5. Statistical analysis

Statistical differences for all growth profiles data, percentages, and quantification of EPA were performed by Student's t-test, with three samples number (n=3). Array one was for wild-type *Nannochloropsis oculata,* and array two was tested environmental conditions; 2-tails, and type 1 were set using Microsoft® Excel® for Microsoft 365 MSO (Washington, United States). The data were considered significant when the p-value was at least < 0.05.

2.3. Results

The *Nannochloropsis oculata* inoculum was first maintained at an exponential growth phase before starting the experiments. Figure 2.3 shows that the *Nannochloropsis oculata* cells viewed under 1000 × magnifications by a light microscope do not undergo significant changes. At the exponential phase, the cell size average was 3 µm, while at a later stage, the cell size increased to 4 µm due to the increase of lipid bodies (Figure 2.4). Green microalgae cells are multiplicated from a single cell and up to several thousand daughter cells through binary fusion, multiple fusion, or both (Metsoviti et al., 2019). Growth development can be observed during cultivation with light green colour changes to dark green from lag phase to mid-exponential phase, and then from dark green to milky-yellow colour from the end of the exponential phase to the stationary phase.

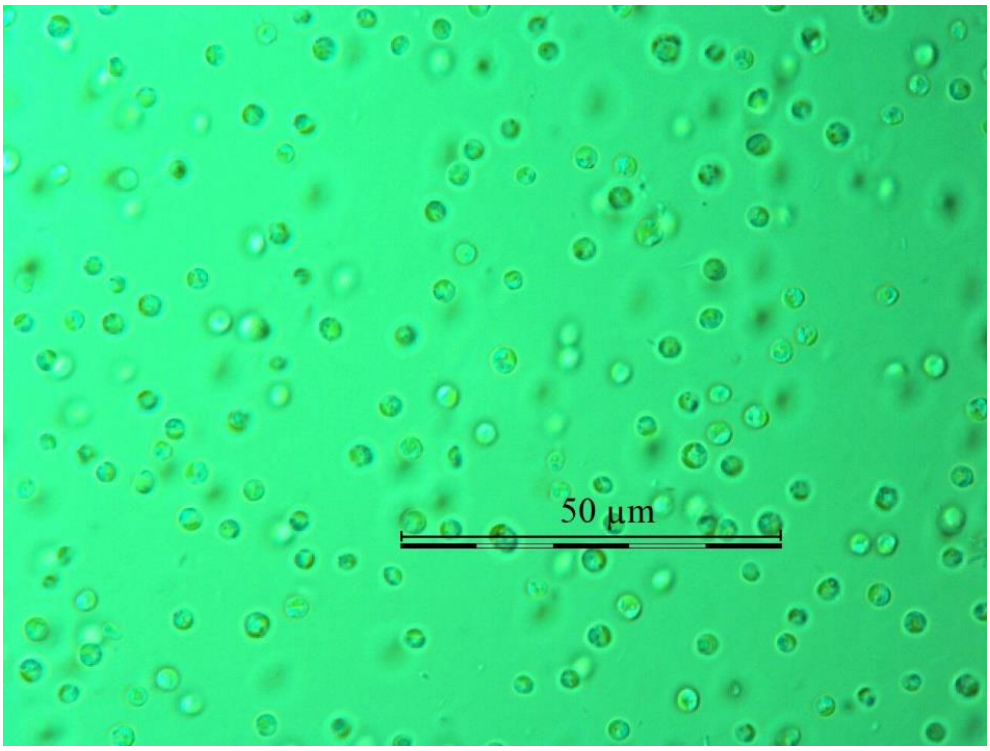

Figure 2.3: *Nannochloropsis oculata* image during mid-exponential phase at 1000 × magnifications. The overall measuring bar represents 50 µm, and one bar segment represents 10 µm.

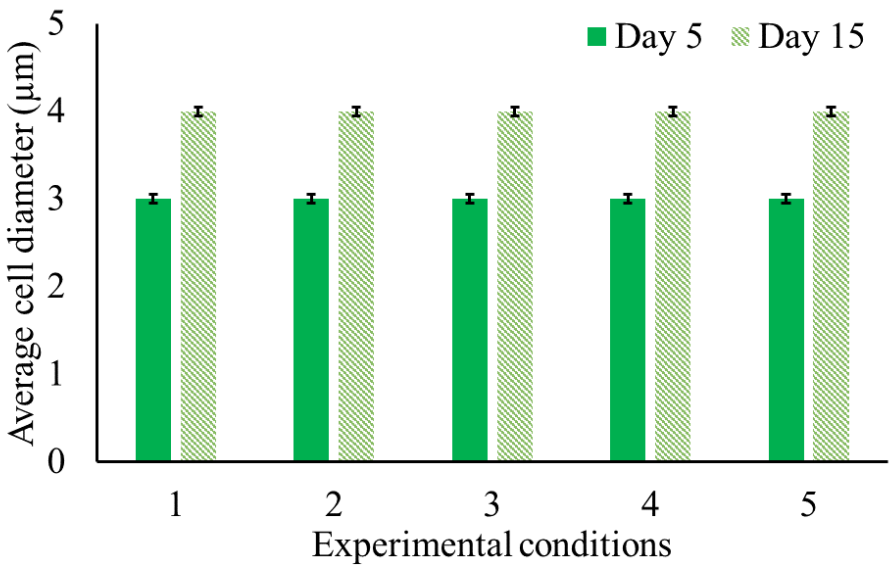

Figure 2.4: The average cell sizes (six cells) of *Nannochloropsis oculata* cells at exponential growth phase (day 5) and stationary phase (day 15) that were measured under 1000 × magnifications microscope image.

A continuous supply of 2 L/minutes air also helped in maintaining the pH. The bubble supported the microalga cell culture mixing and nutrient uptake. The pH was recorded at 8-9 for E1 to E8 experiments throughout the culturing periods. A previous study stated that using tris buffer in the f/2 medium and supplying CO_2 is necessary to maintain the pH within an acceptable range for wild-type *Nannochloropsis oculata* (Rocha et al., 2003). In addition, high alkalinity causes less stability to microalga cell suspension (Rodolfi et al., 2003). Therefore, maintaining the pH was essential to attain high biomass accumulation.

Figure 2.5 shows the OD, growth rate and nitrogen and phosphate uptake throughout the culturing period. E5 and E7 recorded the highest OD at 3.65 and 3.46 on day 15, respectively (Figure 2.5 (a)). At the exponential growth phase, the average growth rate showed only E7 (0.42/day) had the highest growth while E1 (0.37/day), E4 (0.35/day), E5 (0.36/day) and E6 (0.36/day) recorded a comparable growth rate (Figure 2.5 (b)). Based on the OD readings, the cells reached the stationary growth phase on day 15 for E1, E2, E3, E4, and E8, while E5, E6 and E7 continued the exponential growth phase on day 15.

E1, E2, E3, E4 and E6 recorded a comparable nitrate uptake, while E5 (80.2 % nitrate uptake) and E8 (79.3 % nitrate uptake) recorded the highest nitrate uptake on day 15 (Figure 2.5 (c)). Theoretically, 882 µM or equivalent to 75 mg/L of nitrate should be presented in f/2 medium. In this study, the initial concentration recorded was 330 µM on day 0. The initial concentrations were comparable to another study (Tran et al., 2016), where the nitrate concentration was approximately reduced by 50 % at day 0 of culturing. There was a significant difference in low salinity E2 and E8, where the nitrate assimilation in condition 8 was higher than in E2.

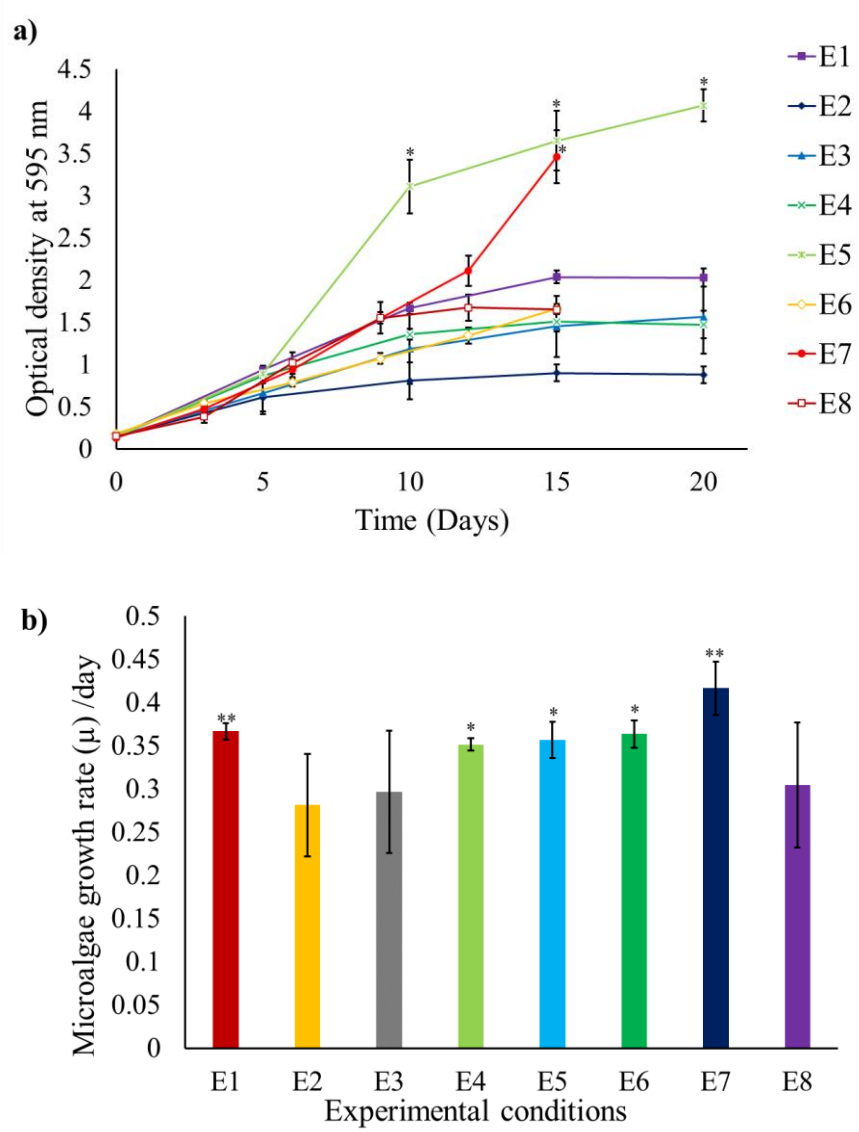

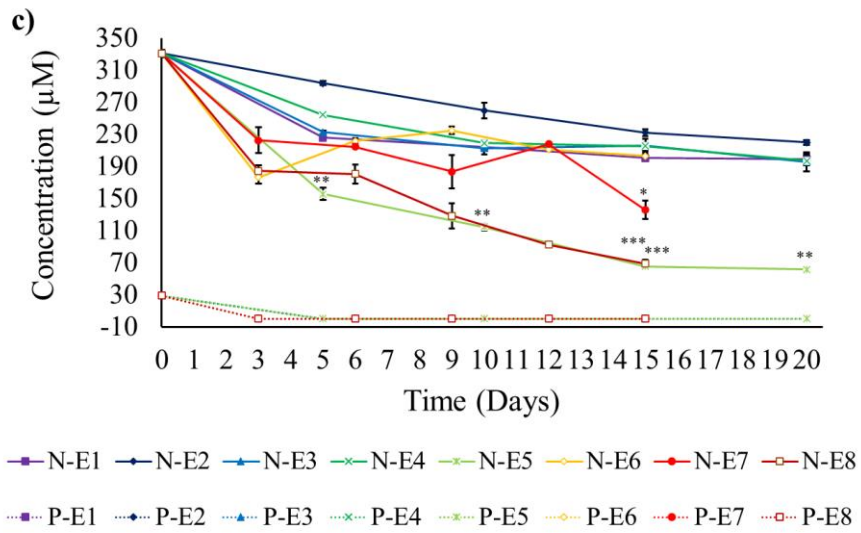

Figure 2.5: a) Growth profiles represented by optical density at 595 nm, b) Growth rates, and c) Nitrate and Phosphate uptake concentrations for environmental conditions (E1-E8). E1-E4 were cultivated under 24 hours photoperiod, while E5-E8 were cultivated under 12:12 (h:h) photoperiod . Mean ± standard deviation is shown (n = 3) and t-tests determine statistical significance ($p < 0.05$ [*]; $p < 0.01$ [**]; $p < 0.001$ [***]). The statistical significance of days 3, 6, 9 and 12 was calculated by referring to the standard condition E7. The statistical significance of days 5, 10, 15 and 20 was calculated by referring to the standard condition E3.

Meanwhile, the phosphorus showed a rapid uptake for all experiments E1 to E8 and was completely consumed within 3 to 5 days. Theoretically, 36.2 µM (4.35 mg/L) of phosphate should be presented in f/2 medium, and an average of 28.86 µM was presented on day 0 of this study. These results showed that all phosphate was rapidly consumed in the early exponential growth phase periods. In a previous study, 2 g/L phosphate in the medium was able to increase the *Nannochloropsis oculata* growth up to 50 % compared to 1 g/L phosphate in the medium (Mahat et al., 2015). 1.57 mg/g biomass/day phosphate uptake rate was recorded for *Nannochloropsis salina* cultured in a standard f/2 medium (Sforza et al., 2018).

Figure 2.6 (a) showed the DCW for E1 to E8 experiments. The highest DCW recorded for E5 (985.0 mg/L), E6 (913.2 mg/L) and E7 (895.1 mg/L) at day 15. E1 (624.5 mg/L), E3 (445.4 mg/L), E4 (461.9 mg/L) and E8 (626.7 mg/L) recorded a decrease of DCW while E2 (276.5 mg/L) showed the lowest DCW.

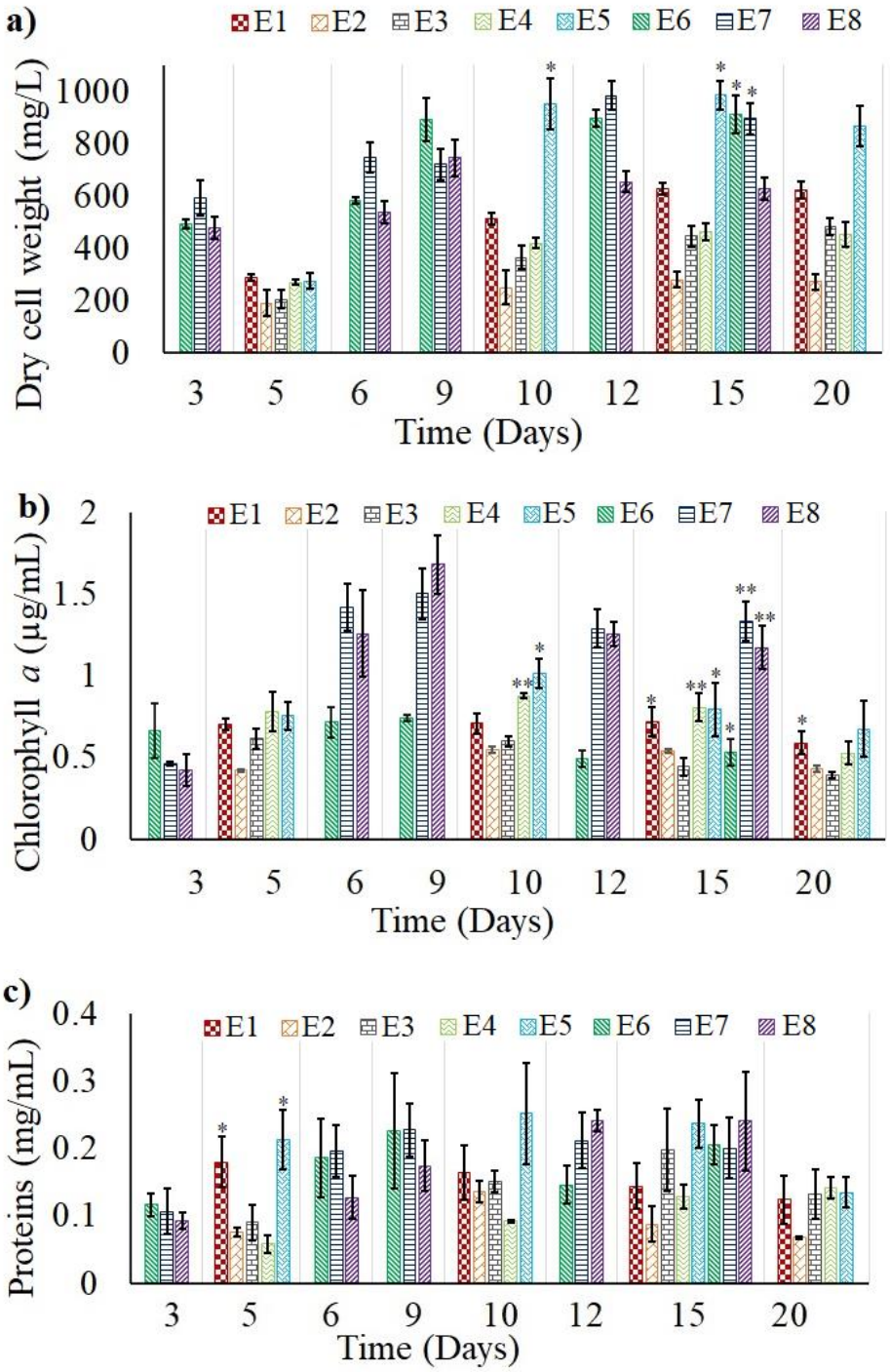

Figure 2.6: a) Dry cell weight profiles. b) Chlorophyll a profiles and c) Protein profiles for eight tested environmental conditions. Mean ± standard deviation is shown (n = 3) and t-tests determine statistical significance ($p < 0.05$ [*]; $p < 0.01$ [**]; $p < 0.001$ [***]). The statistical significance of days 3, 6, 9 and 12 was calculated by referring to the standard E7. The statistical significance of days 5, 10, 15 and 20 was calculated by referring to the standard E3.

In general, chlorophyll-*a* profiles showed the highest content during the mid-exponential growth phase at days 9 and 10 (Figure 2.6 (b)). E7 (1.50 µg/mL) and E8 (1.68 µg/mL) were the highest chlorophyll-*a* content on day 9 compared to other experimental conditions. In another *Nannochloropsis oculata* study, the highest chlorophyll-*a* content was quantified at around 0.95 µg/mL in nitrogen-repleted condition on day 11 (Tran et al., 2016).

The protein contents were increased until the mid-exponential growth phase on day 10 and decreased towards the end of the stationary growth phase (Figure 2.6 (c)). However, E1 showed a decrease in protein content, while E4 and E8 were increased throughout the experimental periods. The results agreed with other studies (Ma et al., 2016a), where the highest protein level was recorded at the exponential phase, and the protein level was decreased under unfavourable conditions. Overall, the protein levels for 12-h (light/dark) cycles had a higher protein level.

EPA percentage of TFA was divided into two groups, E1 to E5 and E6 to E8. E1 to E5 group showed E5 (17.39 %) had the highest percentage, followed by E1 (16.05 %), E3 (14.23 %), E2 (11.61 %) and E4 (10.50 %), at the exponential growth phase day 5 (Figure 2.7). EPA content decreased to around 8-10 % in E3, E4 and E5, while 4-6 % EPA was recorded for E1 and E2, towards the end of the experimental growth period.

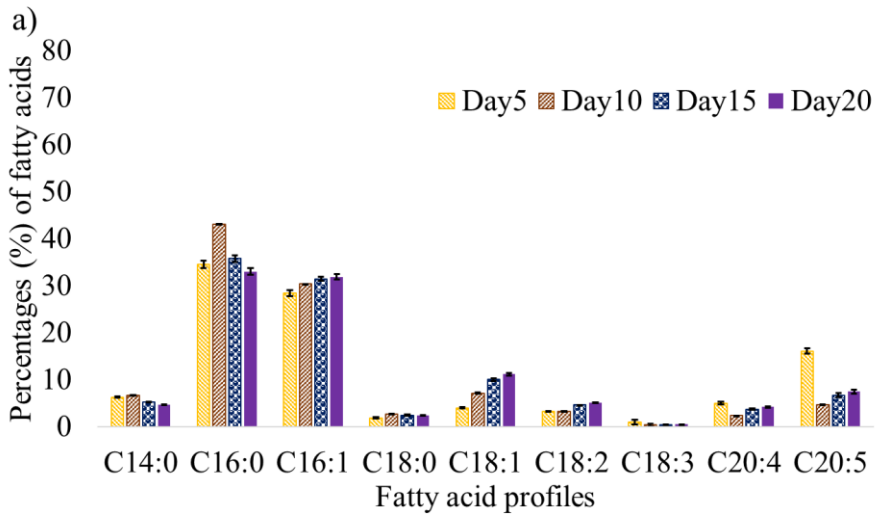

b)

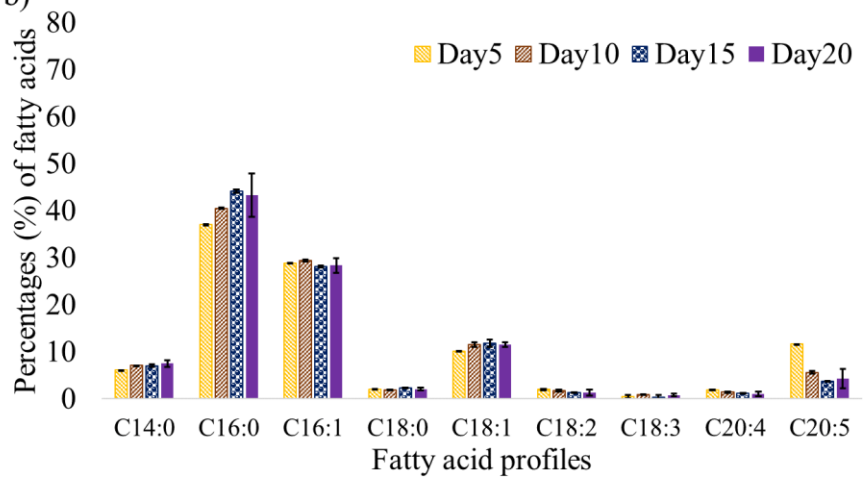
Day5 Day10 Day15 Day20
Percentages (%) of fatty acids
0 10 20 30 40 50 60 70 80
C14:0 C16:0 C16:1 C18:0 C18:1 C18:2 C18:3 C20:4 C20:5
Fatty acid profiles

c)

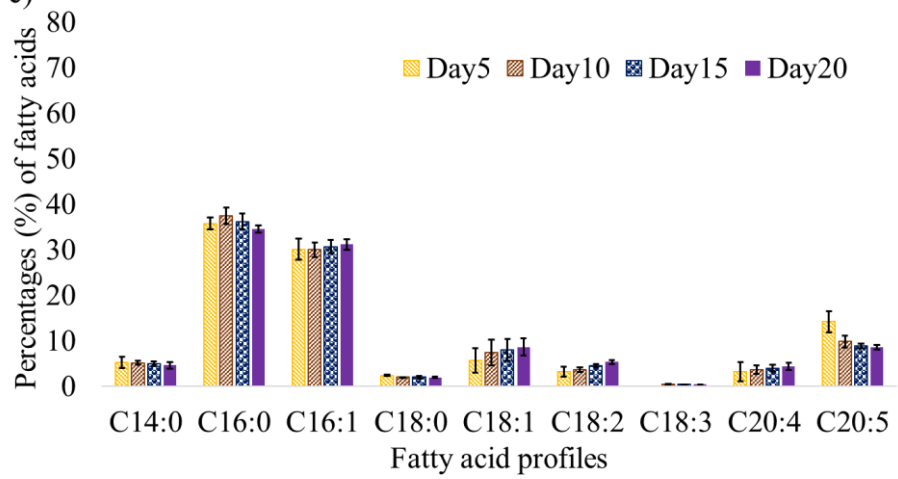
Day5 Day10 Day15 Day20
Percentages (%) of fatty acids
0 10 20 30 40 50 60 70 80
C14:0 C16:0 C16:1 C18:0 C18:1 C18:2 C18:3 C20:4 C20:5
Fatty acid profiles

d)

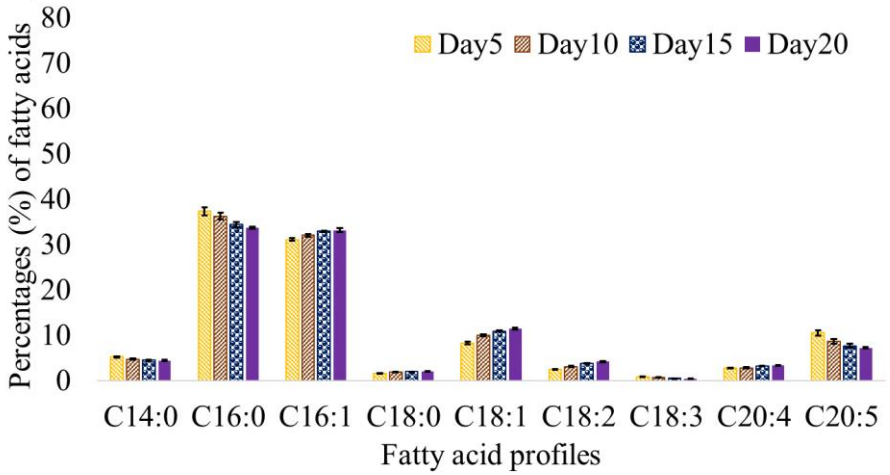
Day5 Day10 Day15 Day20
Percentages (%) of fatty acids
0 10 20 30 40 50 60 70 80
C14:0 C16:0 C16:1 C18:0 C18:1 C18:2 C18:3 C20:4 C20:5
Fatty acid profiles

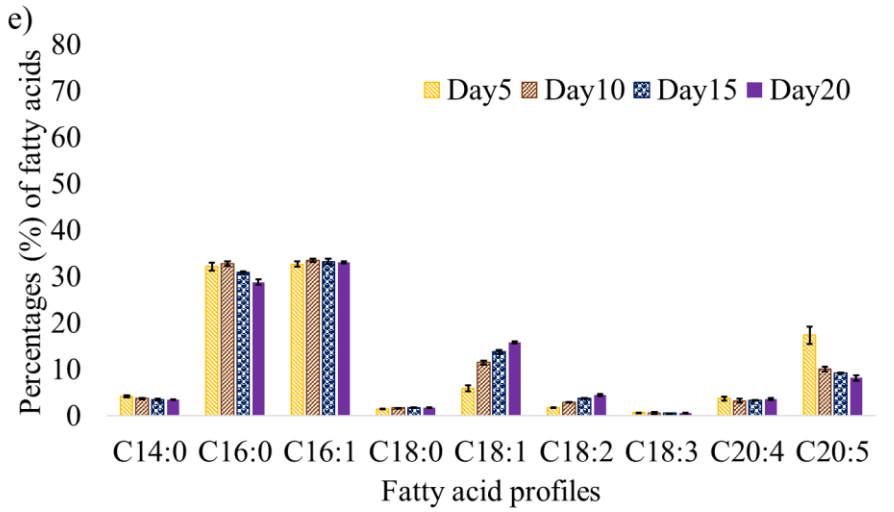
e)
Percentages (%) of fatty acids
80
70
60
50
40
30
20
10
0
Day5 Day10 Day15 Day20
C14:0 C16:0 C16:1 C18:0 C18:1 C18:2 C18:3 C20:4 C20:5
Fatty acid profiles

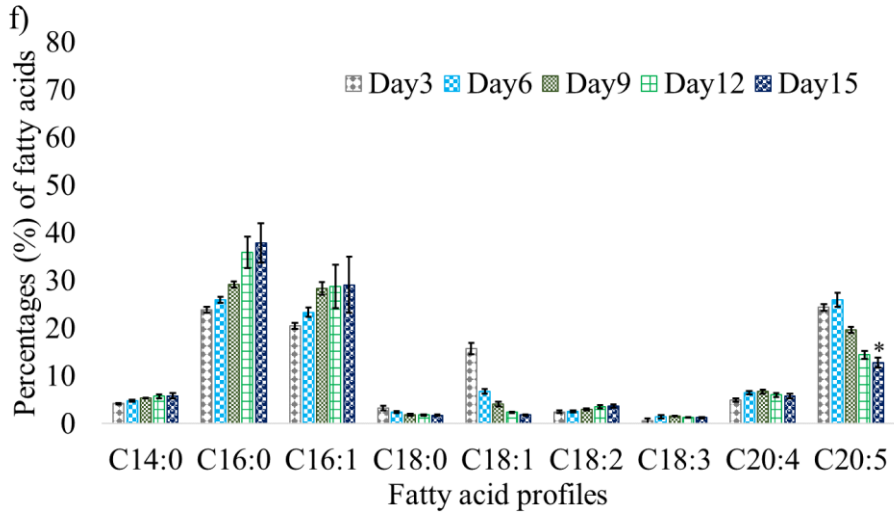
f)
Percentages (%) of fatty acids
80
70
60
50
40
30
20
10
0
Day3 Day6 Day9 Day12 Day15
*
C14:0 C16:0 C16:1 C18:0 C18:1 C18:2 C18:3 C20:4 C20:5
Fatty acid profiles

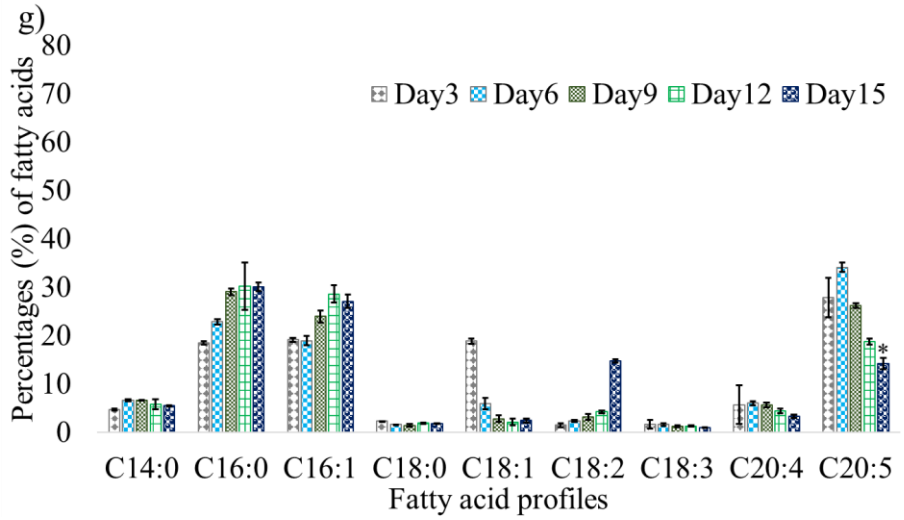
g)
Percentages (%) of fatty acids
80
70
60
50
40
30
20
10
0
Day3 Day6 Day9 Day12 Day15
*
C14:0 C16:0 C16:1 C18:0 C18:1 C18:2 C18:3 C20:4 C20:5
Fatty acid profiles

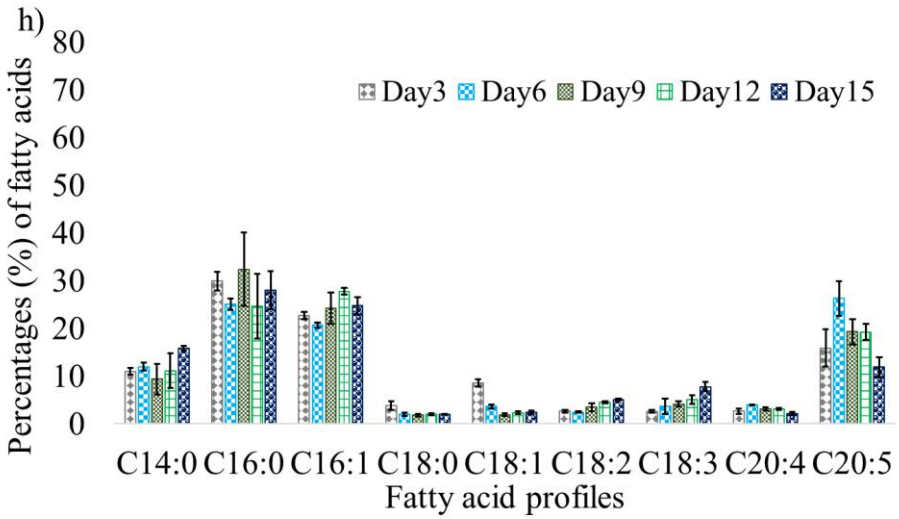

Figure 2.7: Percentage of fatty acids for wild-type *Nannochloropsis oculata* for experimental conditions: a) E1, b) E2, c) E3, d) E4, e) E5, f) E6, g) E7, and h) E8. Mean ± standard deviation is shown (n = 3) and t-tests determine statistical significance ($p < 0.05$ [*]; $p < 0.01$ [**]; $p < 0.001$ [***]).

On the contrary, EPA content in E6, E7 and E8 showed a positive increase on days 3 and 6. The highest percentage were E7 (34.09 %), followed by E8 (26.28 %) and E6 (26.02 %) at day 6. In E6 and E7, the EPA was decreased from day 9 onwards, while the C16:0 profile was concomitantly increased. E8 indicated a fluctuation in the C16:0 profile while the EPA was slightly decreased and then maintained at 19 % on days 9 and 12. No significant differences were recorded in the percentage of EPA for E6 and E8 against standard growth E7. The E6, E7 and E8 were then statistically compared with a standard growth E3 experiment. E6 and E7 on day 15 showed statistical significance with a p-value of 0.02 and 0.01, respectively. The primary FAs in *Nannochloropsis oculata* are myristic acid (C14:0), palmitic acid (C16:0), palmitoleic acid (C16:1), stearic acid (C18:0), oleic acid (C18:1), linoleic acid (C18:2), α-linolenic acid (C18:3) and EPA (C20:5) (Su et al., 2011; Ma et al., 2016b; Cecchin et al., 2020).

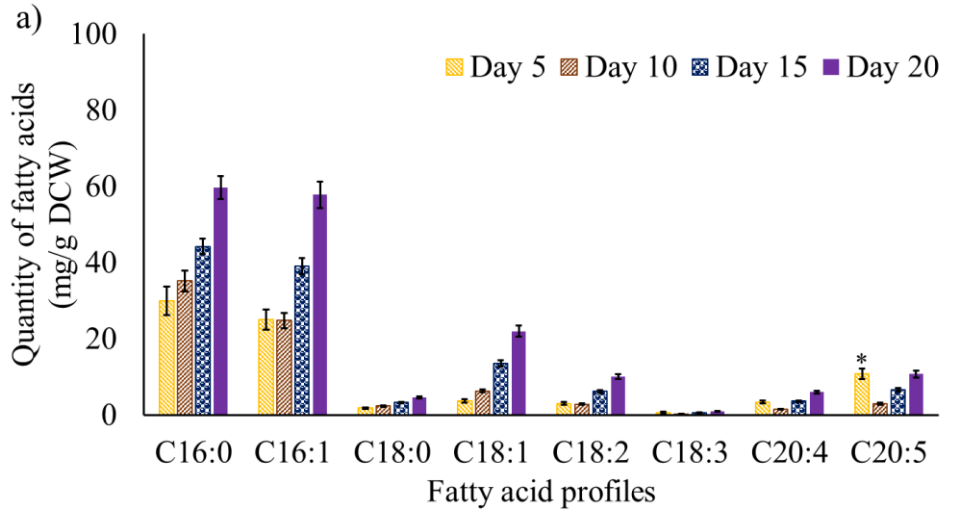
a)
Quantity of fatty acids (mg/g DCW)
100
80
60
40
20
0
Day 5
Day 10
Day 15
Day 20
*
C16:0
C16:1
C18:0
C18:1
C18:2
C18:3
C20:4
C20:5
Fatty acid profiles

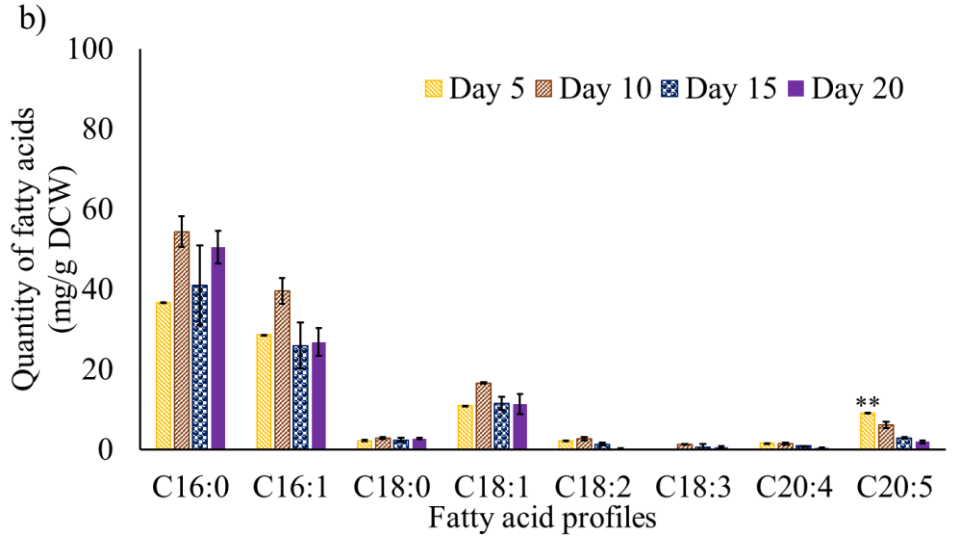
b)
Quantity of fatty acids (mg/g DCW)
100
80
60
40
20
0
Day 5
Day 10
Day 15
Day 20
**
C16:0
C16:1
C18:0
C18:1
C18:2
C18:3
C20:4
C20:5
Fatty acid profiles

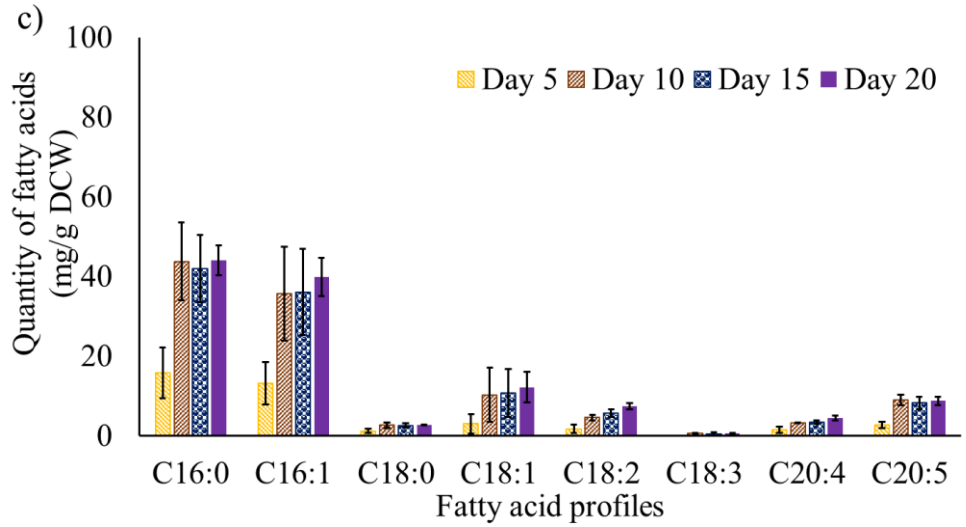
c)
Quantity of fatty acids (mg/g DCW)
100
80
60
40
20
0
Day 5
Day 10
Day 15
Day 20
C16:0
C16:1
C18:0
C18:1
C18:2
C18:3
C20:4
C20:5
Fatty acid profiles

d)

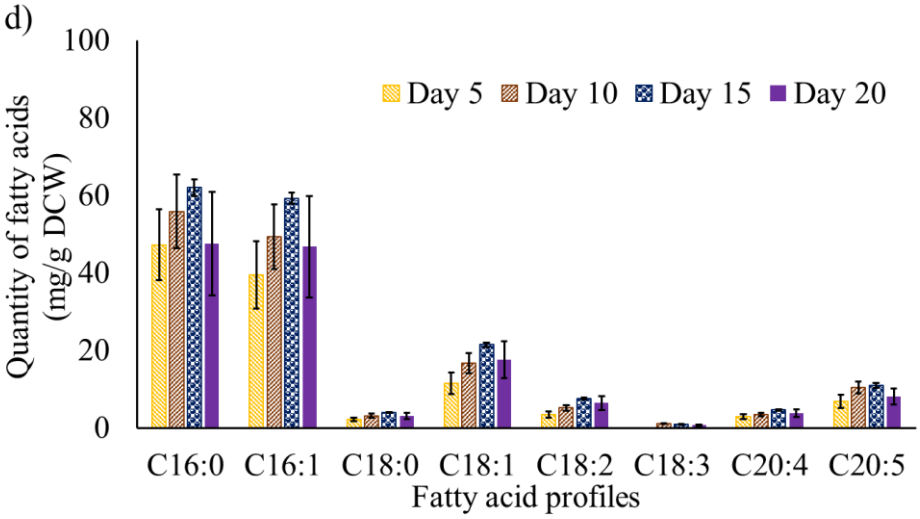
Day 5
Day 10
Day 15
Day 20
Quantity of fatty acids (mg/g DCW)
100
80
60
40
20
0
C16:0
C16:1
C18:0
C18:1
C18:2
C18:3
C20:4
C20:5
Fatty acid profiles

e)

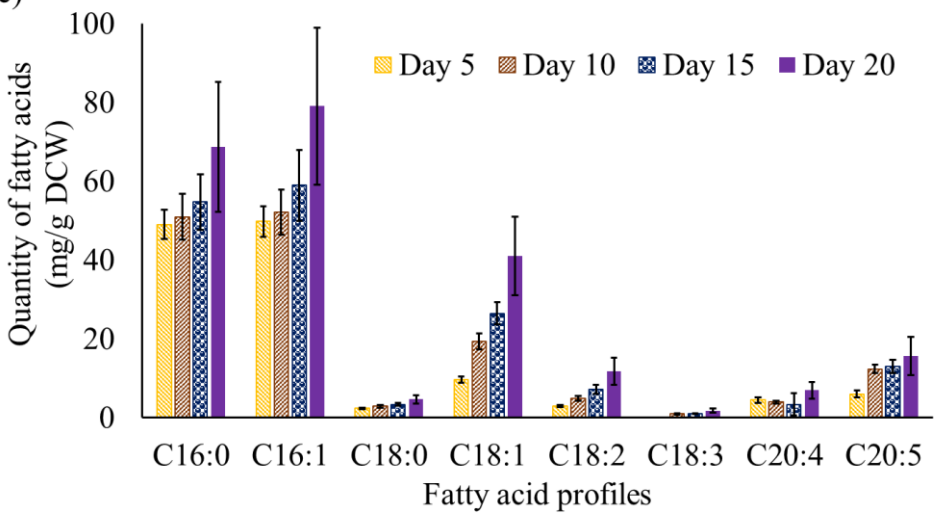
Day 5
Day 10
Day 15
Day 20
Quantity of fatty acids (mg/g DCW)
100
80
60
40
20
0
C16:0
C16:1
C18:0
C18:1
C18:2
C18:3
C20:4
C20:5
Fatty acid profiles

f)

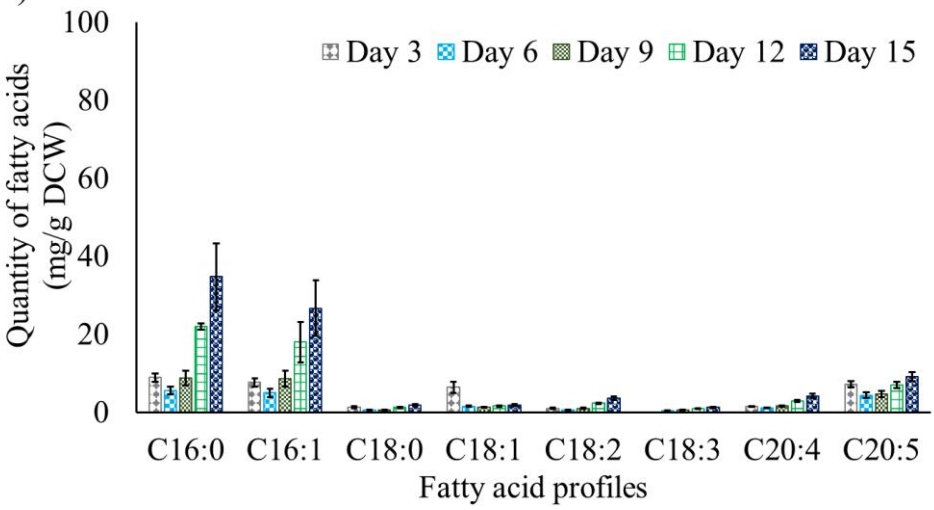
Day 3
Day 6
Day 9
Day 12
Day 15
Quantity of fatty acids (mg/g DCW)
100
80
60
40
20
0
C16:0
C16:1
C18:0
C18:1
C18:2
C18:3
C20:4
C20:5
Fatty acid profiles

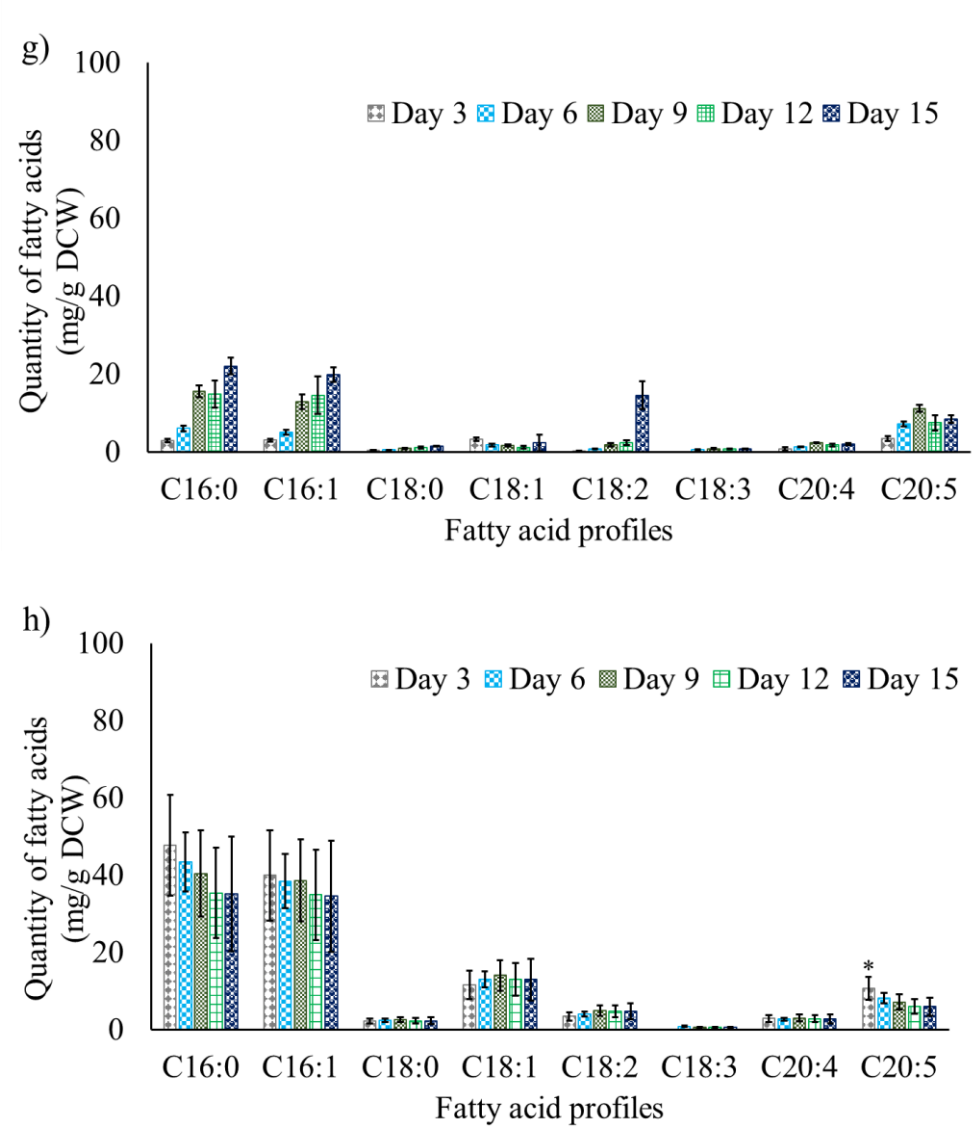

Figure 2.8: Quantification of fatty acids for wild-type *Nannochloropsis oculata* for experimental conditions: a) E1, b) E2, c) E3, d) E4, e) E5, f) E6, g) E7, and h) E8. Mean ± standard deviation is shown (n = 3) and t-tests determine statistical significance ($p < 0.05$ [*]; $p < 0.01$ [**]; $p < 0.001$ [***]).

Figure 2.8 shows the quantity of EPA and other FAs that dominate the *Nannochloropsis oculata* cells for E1 to E8. Overall, the EPA quantity recorded below 11 mg/g DCW for all experiments, a meagre amount compared to other studies (Table 1.1-1.3). Low salinity (15 g/L NaCl) E2 and E8 showed a slightly higher EPA quantity than the standard E3 experiment on days 5 and 3, respectively. High salinity (40 g/L NaCl) E1 also had a somewhat higher EPA quantity than the standard E3 experiment on day 5. E1, E3, E4, E5, E6 and E7 showed a steady increase in C16:0 towards the end of the experimental period. In addition, the C16:0 content

fluctuated in E2 while a decreased profile trend was recorded for E8. In general, the C16:0 and C16:1, which refer to neutral lipids, showed the highest quantity when the culture reached the stationary growth phase. The highest TAG was recorded for C16:0 (68.76 mg/g) and C16:1 (79.11 mg/g) on day 20 for E5, where high salinity (40 g/L), high light intensity (400 µmol m^{-2} s^{-1}) and 12-h (light/dark) cycles induced the accumulation of neutral lipids. On average, 50-60 mg/g DCW of C16:0 and C16:1 was recorded at the stationary growth phase.

2.4. Discussions

2.4.1. Growth, physiological and biochemical analyses

This chapter aimed to get baseline data to study physiological and biochemical analyses corresponding to the EPA synthesis under different environmental conditions for wild-type *Nannochloropsis oculata*. Eight experimental conditions (E1 to E8) were conducted to achieve the first objective. The E1 to E4 were cultured under a 24-h continuous light regime, while E5 to E8 were cultured under 12 h (light/dark) cycles. Wild-type *Nannochloropsis oculata* stock inoculum for E1 to E5 was in a mid-exponential growth phase, while E6 to E8 were in an early exponential growth phase.

Reviving and culturing the wild-type *Nannochloropsis oculata* strain was done to familiarise with the growth characteristics. The microalga cells were observed under 1000 × magnifications to observe the cell's morphology during the early exponential, mid-exponential, and stationary growth phases. Initially, the mid-exponential phase *Nannochloropsis oculata* culture was used for inoculum E1 to E5 because the cells were in healthy conditions with dense enough culture to meet the initial concentration of 0.15 OD at 595 nm. The E1 to E5 were the earliest five experiments conducted to achieve the first objective. Besides getting baseline data, these experiments were conducted to master the fundamental techniques in culturing microalgae, doing physiological and biochemical analyses, and extracting total lipids for EPA quantification. In addition, the developed lab-scale flask photobioreactor system was tested (Figure 2.1).

In this study, OD was used to represent cell growth. A turbidimetric method such as OD was used because it is the quickest way to observe the development of microalga cells. The other

option is direct cell counting using a haemocytometer or an automated cell counter. However, due to the small *Nannochloropsis oculata* cell size, the cell counting methods by haemocytometer require a vast amount of time and tend to be user biased. On the contrary, an automated cell counting machine could not accurately count a small microalgae cell size ~3 µm, based on the surveys made with a few suppliers. Therefore, the automated cell counting machine needs an upgrade to detect and count the species of *Nannochloropsis* as the microalgae have a size of 2 to 5 µm in diameter (Rodolfi et al., 2003). In a recent study, an automated cell counter (Countess II FL; Thermo Fisher Scientific, United Kingdom) demonstrated that using a fluorescence filter could distinguish microalgae starting from 2 µm diameter and bigger (Takahashi, 2018). Therefore, this method is one of the viable approaches in the future for monitoring the microalgae cell culture quantity and quality.

The OD growth curve (Figure 2.5 (a)) had reached a plateau state at day 15 in four out of five conditions, indicating the microalga cells were in the stationary growth phase. The increase of OD after day 15 might be contributed by the increase of microalga cell size bigger than 4 µm. The growth rate for E1, E4 and E5 were comparable at the exponential phase, indicating a range of 0.35-0.37/day could be the optimum growth rate for E1 to E5. However, the increase of DCW, chlorophyll-*a* content, and proteins in the E5 on day 10, implies that 12:12 (h:h) light could increase the growth of microalga cells. The increased cell density is consistent with the other study (Wahidin et al., 2013). *Nannochloropsis* sp. cultured under 200 µmol m^{-2} s^{-1} light intensity with 12:12 (h:h) photoperiod had a higher cell density compared to 18:6 (h:h) and 24:0 (h:h) photoperiod (Wahidin et al., 2013). A lower cell density in E1 to E4 could be caused by the photoinhibition phenomenon when the microalga cells are exposed to a high light intensity of 200 µmol m^{-2} s^{-1} (Wahidin et al., 2013).

The low salinity condition E2 experiment had the lowest growth rate at the exponential phase, implying that the microalgae cell might need a more extended period to adapt to a low salinity level. This adaptation period might cause the bacteria to consume the carbon source from the microalgae and compete with microalga cells for growth. A transmission electron micrograph (TEM) illustrated that the microalgae and bacteria cells were stuck together (Rodolfi et al., 2003), indicating that the microalgae and bacteria form consortia for growth.

Therefore, *Nannochloropsis oculata* cells were adapted for 12 cycles (5 days in each cycle) according to the experimental conditions E6, E7 and E8. In a previous study, 8 cycles of ALE positively affected the carotenoids and growth production (Fu et al., 2013). In addition, early exponential growth phase stock inoculum was used for E6, E7 and E8 experiments to further increase the growth rate and enhance the EPA content. The growth rate slightly improved for the E8 experiment compared to the previous low salinity E2 experiment. The standard E7 had the highest growth rate (0.42/day) than the preceding standard salinity E3 experiment. The increase in growth rate could be attributed to the healthy inoculum stock at the early exponential growth phase, and the 12:12 cycle prevents light from exceeding the saturation point, which causes light inhibition and kills the microalga cells (Wahidin et al., 2013). The increase of the chlorophyll-*a* profile for E8 indicates that the microalga cells dominate the low salinity culture medium. Chlorophyll pigment is necessary for light harvesting (Ma et al., 2016a), and the chlorophyll-*a* quantities could reflect the light harvested for photosynthesis and growth performance of microalga. Chlorophyll content was decreased after day 9, which could be associated with stress conditions when the culture reached the late exponential growth periods.

Furthermore, adapting the stock inoculum to the designated salinity level before experiments could have contributed to the significant nitrate uptake in E7 and E8. Microalgae can assimilate nitrogen from nitrate, a crucial macronutrient for microalgal growth and are involved in the production of protein, lipids, and carbohydrates (Yaakob et al., 2021). Hence, the high level of nitrate uptake in E5, E7 and E8 represents a healthy growth of *Nannochloropsis oculata* cells. This result could prove that wild-type *Nannochloropsis oculata* was successfully adapted to low salinity 15 g/L and growth faster than E2. In another study, an increased amount of nitrate (300 mg/L) had increased the growth rate of *Nannochloropsis oculata* from 0.10 to 0.13/day (Converti et al., 2009). Furthermore, the protein content of E5 and E8 could be associated with nitrate uptake at day 15, as shown in Figure 2.6 (c), demonstrating that more protein is synthesized as nitrogen uptake increases.

Photoinhibition caused by high light intensity and the continuous light regime could decrease the protein levels when the microalgae cells are in stress conditions. In contrast, the 12:12 (h:h) light to dark cycle could increase the EPA biosynthesis due to the consumption of storage

materials such as carbohydrates, and saturated and monosaturated FAs (Chini Zittelli et al., 1999).

2.4.2. Wild-type *Nannochloropsis oculata* fatty acids

FA profile changes throughout the experimental periods were monitored, especially C16:0 and C20:5, which refer to TAG and EPA, respectively. A low amount of EPA percentage (~10-16 %) presented in the E1 to E4 experiments, while a high amount of TAG (~34-44 %) on day 5 indicates the microalga cells could be stressed conditions due to photoinhibitions. Interestingly, this study's percentage of EPA and TAG is in line with a previous study when the *Nannochloropsis oculata* sample is taken at the exponential growth phase (Tonon et al., 2002). Meanwhile, E5 showed a lower percentage of TAG (~30-32 %) and a higher EPA (17.4 %), indicating that the light and dark cycle play a crucial role in microalga biogenesis. The dark period is proved helpful for countering the excess light in the microalga cells (Wahidin et al., 2013). In addition, the increase of EPA content in the E5 experiment is in line with results reported in other *Nannochloropsis* sp. studies (Chini Zittelli et al., 1999). The saturated and monosaturated FAs were consumed during the dark cycle, increasing the EPA content (Chini Zittelli et al., 1999). E6 to E8 experiments showed a significant increase in EPA percentage (~26-34 %) while TAG content (~22-25 %) was decreased on day 6, proving the adaptation strategy in enhancing the EPA synthesis. In addition, early exponential phase inoculum stock could be efficient in improving the photosynthetic rates for E6 to E8.

Standard salinity level (33.5 g/L NaCl), E7 produced the highest EPA percentage compared to low salinity (15 g/L NaCl) and high salinity (40 g/L and 55.5 g/L NaCl). High EPA content in standard salinity (33-35 g/L NaCl) agrees well with the previous studies on other species of *Nannochloropsis* (Mitra et al., 2015a; Chen et al., 2018a). However, the results are also in contrast with the findings from previous studies (Hu and Gao, 2006; Pal et al., 2011; Gu et al., 2012; Solovchenko et al., 2014), when low salinity (<25 g/L NaCl) shows the highest EPA level compared to standard and high salinity levels. A previous study stated that membrane lipids' predominance in microalgae cells could contribute to high EPA at low salinity (Pal et al., 2011). Since E8 showed a higher chlorophyll-*a* content than E7, E8 could contain at least a comparable EPA percentage to E7.

Monitoring the EPA quantity per cell or EPA per gram biomass could be used to find the effect of salinity on EPA synthesis at the same cell density and a similar point of growth condition. Unfortunately, the results for EPA quantity per gram in low salinity are inconsistent with the EPA percentage results. In addition, the average EPA quantity (mg/g DCW) for E1 to E8 was far behind compared to other species of *Nannochloropsis* in previous studies (Chen et al., 2013, 2015; Meng et al., 2015; Hulatt et al., 2017; Willette et al., 2018). It should be noted that other studies reported 20-25 % of EPA, while the EPA quantity recorded 50-60 mg/g DCW of EPA (Yang et al., 2019a). Hence, troubleshooting is necessary in order to increase the EPA per DCW quantity. However, it is quite a surprise that the EPA quantity was increased again on day 20 for high salinity experiments, indicating that the EPA could be optimally translocated to TAG under high salinity and nutrient limitation conditions, especially under 200 µmol m^{-2} s^{-1} in E1 and E6. In addition, a high EPA quantity was also recorded in E5 experiment on day 20 under 400 µmol m^{-2} s^{-1}. Many studies demonstrate that having repleted nitrate in the culture enhances the production of polar lipids and biomass while depriving nitrogen induces the neutral lipids, TAG (Janssen et al., 2020).

2.5. Conclusion

A baseline data was developed using feasible methods to investigate microalgae growth, physiological and biochemical changes, and FAs analysis. A set of eight preliminary experiments were conducted and highlighted the correlation of the growth parameters, physiological and biochemical changes with FAs profile, especially EPA and TAG. Generally, culturing wild-type *Nannochloropsis oculata* under unfavourable conditions such as low and high salinity, high light intensity, and the continuous light regime have decreased the growth rate, resulting in a lower EPA content produced. On the bright side, high salinity experiments indicate the EPA could be optimally translocated to TAG in the late stationary growth phase. In addition, enhancing microalgae's environmental tolerance was crucial before starting the experiments. However, the low EPA quantity (mg/g DCW) compared to the EPA percentage needs further investigation. Overall, the objective for this chapter was successfully achieved, and the methods and techniques learned were essential for strain development and scale-up experiments in chapters 3 and 5, respectively.

CHAPTER 3: *NANNOCHLOROPSIS OCULATA* EPA-OVERPRODUCING STRAIN DEVELOPMENT

3. Enhancement of Eicosapentaenoic Acid Synthesis in The *Nannochloropsis Oculata* Mutant by an Ethyl Methanesulfonate Random Mutagenesis-Screening Procedure

3.1. Introduction

Random mutagenesis combined with screening and selection strategies is a helpful tool for developing algal strains with desirable functional features (Arora et al., 2020). In the species of *Nannochloropsis*, random mutagenesis was notably used in developing and screening for higher neutral lipids for the biofuel industry (Doan and Obbard, 2012; Ma et al., 2013; Beacham et al., 2015). In another study, gamma-ray-mediated random mutagenesis screened by selecting yellowish colonies showed a 43.54 % violaxanthin increase in the mutant compared to the wild-type *Nannochloropsis oceanica* strain (Park et al., 2021). Neutral lipids and violaxanthin screening could be simply conducted by measuring the physical conditions of microalga cells using any fluorescence methods such as fluorescence dye or FACS machine.

Currently, there is little published literature on developing EPA-overproducing mutants by random mutagenesis methods. UV light was used as a mutagenised agent in inducing mutants with higher EPA and DHA in *Pavlova lutheri* at the stationary growth phase (Meireles et al., 2003b). The screening was conducted by selecting mutants with higher quantities of EPA and DHA than the wild-type strain (Meireles et al., 2003b). A similar method demonstrated 2.2-fold EPA increase in *Phaeodactylum tricornutum* compared to the wild-type strain (Alonso et al., 1996). Interestingly, the UV mutagenesis along with FACS that purposely screened the mutant with enhanced neutral lipids, concomitantly increased the TFA and EPA in mutants *Tetraselmis suecica* (Lim et al., 2015), indicating the UV could effectively be used to induce EPA-overproducing mutant. The screening procedure for finding the EPA-overproducing mutant needs a novel approach to screen down the potential mutants prior to GC analysis. Quantifying the FAs of all mutants is indeed the best in screening EPA-overproducing mutants, however, the screening method is less practical and time consuming.

Alternatively, chemical inhibitors targeting a specific enzyme in FA synthesis are used to screen the mutants (Chaturvedi et al., 2004; Chaturvedi and Fujita, 2006). A mutant induced

by UV and then screened by ACCase inhibitor quizalofop shows an increase in TFA while no record of EPA content (Moha-León et al., 2019). The EPA profile could be affected due to the adaptation of *Nannochloropsis oculata* in freshwater (Moha-León et al., 2019). Cerulenin is known as an inhibitor for β-Ketoacyl-ACP synthase (KASI, KASII, and KASIII) (Meng et al., 2018), and is reported to effectively inhibit KASI (Liu et al., 2016a), while Erythromycin could be associated with the nuclear and chloroplast loci (Chaturvedi and Fujita, 2006). Selective pressure on the FA synthesis enzymes could increase the carbon flux in the mutant, hence increasing the EPA level. Besides, a previous study indicates the use of fluorescence video imaging apparatus for screening mutants with higher photosynthetic capabilities in *Nannochloropsis gaditana* (Perin et al., 2015). As a result, a higher growth rate mutant is produced. In addition, several PSII inhibitors (Thomas et al., 2020) could be used as a selective pressure for inducing high growth rate mutants. A higher photosynthetic rate could also increase the carbon flux, hence contributing to the increase of TFA.

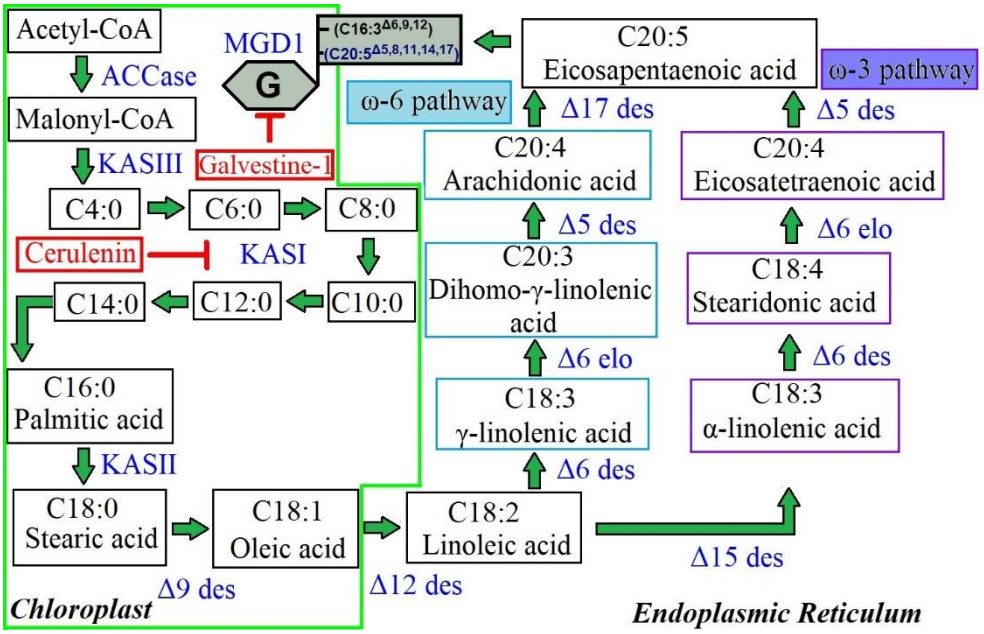

Figure 3.1: Fatty acid synthesis acid in the species of *Nannochloropsis*—modified from a previous study (Beacham et al., 2015). Blue boxes and purple boxes indicate omega-6 and omega-3 pathways, respectively. The light green line indicates the chloroplast.

Figure 3.1 shows two FA synthesis pathways, omega-3 and omega-6, for the species of *Nannochloropsis*. The inhibitors of cerulenin and galvestine-1 are shown in red. As the review in chapter 1, MGDG synthase inhibitor, galvestine-1 could be used to exploit the EPA and

MGDG connections hence potentially modifying the EPA trafficking routes. Other FAS inhibitors that could be used are thiolactomycin and triclosan (Li-beisson, 2016). Although triclosan is known to inhibit ER enzyme (Arora et al., 2020), there is no report on the use of triclosan as a screening inhibitor on any species of *Nannochloropsis*.

Hence, the initial purpose was to develop a *Nannochloropsis oculata* strain that could yield a higher EPA level while maintaining a high growth rate. A random mutagenesis approach using EMS, inspired by a previous study (Chaturvedi and Fujita, 2006), was conducted to generate *Nannochloropsis oculata* mutants. Combinational chemical inhibitors cerulenin and galvestine-1 were applied to screen the mutant and potentially develop EPA-overproducing mutant strains. The most significant mutant strain named M1 was cultured, and the growth, physiological and biochemical, and FAs analyses were compared with the wild-type *Nannochloropsis oculata strain*. Based on investigations, two-time points were identified for LFQ proteomics analysis.

3.2. Materials and Methods

3.2.1. Microalga strain

Wild-type strain *Nannochloropsis oculata* (849/1) was provided by the Culture Centre of Algae and Protozoa (CCAP, UK) and was cultured in f/2 media (CCAP, Scotland). The details of the f/2 medium compositions were described in the previous chapter 2 (Section 2.2.1).

3.2.2. Mutagenesis and selection of EPA-overproducing mutant strains

Different concentrations of FAS inhibitor, cerulenin and MGDG synthase inhibitor (Boudière et al., 2012), uridine 5'-diphosphate disodium salt hydrate (UDP), N-Ethylmaleimide (NEM), and galvestine-1 were tested with wild-type *Nannochloropsis oculata*. Cerulenin, UDP, NEM and galvestine-1 were freshly prepared and mixed with early exponential growth *Nannochloropsis oculata* stock culture. The experiments were conducted in triplicates for each chemical concentration in 24-well culture plates (culture volume = 1.0 ml). The sub-lethal chemical concentrations were determined by measuring OD at 595 nm using a GENios Tecan plate reader (TECAN, Germany) (Supplementary Figures S3.1). The sub-lethal concentration of FAS and MGDG synthase inhibition were selected for two-stage screening

processes. Cells in the early exponential phase (7×10^6 cells/ml) were refreshed with sterile f/2 medium and centrifuged at 3,488 × g for 5 minutes, and EMS was added to make a final concentration of 100, 200, and 300 mM. The cells were mutagenised for 60 minutes, washed three times with sterile f/2 medium, and allowed to grow for seven days before initiating selection. Equal cell numbers (2×10^7 cells/ml) were spread uniformly on f/2 medium plates (1.5% w/v) containing 50 µM of cerulenin. After three weeks of incubation at 20 °C, the number of resistant colonies from each plate was counted. The countable plate was selected, and each colony was inoculated in a 3 ml f/2 medium containing 50 µM of cerulenin in 24-well plates placed under light (130 µmol m^{-2} s^{-1}). The absorbance was measured at 595 nm on the plate reader for ten days. The mutant colonies with a higher OD at 595 nm than wild-type *Nannochloropsis oculata* were selected and cultured in f/2 media containing a higher concentration of cerulenin, 60 µM. The three fastest-growing mutants were selected for the next stage using an MGDG synthase inhibitor, galvestine-1 (Botté et al., 2011; Boudière et al., 2012). The mutants were cultured in f/2 media containing 10 µM of galvestine-1, and the fastest-growing mutant was selected for further studies. The equation for growth rate was described in the previous chapter 2 (section 2.2.2). FA analyses for the wild-type strain, M1 mutant strain treated with cerulenin, M1, M18 and 45 mutant strains treated with galvestine-1 were conducted by referring to the methods described in the previous chapter 2 (section 2.2.4). M1, M18 and M45 were cultured in the f/2 medium containing 10 µM galvestine-1 in a series of adaptation experiments, and FA profiles were monitored. The experiments were carried out by culturing the mutants in f/2 medium containing 10 µM galvestine-1in sterile cell culture flasks (Nunc™, Thermo Fisher Scientific, United Kingdom) at 130 µmol m^{-2} s^{-1}, 20 °C, and 12-h light/dark cycles, and 160 RPM shaking for three cycles (8 days for each cycle). After each cycle, 10 mL (half of the total culture volume) microalga culture volume was removed and replaced with 10 mL f/2 medium containing 10 µM galvestine-1.

3.2.3. Lab Scale experiment for Selecting Two-Time Points for Label-Free Quantitative Proteomics

Nannochloropsis oculata cultures were set up in triplicates using a 1 L flask photobioreactor system, as previously described in chapter 2 (Figure 2.1). The starting OD at 595 nm was 0.3. All flasks were maintained at a temperature of 20 °C and illuminated under 130 µmol m^{-2} s^{-1} under a 12-h (day/night) cycle. Cultures were subjected to continuous filtered aeration and

bubbling at 2 L/minutes. The algal culture was aerated and mixed in the same way as the pre-culture. The OD at 595 nm, and pH was monitored using a portable pH meter LAQUA B-712 (Horiba, Moulton Park, United Kingdom) every day throughout the experiments over a 12-day period. The samples were taken on days 3, 5, 7, 9, and 12 for wild-type *Nannochloropsis oculata* and days 2, 5, 7, 9, and 12 for the selected mutant *Nannochloropsis oculata*. The sample was taken on day 2, considering that the selected mutant grew faster than the wild-type *Nannochloropsis oculata*. Then 5 ml culture was taken for each analysis of DCW, proteins and chlorophylls, lipids, and EPA. The details of analytical and FAME methods were described in chapter 2 (2.2.3 and 2.2.4). A sample volume of 50 ml was taken for LFQ proteomics analysis. The samples were collected in three biological replicates for all analyses. All the sampling was done during the dark period, 2-h before the light period started. Harvested cells pellets (centrifuge at 4,415 × g for 5 minutes) were washed with phosphate-buffered saline and centrifuged (11,337 × g for 2 minutes) prior to storage at −20°C, while proteomic samples were kept at −80°C until further analysis.

3.3. Results

3.3.1. Sensitivity of *Nannochloropsis oculata* to cerulenin and galvestine-1

The wild-type *Nannochloropsis oculata* grew in all tested cerulenin concentrations with 40 µM was identified as a sub-lethal concentration for wild-type *Nannochloropsis oculata* (Supplementary Figure S3.1). 50 µM cerulenin concentration was selected for the first stage of mutants screening. The results showed there was no lethal dose identified. In another study, 25 µM cerulenin was determined as a lethal dose for wild-type *Nannochloropsis oculata*, while a concentration higher than 75 µM cerulenin was identified as a lethal dose for mutant *Nannochloropsis oculata* (Chaturvedi and Fujita, 2006).

The amounts of 20, 60, and 10 µM were determined as the sub-lethal concentrations for NEM, UDP and galvestine-1, respectively (Supplementary Figure S3.1). There was a 34.5 % growth inhibition at 10 µM galvestine-1, whereas only 20.43 % and 8.68 % were observed at 20 µM NEM and 60 µM UDP, respectively. Therefore, 10 µM galvestine-1 was selected as an MGDG synthase inhibitor for the mutants screening. The way to choose the range of quantities for inhibitors and organics solvent was not to exceed 0.3 % of the total culture volume, as the higher than 0.3 % organic solvent is toxic to microalga cells (Miazek et al., 2017).

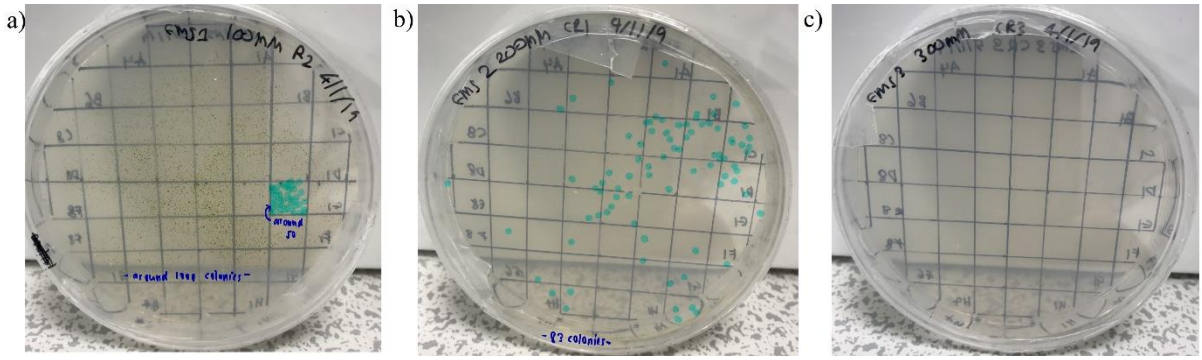

Figure 3.2: *Nannochloropsis oculata* mutant colonies of (a) 100 mM, (b) 200 mM, and (c) 300 mM EMS were grown on the f/2 medium agar containing 50 µM cerulenin after 3 weeks of incubation at 130 µmol m^{-2} s^{-1}, 20 °C, and 12-h (light/dark) cycles. Approximately more than 1000, 82, and no colonies were presented on the plate (a), (b), and (c), respectively, after 3 weeks of incubation.

The amount of 100, 200, and 300 mM EMS concentrations were used to develop mutants from wild-type *Nannochloropsis oculata*. A number of 82 colonies were counted for wild-type *Nannochloropsis oculata* treated with 200 mM EMS spread on an f/2 medium agar plate containing 50 µM cerulenin after 3 weeks of incubation (Figure 3.2). On the other hand, too many colonies and no colonies were recorded growing on the f/2 medium agar plates containing 50 µM cerulenin after 3 weeks of incubation for wild-type *Nannochloropsis oculata* that were treated with 100 and 300 µM, respectively. Therefore, 82 colonies were isolated and grew in 24 well-plates in f/2 medium containing 50 µM cerulenin and cultivated under 130 µmol m^{-2} s^{-1} illuminations at 20 °C.

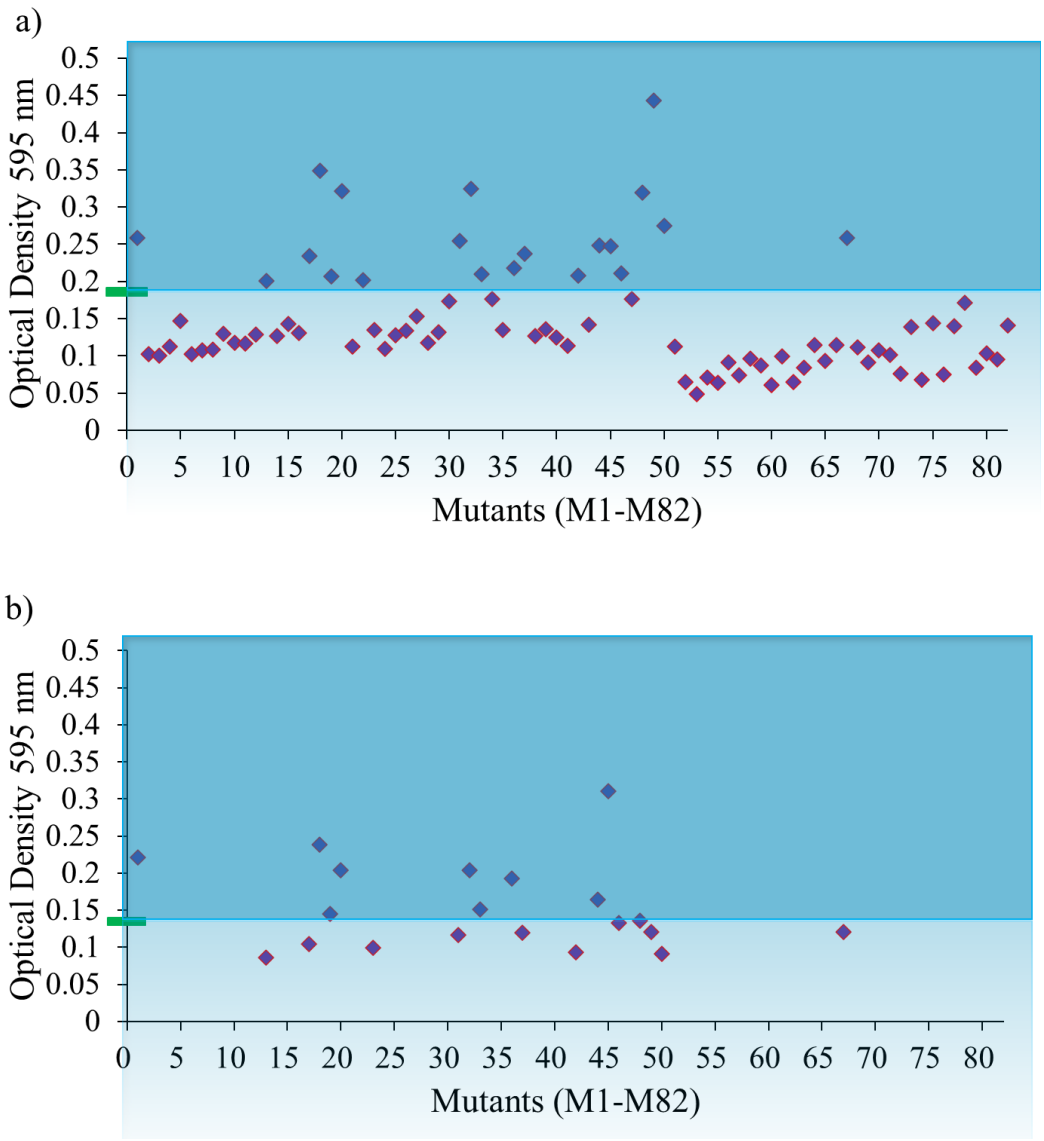

Figure 3.3: a) Growth of 82 *Nannochloropsis oculata* mutants b) Growth of 20 *Nannochloropsis oculata* mutants, cultured in f/2 medium containing 60 µM cerulenin, incubated at 130 µmol m^{-2} s^{-1}, 20 °C, and 12-h light/dark cycles for 8 days. 9 mutants were grown faster than wild-type *Nannochloropsis oculata* (represented by green rectangular).

After 10 days, 20 mutants were recorded with a higher OD at 595nm than wild-type *Nannochloropsis oculata* (Figure 3.3 (a)). These 20 mutants were then cultivated in f/2 medium containing a higher cerulenin concentration, 60 µM, and 3 mutants that reached the highest OD at 595 nm were selected for galvestine-1 screening (Figure 3.3 (b)). The selected mutants were known as M1, M18 and M45. The M1 and M18 mutants showed a significant

growth rate per day compared to the wild-type strain, with p-value of 0.005 and 0.007, respectively (Figure 3.4).

3.3.2. Fatty acids content

The percentage of FAs for wild-type, M1, M18, and M45 *Nannochloropsis oculata* harvested at an exponential growth phase having OD 0.8 at 595 nm was shown in Figure 3.5. C16:0, C16:1, and C20:5 represented the highest component of TFA. The highest percentage of EPA was identified in M1, M18, and M45 with 29.20 %, 26.42 %, and 25.08 %, respectively, while 18.57 % of EPA was identified in wild-type *Nannochloropsis oculata*. TFA quantities in mutants were comparable, while wild-type *Nannochloropsis oculata* had approximately 30 % TFA less than the mutants. A recent investigation of UV mutagenesis with quizalofop showed an increase in total lipid and chlorophyll-*a* content by 12.34 % and 1.10 µg/ mL, respectively (Moha-León et al., 2019).

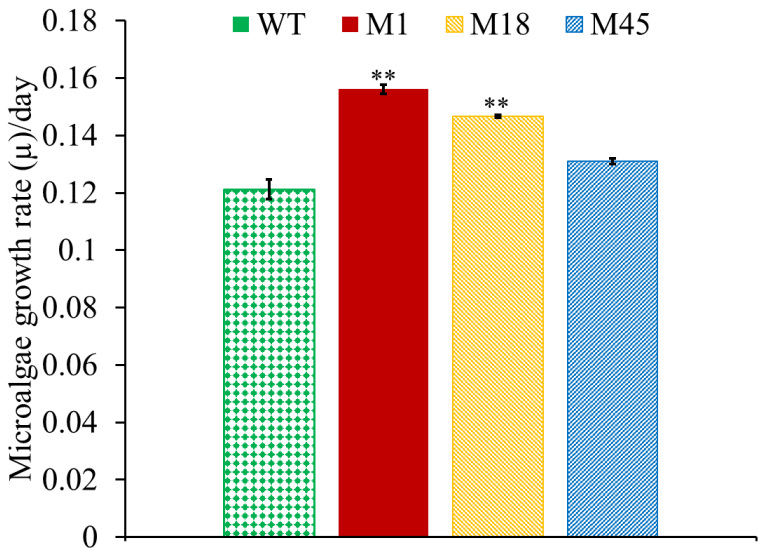

Figure 3.4: Growth rate comparisons of mutants M1, M18, M45, and wild-type *Nannochloropsis oculata*, incubated at 130 µmol m^{-2} s^{-1}, 20 °C, and 12-h light/dark cycles, 160 RPM shaking for 10 days. Mean ± standard deviation is shown (n = 3) and t-tests determine statistical significance ($p < 0.05$ [*]; $p < 0.01$ [**]; $p < 0.001$ [***]).

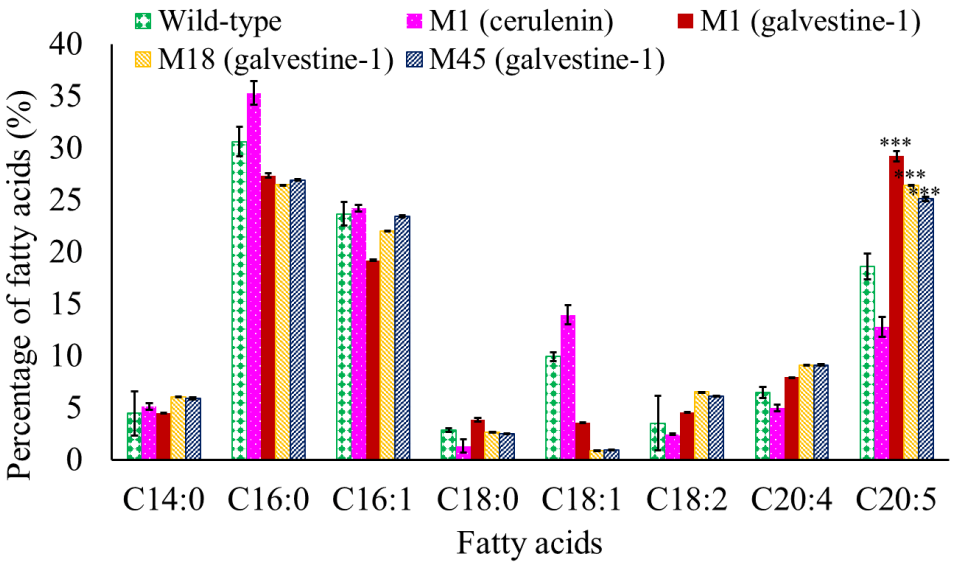

Figure 3.5: Comparative analysis of percentage (%) changes in the fatty acid composition of TFA in wild-type (WT), M1 mutant (treated with 60 µM cerulenin), M1, M18, and M45 (treated with 10 µM galvestine-1) *Nannochloropsis oculata* at exponential growth phase cells having $OD_{595\ nm}$ 0.8. Mean ± standard deviation is shown (n = 3) and t-tests determine statistical significance ($p < 0.05$ [*]; $p < 0.01$ [**]; $p < 0.001$ [***])

M1 mutant (cerulenin) had the highest C16:0 with 35.28 % and lowest C16:1 with 19.16 % of TFA. C16:1 showed a comparable percentage of roughly 23 % for wild-type, M1 (cerulenin), M18 (galvestine-1), and M45 (galvestine-1). Wild-type and M1 (cerulenin) *Nannochloropsis oculata* had a higher C18:1 component than the other galvestine-1 mutant, with 9.91 and 13.94 %, respectively.

The EPA quantities expressed as mg EPA/g DCW for wild-type, M1 (cerulenin), M1, M18, and M45 (galvestine-1) *Nannochloropsis oculata* was shown in Figure 3.6. M1, M18, and M45 (galvestine-1) had the highest EPA mg/g DCW ranging from 78.8-95.86 mg of EPA/g DCW, while the amount of wild-type and M1 (cerulenin) *Nannochloropsis oculata* were comparable with 27.49 and 26.3 EPA/g DCW, respectively. The EPA quantity ranged from 2.9 to 3.7-fold higher than wild-type and M1 (cerulenin) *Nannochloropsis oculata*.

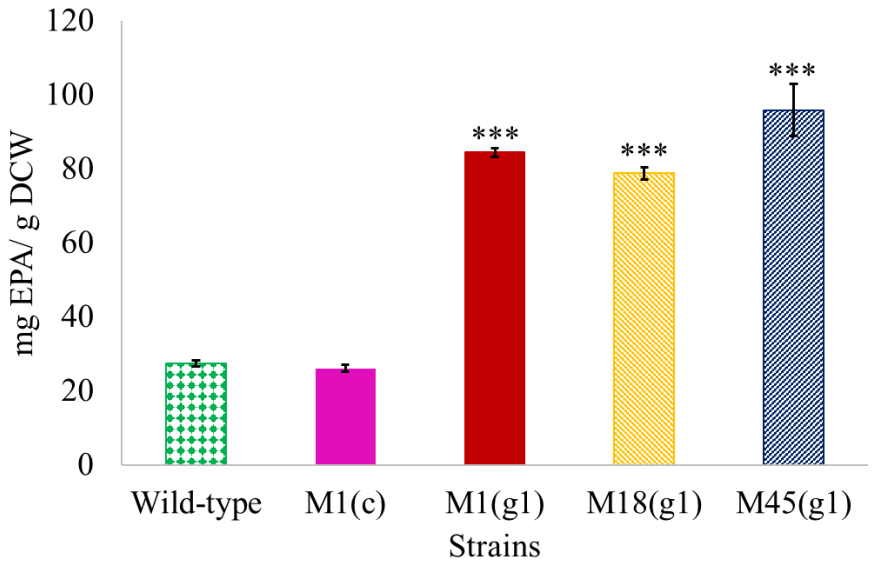

Figure 3.6: Quantities (mg EPA/g DCW) comparison for wild type, wild-type *Nannochloropsis oculata*, M1 mutant (treated with 60 µM cerulenin), M1, M18, and M45 (treated with 10 µM galvestine-1) at exponential growth phase cells having 0.8 OD at *595 nm*. Mean ± standard deviation is shown (n = 3) and t-tests determine statistical significance ($p < 0.05$ [*]; $p < 0.01$ [**]; $p < 0.001$ [***]).

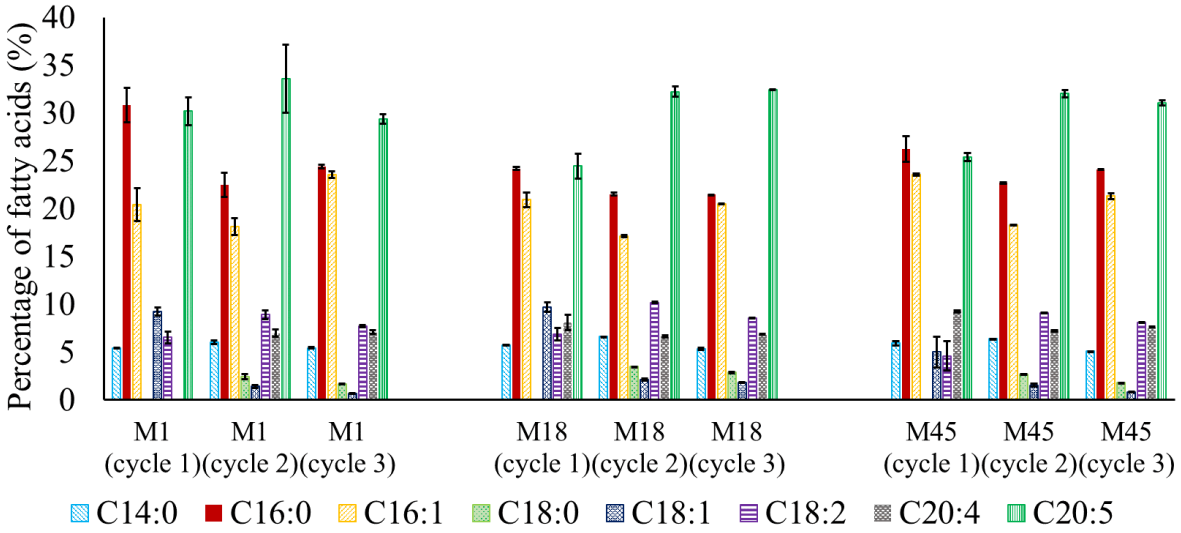

Figure 3.7: Percentage of primary fatty acids of TFA comparison for M1, M18, and M45 *Nannochloropsis oculata* mutants over 3 cycles adaptation in f/2 medium containing 10 µM galvestine-1. The experiments were carried out in sterile cell culture flasks (Nunc™) at 130 µmol m^{-2} s^{-1}, 20 °C, and 12-h light/dark cycles, 160 RPM shaking for 24 days (8 days for 1 cycle).

Further observations of FAs profiles of three cycle ALE in an f/2 medium containing 10 µM showed the EPA percentage was maintained around 30-33 %, while the C16:0 component was decreased by 5-7 % in M1 *Nannochloropsis oculata* mutant. Interestingly, the percentage of EPA in M18 and M45 *Nannochloropsis oculata* mutant were also increased from 24 to 32 % of TFA in cycles 2 and 3. On the other hand, the percentage of the C16:0 component was slightly decreased in cycles 2 and 3 for M18 and M45 *Nannochloropsis oculata*.

3.3.3. Growth profiles of wild-type and M1 mutant *Nannochloropsis oculata*

Figure 3.8 shows the growth profiles of wild-type and M1 mutant *Nannochloropsis oculata*. M1 mutant *Nannochloropsis oculata* growth showed no statistical significance compared to wild-type *Nannochloropsis oculata* (Figure 3.8 (a)), even though M1 mutant recorded a higher growth rate than wild-type *Nannochloropsis oculata* during mutant selections. Despite not much difference in OD profiles, the final DCW for M1 mutant *Nannochloropsis oculata* was slightly higher on day 12, as shown in Figure 3.8 (b). The total DCW are related to the photosynthetic rate and the chlorophyll levels in the microalga cells. Chlorophyll is a crucial component for harvesting light energy and converting it to carbohydrate biomass (Wang and Yin, 2018). M1 mutant *Nannochloropsis oculata* contained a higher chlorophyll-*a* content than wild-type strain Figure 3.8 (c)). Overall, the chlorophyll concentration was comparable with other studies (Ma et al., 2016a; Wei and Huang, 2017; Wang and Jia, 2020).

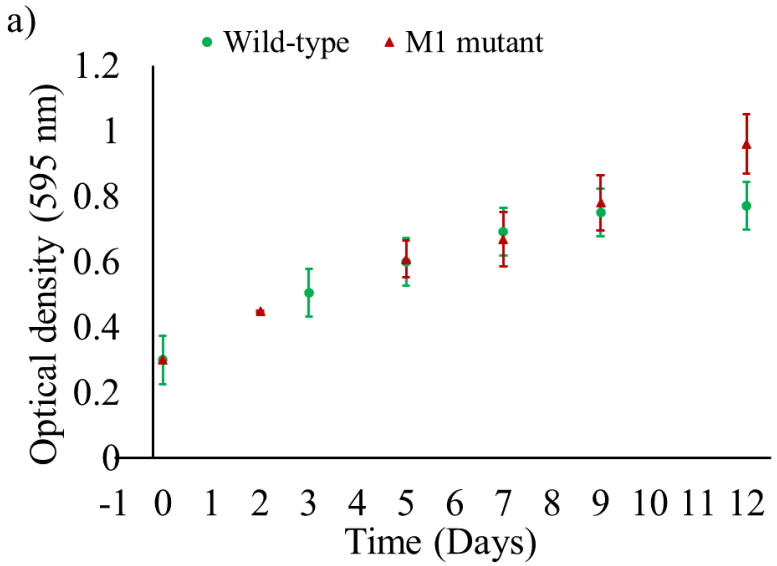

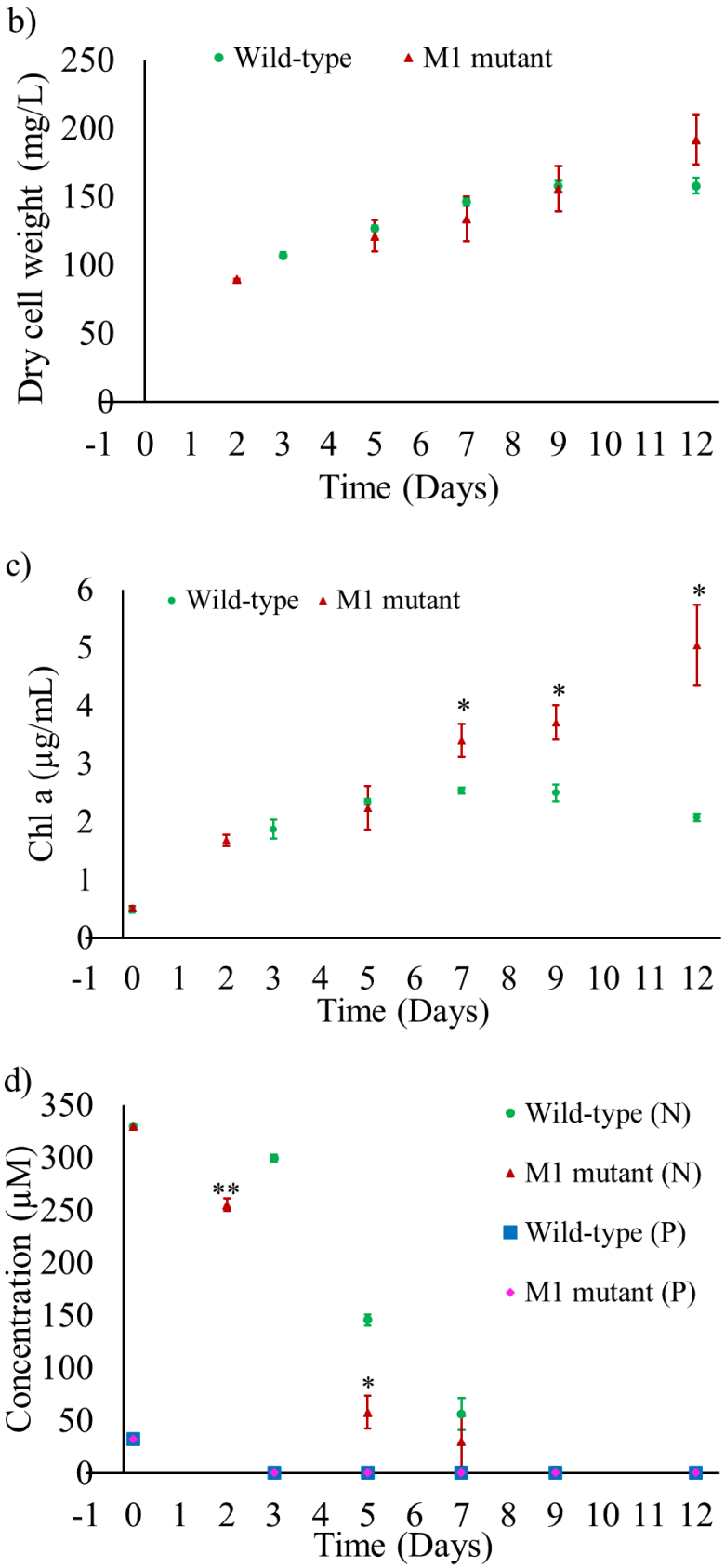

Figure 3.8: Growth profiles for wild-type and M1 mutant *Nannochloropsis oculata* cultivated in 1 L flasks under 150 µmol m^{-2} s^{-1}, 20 °C, and aerated bubbling for mixing and carbon source

for 12 days. a) Growth curves illustrated by optical density at 595 nm and b) Dry cell weight. Comparison of wild-type and M1 mutant *Nannochloropsis oculata* over 12 days of culturing for c) chlorophyll concentration and d) phosphate (P) and nitrate (N) uptake profiles. Mean ± standard deviation is shown (n = 3) and t-tests determine the statistical significance ($p < 0.05$ [*]; $p < 0.01$ [**]; and $p < 0.001$ [***]) of the M1 mutant strain compared to the wild-type strain.

Nitrate was rapidly absorbed till day 5 and was below detection limits by day 9 of culturing (Figure 3.8 (d)). The M1 mutant had a quicker nitrate uptake, with the nitrate concentration in the media reducing from 330 μM to 255 μM after two days of culturing, whereas the nitrate content in the wild-type *Nannochloropsis oculata* flasks decreased from 330 μM to 299 μM after three days of culturing. As seen in several oleaginous microalgae, a nitrate-limited condition in the f/2 medium after day 9 could promote the synthesis of neutral lipids (Burch and Franz, 2016; Tran et al., 2016; Remmers et al., 2017). Whereas phosphate was completely consumed within 2 and 3 days for M1 mutant and wild-type *Nannochloropsis oculata*, respectively. The concentration of phosphate in f/2 medium was sufficient to support the microalga growth. A study discovered that low or excess phosphate concentration reduced the growth rate of *Nannochloropsis salina*, when compared with standard f/2 medium that contains 4.35 to 5 mg/L of phosphate concentrations (Sforza et al., 2018).

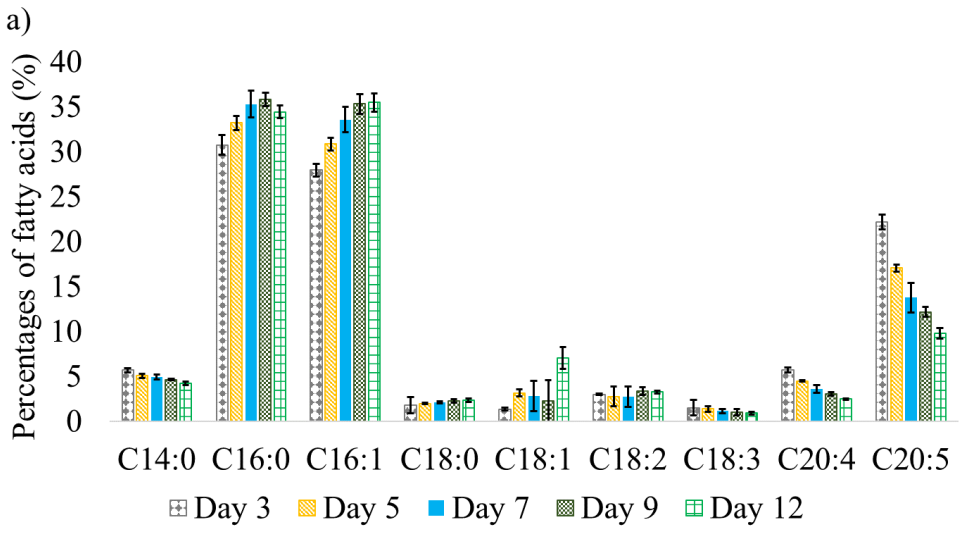

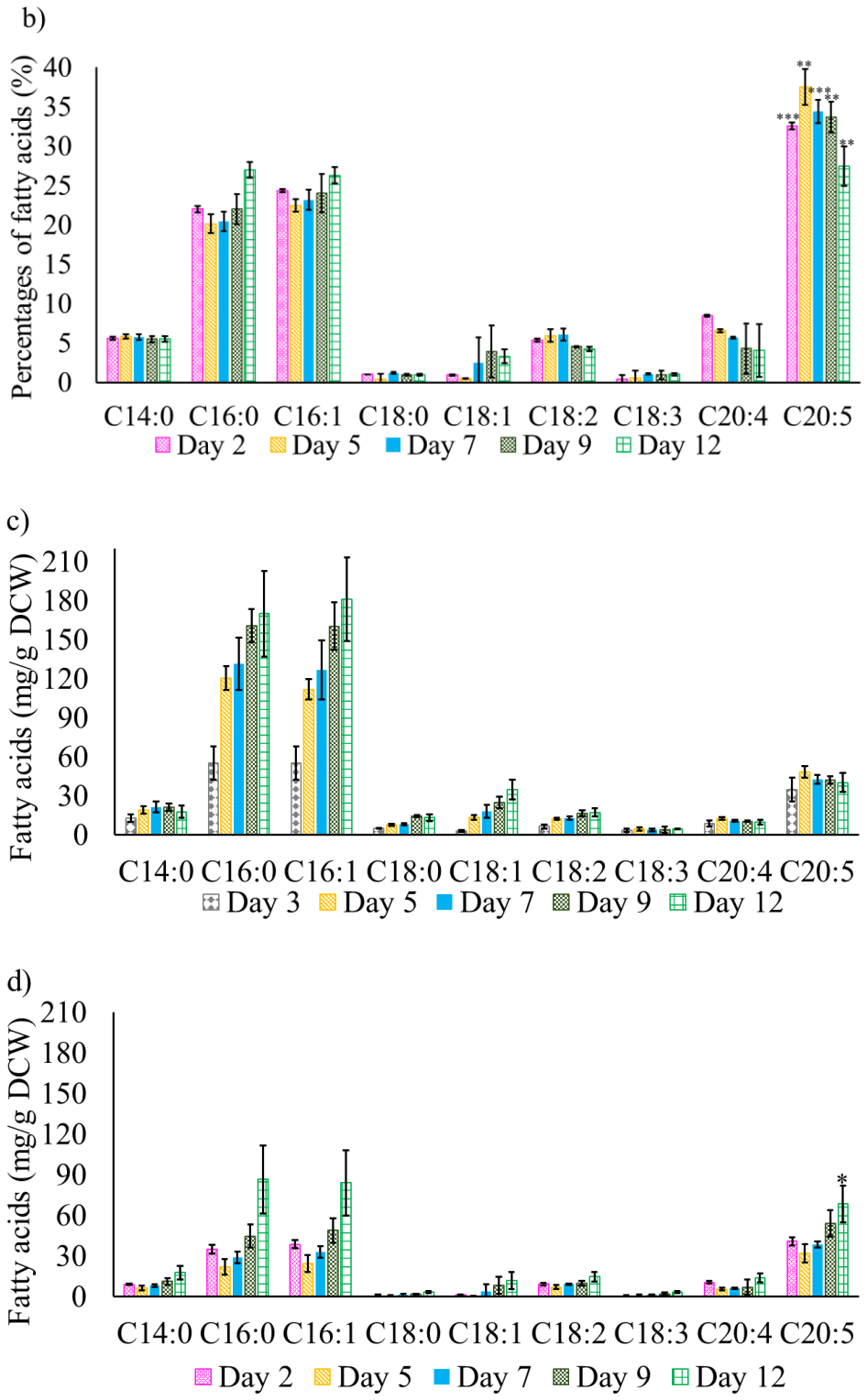

Figure 3.9: Percentages (%) of fatty acids at day 12. a) Wild-type and b) M1 mutant *Nannochloropsis oculata*. Quantification (mg/g) of fatty acids at day 12. c) Wild-type and d) M1 mutant *Nannochloropsis oculata*. Mean ± standard deviation is shown (n = 3) and t-tests determine the statistical significance ($p < 0.05$ [*]; $p < 0.01$ [**]; $p < 0.001$ [***]) for EPA content in the M1 mutant strain compared to the wild-type strain.

The major FAME observed in wild-type, and M1 mutant *Nannochloropsis oculata* were C16:0, C16:1, and C20:5 (EPA). The other FAME identified were C14:0, C18:0, C18:1, C18:2, C18:3, and C20:4. TAG (C16:0) to EPA ratios were monitored throughout 12 days of cultivation. The percentage of the FAs of wild-type and M1 mutant *Nannochloropsis oculata* is shown in Figures 3.9 (a) and (b). The highest percentage of EPA was recorded on day 5, with 37.54 % for M1 mutant *Nannochloropsis oculata,* while 22.17 % was recorded on day 3 for wild-type *Nannochloropsis oculata*. The ratio of C16:0 and C16:1 to EPA was lowest at the exponential phase on days 2 and 3 for M1 mutant and wild-type *Nannochloropsis oculata*, respectively. On the other hand, day 12 had the highest C16:0 and C16:1 to EPA ratio for wild-type and M1 mutant *Nannochloropsis oculata*. During batch growth, both strains produced more neutral lipids (C16:0 and C16:1), which were inversely related to the nutrient level in f/2 medium, as predicted. Both the wild-type and M1 mutant strains gradually increased their percentage of neutral lipids, reaching their greatest levels (35 and 27 %, respectively) on day 12. TAG accumulation is known to occur as a stress reaction when nutrients are scarce, and a previous study found that under these conditions, C16:0 reached a high of roughly 40% of TFA (Wei and Huang, 2017).

Figure 3.9 (c) and (d) demonstrate the total FAME amounts (mg/g DCW) were determined using the standard FAME intensity. The EPA content in M1 mutant *Nannochloropsis oculata* rose from day 2 and peaked at 68.5 mg/g DCW on day 12. On day 5, the wild-type strain had the greatest EPA of 48.6 mg/g DCW. Compared to previous studies, the amount of EPA found in the M1 mutant was significantly higher. Shi et al. (2021) recorded EPA at 40 and 45 mg/g DCW on day 4 for a wild-type *N. oceanica* strain and a Δ6 elongase overexpression strain, respectively. Yang et al. (2019a) described a Δ6 desaturase overexpression *Nannochloropsis oceanica* strain with 62.35 mg/g DCW on day 10, decreasing to around 50 mg/g DCW at day 13, while the wild-type strain had around 40 mg/g DCW at day 10, increasing to around 60 mg/g DCW at day 13.

3.4. Discussion

3.4.1. *Nannochloropsis oculata* mutants screening procedure

Enhancing the EPA content in microalgae could boost the market competitiveness of omega-3 microalgae. This chapter aimed to develop EPA-overproducing mutant strains *Nannochloropsis oculata* via a random mutagenesis approach. EMS and chemical inhibitors were combined to induce and screen down the desired phenotype mutant strains.

In the literature, cerulenin is a practical chemical component to inhibit FAS-KR or KASI, an essential enzyme in the FA synthesis cycle (Liu et al., 2016b). Hence, the cerulenin was selected and combined with an MGDG synthase inhibitor to optimise the mutant screening. Interestingly, no MGDG synthase inhibitor was tested on any species of *Nannochloropsis* to enhance EPA production. Galvestine-1 is indicated as the most suitable MGDG synthase inhibitor compared to UDP and NEM. However, a higher growth rate recorded in UDP screening experiments (Supplementary Figure S3.1) requires further investigation even though the environmental conditions were similar to cerulenin, galvestine-1 and NEM.

A higher concentration of EMS than in the previous study was applied to optimise the effect of EMS on microalga cells; hence, only tough microalga phenotype could survive. Besides, 1000 mutants induced by 100 mM could not be selected because of the limited chemical inhibitor compound and laboratory space to facilitate all the mutants. In addition, FACS could be used to screen the mutants with enhanced total lipid content (Beacham et al., 2015). However, EPA-overproducing mutant strains could not be screened by any fluorescence method as all the selected mutants showed a lower EPA content in exponential and stationary growth periods (Beacham et al., 2015). Hence, working on a smaller number of mutants, such as 82 mutants induced by 200 mM, would be the most convenient to screen a potential EPA-overproducing mutant strain.

A higher concentration of 50 µM of cerulenin was selected instead of 40 µM for the first screening. Considering the light intensity could affect the cerulenin content, a slightly higher than the minimum sub-lethal concentration was applied. The material safety data sheet of cerulenin shows that the chemical is sensitive to light and stable at room temperature.

However, there is no detailed information on the specific light intensity that could damage cerulenin. A range of 90-400 µmol m^{-2} s^{-1} light intensity indicates no effect on cerulenin (Chaturvedi and Fujita, 2006; Liu et al., 2012, 2016b; Suhaimi et al., 2022). A concentration of 60 µM was also tested on the first screening mutants to avoid a false positive selection. Nine mutants, M1, M18, M19, M20, M32, M33, M36, M44, and M45, showed higher growth than wild-type strains in both screenings by cerulenin (Figure 3.3). However, only three mutant strains were chosen for galvestine-1 testing due to the low amount of galvestine-1 available for this study.

M1, M18, M45 and wild-type *Nannochloropsis oculata* were cultured in 20 mL f/2 medium containing 10 µM galvestine-1 to get enough biomass for FAs analysis. FA analysis results confirmed that the M1, M18 and M45 mutants had higher EPA percentage and EPA quantity (mg/g DCW), as evidenced by statistical analysis (t-test $p < 0.05$) (Figures 3.4 and 3.5). The FAs analyses for ALE experiments indicate the competitiveness of mutant strains in enhancing EPA production. However, the mutants were monitored for 3 cycles only because of the limited source of galvestine-1. The length of the ALE period should be a minimum of a few weeks and could last several years to generate an improved phenotype (Arora et al., 2020). The entire impact of ALE, also known as the whole genome, might take anywhere from 95 days to 4 years, where the evolution caused the alteration in coding sequences, which then alter the genes involved in cell division, cycle regulation, and nucleotide synthesis and binding (Arora et al., 2020).

The mutants could be cultured without the presence of galvestine-1 and show a similar performance. The mutant DNA structures could remain because EMS has randomly generated point mutations such as the replacement of A-T to G-C (Barati et al., 2021). However, the details of point mutations in mutants will be conducted in future studies.

3.4.2. Growth profiles of wild-type and M1 mutant *Nannochloropsis oculata*

Growth performance, nutrient uptake, and variations in FAME profiles were all observed in identifying two-time points when EPA and TAG production were at an optimum level. Despite the fact that the M1 mutant grew faster than wild-type cells during screening in 24 well plates and had a higher final DCW (day 12), no statistical significance was found (Figure 3.8 (a) and

(b)). From day 7 onwards, however, chlorophyll-*a* levels in the M1 mutant were statistically substantially greater than in wild-type cells (Figure 3.8 (c)), implying more efficient light-harvesting and photosynthetic capability than in wild-type strain.

The pH of both the wild-type and M1 mutant cultures was approximately 7 to 8.5, indicating that aeration was sufficient to maintain the pH at the ideal levels. The perfect pH for *Nannochloropsis* sp. growth was previously reported to be 8.5 (Khatoon et al., 2014).

During microalga growth, the amounts of nitrate and phosphate in the f/2 media were also measured. Despite the fact that these macronutrients are required for microalgae growth (Hu and Gao, 2006), their absorption rates may have an impact on FA profiles (Rasdi and Qin, 2015). Nitrate was rapidly absorbed till day 5 and was below detection limits by day 9 of culturing (Figure 3.7 (d)). The M1 mutant had a quicker nitrate uptake, with the nitrate concentration in the media reducing from 330 μM to 255 μM after two days of culturing, whereas the nitrate content in the wild-type *Nannochloropsis oculata* flasks decreased from 330 μM to 299 μM after three days of culturing. As seen in several oleaginous microalgae, a nitrate-limited condition in the f/2 medium after day 9 could promote the synthesis of neutral lipids (Burch and Franz, 2016; Tran et al., 2016; Remmers et al., 2017).

Similarly, during growth, phosphate concentrations fell below detectable levels in M1 mutant and wild-type cells within 2 and 3 days, respectively (Figure 3.7 (d)). Overall, the nitrate and phosphate data indicated that the wild-type and M1 mutant cultures had finished their batch development in nine days.

3.4.3. Fatty acid methyl ester (FAME) profiles

Wild-type and M1 mutant *Nannochloropsis oculata* had a larger percentage of EPA in total lipids in the early exponential phase, implying that EPA synthesis preferred favourable growth conditions. A higher EPA percentage at the exponential growth phase could also be related to MGDG, part of membrane lipid. In *Nannochloropsis salina*, an earlier study found that chlorophyll-*a* was directly proportional to MGDG quantity, with higher chlorophyll-*a* and MGDG quantity on day 8 (exponential phase) than on day 12 (Koh et al., 2019). Contrarily, the M1 mutant showed the highest quantity on day 12, indicating a higher EPA content could be

incorporated with neutral lipids than the wild-type strain. Another hypothesis was that the EPA pool in M1 mutant is higher than the wild-type strain; hence the EPA could be translocated easier from the membrane lipid to neutral lipids. Therefore, the two time-point were chosen based on the significant FA profiles between TAG and EPA, EPA percentages, and absolute EPA quantifications for LFQ proteomics analysis. The first time point was the early exponential growth phase (days 2 and 3), where the percentage of EPA was highest, and the neutral lipid content was at the lowest was selected. The second time point was day 12, where neutral lipids and EPA quantity in M1 were at the highest quantity.

3.5. Conclusion

A novel strategy to increase EPA productivity in *Nannochloropsis oculata* was devised using a combination of EMS-induced random mutagenesis and screening with chemical inhibitors that haven't been applied together previously. The combination of EMS random mutagenesis and supported by a 2-stage screening with cerulenin and galvestine-1, indicates a compatible match for developing EPA-overproducing mutants in *Nannochloropsis oculata*. In addition, other chemical inhibitors could be tested by targeting different FA synthesis-related enzymes to increase the EPA content further. Besides, combining this study with a photosynthetic membrane protein complex, PSII inhibitor could further increase the developed mutant's growth rate, hence, offering the omega-3 industry a greater option.

CHAPTER 4: LABEL-FREE QUANTITATIVE PROTEOMICS ANALYSIS

4. Comparative proteomics reveals proteins involved in eicosapentaenoic acid trafficking of wild-type and mutant *Nannochloropsis oculata*

4.1. Introduction

Microalgae molecular biology has gained a lot of attention in recent years due to its potential for maximising the yield of high-value bioactive compounds from microalgae cells. Studying the different environmental conditions and the changes in the improved microalgae strains compared to the wild-type microalgae species could reveal the trigger for the metabolic changes. Algomics, or omics for algae, help acquire a broad perspective of algae and its working system and give massive data that can be interpreted using computer tools and software (Mishra et al., 2019). Combining omics technologies such as genomics, transcriptomics, proteomics, and metabolomics has significantly impacted microalgae advancement and manipulation (Anand et al., 2017). Among the omics analysis techniques, proteomics is considered one of the perfect choices for analysing the various biological processes at the protein level, such as identifying proteins, finding the protein role in the microalgae evolution and studying biochemical pathways (Anand et al., 2019).

LFQ and label-based proteomics are two general quantification strategies for MS-based proteomics. LFQ compares two or more experiments by comparing the direct MS intensity of any measured peptide or utilising the number of obtained spectra matching a protein as a proxy for their respective quantities in a given sample (Bantscheff et al., 2007). In the label-based approach, an internal standard is incorporated into amino acids metabolically, chemically, enzymatically, or via spiked synthetic peptides in order to investigate the differently expressed proteins (Latosinska et al., 2015).

Referring to the www.uniprot.org website, *Nannochloropsis gaditana* is the only species of the *Nannochloropsis* genus with a complete genome representation, while other species of *Nannochloropsis* are at the scaffold level (Wang et al., 2014). On the contrary, *Nannochloropsis oceanica* were reported to have a complete proteome database (Wei et al., 2019, 2020). Table 4.1 shows that LFQ proteomics analysis is preferred for species of *Nannochloropsis* that do not have full genome representation. A cross-microalgae species

sequenced protein database was used for *Nannochloropsis oculata* proteomics analysis (Kim et al., 2005; Tran et al., 2016).

Table 4.1: All proteomics analysis articles published for species of *Nannochloropsis* were based on google scholar and StarPlus - University Library Discovery searched in April 2022.

Microalga species	**Study topic**	**Experimental setup**	**References**
Nannochloropsis oculata	Finding out the effect of Cadmium to marine microalga cells	2D-gel electrophoresis and LFQ proteomic analysis	(Kim et al., 2005)
Nannochloropsis oculata	Finding out the effect of nitrogen repleted and depleted on FA biosynthesis and accumulation	LFQ proteomics analysis	(Tran et al., 2016)
Nannochloropsis gaditana	Discovering the first proteomic analysis under industrial conditions	LFQ proteomics analysis	(Fernández-Acero et al., 2019)
Nannochloropsis oceanica	Studying about carbon concentration mechanism (CCM) in microalga cells	LFQ proteomics analysis	(Wei et al., 2019)
Nannochloropsis oceanica	Finding out the effect of blue and red colour light to microalga cells	LFQ proteomics analysis	(Wei et al., 2020)
Nannochloropsis oceanica	Finding out the effect of nitrogen repleted and depleted on lipid storage	LFQ proteomics analysis	(Chen et al., 2019)
Nannochloropsis gaditana	Studying the effects of bioavailable nitrogen (N) and phosphorus (P) deprivation on the proteome and transcriptome	TMT labelling quantification analysis	(Hulatt et al., 2020)

A phylogenomic study of five oleaginous *Nannochloropsis* species shares similar lipid biosynthesis traits and has a comparable number of protein-coding genes (Wang et al., 2014). Hence, the sequenced proteins of other *Nannochloropsis* species could also be used for proteomics study for *Nannochloropsis* species that have not been fully sequenced yet. In addition, the number of sequenced proteins deposited in the primary repositories such as Uniprot has increased enormously, which could make the proteomics analysis for unsequenced microalgae species possible.

In this chapter, LFQ proteomics analysis was conducted to investigate the proteome level changes on early exponential and late exponential growth phase in mutant *Nannochloropsis oculata* compared to wild-type strains. Cross-species of *Nannochloropsis* quantitative proteomics was applied to generate specific hypotheses on how metabolism has been re-wired to generate the mutant phenotype.

4.2. Materials and Methods

4.2.1. Protein extraction and quantification

Crude proteins were extracted by referring to a previous study (Posch, 2014). A volume of 1 ml lysis buffer (2 % sodium dodecylsulfate (SDS), 40 mM Tris base, 60 mM dithiothreitol (DTT)) and 10 µL Halt™ protease inhibitor cocktail (Thermo Fisher Scientific, United Kingdom) were added to the samples pellets and put on ice for thawing. Approximately 500 µL volume of glass beads were added to the sample tubes. The samples were vortexed for 20 cycles (30 seconds vortexed and then 30 seconds cooled on ice. Lysed samples were centrifuged at 18,000 × g for 5 minutes at 4 °C. The samples were kept on ice for 30 minutes until the foam subsided. The supernatants (crude protein) were transferred to 1.5 mL protein LoBind Eppendorf tubes and stored at -80 °C.

Two set of samples were purified from lipids, pigments, and other contaminants by using a protein 2D Clean-up kit (GE Healthcare) by following the manufacturer's protocols. Generally, the protocols started by adding 300 µL precipitant to 100 µL crude protein samples. The samples were vortexed for 30 seconds and incubated on ice for 15 minutes. Then, 300 µL co-precipitant were added, and the samples were vortexed for 30 seconds for mixing. The samples were centrifuged at 18,000 × g for 5 minutes at 4 °C, with the tubes' cap hinges facing outward. Then, supernatants were removed, and 40 µL of co-precipitant was added on top of the pellet and incubated on ice for 5 minutes. The samples were centrifuged at 18,000 × g for 5 minutes at 4 °C again, with the tubes' cap hinges facing outward. 25 µL of HPLC grade water was added to the pellet to disperse the pellet. 1 mL chilled wash buffer (kept at -20 °C) and 5 µL of wash additive were added. The samples were vortexed for 30 seconds and kept on ice for 10 minutes. The samples were centrifuged again at 18,000 × g for 5 minutes with the cap hinge facing outward. The supernatants were removed, and pellets were dried (not more than

5 minutes), and the pellets were resuspended in 100 µL lysis buffer and urea buffer (8M urea, 100 mM Tris-HCl (pH 8.5), 5 mM DTT) for 1D-SDS PAGE and in-solution digestion, respectively.

The sonication bath was used for 5 minutes to dissolve protein into a urea buffer. The protein samples were quantified by using NanoDrop™ 2000 (Thermo Fisher Scientific, United Kingdom) spectrophotometer. The spectrophotometer setting was set as 1 mg/mL equals 1 OD at 280nm. The urea buffer was used as a blank. 4 µL BSA (1, 0.8, 0.6, 0.4, 0.2, 0.1 mg/mL), which was prepared by using urea buffer, were placed in the spectrophotometer sample holder, and the standard curve data were run in triplicates (Supplementary Figure S4.1). 4 µL samples were placed on the spectrophotometer sample holder, and the protein was measured and quantified.

4.2.2. 1D SDS-PAGE protein visualisation

An amount of 10 µg crude protein samples and a 2D cleaned-up sample solution were run on 1D SDS-PAGE gel to visualise the protein quantities. A precast gel (NuPAGE™,Thermo Fisher Scientific, United Kingdom) was used to minimise the preparation steps and reduces the chances of contamination (Posch, 2014). The running buffer was prepared as follows; 1 × SDS running buffer was prepared by diluting 50 mL 20× SDS running buffer (Thermo Fisher Scientific, United Kingdom) with 950 mL of distilled water. For diluted samples, 0.5 mL antioxidants (NuPAGE™, Thermo Fisher Scientific, United Kingdom) were added to 200 mL 1 × running buffer. 200 mL of 1 × SDS running buffer containing antioxidants were poured for the upper running buffer, followed by 750 mL 1 × SDS running buffer added for the lower running buffer. 20 µL (13 µL protein samples + 5 µL sample buffer 4 × and 2 µL reducing agent 10 × were prepared and incubated in the water bath at 70 °C for 10 minutes. 5 µL EZ-RUN Prestained Protein ladder PB3603-500 (Thermo Fisher Scientific, United Kingdom) and 0.5 µg of BSA was used as standard internal quantification. 20 µL samples were loaded into the gel's well. The gel was run for 2 hours with an initial voltage of 200 V and 90 mA current. The gels were stained by Coomassie blue staining solution (InstantBlue™, VWR, United Kingdom) for 24 hours at 4 °C. The gels were washed with distilled water three times, and the pictures were taken and analysed by using the GelAnalyzer 19.1 software version (downloaded via http://www.gelanalyzer.com/). The percentage of proteins purified after 2D cleaning were determined.

4.2.3. In solution digestion

An amount of 5 µg protein solution were visualised by 1D SDS PAGE. 50 µg proteins were transferred to a sterile protein LoBind Eppendorf tubes. Protein samples were reduced to 10 µL by diluting with urea buffer and incubated at 37 °C for 30 minutes. 1 µL 100mM iodoacetamide was added and incubated in the dark for 30 minutes at 20 °C to s-alkylate the protein samples. 2 µg Trypsin/Lys-C mix (Promega, United States) was added to the protein solutions and incubated for 3 hours at 37 °C. 75 µL (50 mM Tris-HCl (pH 8.5), 10 mM $CaCl_2$) was added to the protein solution and incubated overnight (16-20 hours) at 37 °C for trypsin digestion (check Phil Jackson). 5 µg of protein samples were aliquot and ran 1D SDS PAGE to confirm that the protein was denatured. 4.8 µL (5 % of the total protein solution) of 10 % TFA was added to the protein solution to stop the digestion process. Pierce® C18 spin columns (Thermo Fisher Scientific, United Kingdom) were used for desalting the samples by following the manufacturer's protocols. Activation solution (50 % methanol; 400 µL per sample), Equilibrium solution (0.5 % TFA in 5 % ACN, 400 µL per sample), sample buffer (2 % TFA in 20 % ACN, 1 µL for every 3 mL sample), wash solution (0.5 % TFA in 5 % ACN, 800 µL per sample), and elution buffer (70 % ACN, 40 µL per sample) were prepared in sterile glass bottles. Sample buffer was added to each sample and kept on ice while preparing the column. The column was tapped to settle down the resin, the top and bottom cap were removed, and the column was placed into receiver 2 mL Eppendorf tubes. 200 µL of activation solution was added to the column to rinse the wall of the spin column and to wet resin. The column cap was placed back, and the columns were centrifuged at 1500 × g for 1 minute. The flow-through was then discarded. The activation solution step was repeated twice. 200 µL equilibrium solution was added, and the columns were centrifuged at 1500 × g for 1 minute. The equilibrium solution step was repeated twice. The protein samples were loaded on top of the resin bed. The column cap was placed back, and the columns were centrifuged at 1500 × g for 1 minute. The flow-through samples were re-added 3 times to the columns to secure the sample binding. 200 µL wash solution was added, and the columns were centrifuged at 1500 × g for 1 minute. The wash solution step was repeated 4 times to make sure the samples were washed thoroughly to discard all contaminants. Sterile 1.5 mL LoBind tubes were used as sample receiver tubes. 20 µL of elution buffer was added to the top of the resin bed. The columns were centrifuged at 1500 × g for 1 minute. The elution buffer step was repeated 3 times to

collect 60 µL purified protein samples. Samples were dried using a vacuum evaporator (speedVac, United Kingdom) and stored at -80 °C for further mass spectrometry analysis.

4.2.4. LC-MS/MS for proteomics

LC-MS/MS was performed and analysed by nano-flow liquid chromatography (U3000 RSLCnano, Thermo Fisher Scientific, United Kingdom) coupled to a hybrid quadrupole-orbitrap mass spectrometer (Q Exactive HF, Thermo Fisher Scientific, United Kingdom). Peptides were separated on an Easy-Spray C18 column (75 µm × 50 cm) using a 2-step gradient from 3 % solvent A (0.1 % formic acid in water) to 10 % B over 5 minutes and then to 50 % solvent B (0.1 % formic acid in 80 % acetonitrile) over 180 minutes at 300 nl min-1, 40 °C. The mass spectrometer was programmed for data-dependent acquisition with 10 product ion scans (resolution 30,000, automatic gain control 1e5, maximum injection time 60 ms, isolation window 1.2 Th, normalised collision energy 27, and intensity threshold 3.3e4) per full MS scan (resolution 120,000, automatic gain control 1e6, maximum injection time 60 ms) with a 20-s exclusion time. Each sample was run in triplicate.

4.2.5. Data analysis

Triplicates fraction files for WT *Nannochloropsis oculata* for days 3 and 12 and triplicates fraction files for M1 mutant *Nannochloropsis oculata* days 2 and day 12 were processed by proteomics analysis software MaxQuant (version 1.6.17). The settings used were as followed: Initial maximum precursor and fragment mass deviations were set to 7 ppm and 0.5 Da, respectively. Variable modification (methionine oxidation and N-terminal acetylation) and fixed modification (cysteine carbamidomethylation) were set trypsin/P with a maximum of two missed cleavages were chosen for searching. 7 amino acids were set at the minimum peptide length, and the false discovery rate (FDR) for peptide and protein identification was set to 0.01. The database used was all protein sequences for *Nannochloropsis* downloaded from NCBI (December 2020), Uniprot (December 2020) and extracted from MSPnr100 database (Tran et al., 2016). The total number of protein sequences in the combined *Nannochloropsis* proteome database were 16270 proteins. LFQ analyst (https://bioinformatics.erc.monash.edu/apps/LFQ-Analyst/) was used for LFQ protein quantifications and visualisations.

4.2.6. Quantifications of fatty acid profiles in TAG and polar lipids

The quantification of FA within TAG and polar lipids was adapted from a previous study with modifications (Janssen et al., 2019). In brief, total lipids were extracted from wet microalgae biomass using a standard Folch method (Axelsson and Gentili, 2014). C17:0 PC and C17:0 triheptadecanoin were added to the samples prior to the extraction of total lipids. Then 2 ml of methanol was added to the samples and homogenised for 1 minute using a homogeniser Ultra-Turrax®T 25 (Ultra-Turrax, Germany), followed by the addition of 4 ml of chloroform and further homogenisation for 2 minutes. The total lipid solution was filtered through a 0.22-µm filter (SLS, United Kingdom). The cell debris was rinsed with 2 ml fresh solvent (chloroform and methanol, ratio 2:1, v/v) and combined with the previous filtrate. 2 ml of potassium chloride solution (8.8 g/L) was added, and the mixture vortexed for 1 minute. The top solvent layer was discarded, and the bottom solvent was evaporated using a centrifugal evaporator (Jouan, United States). The total lipid extract was dissolved in chloroform and spotted onto a thin liquid chromatography (TLC) plate along with TAG and polar lipid standard. The mobile phase used was iso-hexane, ether, and formic acid (80:20:2, v/v/v) to separate the TAG and polar lipids. The TAG and polar lipid fractions were removed by scraping the silica into test tubes, followed by re-extraction using iso-hexane and ether (1:1, v/v) and chloroform, methanol, and distilled water (5:5:1, v/v/v), respectively. A total of 1 ml of toluene and 2 ml of 1 % sulfuric acid in methanol were added for transesterification, and the samples were incubated at 50 °C for 16 h. Then 5 µl FAME sample was identified and quantified using a GG, Agilent 6890 model (Agilent Technologies, United States), onto a CP-Wax (52 CB) GC column (30 m × 0.25 mm × 0.15 µm). In total, 1 µl of FAME standard (Nu-Chek Prep, United States) was injected as a reference, and 1 µl of sample volume was injected in split injection mode at 230 °C. The GC was operated at a constant flow of 1 ml/ minute hydrogen. The temperature program was started at 170 °C for 3 minutes, followed by temperature ramping at 4 °C/ minute to a final temperature of 220 °C and held constant at 220 °C for 10 minutes. Peak areas were integrated using a chromatography data system, Agilent Chemstation software (Agilent Technologies, United States). The EPA of TFA in TAG and polar lipids were determined by their peak areas and quantified against the added internal standard.

4.3. Results

4.3.1. Protein profiles

Protein quantifications were crucial for LFQ proteomics analysis. In this chapter, the microbiuret method was used to quantify the protein for 12 days culturing periods as previously described in the previous chapter 3. Whereas the protein extracted for LFQ proteomics analysis used the nanodrop method for quantification. Referring to Figure 4.1, the protein quantity for 12 days showed a comparable amount for wild-type and M1 mutant *Nannochloropsis oculata*. However, there were 35.3 % and 3.88 % protein reduction by the nanodrop method in M1 mutant days 2 and 12, respectively. A 12.1 % and 18.5 % decrease was recorded for wild-type day 3 and day 12, respectively. Supplementary Figure S4.1 shows the standard BSA curve for the nanodrop method.

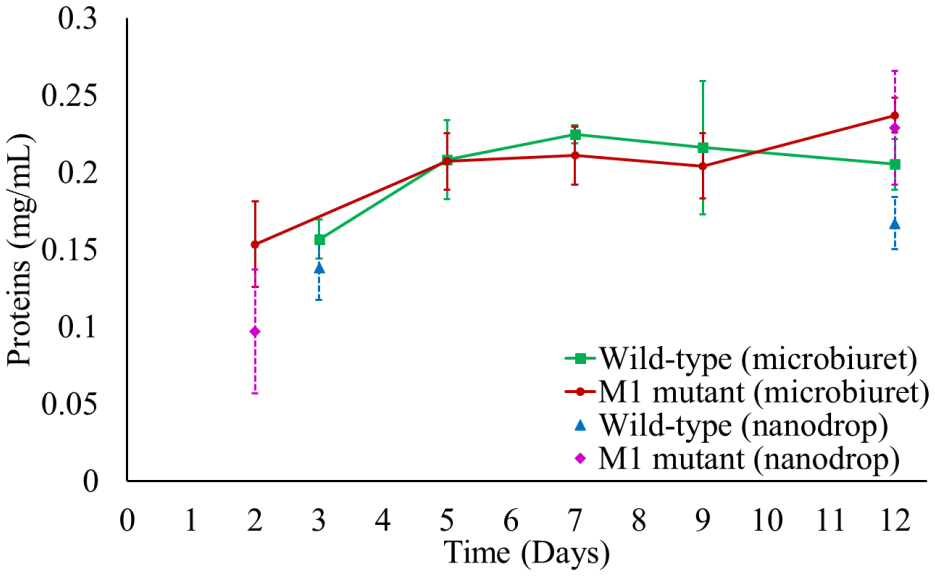

Figure 4.1: Protein quantifications comparison for M1 mutant and wild-type *Nannochloropsis oculata* by Microbiuret method (Itzhaki and Gill, 1964) and Nanodrop 2000 method (Thermo Fisher Scientific, United Kingdom). The protein was quantified for all samples using the microbiuret method, while two-time proteins were determined using the Nanodrop 2000 method and compared with the microbiuret method.

Based on the microbiuret method quantified protein, 10 µg of protein was compared before and after 2D cleaned-up by one-dimensional SDS-polyacrylamide gel electrophoresis (1D-SDS PAGE) to determine the percentage of protein recovery as shown in Supplementary Figure

S4.2. The percentage of protein recovery after 2D cleaned up was around 63 to 85 %. The 2D cleaned-up protein sample then proceeds with in-solution digestion. Nanodrop 2000 (Thermo Fisher Scientific, UK) was used to quantify 2D cleaned-up two-time points protein samples due to a small, digested protein volume. 0.5 µg protein samples were compared before and after in-solution digestion by 1D-SDS PAGE to ensure all the protein was completely digested by Trypsin/Lys-C mix (Promega, United States) (Supplementary Figure S4.3).

MS/MS scans for label-free quantitative experiments for wild-type and M1 mutant *Nannochloropsis oculata* in early exponential phase and end of exponential phase samples is shown in Supplementary Table S4.1. The MS/MS scans showed comparable scans for each replicated sample, except for M1 mutant day 2 replicate number 3 (M1D2F3) sample, having the lowest scan and a 39.6 % scan decrease compared to M1 mutant day 2 replicate number 3 (M1D2F2) sample.

The UniProt's website proteome database search (December 2020) showed 219 protein groups reported for *Nannochloropsis oculata*. The number of protein sequences for *Nannochloropsis oculata* is small compared to *Nannochloropsis gaditana,* with 15,363 protein groups. Hence, for this study, all *Nannochloropsis* proteome databases were combined from UniProt, NCBI, and MSPnr100 (Tran et al., 2016). The *Nannochloropsis* proteome database was used in a proteomics article reported for *Nannochloropsis oceanica* (Wang and Jia, 2020). Using a cross-species proteomics database must be used especially for un-sequenced microalgae species (Wright, J.C., Beynon, R.J., and Hubbard, 2010). The combined proteome database of the *Nannochloropsis* genus consisted of 16270 protein sequences.

Figure 4.2 shows a PCA plot for sample clustering and volcano plots revealing significantly differently quantified proteins. The number of protein groups with at least two peptides was 422 and 434 for wild-type and M1 mutant *Nannochloropsis oculata*, respectively. The numbers of significant proteins (> 2-fold changes and p-value < 0.05) were 123 and 103 for the wild-type and M1 mutant strain, respectively (Supplementary Tables S4.1, S4.2).

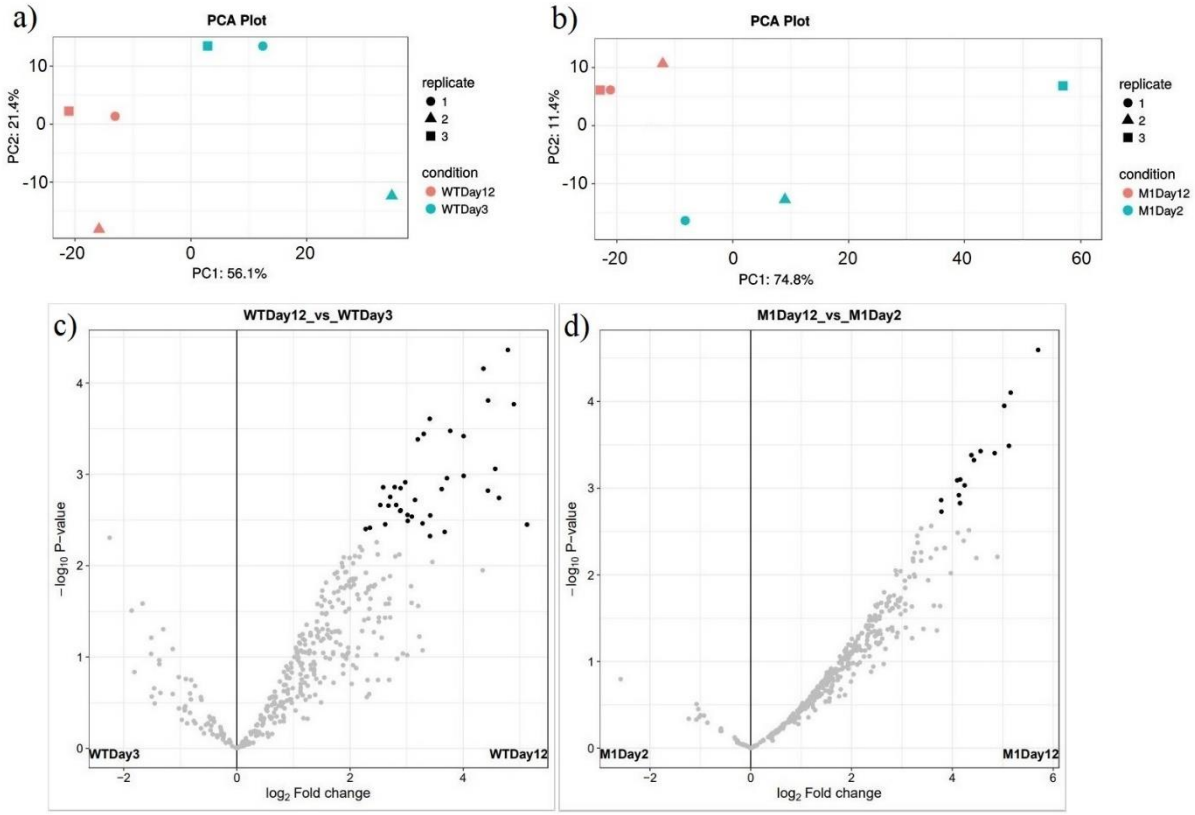

Figure 4.2: PCA plots show 12 samples clustered by biological replicates: Figure 7.8 (a) wild-type *Nannochloropsis oculata* samples day 3 (light blue) and day 12 (pink), Figure 7.8 (b) M1 *Nannochloropsis oculata* samples day 2 (light blue), and day 12 (pink). Volcano plots show the significant protein distributions in wild-type (Figure 7.8 (c)) and M1 mutant (Figure 7.8 (d)) *Nannochloropsis oculata.*

4.3.2. Photosynthetic system

Cell division protein was shown to be 10.4-fold elevated in the M1 mutant strain from early to late exponential phase, compared to 7-fold upregulation in the wild-type strain (Supplementary Table S4.1, S4.2). From the early to late exponential phase, photosynthetic proteins in the M1 mutant were mostly upregulated, including PS I iron-sulfur centre (22.3-fold increase), PS I subunit III (15.7-fold increase), chlorophyll A-B binding protein (13.6-fold increase), PS II 12 kDa extrinsic protein (12.9-fold increase), PS II 11 kDa protein (12.4-fold increase), PS II CP43 reaction centre protein (5.6-fold increase), chloroplast light-harvesting protein isoform 4 (5.5-fold increase), PS I reaction centre subunit IV (5.2-fold increase) and PS I reaction centre subunit XI (4.6-fold increase). The only photosynthetic protein found to increase significantly in the wild-type strain during the period of exponential phase was PS I

reaction centre subunit IV (3-fold increase). From the early exponential to late exponential phase, the M1 mutant strain's Rieske (2f3-2s) region protein was 52-fold increased, while ferredoxin was 29.7-fold elevated. In the wild-type strain, however, the Rieske (2f3-2s) region protein and ferredoxin were not significantly altered during the same growth period (Supplementary Table S4.1, S4.2). Rieske (2f3-2s) region protein and ferredoxin are proteins with similar roles in electron transport chains in the mitochondria and chloroplast for NADPH production (Fukuyama, 2004; Kameda et al., 2011).

4.3.3. FA, TAG, and EPA Synthesis

Figures 4.3 and 4.4 depict the highly expressed protein that may contribute to the production of FAs, EPA, and TAG. LDSP was 8.5-fold elevated in wild-type *Nannochloropsis oculata* from day 3 to day 12 (Figure 4.3). However, LDPS was 34.8-fold elevated from day 2 to day 12 in M1 mutant *Nannochloropsis oculata* (Figure 4.4). At the late exponential phase, the quantity of C16:0 (mg/g DCW) increases by 2.7-fold in wild-type cells, predicting an increase in LDPS production. This amount of change was previously observed in *Nannochloropsis oculata* cells (Tran et al., 2016), where LDSP was elevated 2.4-fold after 11 days of the experimental period. In contrast, In contrast, acyl-coenzyme A dehydrogenase (ACAD) was 35-fold higher in the wild-type strain than in the M1 mutant, where it was just 9.2-fold higher. ACAD is responsible for FA beta-oxidation in mitochondria (Tan and Lee, 2016). The M1 mutant had a 23.6-fold increase in 3-hydroxyacyl-CoA dehydrogenase (HCDH), which was much larger than the increase seen in wild-type *Nannochloropsis oculata* (3.7-fold). The M1 mutant strain had a 13.7-fold upregulation of fatty acid desaturase type 2 (FAD2), whereas the protein was not significant in the wild-type strain. FAD2 is an important membrane protein in the endoplasmic reticulum (ER) that is responsible for the biological switch from oleic acid (C18:1) to linoleic acid (C18:2) (Dar et al., 2017). In the wild-type, 3-ketoacyl-mitochondrial expression was 6.5-fold higher than in the M1 mutant, but there was no difference in expression. On the contrary, 3-ketoacyl-mitochondrial with was 6.5-fold upregulated in the wild-type strain, and no significant changes were recorded in the M1 mutant.

4.3.4. Membrane Lipid Remodelling

Phosphoglucomutase was elevated 11.5-fold in M1 mutant cells compared to only 4-fold in wild-type cells. Phosphoglucomutase is engaged in chrysolaminarin synthesis and serves as a

crucial node in exchanging carbon precursors between carbohydrate and lipid metabolism (Yang et al., 2019b). In this investigation, there were no highly expressed proteins associated to membrane lipids.

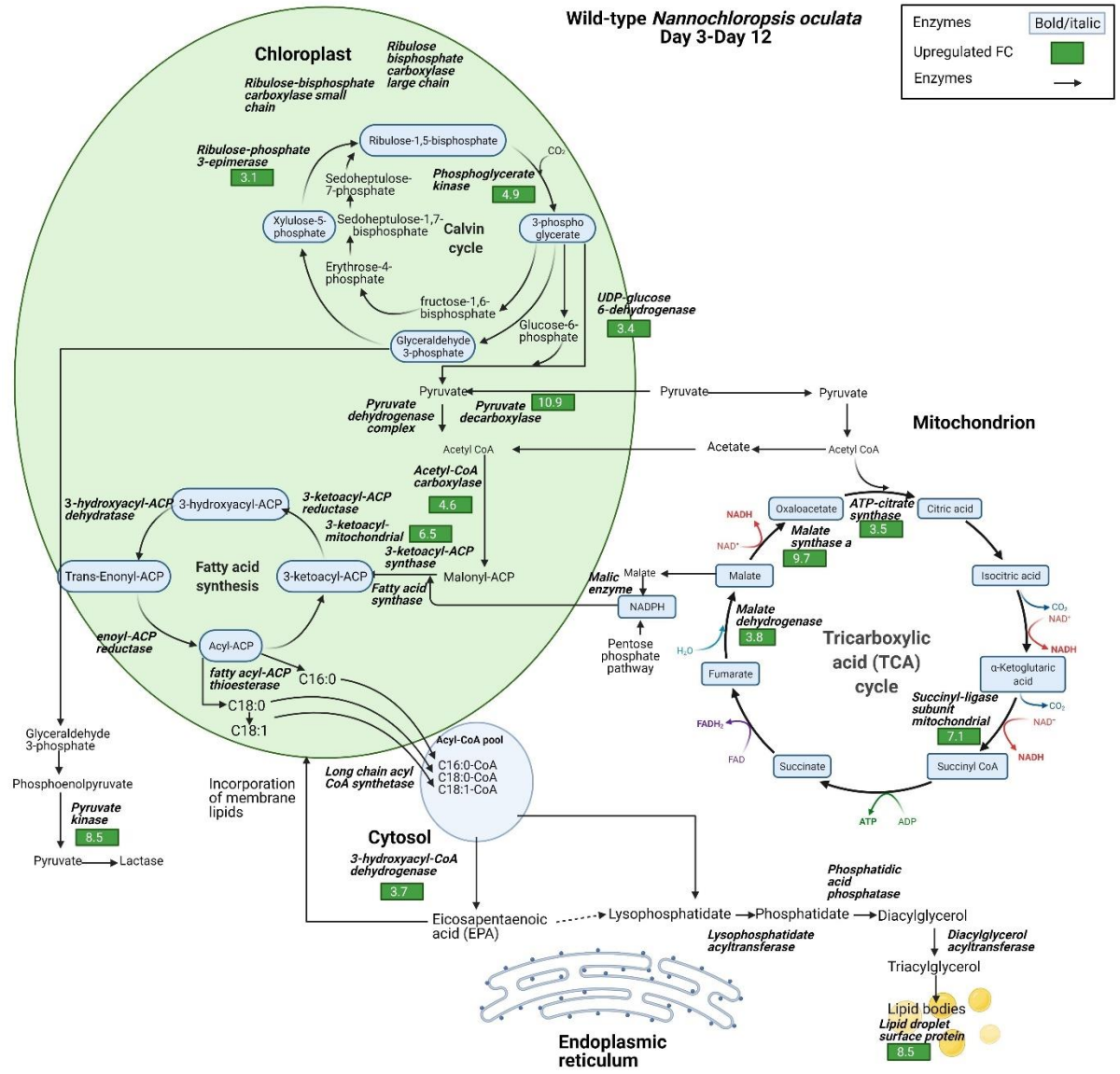

Figure 4.3: Diagram of enzyme regulations from day 3 to day 12 for carbon fixation toward TAG biosynthesis pathways for wild-type *Nannochloropsis oculata*. The diagram shows the pathways and their relation to fatty acid synthesis pathways. Upregulated proteins are shown in the green boxes (Wan Razali et al., 2022).

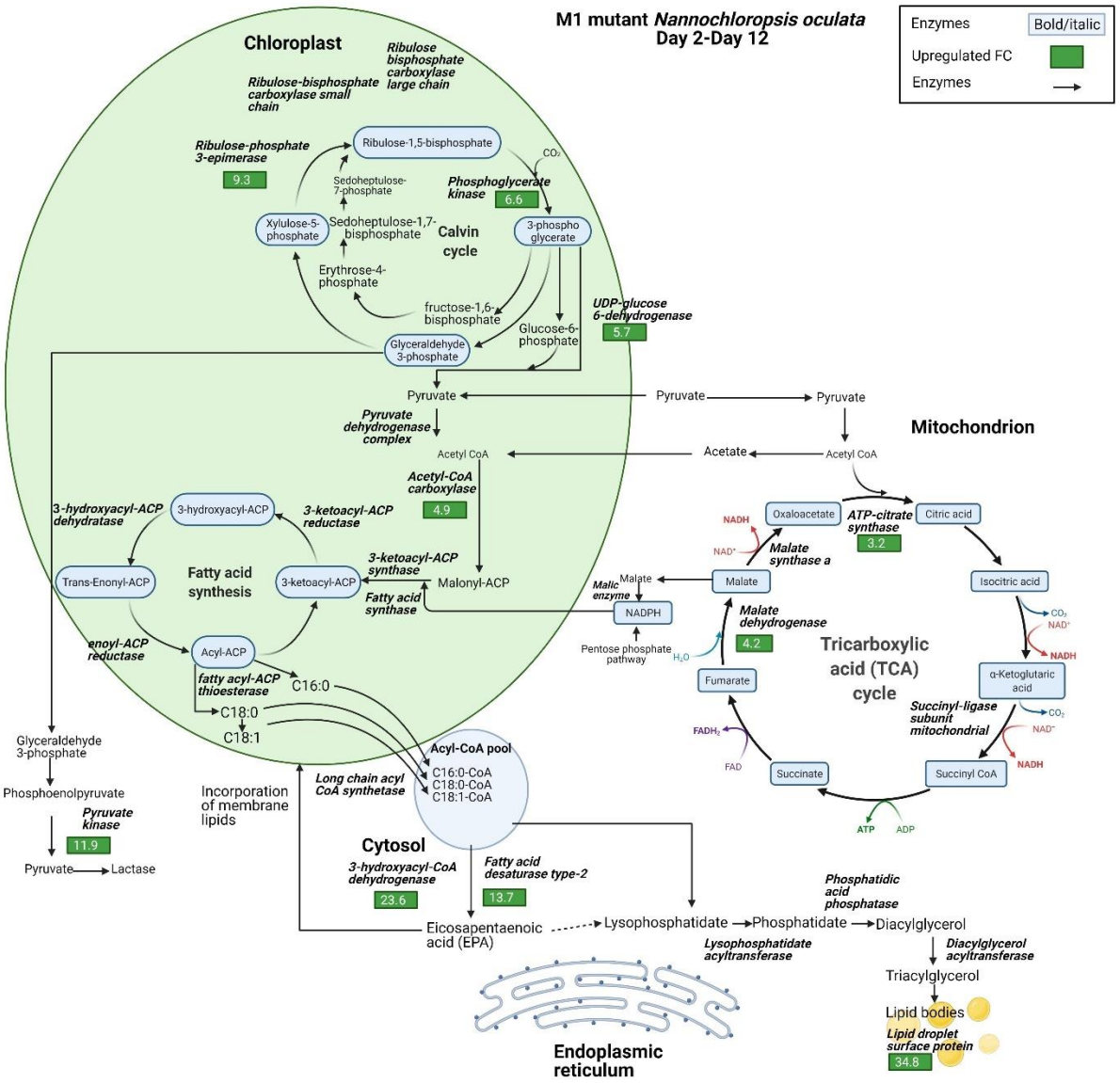

Figure 4.4: Diagram of enzyme regulations from day 2 to day 12 for carbon fixation toward TAG biosynthesis pathways for M1 mutant *Nannochloropsis oculata*. The diagram shows the pathways and their relation to fatty acid synthesis pathways. Upregulated proteins are shown in the green boxes (Wan Razali et al., 2022).

4.3.5. Cellular Location of EPA

Figure 4.5 (a) and (b) show FA analysis that is related to EPA levels in polar lipid and TAG. As the proteomics data suggested that the EPA in the M1 mutant of *Nannochloropsis oculata* may be translocated outside of the chloroplast, the absolute amount and percentage composition of FAME were also determined in the TAG and polar lipid cellular components. The percentage of EPA in TAG was 1.9 times more in the M1 mutant compared to the wild-

type strain. During the early and late exponential phases, the percentage of EPA in the M1 mutant was 2 times and 3.7 times higher than in the wild strain, respectively. The ratio of polar membrane lipids to TAG reduced after 12 days of culturing, demonstrating that TAG was deposited in both wild-type and M1 mutant cells, as shown in Figure 4.5 (b). In the FA pathways, membrane lipids have been reported to translocate to TAG, particularly under nutrient-limited conditions (Janssen et al., 2020).

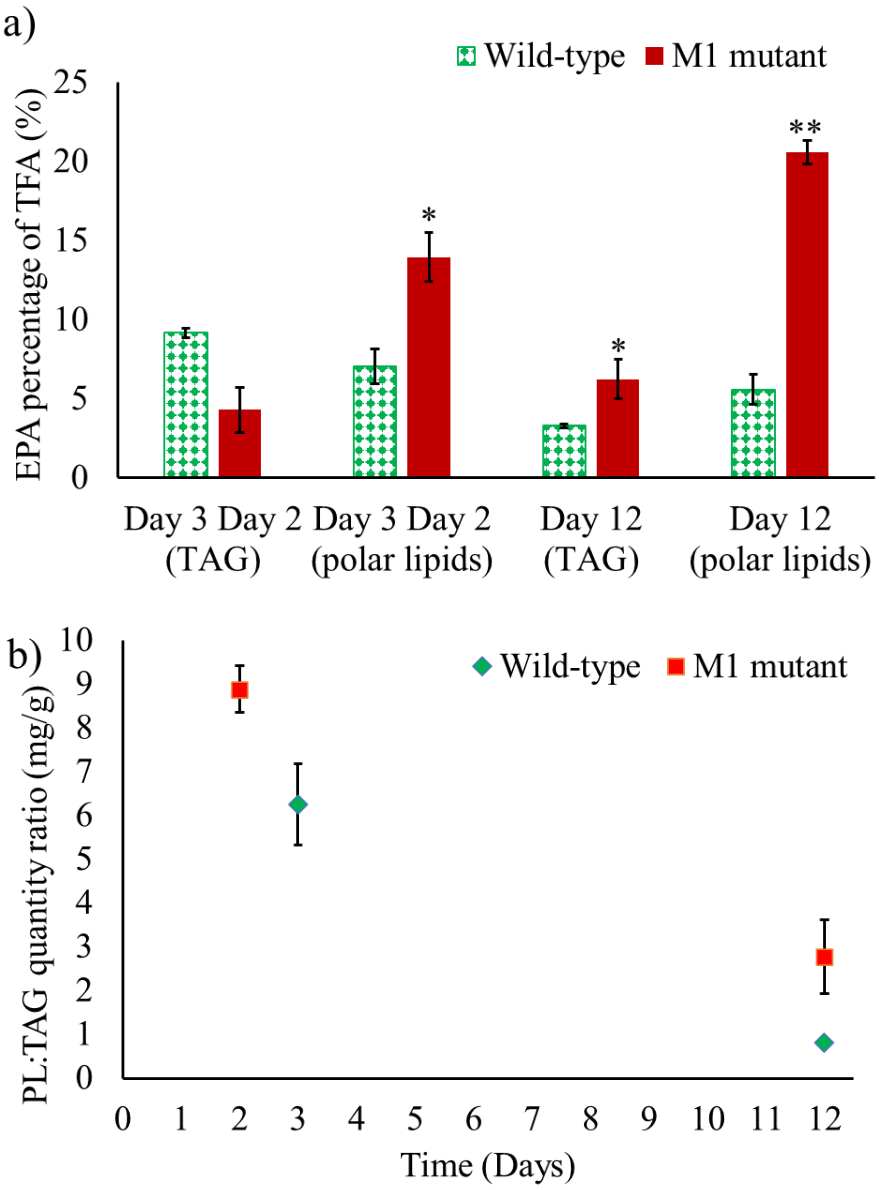

Figure 4.5: Fatty acid content. a) EPA percentages (%) of TFA in polar lipids and TAG at day 2 (M1 mutant), day 3 (wild-type), and day 12 (wild-type and M1 mutant) *Nannochloropsis oculata*. b) Polar lipid (PL):TAG quantity ratio (mg/g) at day 2 (M1 mutant), day 3 (wild-type), and day 12 (wild-type and M1 mutant) *Nannochloropsis oculata*. Mean ± standard deviation

is shown (n = 3) and t-tests determine the statistical significance ($p < 0.05$ [*]; $p < 0.01$ [**]; $p < 0.001$ [***]) for EPA content in the M1 mutant strain compared to the wild-type strain.

4.4. Discussion

4.4.1. Protein profiles

Differential protein expression patterns that potentially contribute to greater EPA production in the M1 mutant *Nannochloropsis oculata* strain were investigated using LFQ proteomics at specific time points. Growth, photosynthetic systems, FA, TAG, EPA synthesis, and membrane remodelling will all be addressed in connection to differential protein analysis. Following a discussion on how they differed, the data were analysed by comparing the early versus late exponential growth phase for the wild-type strain and then the same changeover in the growth phase for the mutant strain.

Quantifying protein content in the microalga cells was crucial for LFQ proteomics analysis. In this study, the microbiuret method was initially used because of the combined sample for chlorophyll-*a* and protein assays. However, the OD reading for the microbiuret method could be interfered with the pigments, especially towards the end of the culturing period. The quartz cuvette requires a thorough cleaning prior to measuring a new sample. In contrast, the nanodrop method used 2D-cleaned samples free from pigment interference. Besides, only 4 µL volume was required, making it a more suitable option for quantifying the protein for LFQ proteomics analysis. 2-D cleaned up-protein (Supplementary Figure S4.3 (a), S4.3 (b)) illustrated protein bands with comparable intensities, indicating the accuracy of the nanodrop method in quantifying the protein.

4.4.2. Photosynthetic system

Photosynthesis is converting and storing solar energy as energy-rich organic compounds by microalgae as a form of energy for cell growth. Cell growth is related to cell division and complex biochemical processes, including cell cycle machinery, cytoskeletal elements, chromosomes and membranes (Üretmen Kagıalı et al., 2017). The M1 mutant's increased cell division protein could be linked to faster cell division compared to the wild-type strain. Microalgae cells use light energy captured by chlorophyll-a molecules to convert CO_2 and

water to carbohydrates and oxygen during autotrophic development. Varying microalgae species and growing conditions have different photosynthesis rates (Costache et al., 2013). The photosynthetic mechanism is organised in organelles, thylakoids, and stroma in chloroplasts. Different microalgae species have different preferences for the chlorophyll-binding group. Chl a/b binding proteins (LHCA/LHCB) are found in Viridiplantae, fucoxanthin Chl a/c binding protein (FCP, or LHCF) is found in diatoms, and LHCR is found in red algae (Carbonera et al., 2014). *Nannochloropsis oculata* has only one plastid and only one photosynthetic pigment, chlorophyll-*a* (Szabó et al., 2014). Increasing the light absorption of light-harvesting antennae is a sustainable strategy to boost microalgae cells' growth rate and biomass output.

The M1 mutant has better photosynthetic efficiency, according to the findings. Since more NADPH is accessible for reductive synthesis processes in the M1 mutant, it contributes to the high efficiency of EPA synthesis. The NADPH availability has been demonstrated to improve the reaction velocity of NADPH-dependent enzymes involved in FA syntheses, such as acetyl-CoA carboxylase (ACCase) and ATP citrate lyase (ATP: CL) (Mühlroth et al., 2013). Overexpression of the Rieske (2f3-2s) region protein, which is involved in NADPH generation, could further confirm NADPH's role in improving photosynthetic activity in the M1 mutant. In a previous study, increased NADPH levels have recently been linked to greater FA production in *Nannochloropsis salina* (Jeon et al., 2021).

4.4.3. FA, TAG, and EPA Synthesis

The proteomic data revealed changes in the relative expression of major enzymes involved in FA, TAG, and EPA production. In both wild-type and M1 mutant *Nannochloropsis oculata*, lipid droplet surface protein (LDSP) was shown to be one of the most differentially expressed proteins. LDSP are putative proteins previously connected to the TAG storage compartment and also linked to lipid droplets in *Nannochloropsis* sp. (Vieler et al., 2012). Furthermore, lipid droplet form is highly dynamic and plays a role in a variety of cellular functions, including energy homeostasis, membrane remodelling, and signalling. (Zienkiewicz and Zienkiewicz, 2020). The significantly larger fold shift in LDSP in the M1 mutant strain, on the other hand, suggests a major change in cell regulation that increases FAs.

ACAD is highly regulated in the wild-type strain, implying that the mutant has a slower rate of FA breakdown than the wild-type. ACAD is responsible for FA beta-oxidation in mitochondria (Tan and Lee, 2016). In the plastid, ACCase converts acetyl-CoA to malonyl-CoA and acts as a carbon donor for FA chain extension (Li et al., 2014). In FA metabolism, 3-hydroxyacyl-CoA dehydrogenase (HCDH) catalyses the conversion of 3-hydroxyacyl-CoA to 3-oxoacyl-CoA. Short and medium-chain HCDH are found in the mitochondrial matrix, while long-chain HCDH is found in mitochondria and peroxisomes as part of the membrane-associated multifunction protein (Xu et al., 2014). Although various enzymes are involved in FA elongation, such as 3-oxoacyl-reductase, 3-hydroacyl-CoA dehydratase, and enoyl-CoA reductase (which converts C16:0 toC18:0) (Kapase et al., 2018), however, the mentioned enzymes were not overexpressed in this study.

The FAD2 protein may play a role in EPA production in the ER. According to the UniProt database and gene ontology functions, 3-ketoacyl-CoA thiolase and 3-ketoacyl-mitochondrial have a similar function that allows for acetyl-CoA C-acyltransferase activity. The 3-ketoacyl-CoA thiolase enzyme involves in FA beta-oxidation in the chloroplast, where acetyl-CoA is catalysed for FA production (Osumi, T., Tsukamoto, T., and Hata, 1992; Kechasov et al., 2020). Another protein with a potential role is 3-ketoacyl-ACP synthase (KAS), an important enzyme involved in FA elongation in plastids (Chaturvedi and Fujita, 2006; Morales-Sánchez et al., 2016).

Three possible spatial routes have been previously suggested for EPA synthesis (Mühlroth et al., 2013); 1) Chloroplast → acetyl-CoA → ER → membrane lipids, 2) Chloroplast → mitochondrion → acetyl-CoA → ER → membrane lipids, 3) Chloroplast → citrate lyase → acetyl-CoA → ER → membrane lipids. It's unclear which pathway is most likely for *Nannochloropsis oculata* wild-type and M1 mutant cells because of the nature of proteomics data with missing proteins. However, when 3-ketoacyl-mitochondrial was 6.5-fold elevated in the chloroplast-mitochondria pathway, it's possible that wild-type *Nannochloropsis oculata* adopted the first or second pathway based on differential protein expression. In the M1 mutant, EPA synthesis may be maximised outside the chloroplast; in the cytosol and ER.

4.4.4. Membrane Lipid Remodelling

Lipidomic studies revealed an increase in neutral lipids accumulation during nitrogen-deprived conditions, in addition to a decrease in membrane lipids (Han et al., 2017; Liang et al., 2019). This suggests that the cellular responses that cause TAG accumulation are linked to membrane lipid alteration. Under nitrogen restriction, MGDG was the most commonly decreased membrane lipid component in *Nannochloropsis oceanica*, which was hypothesised as a protective strategy to avoid thylakoid and chloroplast envelope membrane breakdown (Han et al., 2017). Under phosphate deprivation, the membrane lipid composition was similarly rearranged, with phospholipids being replaced by betaine lipids (Murakami et al., 2020). Membrane lipids in *Nannochloropsis oculata* were similarly remodelled in this study using a combined mutagenesis and selection with galvestine-1 approach. The increase amounts of LDSP expression in M1 mutant *Nannochloropsis oculata* cells suggests that membrane lipids were changed and converted to TAG at considerably greater levels, and thus EPA, which is generally abundant in membrane lipids, was transferred to TAG. The availability of acetyl-CoA and NADPH is a rate-limiting step in balancing growth rate and FA accumulation because both biomass growth and FA synthesis compete for the same substrates (Tan and Lee, 2016). The glycolysis process produces acetyl-CoA conversion, and the key photosynthate enzymes pyruvate kinase (PK) and enolase have been identified (Tran et al., 2016). Carbohydrates in the form of pyruvate are converted to acetyl-CoA to supply the cell with energy and reduced carbon (Mühlroth et al., 2013). Besides, Acetyl-CoA also is a key metabolite in both the TCA cycle in the mitochondrion and FA synthesis in the chloroplast (Mühlroth et al., 2013). A higher carbohydrate metabolic process in M1 mutant cells could indicate a higher quantity of membrane lipids, which could be employed to facilitate higher EPA amounts compared to the wild-type strain.

Identifying protein modifications that contribute to membrane lipid composition remains difficult since very few membrane proteins in algae have been sequenced and analysed. (Garibay-Hernández et al., 2017). MGDG and DGDG are the primary lipids of the photosynthetic membrane, with MGDG being synthesised in the chloroplast and DGDG being synthesised in both the chloroplast and ER (Dolch et al., 2017; Cecchin et al., 2020). The formation of polar membrane lipids is strongly linked to photosynthesis; for example, research suggests that the light-harvesting complex may stabilise the MGDG component in

thylakoid membranes (Han et al., 2017). It's possible that the M1 mutant's elevated membrane lipid content is attributable to more efficient light-harvesting during photosynthesis. As a result, more EPA may be synthesized during the early exponential phase of growth. The reduced MGDG caused more EPA to be translocated outside the membrane lipid as the mutant cells approached the end of the exponential phase, resulting in a higher overall EPA level. Polysaccharides constitute a large part of *Nannochloropsis oculata*'s cell wall architecture, with glucose subunits accounting for 68 % (Scholz et al., 2014). Glucose sourced from the cell wall can be oxidised to provide energy that can be diverted to FA synthesis through the glycolysis process. In a recent study, the *Nannochloropsis oceanica* cell wall altered from two layers with a thickness of 32.9 nm to a one-layer cell wall with a thickness of 37.8 nm under nitrogen starvation (Roncaglia et al., 2021). This suggested that cell wall breakdown may also play a role in FA production.

4.4.5. Cellular Location of EPA

The results of FAME within the TAG and polar lipid provide evidence for the enhanced translocation of EPA to TAG in the M1 mutant strain and could be linked to the elevated abundance of LDSP in this strain. The increased EPA quantity in the M1 mutant is most likely due to the M1 mutant's comparatively high polar lipid production, particularly MGDG. It's likely that the M1 mutant's high MGDG content was preserved until the late exponential phase due to the amount of polar lipids synthesised in comparison to the wild-type strain. As a result, more EPA in the M1 mutant could be translocated to TAG by day 12. In contrast, less MGDG content in the MGDG in the wild-type strain implies that a lower EPA content could be converted to TAG. Hence, EPA could be translocated with membrane lipids to TAG by a structural reform to saturated FA. The EPA, on the other hand, could be directly translocated from the ER to TAG (Ma et al., 2016b); however, this pathway has received less attention in the literature.

4.5. Conclusion

LFQ proteomics analysis was conducted and highlighted metabolic pathways that could contribute in enhancing EPA synthesis, as well as alternative translocation routes between a selected mutant strain and the wild-type strain. Overall, the developed method could be used

as an alternative to genetic engineering methods for increasing EPA production, although cell engineering targets were highlighted for further improvement studies. The developed method could be combined with other selective pressure, such as PSII inhibitors and other related FA synthesis enzymes, to further explore the EPA trafficking route and synthesis. Increasing EPA productivity in industrially relevant microalgal strains increases the sustainable manufacturing of this LC-PUFA.

CHAPTER 5: PILOT-SCALE EXPERIMENTS

5. Feasibility Study of Eicosapentaenoic Acid Production from wild-type and Mutant *Nannochloropsis oculata* using a Pilot-Scale 300 L PhycoFlow® photobioreactor

5.1. Introduction

Currently, there are a variety of studies that have successfully engineered and developed EPA-overproducing *Nannochloropsis* strains, as described in chapter 1 (Chaturvedi et al., 2004; Chaturvedi and Fujita, 2006; Kaye et al., 2015; Poliner et al., 2018; Yang et al., 2019a; Shi et al., 2021). However, most engineered strains are cultivated at a laboratory scale, whereas more research is required at a pilot-scale.

Strains of wild-type *Nannochloropsis* cultured at a pilot-scale are reported in a few studies. In one study, a *Nannochloropsis oceanica* strain cultured in an outdoor pilot-scale raceway pond having a 6000 L culture volume produced 26-29.5 % EPA per cell (Cunha et al., 2020), indicating average EPA content compared to other species of *Nannochloropsis*. The EPA reached 41.56 % of TFA in the *Nannochloropsis gaditana* strain cultured by semi-continuous mode in an outdoor 100 L tubular photobioreactor (Nogueira et al., 2020). In addition, culturing *Nannochloropsis oceanica* in an outdoor 5 L plastic-bag type photobioreactor could reach 41.2 mg/g DCW EPA quantity (Chen et al., 2018b). Furthermore, *Nannochloropsis oculata* and *Nannochloropsis salina* show consistent productivities, indicating the stability and resistance of the microalgae in outdoor photobioreactor systems (Quinn et al., 2012). Therefore, the species of *Nannochloropsis* is expected to reach an optimum growth in outdoor photobioreactor systems.

In general, TEA on the EPA and DHA productivity in wild-type microalgae strains are not able to attain economic parity with fish oils (Chauton et al., 2015). Until recently, there have been only a few published results on techno-economic assessment for the main industrial *Nannochloropsis* species. Besides, all of the studies use prediction models to assess the performance of the species of *Nannochloropsis* from an economic and technical standpoint (Kang et al., 2019; Schade and Meier, 2021; Vázquez-Romero et al., 2022). Alternatively, a pilot-scale photobioreactor experiment offers a better option for predicting the actual EPA

content, increasing the accuracy of developed TEA models. High accuracy data is needed in bridging the models' findings for the future microalga biorefinery plant setup.

This chapter evaluated the performance of wild-type and the M1 mutant *Nannochloropsis oculata* culturing in a 300 L outdoor photobioreactor with standard air and CO_2 as carbon sources. Then, the TEA was conducted to evaluate microalgae oil from an economic standpoint. The EPA content produced at the optimum conditions was integrated into the developed TEA model from a previous study (Schade and Meier, 2021). Net present value (NPV) and return on investment (ROI) were two economic tools used to evaluate the sustainability of developed strain in the scale-up outdoor setup.

5.2. Materials and methods

5.2.1. Microalgae strains

Wild-type strain *Nannochloropsis oculata* (849/1) and EPA-overproducing M1 mutant, developed in chapter 3, were cultured in f/2 media (CCAP, Scotland). 40 L inoculum was prepared in two units of 20 L polycarbonate carboy for the first wild-type experiment. The culture conditions were 130-200 µmol m^{-2} s^{-1} with 12-h light/dark cycles, 20 °C and standard aeration at 2 L/minute. Generally, f/2 medium was added at a 1:1 ratio when the microalgae stock culture reached 0.7 OD at 595 nm.

However, due to difficulty in reaching 1.0 OD at 595 nm of microalga culture, the inoculum for the second, third and fourth batch experimental were initiated in three units of 1 L flasks photobioreactor. The flasks were exposed to 150-200 µmol m^{-2} s^{-1} at 20 °C. When the OD reached 0.7 OD at 595 nm, half of the volume of microalga culture was transferred to 20 L polycarbonate carboy. The carboy was illuminated (130-200 µmol m^{-2} s^{-1}) at 20 °C, while the culture in 1 L flasks was added with a sterile f/2 medium and continued the growth under the mentioned conditions. The cultivating steps were repeated until the inoculum reached 40 L.

5.2.2. Description of Pilot-scale photobioreactor

An outdoor 300 L pilot-scale PhycoFlow® photobioreactor was installed at Arthur Willis Environmental Centre (53.3832000157627° North, -1.4995194567741421° West),

Department of Animal and Plant Sciences, University of Sheffield. The photobioreactor consisted of two stages, the photo stage and the dark stage. The photo stage comprises transparent glass tubes (length: 2.5 m; outer diameter: 54 mm; wall thickness: 1.8 mm) and u-bend glass tubes (width: 234 mm; outer diameter: 54 mm; wall thickness: 2.5 mm; height: 200 mm) connected by using compression twist couplers in a serpentine's arrangement. The serpentine arrangement helps in reducing the pumping requirements and prevents biofilm build-up and contamination. The dark stage consisted of a 300 L holding tank, where the nutrient dosing line, PT 100 thermocouple, and NTC probe for temperature measurement and pH probe were located. The photobioreactor was equipped with a heating and cooling system. An electric heater (Marko Electrical, United Kingdom) and a tap water sprayer (Varicon Aqua, United Kingdom) at the top of glass tubes were used to maintain the set temperature for microalgae growth. Aeration, either filtered-pump air or CO_2, was supplied at the bottom of the holding tank and the initial point of the light stage. A control system was located next to the holding tank, as shown in Figure 5.1. The housing for the control system is an IP66-rated GRP enclosure that is a waterproof system. The control system consisted of 1) a timer controller for aeration; 2) solenoid operation for nutrients dosing; 3) a water-powered injector system for cooling; 4) a temperature and a pH meter controller; 5) a heating control circuit; 6) variable drive pump motor controller; 7) a low-level protection circuit for the pump, heating and cooling circuits; and 8) buttons for initiating and shutting down the photobioreactor.

Commissioning the photobioreactor was started by sterilising the photobioreactor system. Chemical sterilisation is the only appropriate method of cleaning the system from any contaminations. 3 L of 2 % sodium hypochlorite (Alfa Aesar, United Kingdom) was added to approximately 297 L of tap water to give an available chlorine concentration of 200 mg/L. The solution was circulated in the photobioreactor for 24-h. The chlorine was neutralised with 3.42 L of 5 % sodium thiosulphate (Thermo Fisher Scientific, United Kingdom), which is 2.85 times higher concentrations than sodium hypochlorite. The solution was circulated for another 24-h and then drained to remove any particulate in the photobioreactor.

Figure 5.1: An outdoor 300 L PhycoFlow® Photobioreactor that was installed at Arthur Willis Environmental Centre (53.3832000157627° North, -1.4995194567741421° West), Department of Animal and Plant Sciences, University of Sheffield.

Prior to starting the culturing, 270 L of tap water was supplied to the holding tank, 10 kg of instant ocean marine salt was added to make the artificial seawater that had 33.5 g/L salinity levels, 750 mL of 2% sodium hypochlorite was added to give an available chlorine concentration of 50 mg/L, and the solution was circulated for 24-h. 855 mL of 5 % sodium thiosulphate was added, and the solution was circulated for 24-h. Sterile nutrients were added to prepare f/2 medium (CCAP, Scotland) in the photobioreactor.

In general, 40 L of exponential phase *Nannochloropsis oculata* having approximately 1.125 OD at 595 nm was added to the prepared f/2 medium in the 300 L photobioreactor to prepare the initial culture concentration of around 0.15 OD at 595 nm. During operation, the culture was circulated at a liquid velocity of approximately 0.42 m/s for 24-h by a CO4-350/02K 3-phase SS pump (ITT Lowara, United Kingdom). During the operation of the first and second batch experiments, the culture was aerated with non-sterile air continuously for 24-h using an ACQ-007 air compressor (Boyu, Beijing, China) at a rate of 1.18 L/minute. Meanwhile, pure CO_2 was supplied daily to regulate the pH range of 7-8.5. 4.5 and 4 % CO_2 were used for wild-type and M1 mutant *Nannochloropsis oculata*, respectively. Outdoor temperature was recorded manually by referring to Sheffield's daily weather forecast report. Whereas photobioreactor temperature and pH were recorded from the photobioreactor control panel. In addition, the pH was also monitored using a portable pH meter LAQUA B-712 (Horiba, Moulton Park, United Kingdom). Light intensity was measured using a digital light meter (LX1330B, Dr. meter, China) for the third and fourth experiments.

A volume of 1 L sample was taken at 9 a.m. every day over a 15-day experimental period and immediately transferred to the A03 laboratory in Sir Robert Hadfield Building, University of Sheffield. Then, the OD at 595 nm was measured to monitor microalga growth quickly. A volume of 5 ml culture was allocated for each analysis of DCW, proteins and chlorophylls, lipids, and EPA. The samples were collected in three technical replicates for all analyses. Harvested cells pellets (centrifuge at 4,415 × g for 5 minutes) were washed with phosphate-buffered saline and centrifuged (11,337 × g for 2 minutes) prior to storage at −20 °C. The supernatant was used for the nitrate and phosphate uptake assays, as described in chapter 2.

5.2.3. Techno-economics assessment

The TEA was conducted by integrating the optimum EPA quantity into the developed TEA model by a previous study (Schade and Meier, 2021). Therefore, the average EPA quantities from day 4 until day 7 for wild-type and M1 mutant cultured with supplied CO_2 were 57.61 and 87.02 g EPA /kg DCW, respectively, selected for TEA analysis. Meanwhile, the baseline data for the TEA model was 42 g EPA / kg DCW and estimated at 13,225 kg/annum of microalga oil production (Schade and Meier, 2021), as shown in Table 5.1.

Table 5.1: Parameters and input of microalga biomass, lipid, and EPA production comparisons for baseline *Nannochloropsis* sp., wild-type, and M1 mutant *Nannochloropsis oculata*. All other parameters and input are considered as constant variables and similar to the baseline *Nannochloropsis* sp.

Parameter	**Unit**	**Baseline *Nannochloropsis* sp. (Schade and Meier, 2021)**	**Wild-type *Nannochloropsis oculata* (this study)**	**M1 mutant *Nannochloropsis oculata* (this study)**
Lipids	g/kg DCW	206	206	206
EPA	g/kg DCW	42	57.6	87.02
Total microalga cell yield	kg/1.2ha/annum	64,200	64,200	64,200
Biomass residue	kg/1.2ha/annum	50,917	50,917	50,917
Microalga oil	kg/1.2ha/annum	13,225	13,225	13,225
Land	ha	1.2	1.2	1.2

The temperature and hours of daylight comparison between the location used for the mentioned model study, Halle, Germany and this study based in Sheffield, United Kingdom, are shown in Table 5.2. The data comparison shows that the high-temperature average is within range for strains of *Nannochloropsis* culturing, and the hours of daylight are comparable, enabling Schade and Meier (2021) model to be used for assessing the wild-type and M1 mutant strain culturing in Sheffield, United Kingdom.

Table 5.2: Average daily temperature and hours of daylight comparison between Halle, Germany and Sheffield, United Kingdom, referring to a forecast website (https://weatherspark.com/). The website uses the NASA climate model, Modern Era Retrospective-analysis for Research and Applications (MERRA-2, https://gmao.gsfc.nasa.gov/reanalysis/MERRA-2/).

Place	**Conditions**	**June**	**July**	**August**
Halle, Germany	High-temperature average (°C)	22	24	24
	Low-temperature average (°C)	12	14	14
	Hours of daylight (h)	16.6	16.1	14.5
Sheffield, UK	High-temperature average (°C)	18	20	20
	Low-temperature average (°C)	10	12	12
	Hours of daylight (h)	16.9	16.4	14.7

Referring to the baseline data by Schade and Meier (2021), the new baseline was obtained for wild-type and M1 mutant *Nannochloropsis oculata*, respectively. Then, there were four scenarios considered for the M1 mutant strain. The first scenario considered a faster growth rate of 28.3 % than the wild-type strain. The faster growth rate indicates that each experiment could reach a higher EPA quantity. In the second scenario, the baseline study increased the culturing operations to 80 % (292 days) instead of 50 % (183 days). The increase of working days to 80 % was considered in order to optimise the profits gained, hence shortening the payback period. In the third scenario, the potential of M1 mutant to produce 50 % higher biomass due to sunlight availability throughout the year in tropical countries such as Malaysia. These scenarios are crucial in influencing production costs (Chauton et al., 2015). The fourth scenario combines the changes made in all scenarios (Scenario 1, 2 and 3) to achieve an overall 'best-case' scenario (Leflay et al., 2020). Net present value (NPV) was calculated by referring to the equation:

$$NPV_n = \frac{NCF}{(1+d)^n},$$

where NCF is the net cash flow of a time period *n*, and *d* is the nominal discount rate set at 12 % (Schade and Meier, 2021). Return on investment (ROI) was calculated by referring to the equation:

$$ROI = \sum_3^n \frac{NPV_n - C_{tot}}{C_{tot}},$$

where total costs C_{tot} represents the sum of payments assigned in the first and second year when all investment costs were paid (Schade and Meier, 2021).

5.3. Results

5.3.1. Physiological and biochemical analysis of wild-type *Nannochloropsis oculata* supplied with standard aeration

The outdoor culturing was conducted for 15 days from 17th august 2018 until 1st September 2018. On day 0, it was a sunny day and partly cloudy weather, with an outdoor temperature of 20 °C, considered ideal for initiating the first experiment, as shown in Figure 5.3 (a). The wild-type *Nannochloropsis oculata* grew well for the first 3 days and reached 0.46 OD at 595 nm, with an average of 0.38/day growth rate, while the pH was escalated to 9.5 as shown in

Figure 5.2 (a). On day 4, the growth rate suddenly dropped to 0.05/day, while on day 5, the growth decreased at a rate of -0.09/day. The pH on days 4 and 5 was maintained at around 9.8. The microalga culture struggled to grow, while the pH was increased until 10 on days 6 and 7. In previous studies, a pH higher than 9 decreased microalga growth, as demonstrated in an earlier study (Bartley et al., 2014), while 8.5 enhanced the growth (Khatoon et al., 2014). Therefore, the pH must be immediately regulated to salvage microalga culture from dying. An amount of 0.25 g/L of sodium bicarbonate was added for 3 days on days 7, 9 and 11. As a result, the growth rate had increased again to 0.26/day. Microalga cells reached the stationary growth phase on day 13, with the 1.39 OD at 595 nm. In this first batch experiment, the average temperature inside the photobioreactor was 24.5 °C with an average 14.14-h/9.86-h (light/dark) cycle.

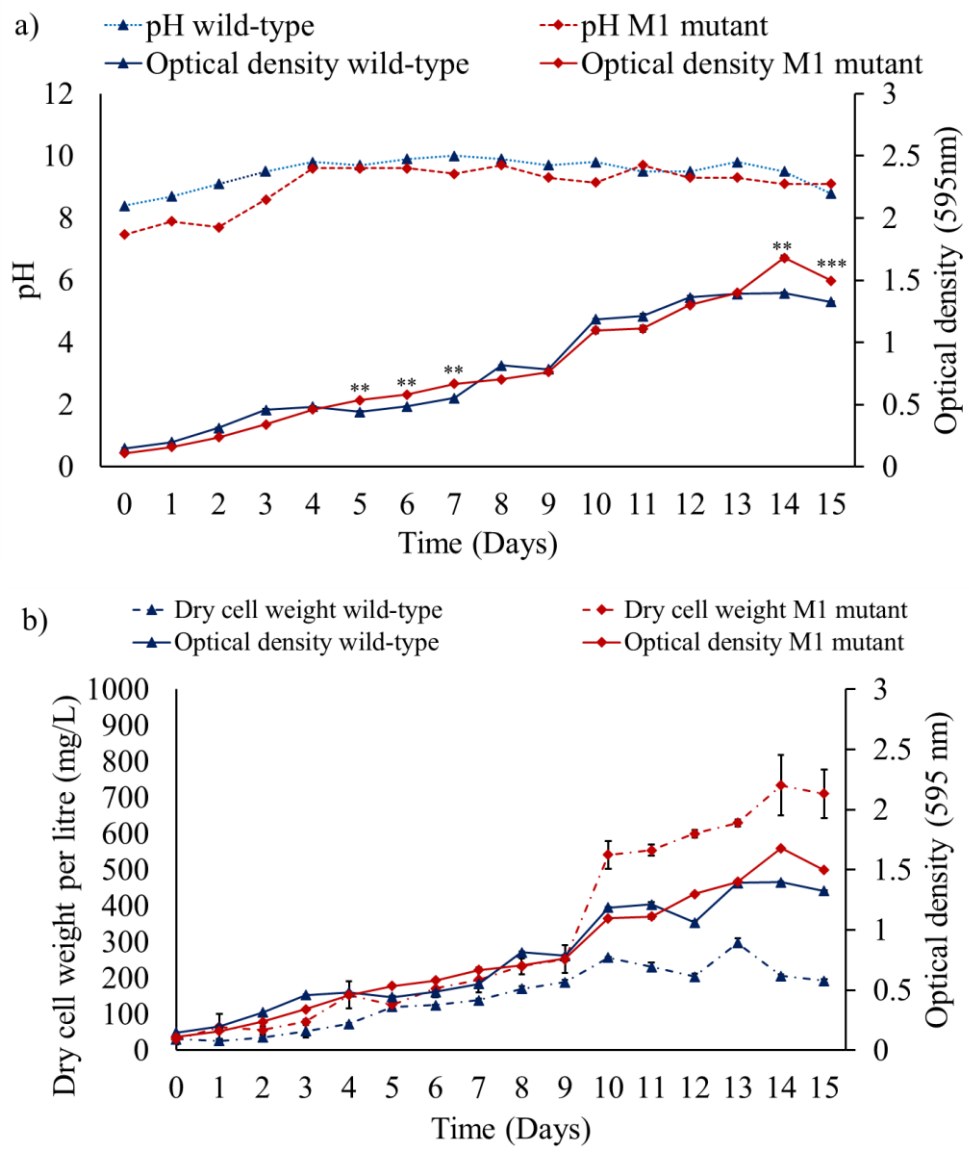

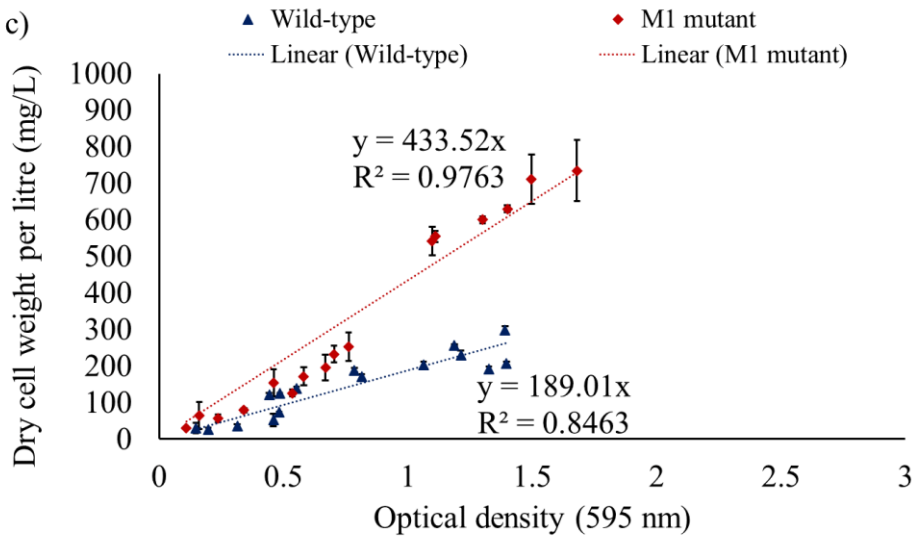

Figure 5.2: Growth profiles for wild-type and M1 mutant *Nannochloropsis oculata* cultivated in an outdoor 300 L Photobioreactor supplied with standard aeration. a) Optical density at 595 nm and pH profiles, b) and c) dry cell weight and optical density correlation. Mean ± standard deviation is shown (n = 3) for each day.

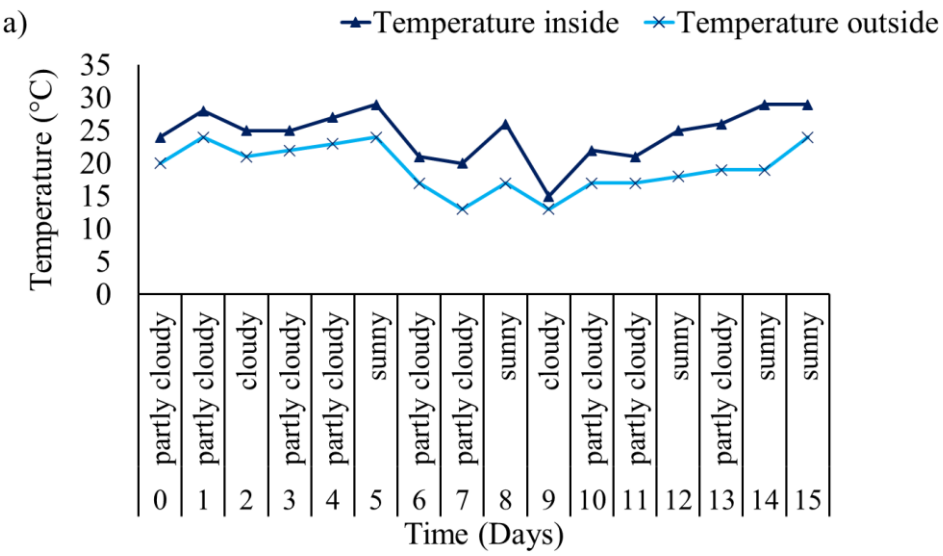

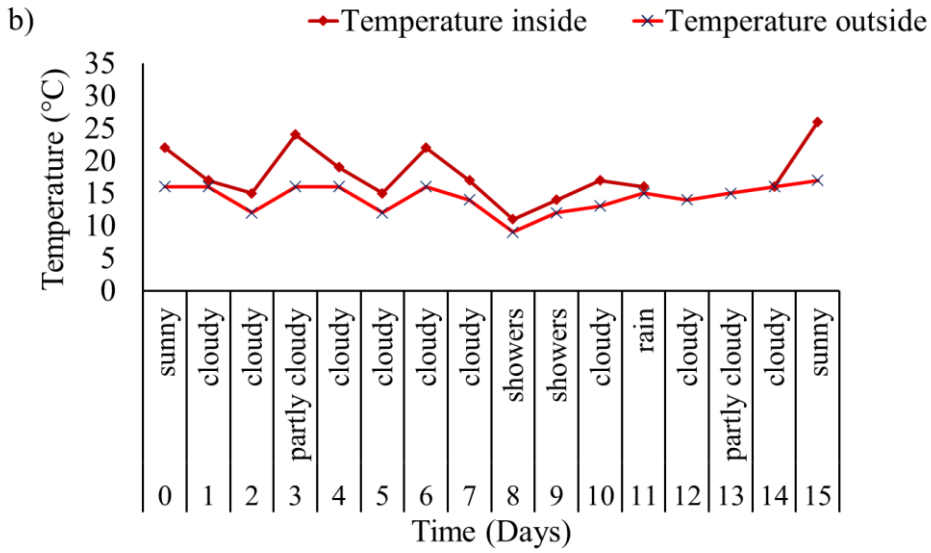

Figure 5.3: Temperature and weather profiles throughout 15 days experimental period: a) wild-type supplied with standard aeration, b) M1 mutant *Nannochloropsis oculata* supplied with standard aeration.

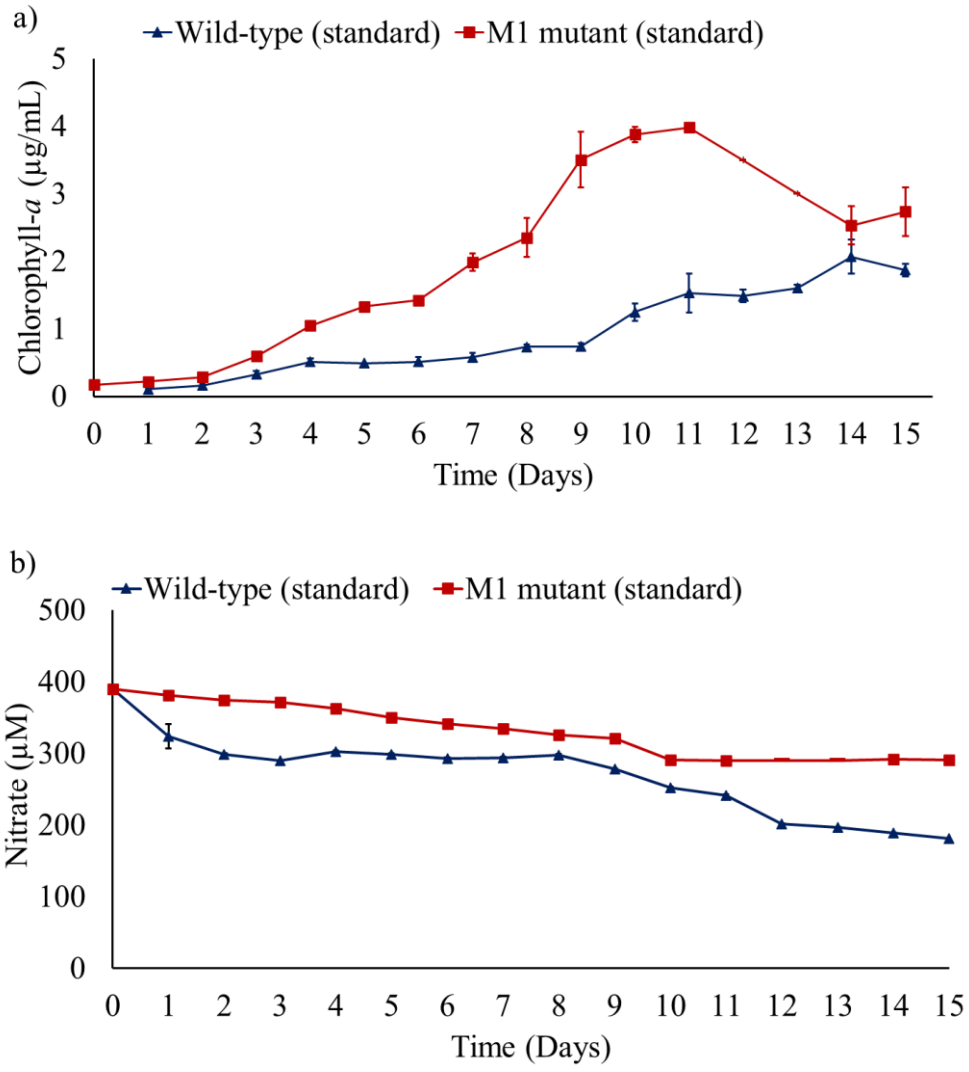

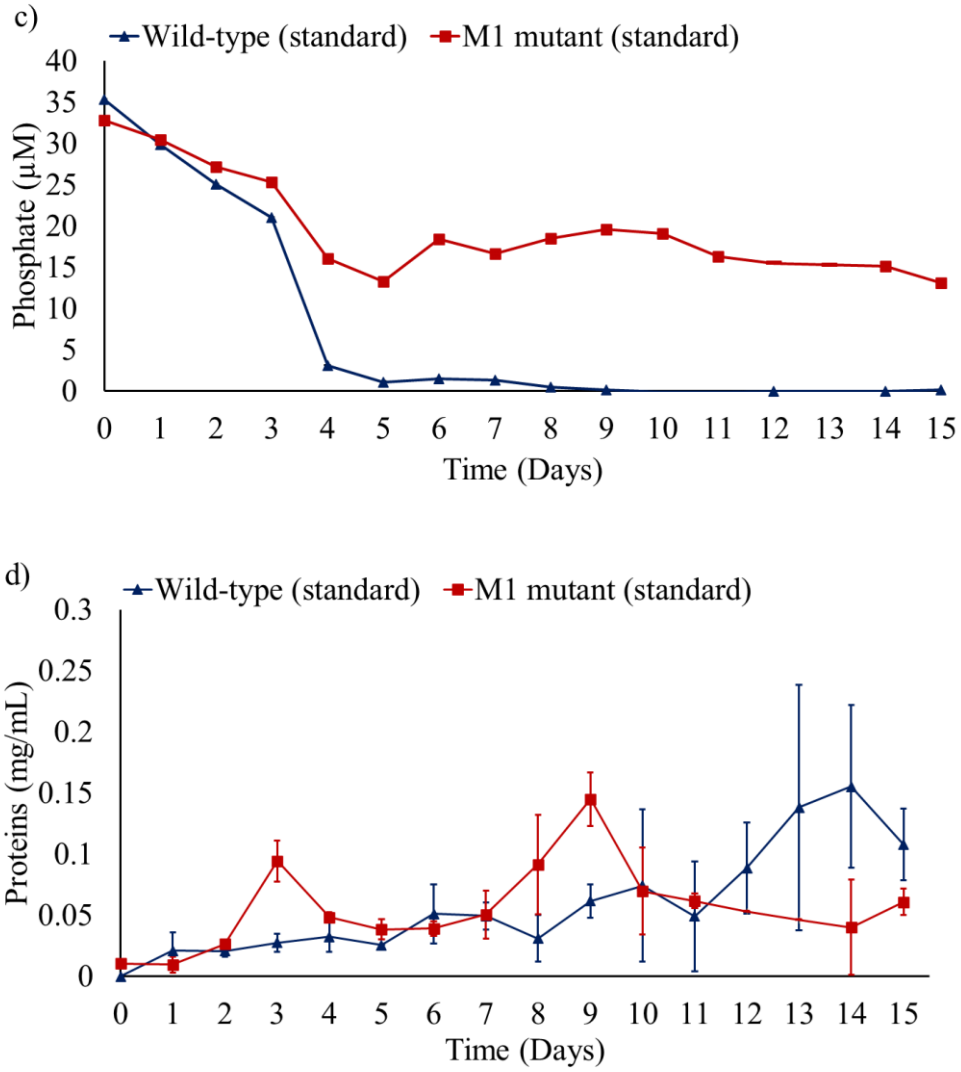

Figure 5.4: Profiles for wild-type and M1 mutant *Nannochloropsis oculata* cultivated in an outdoor 300 L pilot-scale photobioreactor supplied with standard aeration. a) Chlorophyll-*a*, b) nitrate uptake, c) phosphate uptake, and d) protein quantity profiles. Mean ± standard deviation is shown (n = 3) for each day.

Chlorophyll-*a* profile for wild-type strain was directly proportional to the OD profile, as shown in Figure 5.4 (a). The chlorophyll-*a* was increased until day 4 (0.5 µg/mL) and maintained at the same level until day 6. From day 7 onwards, the chlorophyll-*a* was slowly increased and reached the highest chlorophyll-*a* content (2.07 µg/mL) on day 14. Then, the chlorophyll-*a* decreased on day 15 (1.87 µg/mL). Nitrate and phosphate uptakes are shown in Figures 5.4 (b) and (c), respectively. The nitrate uptake rate was 0.14/day until day 2, decreased to 0.03/day on day 3, and no nutrient uptake was demonstrated until day 8. After adding sodium bicarbonate, the nitrate uptake was increased at 0.1/day until day 12 and dropped to

0.04/day until day 15. On the contrary, a rapid phosphate uptake was observed, an average of 0.17/day until day 3 and 4.16/day on day 4. On day 8, all the phosphate was consumed by microalga cells. The protein content profile ranged from 0.021 to 0.025 mg/mL from day 1 until day 5, as shown in Figure 5.4 (d). Then, the protein content was slightly increased to 0.05 mg/mL on days 6 and 7 and reached the highest 0.16 mg/mL on day 14. In contrast, the protein started to drop on day 15 at the end of the exponential growth phase.

FA contents for wild-type *Nannochloropsis oculata* supplied with standard aeration are shown in Figures 5.5 (a) and 5.6 (a). TAG (C16:0) percentage fluctuated throughout the culturing period. The C16:0 had the highest percentage (33.64 %) on day 0 and showed a decrease percentage (29.69 %) on day 4. The EPA had a 6.23 % on day 0 and showed a decrease on day 1 (4.15 %). Then, the EPA gradually increased as the growth progressed and reached 18.30 % on day 5. When the stagnant growth was on days 4 and 5, monounsaturated FA profile C16:1 steadily increased and reached the highest level (36.62 %) on day 10. During the optimum growth from day 8 until day 13, the C16:0 and C16:1 gradually decreased while the EPA percentage (22.33 %) reached the highest level on day 13. Whereas on days 14 and 15, the EPA again reduced to around 17 %, while the C16:0 increased to a range of 28-30 %.

The quantity of FA (mg/g DCW) (Figure 5.6 (a)) indicated an increasing trend and reached the highest EPA quantity (58.85 mg/g) at the end of the experimental period, day 15. The FA C16:0 and C16:1 recorded the highest quantity range of 125-128 and 140-142 mg/g DCW, respectively, from day 14 until day 15.

5.3.2. Physiological and biochemical analysis of M1 mutant *Nannochloropsis oculata* supplied with standard aeration

This time, the weather conditions were completely different from the previous experiment due to the rain and cloudiness on most days. Only 4 days were sunny and partly cloudy, while the rest were cloudy and showers (Figure 5.3 (b)). Despite the unfavourable weather, the growth rate reached 0.36/day from day 0 until day 4, while the pH was around 9.6. Then, the growth rate dropped to 0.13/day from day 4 until day 7, while the pH maintained around 9.6. 0.25 g/L of sodium bicarbonate was added for 3 days on days 7, 9 and 11 to regulate the pH in the M1 mutant culture. As a result, the growth rate increased again to 0.16/day and

reached the maximum of 1.68 OD at 595 nm on day 14. In addition, the pH decreased to around 9.3, as shown in Figure 5.2 (b). The average temperature inside the photobioreactor was 17.93 °C with an average 16.89-h/7.11-h (light/dark) cycle.

Chlorophyll-*a* content for M1 mutant showed a 2.1-fold higher than wild-type strain on day 4, as shown in Figure 5.4 (a). On day 11, when the growth was at an optimum level, the M1 mutant chlorophyll-*a* content was 2.6-fold higher than the wild-type strain. The nitrate uptake showed wild-type strain (0.07/day) had a higher uptake than the M1 mutant (0.05/day) on day 11. The phosphate uptake rate for wild-type was approximately 9 times faster than the M1 mutant on day 4. At the end of culturing period day 15, the final phosphate concentration in the M1 mutant culture was 13.12 µM. The protein profile was directly proportional to the chlorophyll-a profile, as shown in Figure 5.4 (d).

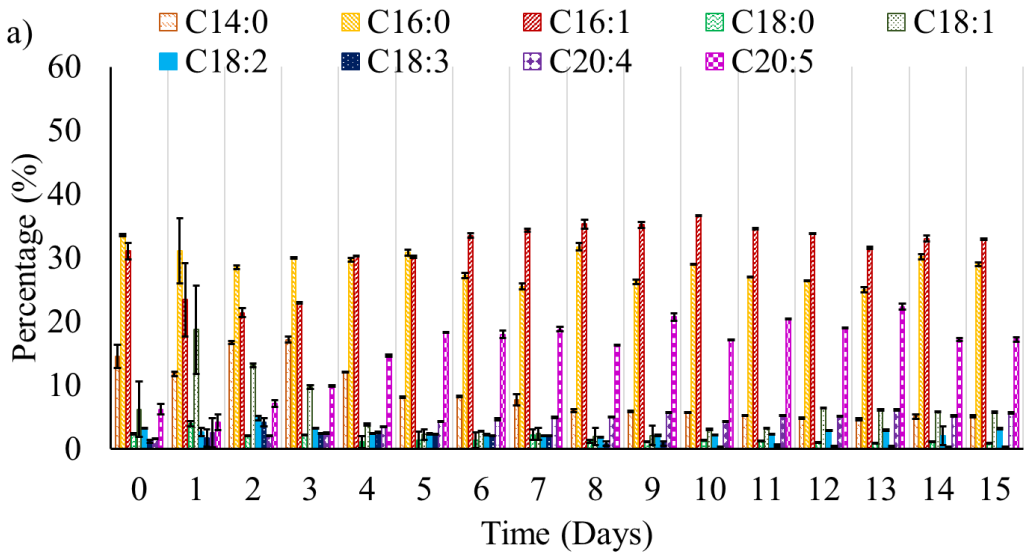

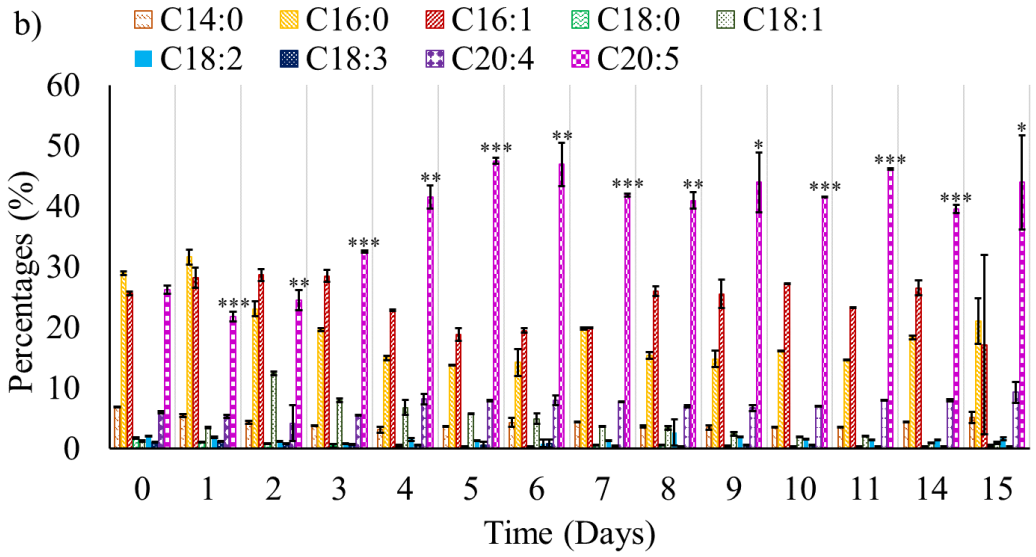

Figure 5.5: Percentage of primary fatty acids profiles: a) wild-type, and b) M1 mutant *Nannochloropsis oculata* (standard aeration). The data show the mean value and standard deviation of three technical replicate samples. Asterisks indicate the significant differences that were determined by Student's t-test (*p<0.05, **p<0.01, ***p<0.001).

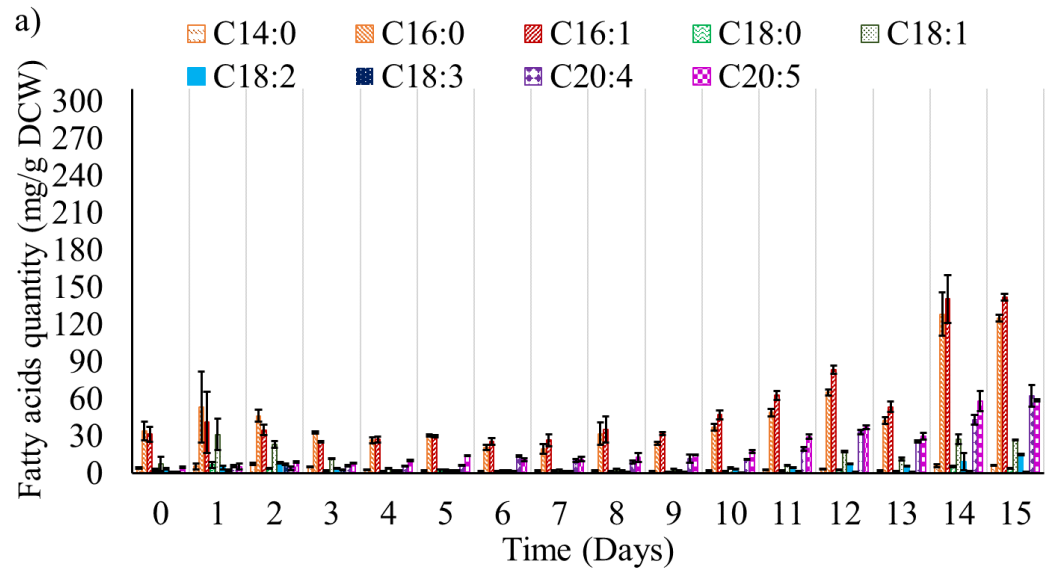

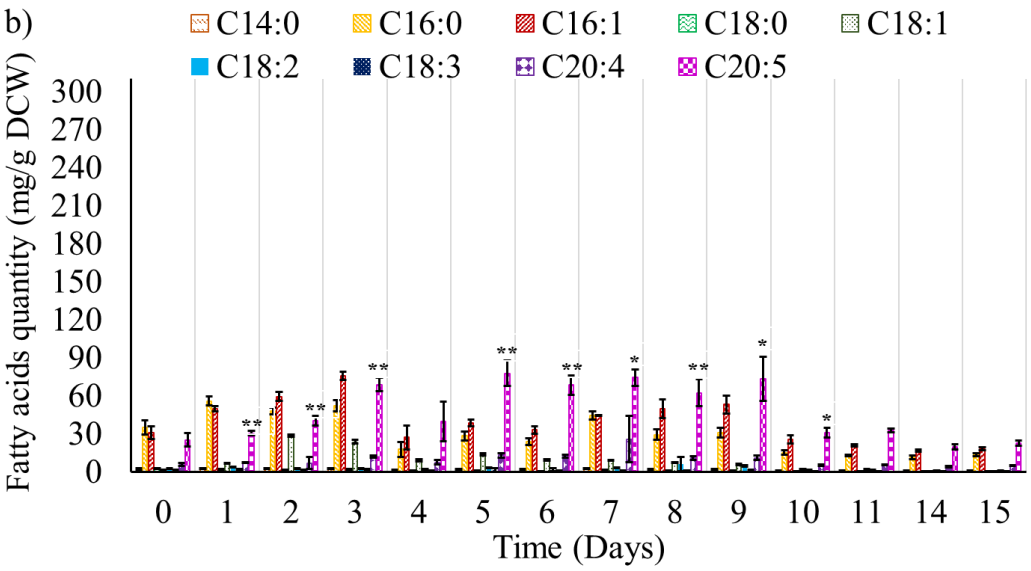

Figure 5.6: Quantification of main fatty acids profiles: a) wild-type, and b) M1 mutant *Nannochloropsis oculata* (standard aeration). The data show the mean value and standard deviation of three technical replicate samples. Asterisks indicate the significant differences that determined by Student's t-test (*p<0.05, **p<0.01, ***p<0.001).

FA contents for M1 mutant *Nannochloropsis oculata* supplied with standard aeration are shown in Figures 5.5 (b) and 5.6 (b). The C16:0 had 28.96 % on day 0 and increased to 31.65 % on day 1. The C16:0 and C16:1 remained below 21 and 27 %, respectively, from day 4 until day 15. The EPA percentage increased starting from day 2 and reached the highest 47.52 % on day 5. The EPA percentage remained at the same level with a range of 39-46 %, which is remarkably more elevated than the wild-type strain. The FA quantity results were consistent with the FA percentage, where the EPA quantity was the highest on day 5 (77.58 mg/g DCW), while the C16:0 and C16:1 were lower in amount than EPA from day 4 until day 15.

5.3.3. Physiological and biochemical analysis of M1 mutant Nannochloropsis oculata supplied with CO2

On 27 July 2019, the M1 mutant Nannochloropsis oculata experiment was conducted in a 300 L photobioreactor for a 15-day period. In order to overcome the pH issue, CO2 was used instead of standard aeration. The growth started with a lag growth phase from day 0 until day 2 due to partly cloudy weather with a temperature range of 16-17 °C, as shown in Figure 5.8 (b).

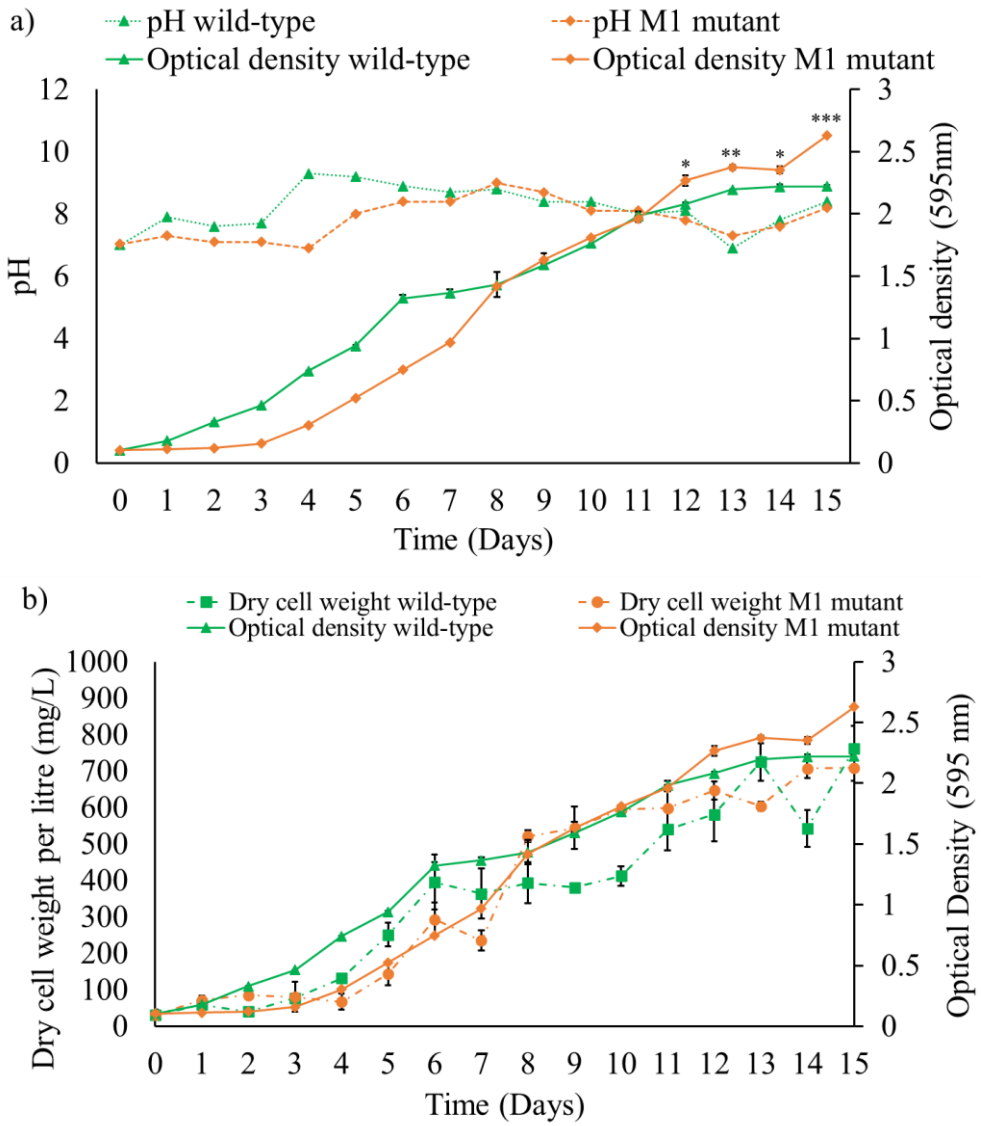

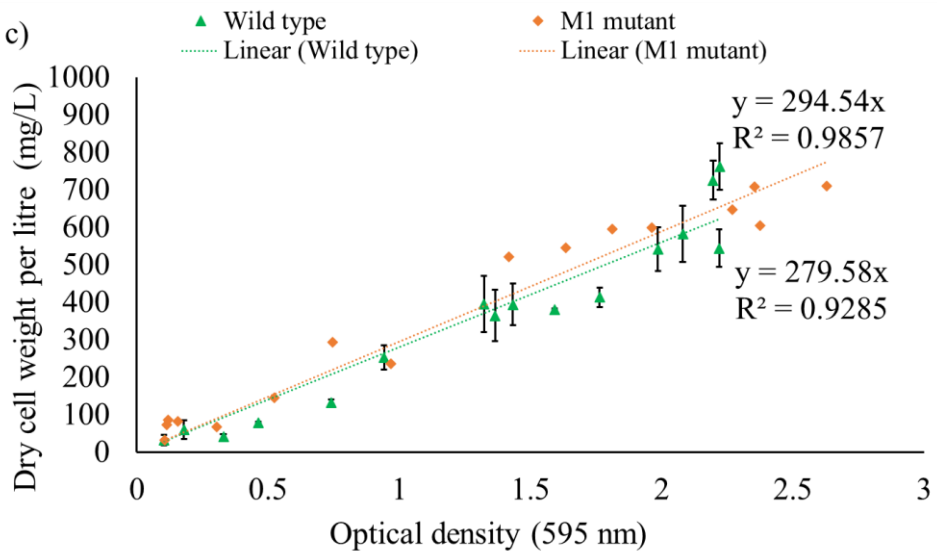

Figure 5.7: Growth profiles for wild-type and M1 mutant *Nannochloropsis oculata* cultivated in an outdoor 300 L Photobioreactor supplied with CO_2. a) Optical density at 595 nm and pH profiles, b) and c) dry cell weight and optical density at 595 nm correlation.

When the weather condition was improved on day 3, the growth rate sharply increased (0.38/day) from day 4 to day 8. The microalga cells continued to grow at a slower rate (0.12/day) from day 9 to day 12 and reached the end of the exponential growth phase on day 13. However, the OD suddenly increased again on day 15 with 2.63 OD at 595 nm. Day 3, 8 and 9 were the highest temperature recorded, with 23, 25 and 24 °C, respectively. The average temperature throughout the experimental period was 19.94 °C, and the average light intensity was 969.6 µmol m^{-2} s^{-1} with a 15:53-h/8.47-h (light/dark) cycle.

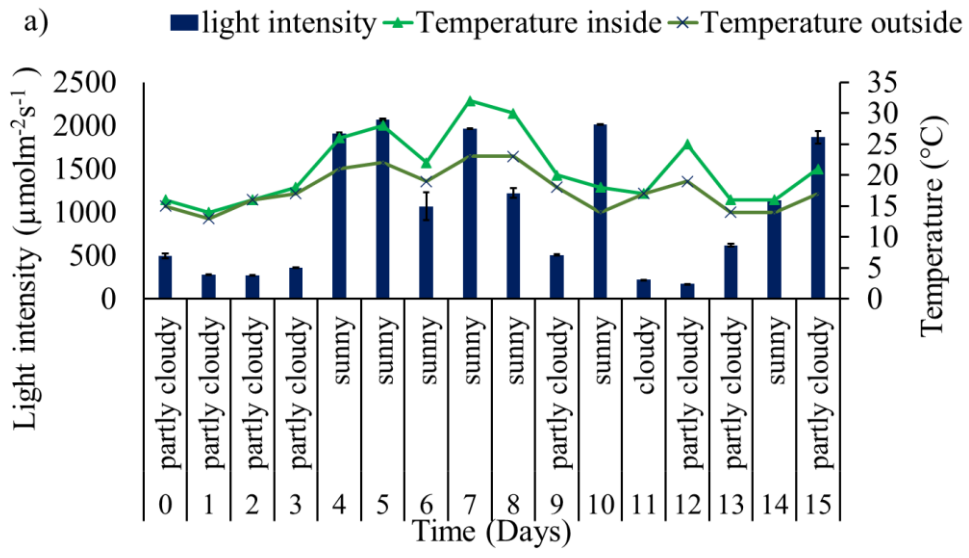

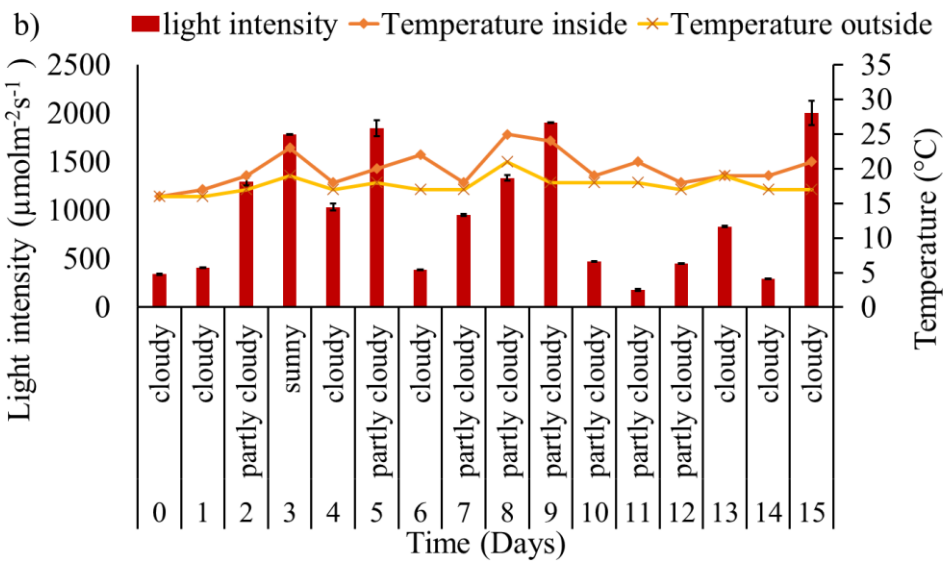

Figure 5.8: Temperature and weather profiles throughout 15 days experimental period: a) wild-type supplied with CO_2, b) M1 mutant *Nannochloropsis oculata* supplied with CO_2.

Chlorophyll-*a* was directly proportional with the OD profile, as expected. The chlorophyll-*a* had a rapid increase from day 4 until day 8, moderately increased until day 14, and showed a decrease amount on day 15, as shown in Figure 5.9 (a). The highest chlorophyll-*a* was recorded on day 14 with 3.94 µg/mL. The nitrate profile showed that the nutrient was thoroughly utilised on day 10, while phosphate was wholly and rapidly used on day 3 as shown in Figures 5.9 (b) and (c), respectively. The nitrate uptake rate was at the optimum level (1.46/day) from day 5 to day 10, while the uptake rate for phosphate was 4.47/day from day 3 until day 4. The protein content for the M1 mutant showed a remarkable higher, especially from day 8 until day 12, with a range of 0.22 to 0.38 mg/mL, as shown in Figure 5.9 (d).

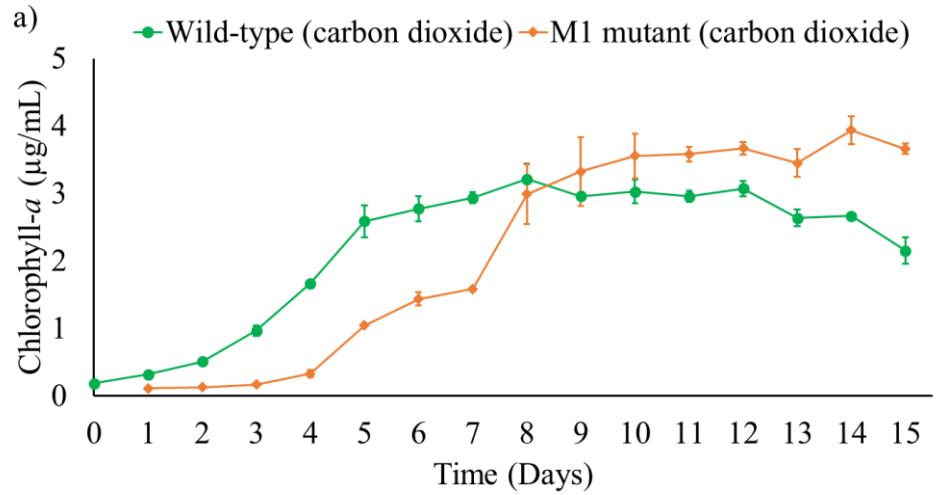
a)
Wild-type (carbon dioxide)
M1 mutant (carbon dioxide)
Chlorophyll-a (µg/mL)
0
1
2
3
4
5
0 1 2 3 4 5 6 7 8 9 10 11 12 13 14 15
Time (Days)

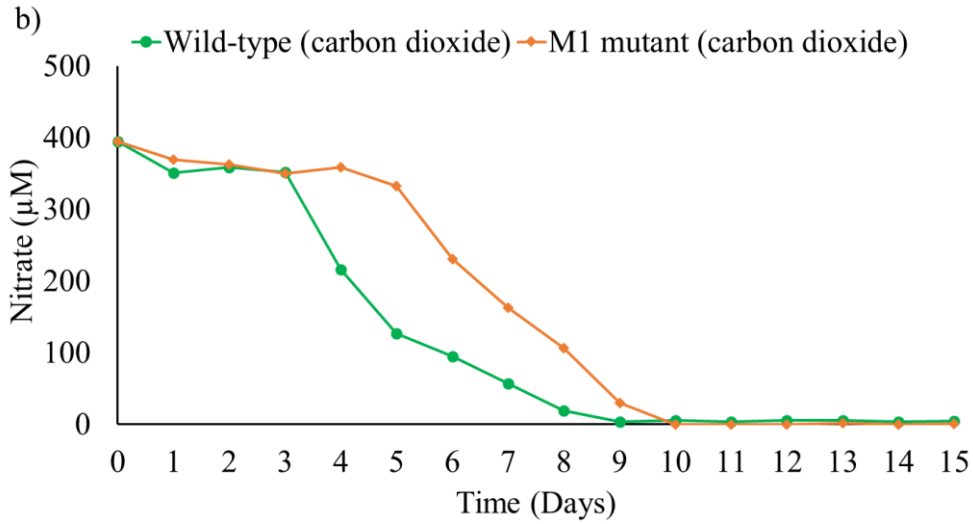
b)
Wild-type (carbon dioxide)
M1 mutant (carbon dioxide)
Nitrate (µM)
0
100
200
300
400
500
0 1 2 3 4 5 6 7 8 9 10 11 12 13 14 15
Time (Days)

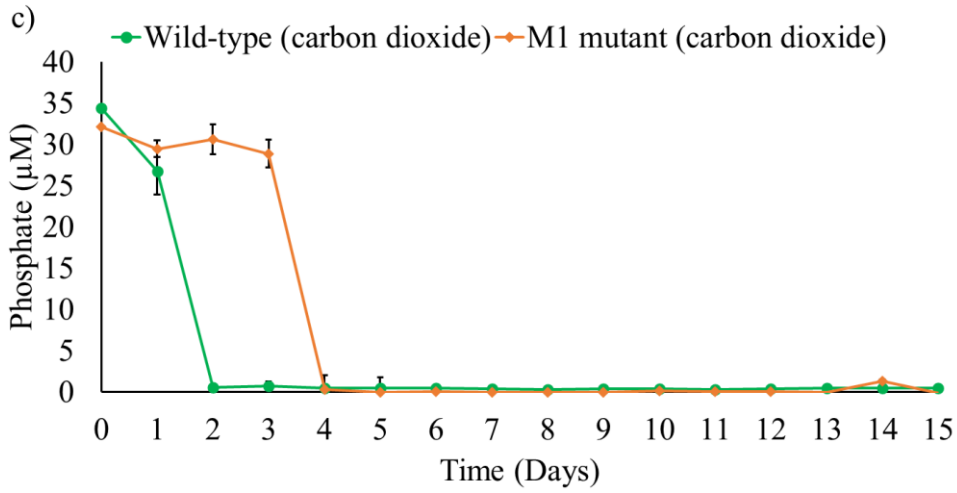
c)
Wild-type (carbon dioxide)
M1 mutant (carbon dioxide)
Phosphate (µM)
0
5
10
15
20
25
30
35
40
0 1 2 3 4 5 6 7 8 9 10 11 12 13 14 15
Time (Days)

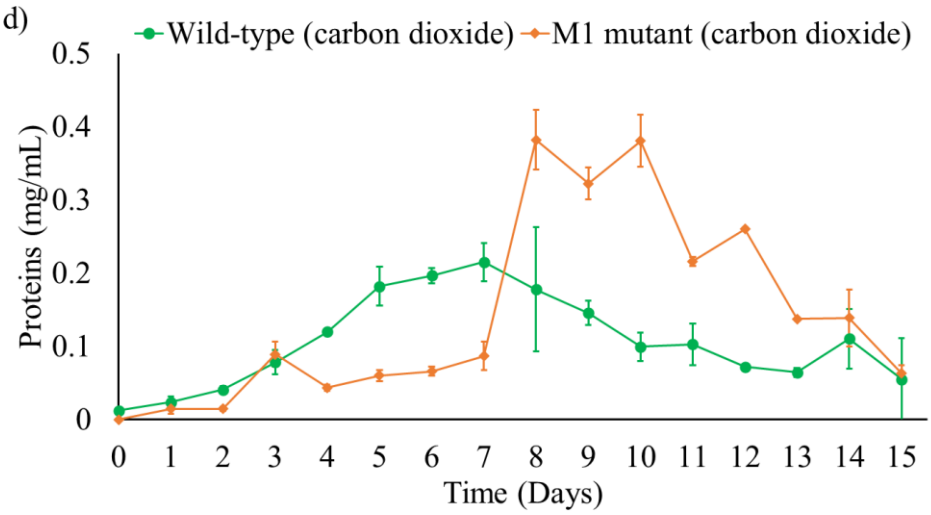

Figure 5.9: Profiles for wild-type and M1 mutant *Nannochloropsis oculata* cultivated in an outdoor 300 L pilot-scale photobioreactor supplied with CO_2. a) Chlorophyll-*a*, b) nitrate uptake, c) phosphate uptake, and d) protein quantity profiles. Mean ± standard deviation is shown (n = 3) for each day.

The FA contents for M1 mutant *Nannochloropsis oculata* supplied with CO_2 are shown in Figures 5.10 (b) and 5.11 (b). The percentage of C16:0 and C16:1 were around 24-30 % from day 0 until day 3. The C16:0 and C16:1 showed a sharp decrease with 13.28 % and 18.85 %, respectively, on day 4 when the growth was at the optimum condition. Concomitantly, the EPA reached the highest percentage from day 4 until day 7. Day 5 showed the most significant 42.77 % EPA of total FA. The ratio of EPA to C16:0 was 2.85, 2.49, and 1.43 for days 4, 5 and 6, respectively, whereas, from day 7 onwards, the ratio fell below 1, indicating C16:0 dominated the microalga cells. The C16:0 and C16:1 again dominated the culture from day 7 until day 15 and reached the highest percentage on day 15 (35-36 %). The EPA quantity recorded 94.86, 61.76 and 61.58 mg/g DCW on days 4, 5 and 6, respectively. The most significant EPA quantity recorded on day 7 with 129.87 mg/g DCW with EPA to C16:0 ratio of 0.73. In comparison, the C16:0 and C16:1 quantity showed a lower amount than the EPA on days 4, 5 and 6. The EPA quantity profile results were directly proportional to the FA percentage profile. The highest C16:0 and C16:1 were recorded on day 15 with 215.20 and 281.74 mg/g, respectively. Interestingly, from day 8 to 15, the EPA quantity remained considerably high, ranging from 41-69.8 mg/g DCW.

5.3.4. Physiological and biochemical analysis of wild-type *Nannochloropsis oculata* supplied with CO_2

On 18th August 2019, the second wild-type *Nannochloropsis oculata* experiment was conducted for 15 days. The microalga showed an exponential growth curve from day 0 until day 6 with an average rate of 0.42/day. Then, the growth rate declined (0.07/day) until the end of the exponential growth phase on day 13. The average temperature throughout the experimental period was 20.94 °C and 1009.90 µmol m^{-2} s^{-1} with a 14:07-h/9.93-h (light/dark) cycle, as shown in Figure 5.8 (a).

Chlorophyll-*a* quantity was rapidly increased until day 5, moderately increased until day 8, and then gradually declined towards the end of 15 days experimental period, as shown in Figure 5.9 (a). Day 8 recorded the highest chlorophyll-*a* quantity, 3.2 µg/mL. Despite of wild-type strain showing rapid growth progress, the average of chlorophyll-*a* was higher in the M1 mutant. The rapid microalga progress indicated a faster nitrate uptake, completely consumed on day 9, one day faster than the M1 mutant, as shown in Figure 5.9 (b). However, the optimum uptake rate (1.22/day) was slightly lower than the M1 mutant strain. The rapid growth of wild-type was also indicated by a rapid phosphate uptake rate, completely consumed on day 2, as shown in Figure 5.9 (c). The protein quantity was gradually increased from day 0 until day 7, reached the highest 0.22 mg/mL, and then gradually decreased from day 8 until day 15, as shown in Figure 5.9 (d). On average, the protein quantity of wild-type strain was lower than M1 mutant *Nannochloropsis oculata*.

The FA contents for wild-type *Nannochloropsis oculata* supplied with CO_2 are shown in Figures 5.10 (a) and 5.11 (a). FA percentage indicated 42.68 % and 37.55 % EPA on days 3 and 4, respectively. The ratio of EPA to C16:0 was 2.23 and 1.47 on days 3 and 4, respectively, while from day 5 until day 15 the ratio fell below 1, indicating C16:0 dominated the microalga cells. C16:0 and C16:1 showed an average of 35-36 % towards the end of culturing period. Although day 3 and day 4 had the highest EPA percentage, the EPA quantity recorded 39.66 and 66.26 mg/g DCW on days 3 and 4, respectively. The highest EPA was recorded on day 10 with 75.43 mg/g DCW with the EPA to C16:0 ratio of 0.58.

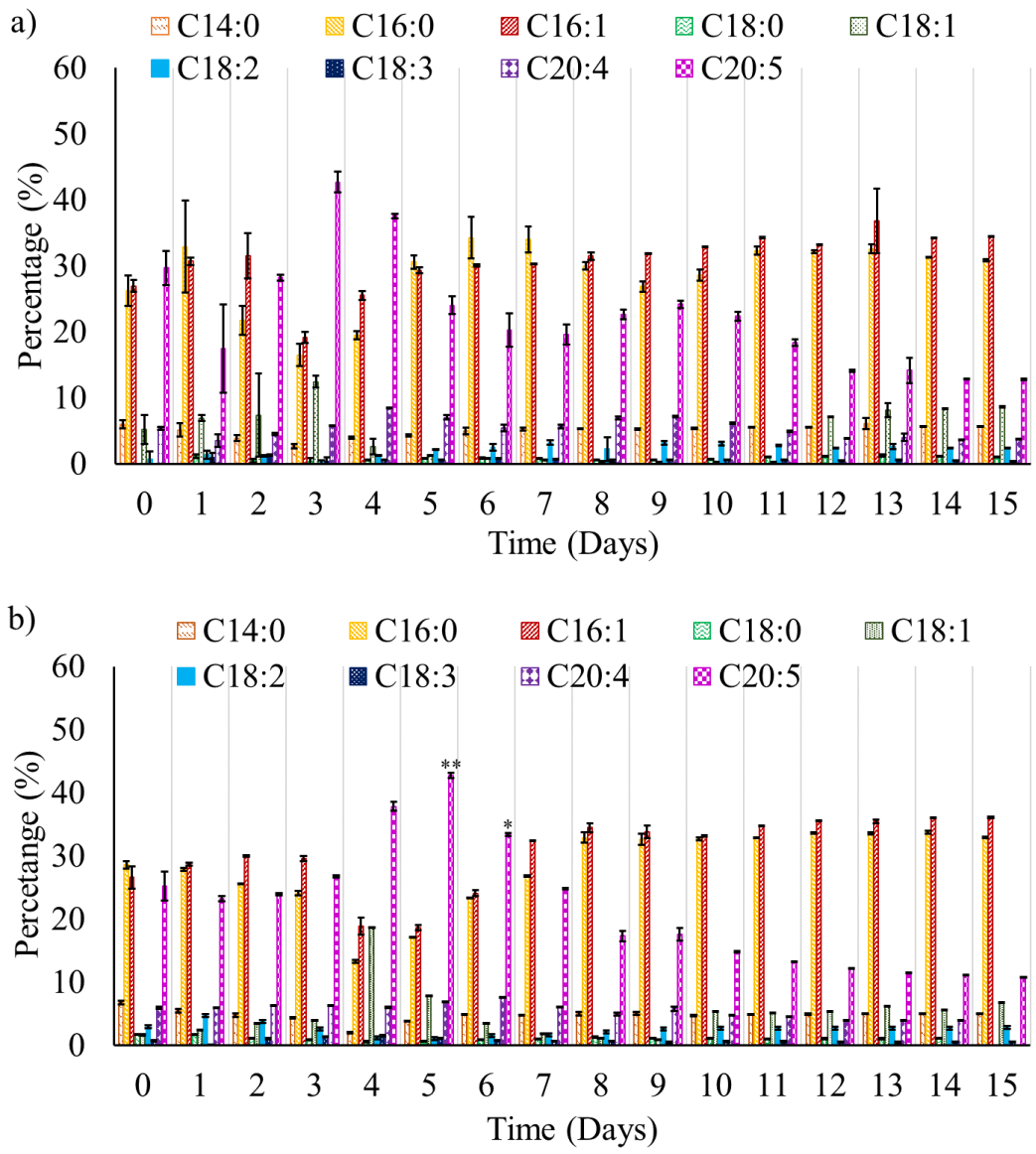

Figure 5.10: Percentages of main fatty acid profiles: a) wild-type, and b) M1 mutant *Nannochloropsis oculata* supplied with 4.5 and 4 % CO_2, respectively. The data show the mean value and standard deviation of three technical replicate samples. The significant differences, that determined by Student's t-test, are indicated by asterisks (*p<0.05, **p<0.01, ***p<0.001).

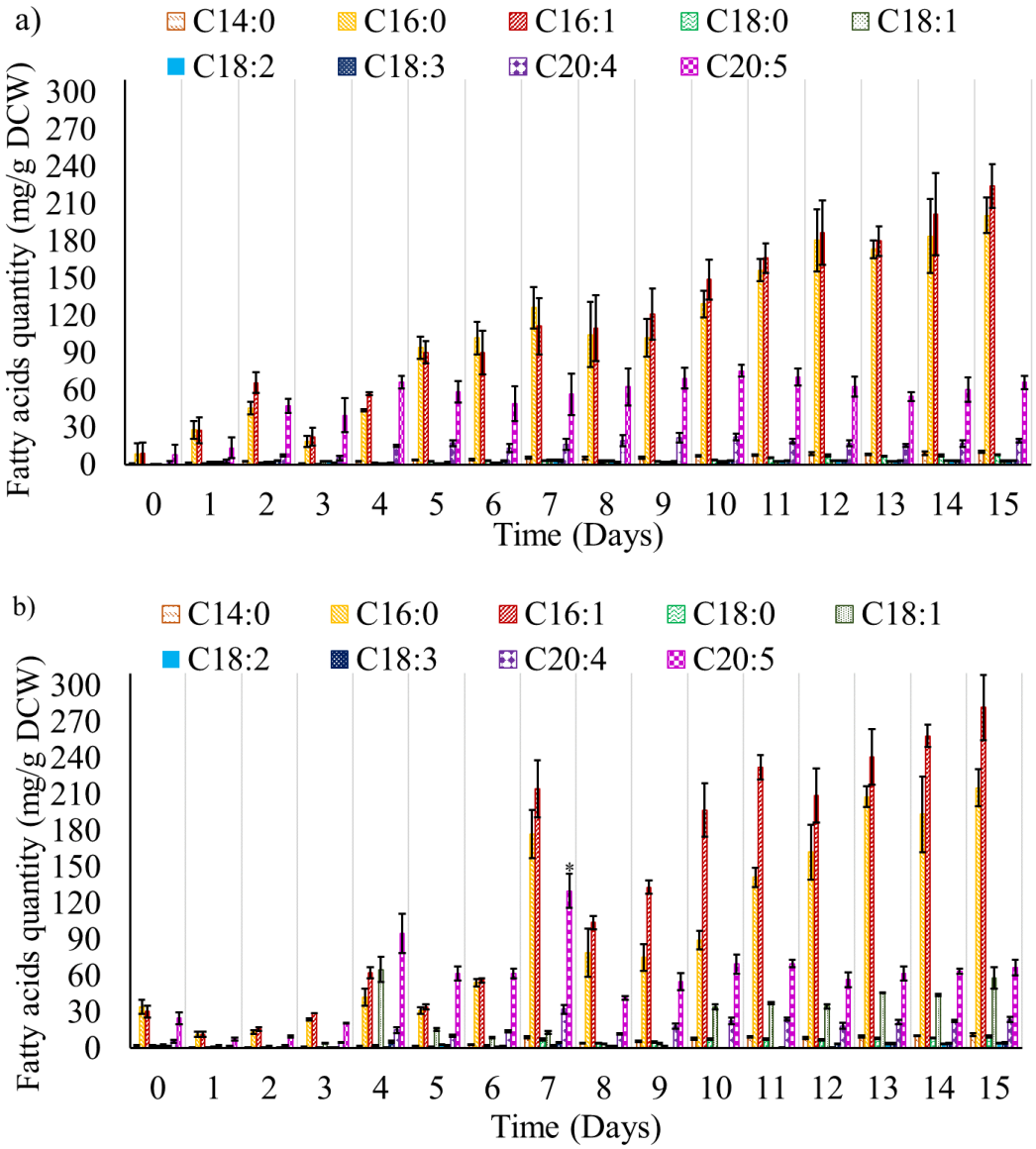

Figure 5.11: Quantification of main fatty acid profiles. a) wild-type and b) M1 mutant *Nannochloropsis oculata* supplied with 4.5 and 4 % CO_2, respectively. The data show the mean value and standard deviation of three technical replicate samples. Asterisks indicate the significant differences determined by Student's t-test (*p<0.05, **p<0.01, ***p<0.001).

TFA comparison for all conducted experiments is shown in Table 5.3. In the experiments supplied with standard air, the wild-type strain showed a higher TFA than the M1 mutant strain *Nannochloropsis oculata* at day 15. In comparison, the M1 mutant indicated a higher TFA than the Nannochloropsis oculata wild-type strain in the experiments supplied with CO_2. The TFA could reach around 270 to 300 mg/g DCW in wild-type *Nannochloropsis oculata*

cultured under nitrate and phosphate limitation for 5 days of culturing period (Gong et al., 2013).

Table 5.3: TFA profiles (mg/g DCW) for wild-type and M1 mutant *Nannochloropsis oculata*. The data show the mean value of three technical replicate samples. The data for M1 mutant (standard) was not available (N/A).

Days	**Wild-type (standard air)**	**M1 mutant (standard air)**	**Wild-type (4.5 % CO_2)**	**M1-mutant (4 % CO_2)**
0	90.82	107.15	27.59	104.85
1	156.15	161.04	77.92	36.66
2	144.48	191.29	174.26	45.04
3	99.43	240.87	92.36	86.27
4	83.38	105.02	188.14	289.21
5	92.09	178.08	270.22	160.69
6	79.96	151.99	266.28	203.06
7	77.09	207.10	328.55	590.10
8	97.35	169.50	310.83	250.86
9	90.27	183.01	327.46	296.73
10	125.03	82.09	393.60	428.63
11	177.90	77.17	432.93	522.43
12	251.32	N/A	472.07	499.76
13	172.72	N/A	446.64	602.58
14	419.63	54.80	487.95	607.80
15	442.00	62.61	536.94	674.45

5.3.5. Techno-economic assessment results

In the TEA analysis, four possible scenarios were evaluated. The cost projection was calculated by referring to the baseline data (Schade and Meier, 2021), as shown in Table 5.4. The scenarios studied the economic impact of M1 mutant EPA quantity (87.02 g/kg DCW) when the microalga oil production was higher than the baseline data. In the baseline scenario, a weight of 64,200 kg of *Nannochloropsis* sp. biomass was produced in one year, and 13,225 kg is accounted for total lipids or microalga oil. The other valuable side product was biomass residue left after the microalga oil was extracted. The yearly production of 50,917 kg/year was accounted for biomass residue; the by-product was left over after the microalga oil was removed. The biomass residue could also be used as animal and fish feed. The price of fish feed was estimated at €1,091 or equivalent to £938.26 per tonne (Shield and Lupatsch, 2012). The conversion rate from euro to pound when this study was conducted was 1 euro equals

0.86 pounds. The NPV and ROI calculations are shown in the supplementary Table S5.1 until S5.7).

Table 5.4: Parameters and input for four possible scenarios to be applied to M1 mutant *Nannochloropsis oculata* to increase microalga oil production productivity. All other parameters and information are considered constant variables similar to the baseline *Nannochloropsis* sp. (Schade and Meier, 2021).

Parameter	**Unit**	**M1 Mutant *Nannochloropsis oculata* (Grow 28.3 % Faster)**	**M1 Mutant *Nannochloropsis oculata* (292 Day Per Year)**	**M1 Mutant *Nannochloropsis oculata* (Tropical Country)**	**M1 Mutant *Nannochloropsis oculata* (Combined Scenarios)**
Lipids	g/kg DCW	206	206	206	206
EPA	g/kg DCW	87.02	87.02	87.02	87.02
Total microalga cell yield	kg/1.2ha/ annum	103,242.20	102,439.34	96,292.72	247,106.8
Biomass residue	kg/1.2ha/ annum	81,881	81,244.61	76,375.5	195,980.4
Microalga oil	kg/1.2ha/ annum	21,267.79	21,102.19	19,837.5	50,903.24
Land	ha	1.2	1.2	1.2	1.2

NPV and ROI are two financial metrics that are used to evaluate the significance indicators for the economic potential of the studied scenarios. The ROI for M1 mutant *Nannochloropsis oculata* was expected at 110.99 % after 10 years of operations. On the contrary, *Nannochloropsis* sp. and wild-type *Nannochloropsis oculata* have ROI -0.10 % and 39.68 %, respectively, after 10 years of operations which are unprofitable. 239.30 % of ROI was recorded for scenario 1, where M1 mutant *Nannochloropsis oculata* had a 28.3 % faster growth rate than wild-type *Nannochloropsis oculata*. The ROI indicates that this is a profitable investment. The other two scenarios are also promising, where ROI was recorded at 236.66 % and 216.49 %, respectively, after 10 years. The ideal situation presents when all the scenarios are combined. The ROI was calculated at 712.11 % after 10 years of the operation as shown in Table 5.5.

Table 5.5: Net present value (NPV) and return of investment (ROI) comparisons for 10 years timeline.

	Case study	**Net present value (NPV) (£) after 10 years**	**Return of investment (ROI) after 10 years**
1	Baseline *Nannochloropsis sp.*	-7,354.08	-0.10 %
2	Wild-type *Nannochloropsis oculata*	2,906,431.17	39.68 %
3	M1 mutant *Nannochloropsis oculata*	8,129,226.70	110.99 %
4	M1 mutant *Nannochloropsis oculata* (28.3 % growth faster)	17,527,277.25	239.30 %
5	M1 mutant *Nannochloropsis oculata* increased to 80 % of running of total days/year	17,333,772.61	236.66 %
6	M1 mutant *Nannochloropsis oculata* (accumulate 50 % more biomass in tropical countries)	15,855,974.41	216.49 %
7	Combine Scenario (4, 5, & 6)	49,051,303.49	712.11 %

5.4. Discussion

5.4.1. Wild-Type Versus M1 Mutant *Nannochloropsis oculata* in Standard Aeration Experiments

EPA-overproducing *Nannochloropsis* strains have been reported in a lot of studies at the laboratory scale. At the time of undertaking the current study, there are very limited studies on the developed strains on a pilot scale. Hence, this chapter evaluates the performance of developed and wild-type *Nannochloropsis oculata* in a 300 L pilot-scale photobioreactor. In addition, the potential of scaling this work to a commercial scale was also investigated by integrating the pilot-scale results into a techno-economic assessment model of *Nannochloropsis* sp. strain.

The first batch experiment was conducted to evaluate the suitability of wild-type *Nannochloropsis oculata* in an outdoor 300 L pilot-scale photobioreactor. An amount of 297.6 mg/L was the highest dry biomass quantified on day 13 despite having a few sunny days during the experiment, as shown in Figure 5.2 (b). However, a sudden temperature shooting up to 29 °C inside the photobioreactor could inhibit the growth rate on day 5. Therefore, the water was sprayed on the top of the photobioreactor when the temperature reached 28 °C.

A previous study demonstrated that *Nannochloropsis* sp. could be cultured at 30 °C (Hu and Gao, 2006). Hence, the 28 °C temperature limit was appropriate to get optimal growth.

Meanwhile, the M1 mutant recorded 734.47 mg/L DCW, 2.5-fold higher than the wild-type strain despite having unfavourable weather. Overall, the biomass attained in this study was lower than that obtained by *Nannochloropsis* sp. in a pilot-scale tubular photobioreactor, which achieved 840 mg/L dry biomass (Chini Zittelli et al., 1999). Mid-exponential growth phase inoculum used for culturing wild-type strain could influence the growth performance under unfavourable conditions. In addition, photoinhibition decreases the growth rate of inoculum in the 20 L, hence taking a long time to reach 0.7 OD at 595 nm. As an improvement, the M1 mutant was cultured in 1 L flasks and pooled in the 20 L carboys when the cells were in the early exponential phase (having OD 0.5-0.6 at 595 nm). Hence, by the time of the experiments, the inoculum was in the early to mid-exponential growth phase conditions. The dry biomass of the M1 mutant could be increased further under optimum growth conditions especially when the pH was controlled in a range from 7 to 8.5.

Chlorophyll-*a* indicates that the M1 mutant could have a higher photosynthetic rate than the wild-type strain, contributing to the increased EPA synthesis in the chloroplast. In another study, low temperature limits chlorophyll build-up by lowering the light-harvesting complex, influencing the values of maximal photochemical efficiency of PSII in the cells (Carneiro et al., 2020). Around 62 % phosphate uptake in the M1 could be sufficient for phospholipids synthesis that attains the minimum membrane function and stability (Manning, 2022), enhancing EPA synthesis. A lower nitrate uptake rate in the M1 mutant implies that the cell division in the M1 mutant could be lower than in the wild-type strain. The protein results could be influenced by the optimum microalga growth. The optimum growth was on day 8 until 9 and 13 until 14 for M1 mutant and wild-type strains, respectively. Nitrate deficiency causes a decrease in protein content, which eventually stops microalga growth (Hulatt et al., 2017). However, the protein content was contradicted by the stagnant OD at the end of culturing period in the wild-type *Nannochloropsis oculata*.

The EPA-overproducing M1 mutant showed the most significant results in enhancing the EPA content. The EPA results produced by M1 was higher than other studies in the species of

Nannochloropsis, as reviewed in chapter 1. The cold weather with a 17.93 °C average during the experimental period could be one of the factors in inducing a higher EPA in the M1 mutant. This finding is in line with the other study, where *Nannochloropsis oceanica* cultured in an outdoor tubular photobioreactor showed that 18 °C had a higher EPA percentage than 28 °C environment condition (Carneiro et al., 2020). The low temperature could inhibit the synthesis of C16:0 and C16:1, while the photosynthetic activity could be at the optimum levels. In addition, the EPA synthesis could follow a different pathway under low-temperature conditions that favours the incorporation of EPA with DGTS, a betaine lipid (Murakami et al., 2018). On the contrary, high light intensity and high temperature during the wild-type experiment could trigger C16:0 and C16:1 synthesis. A higher EPA content on day 14 and 15 could be contributed by the EPA translocation from membrane lipids to lipid bodies (Hulatt et al., 2017). Unfortunately, the quantity and duration of sunlight irradiance to the photobioreactor were not monitored as it was not equipped with light intensity meter. Referring to the previous studies, the light intensity on the sunny days is around 2000 µmol m^{-2} s^{-1} (Stunda-Zujeva et al., 2018), and the light intensity for cloudy and rainy days has about 500 µmol m^{-2} s^{-1} (Metsoviti et al., 2020), which is higher compared to light intensity used in the lab which is around 130-200 µmol m^{-2} s^{-1}.

In this experiment, a larger aeration pump could not be employed to increase the aeration rate and regulate the pH. Besides, the location of Arthur Willis Environmental Centre is very close to the neighbouring houses; hence any mechanical noise had to be avoided where necessary. For photosynthesis, the microalgae cell uses bicarbonate as an external carbon source and produces CO_2 by the action of carbonic anhydrase (Mokashi et al., 2016), demonstrating that sodium bicarbonate is a suitable carbon source for microalgae cells. However, even though sodium bicarbonate enhanced the growth, the pH was more than 9, which was not an optimum condition. Therefore, another two batches of experiments were conducted to evaluate the wild-type and M1 mutant *Nannochloropsis oculata* by supplying 4.5 and 4 % pure CO_2 as a carbon source and regulating the pH.

5.4.2. Wild-Type Versus M1 Mutant *Nannochloropsis oculata* in supplied CO_2 Experiments

In the M1 mutant *Nannochloropsis oculata* growth profile, there was a delay from day 0 until day 3, possibly caused by cloudy, low temperature and limited light intensities. The M1

mutant could have a higher OD and reach the stationary growth phase quicker if not delayed. There was no delay in wild-type *Nannochloropsis oculata* due to partly cloudy weather, where the light intensity was higher than on cloudy days. The light intensity is shown in Figures 5.3 (a) and (b) represents the light intensity during the sampling time from 9 until 10 a.m. There was no equipped device to record the light intensity automatically, and there is a high possibility the light intensity during partly cloudy days is much higher in the afternoon than the cloudy days. In addition, a higher concentration of 4.5 % CO2 was needed to regulate the pH in the wild-type *Nannochloropsis oculata*, indicating a higher carbon available for photosynthesis. In the mutant strain, 4 % CO_2 was used to regulate the pH. Even though less amount of CO_2 was used, the M1 mutant enhanced a higher OD, dry biomass, chlorophyll-*a*, and protein quantity. In a previous study, 8 % CO_2 was an optimum concentration for wild-type *Nannochloropsis oculata* growth in a 1.8 L photobioreactor (Razzak et al., 2015). Another report showed that 8 % total volume of CO_2 had the highest CO_2 fixation in *Chlorella vulgaris*, while 4 % of total CO_2 had the most increased CO_2 fixation in wild-type *Nannochloropsis gaditana* that were cultured in 18 L photobioreactor (Adamczyk et al., 2016). In the photosynthesis process, microalgae cells utilise CO_2 in dissolve CO_2 form. However, the conversion of CO_2 gas to dissolve CO_2 in the culture medium was not measured in this study. In another study, 400 mg/L dissolved CO_2 was determined as the optimum concentration for culturing polyculture, *Scenedesmus acuminatus, Dictyosphaerium sp.*, and *Phormidium sp.*(Kandasamy et al., 2021).

High chlorophyll-*a* content in M1 mutant *Nannochloropsis oculata* was in line with findings in the previous chapter, indicating that light-harvesting capacity in the mutant is better than the wild-type strain hence enhancing chlorophyll-*a* and EPA production. In addition, a higher protein content proves the optimise conditions achieved in the M1 mutant. A faster nitrate uptake rate during optimum growth conditions could also contribute to a higher chlorophyll-*a* and protein content in the M1 mutant strain. In addition, nitrate limited in the medium was reported as a trigger for neutral lipid synthesis in most oleaginous microalgae (Burch and Franz, 2016; Tran et al., 2016; Remmers et al., 2017). The decrease in protein content resulting from nitrogen deprivation is consistent with another study (Sui et al., 2019). In another study, the neutral lipids decreased while the protein increased when the nutrient was replenished in *Nannochloropsis sp.* culture (Li et al., 2020). Phosphate uptake was rapidly

consumed for wild-type and M1 mutant *Nannochloropsis oculata*, indicating that a higher phosphate concentration could be employed in the future. A previous study recorded up to 20.05 mg/g/day phosphate rate in *Nannochloropsis salina* (Sforza et al., 2018), and 2 g/L phosphates showed the highest OD in *Nannochloropsis oculata* (Mahat et al., 2015). In addition, an optimised N:P ratio concentration could be prepared as a 20 N:P ratio showed the highest EPA percentage in *Nannochloropsis oculata* (Rasdi and Qin, 2015).

The biochemical results were in agreement with an enhanced EPA quantity in M1 mutant *Nannochloropsis oculata*, while the wild-type strain EPA quantity was satisfactory to reach 75.53 mg/g DCW, higher than the average EPA produced in the other studies as described in the chapter 1. In addition, it is pretty surprising to find that the EPA percentage reached 42.68 % in wild-type strain, a comparable result to the EPA percentage in M1 mutant strain, which recorded 42.77 %. The variations of microalga culture and experimental conditions, such as continuous temperature monitoring, light intensity, and pH, should be considered in future studies, especially for culturing an outdoor photobioreactor. The ratio of EPA to C16:0 is also crucial in maximising the EPA content, when 0.58 and 0.73 ratios produced the highest EPA quantity in wild-type and M1 mutant *Nannochloropsis oculata*, respectively. During the transition of polar membrane lipids to neutral lipids, the EPA was conserved at the optimum quantity and partially translocated to neutral lipids (Hulatt et al., 2017). Hence, the microalga inoculum should reach an appropriate EPA to C16:0 ratio prior for scaling the microalga in an outdoor pilot-scale photobioreactor. The M1 mutant had a higher TFA percentage than the wild-type strain, which implies that the FA synthesis pathway of FAs has changed in the developed mutant. Therefore, the different levels of TFA content produced in wild-type and M1 mutant could influence the ratio of EPA to C16:0 that could produce the optimum EPA.

5.4.3. Techno-economic assessment

The TEA analysis was conducted by integrating the optimum EPA quantity data for wild-type, and M1 mutant *Nannochloropsis oculata* in this study into a TEA model described in a previous study (Schade and Meier, 2021). The system referred to an outdoor 628 m^3 tubular photobioreactor located in Halle/Saale, Germany (Schade and Meier, 2021). All measured parameters are assumed suitable for growing wild-type and M1 *Nannochloropsis oculata* at the optimal growth rate.

EPA quantity per cell in M1 mutant was significantly higher compared to the EPA quantity reported in the literature review (chapter 1). 110.99 % ROI and £8,129,226,70 NPV after 10 years indicate 87.02 mg/g DCW EPA quantity has doubled the initial investment. The results demonstrated that the M1 mutant reaches the breakeven point after 10 years and gains profits in a few more years. The break-even point is when the investment cost of developing the microalga plant equals the revenue from sales, hence starting to generate a profit (Mohammady et al., 2020). The baseline scenario showed that at least 10 years and 6 months are required for a plant to profit from selling biomass, while at least 24 years is needed for microalga oil of wild-type *Nannochloropsis* sp. industry to get profit (Schade and Meier, 2021). Therefore, further strategies must be implemented to gain profits in a shorter period.

Four scenarios were investigated to determine whether the M1 mutant could be sustained and challenge the fish oil omega-3 industry in the market. The increase in the M1 growth rate could shorten the break-even point to the end of 6 years, as the ROI reaches 98.72 % and NPV achieves £3,137,433.08. Increasing the operation period to 292 days/year also could shorten the break-even point to the end of 6 years, as the ROI reaches 97.17 % and NPV achieves £3,1110,765.08. However, the increase in operating cost for extending the working days period per year was not considered in the calculation of scenario 2. Scenario 3, culturing M1 mutant in tropical countries, showed a slightly lower ROI and NPV compared to other scenarios. Tropical countries with consistent light intensities and temperature could be the ideal place to culture microalgae. For example, in tropical country Malaysia, at the lower altitude place such as Kuala Lumpur, the daily temperature is around 26-28 °C (Abdul Rahman, 2018; Tang, 2019). On the other hand, in a high-altitude place like Cameron Highland, the average daily temperature ranges from 15-22 °C, which could be an ideal place for culturing and maximizing the EPA synthesis (Tan et al., 2021).

The ‘best case’ scenario shows the highest ROI and NPV as expected, with a break-even point as early as year 4 and gaining profit afterwards. After 32 years, the ROI is expected at 1134.54 %, about ten times of initial investments with an NPV £501,254.44.

5.5. Conclusion

Wild-type and M1 mutant *Nannochloropsis oculata* were cultured in an outdoor 300 L pilot-scale photobioreactor to investigate the microalgae growth, physiological and biochemical changes of the developed mutant compared to the wild-type strain. The average EPA quantity in the exponential growth phase was integrated into a developed TEA model and evaluated to determine whether the enhanced EPA-based project is economically feasible. In general, wild-type and mutant strain were compatible with the outdoor setup. However, the pH must be maintained in a range of 7-8.5 to optimise growth performance. The M1 mutant *Nannochloropsis oculata* indicated the capabilities of producing higher amounts of EPA on an outdoor pilot-scale system. Furthermore, the improved scenarios for the M1 mutant demonstrated the financial advantages of the M1 mutant in overcoming the high capital costs that currently exist within the microalgae industry. Overall, the objective for this chapter was successfully achieved, and the developed M1 mutant provides a platform for further process improvements.

CHAPTER 6: FUTURE DIRECTIONS

6. Future Directions

6.1. Future perspectives

The work presented in this thesis offers a lot of potential for future explorations in Malaysia. Future work could be started by isolating the microalgae that originated from the Malaysia environment. The local microalgae species are adapted to Malaysia's hot and humid weather, hence would be an ideal choice for developing a new EPA-overproducing mutant strain. In addition, Malaysia is surrounded by oceans, the South China Sea on the east coast and the Strait of Malacca and the Andaman Sea on the west coast, with a total coastline of 4800 km, offering great aquatic biodiversity, including algae (Mazlan et al., 2005). Hence, testing a native microalgae species with random mutagenesis with a combination of a few chemical inhibitors and followed by ALE is one of the practical plans in the future to develop and improve the microalgae phenotype for maximising the synthesis of EPA. In addition, another method besides random mutagenesis that could be applied is insertional mutagenesis. The insertional mutagenesis can be used to develop a new microalgae phenotype and identify the responsible genes involved (Ryu et al., 2020).

In addition, the other culturing strategy could be implemented to improve EPA production further. Heterotrophic culturing using sugarcane waste as an alternative carbon source could reduce agricultural solid waste and enhance omega-3 production (Oliver et al., 2020). In Malaysia, it would be more interesting to explore the mixotrophic growth, as the microalgae can benefit the sunlight and carbon sources, improving the biomass productivities (Castillo et al., 2021). Consistent sunlight throughout the year could contribute to the fast-growing microalgae in the carotenoids and biofuels industry. Microalgae cells are expected to reach the stationary phase rapidly and favour neutral lipid synthesis for biofuel and carotenoid production. Besides, microalgae bioremediation is one of the exciting research that could be conducted in the future for biofuels, bioplastics and biofertilizer production (Al-Jabri et al., 2021).

Developing photobioreactor systems at a pilot-scale that could optimise microalgae growth is another aim in the future. Low-cost photobioreactor by using renewable materials could

decrease the capital cost for a microalgae photobioreactor system. Besides, this study was funded by the government of Malaysia and the University of Malaysia Terengganu. Therefore, high research impact that could be applied to improve the country's economy and contribute to the community is highly encouraged. EPA-overproducing mutant offers new potential for the aquaculture industry in breeding fish that are enriched with EPA (Hemaiswarya et al., 2011). The biomass produced also benefits the animal feed industry by providing high-quality and nutritious foods (der Poel et al., 2020). Recently in 2022, the Malaysian government has encouraged all Malaysian citizens to start home farming to overcome the global food crisis due to the covid-19 pandemic. Interestingly, microalgae could be beneficial in a hydroponics system. A system that integrates hydroponics, microalgae and fishes could be developed as part of home farming or known as aquaponics (Addy et al., 2017). Developing a simple and reliable aquaponics system could motivate people to enjoy farming besides gaining some extra earnings. Besides, lobster could also be used instead of fish in the aquaponics system due to high demand, and it is regarded as an exclusive cuisine in Malaysia.

All the mentioned research will be contributed towards developing a sustainable biorefinery plant is an ultimate goal in the future. However, the microalgae biorefinery plant is not profitable at the present time due to high capital and processing cost and lack of revenue gained. A recent review article described the principal, challenges and prospects of developing a microalgae biorefinery plant (Chew et al., 2017). In conclusion, microalgae research is far from reaching its full potential, and more explorations are needed. Therefore, the proteomics analysis fundamental techniques learned in this study will be applied in the future for the research on microalgae species originating from Malaysia. Hopefully, the new discoveries at molecular levels will help improve the understanding of physiological and biochemical activities inside the microalgae cells.

7. References

Abdul Rahman, H. (2018). Climate Change Scenarios in Malaysia: Engaging the Public. *Int. J. Malay-Nusantara Stud.* 1, 55–77. Available at: https://www.researchgate.net/publication/329642223_CLIMATE_CHANGE_SCENARIOS_IN_MALAYSIA_ENGAGING_THE_PUBLIC.

Adamczyk, M., Lasek, J., and Skawińska, A. (2016). CO2 Biofixation and Growth Kinetics of Chlorella vulgaris and Nannochloropsis gaditana. *Appl. Biochem. Biotechnol.* 179, 1248–1261. doi:10.1007/s12010-016-2062-3.

Adarme-Vega, T. C., Lim, D. K. Y., Timmins, M., Vernen, F., Li, Y., and Schenk, P. M. (2012). Microalgal biofactories: a promising approach towards sustainable omega-3 fatty acid production. *Microb. Cell Fact.* 11, 96. doi:10.1186/1475-2859-11-96.

Adarme-Vega, T. C., Thomas-Hall, S. R., and Schenk, P. M. (2014). Towards sustainable sources for omega-3 fatty acids production. *Curr. Opin. Biotechnol.* 26, 14–18. doi:10.1016/j.copbio.2013.08.003.

Addy, M. M., Kabir, F., Zhang, R., Lu, Q., Deng, X., Current, D., et al. (2017). Co-cultivation of microalgae in aquaponic systems. *Bioresour. Technol.* 245, 27–34. doi:10.1016/j.biortech.2017.08.151.

Al-Jabri, H., Das, P., Khan, S., Thaher, M., and Abdulquadir, M. (2021). Treatment of wastewaters by microalgae and the potential applications of the produced biomass—a review. *Water (Switzerland)* 13. doi:10.3390/w13010027.

Alonso, D. L., Segura, C. I., and Grima, E. M. (1996). First Insights I N T O Improvement of Eicosapentaenoic Acid Content in. *J. Phycol.* 32, 339–345.

Anand, V., Kashyap, M., Samadhiya, K., and Kiran, B. (2019). Strategies to unlock lipid production improvement in algae. *Int. J. Environ. Sci. Technol.* 16, 1829–1838. doi:10.1007/s13762-018-2098-8.

Anand, V., Singh, P. K., Banerjee, C., and Shukla, P. (2017). Proteomic approaches in microalgae: perspectives and applications. *3 Biotech* 7, 1–10. doi:10.1007/s13205-017-0831-5.

Arif, M., Bai, Y., Usman, M., Jalalah, M., Harraz, F. A., Al-Assiri, M. S., et al. (2020). Highest accumulated microalgal lipids (polar and non-polar) for biodiesel production with advanced wastewater treatment: Role of lipidomics. *Bioresour. Technol.* 298, 122299.

doi:10.1016/j.biortech.2019.122299.

Arora, N., Pienkos, P. T., Pruthi, V., Poluri, K. M., and Guarnieri, M. T. (2018). Leveraging algal omics to reveal potential targets for augmenting TAG accumulation. *Biotechnol. Adv.* 36, 1274–1292. doi:10.1016/j.biotechadv.2018.04.005.

Arora, N., Yen, H. W., and Philippidis, G. P. (2020). Harnessing the power of mutagenesis and adaptive laboratory evolution for high lipid production by Oleaginous Microalgae and yeasts. *Sustain.* 12. doi:10.3390/su12125125.

Aussant, J., Guihéneuf, F., and Stengel, D. B. (2018). Impact of temperature on fatty acid composition and nutritional value in eight species of microalgae. *Appl. Microbiol. Biotechnol.* 102, 5279–5297. doi:10.1007/s00253-018-9001-x.

Axelsson, M., and Gentili, F. (2014). A single-step method for rapid extraction of total lipids from green microalgae. *PLoS One* 9, 17–20. doi:10.1371/journal.pone.0089643.

Bai, X., Song, H., Lavoie, M., Zhu, K., Su, Y., Ye, H., et al. (2016). Proteomic analyses bring new insights into the effect of a dark stress on lipid biosynthesis in Phaeodactylum tricornutum. *Sci. Rep.* 6, 1–10. doi:10.1038/srep25494.

Bajpai, P., and Bajpai, P. K. (1993). Eicosapentaenoic acid (EPA) production from microorganisms: a review. *J. Biotechnol.* 30, 161–183. doi:10.1016/0168-1656(93)90111-Y.

Bantscheff, M., Schirle, M., Sweetman, G., Rick, J., and Kuster, B. (2007). Quantitative mass spectrometry in proteomics: A critical review. *Anal. Bioanal. Chem.* 389, 1017–1031. doi:10.1007/s00216-007-1486-6.

Barati, B., Zeng, K., Baeyens, J., Wang, S., Addy, M., Gan, S. Y., et al. (2021). Recent progress in genetically modified microalgae for enhanced carbon dioxide sequestration. *Biomass and Bioenergy* 145, 105927. doi:10.1016/j.biombioe.2020.105927.

Barbosa, M. J., Hadiyanto, and Wijffels, R. H. (2004). Overcoming Shear Stress of Microalgae Cultures in Sparged Photobioreactors. *Biotechnol. Bioeng.* 85, 78–85. doi:10.1002/bit.10862.

Bartley, M. L., Boeing, W. J., Corcoran, A. A., Holguin, F. O., and Schaub, T. (2013). Effects of salinity on growth and lipid accumulation of biofuel microalga Nannochloropsis salina and invading organisms. *Biomass and Bioenergy* 54, 83–88. doi:10.1016/j.biombioe.2013.03.026.

Beacham, T. A., Macia, V. M., Rooks, P., White, D. A., and Ali, S. T. (2015). Altered lipid

accumulation in Nannochloropsis salina CCAP849/3 following EMS and UV induced mutagenesis. *Biotechnol. Reports* 7, 87–94. doi:10.1016/j.btre.2015.05.007.

Blasio, M., and Balzano, S. (2021). Fatty Acids Derivatives From Eukaryotic Microalgae, Pathways and Potential Applications. *Front. Microbiol.* 12, 1–21. doi:10.3389/fmicb.2021.718933.

Bleakley, S., and Hayes, M. (2017). Algal Proteins: Extraction, Application, and Challenges Concerning Production. *Foods* 6, 33. doi:10.3390/foods6050033.

Botté, C. Y., Deligny, M., Roccia, A., Bonneau, A. L., Saïdani, N., Hardré, H., et al. (2011). Chemical inhibitors of monogalactosyldiacylglycerol synthases in Arabidopsis thaliana. *Nat. Chem. Biol.* 7, 834–842. doi:10.1038/nchembio.658.

Boudière, L., Botté, C. Y., Saidani, N., Lajoie, M., Marion, J., Bréhélin, L., et al. (2012). Galvestine-1, a novel chemical probe for the study of the glycerolipid homeostasis system in plant cells. *Mol. Biosyst.* 8, 2023–2035. doi:10.1039/c2mb25067e.

Boudière, L., Michaud, M., Petroutsos, D., Rébeillé, F., Falconet, D., Bastien, O., et al. (2014). Glycerolipids in photosynthesis: Composition, synthesis and trafficking. *Biochim. Biophys. Acta - Bioenerg.* 1837, 470–480. doi:10.1016/j.bbabio.2013.09.007.

Briassoulis, D., Panagakis, P., Chionidis, M., Tzenos, D., Lalos, A., Tsinos, C., et al. (2010). An experimental helical-tubular photobioreactor for continuous production of Nannochloropsis sp. *Bioresour. Technol.* 101, 6768–6777. doi:10.1016/j.biortech.2010.03.103.

Burch, A. R., and Franz, A. K. (2016). Bioresource Technology Combined nitrogen limitation and hydrogen peroxide treatment enhances neutral lipid accumulation in the marine diatom Phaeodactylum tricornutum. *Bioresour. Technol.* 219, 559–565. doi:10.1016/j.biortech.2016.08.010.

Caffarri, S., Tibiletti, T., Jennings, R. C., and Santabarbara, S. (2014). Send Orders for Reprints to reprints@benthamscience.net A Comparison Between Plant Photosystem I and Photosystem II Architec-ture and Functioning. *Curr. Protein Pept. Sci.* 15, 296–331.

Camacho-Rodríguez, J., González-Céspedes, A. M., Cerón-García, M. C., Fernández-Sevilla, J. M., Acién-Fernández, F. G., and Molina-Grima, E. (2014). A quantitative study of eicosapentaenoic acid (EPA) production by Nannochloropsis gaditana for aquaculture as a function of dilution rate, temperature and average irradiance. *Appl. Microbiol. Biotechnol.* 98, 2429–2440. doi:10.1007/s00253-013-5413-9.

Cao, J. Y., Kong, Z. Y., Ye, M. W., Zhang, Y. F., Xu, J. L., Zhou, C. X., et al. (2019). Metabolomic and transcriptomic analyses reveal the effects of ultraviolet radiation deprivation on Isochrysis galbana at high temperature. *Algal Res.* 38, 101424. doi:10.1016/j.algal.2019.101424.

Carbonera, D., Agostini, A., Di Valentin, M., Gerotto, C., Basso, S., Giacometti, G. M., et al. (2014). Photoprotective sites in the violaxanthin-chlorophyll a binding Protein (VCP) from Nannochloropsis gaditana. *Biochim. Biophys. Acta - Bioenerg.* 1837, 1235–1246. doi:10.1016/j.bbabio.2014.03.014.

Carneiro, M., Cicchi, B., Maia, I. B., Pereira, H., Zittelli, G. C., Varela, J., et al. (2020). Effect of temperature on growth, photosynthesis and biochemical composition of Nannochloropsis oceanica, grown outdoors in tubular photobioreactors. *Algal Res.* 49, 101923. doi:10.1016/j.algal.2020.101923.

Castillo, T., Ramos, D., García-Beltrán, T., Brito-Bazan, M., and Galindo, E. (2021). Mixotrophic cultivation of microalgae: An alternative to produce high-value metabolites. *Biochem. Eng. J.* 176. doi:10.1016/j.bej.2021.108183.

Cavonius, L. R., Carlsson, N. G., and Undeland, I. (2014). Quantification of total fatty acids in microalgae: Comparison of extraction and transesterification methods. *Anal. Bioanal. Chem.* 406, 7313–7322. doi:10.1007/s00216-014-8155-3.

Cecchin, M., Berteotti, S., Paltrinieri, S., Vigliante, I., Iadarola, B., Giovannone, B., et al. (2020). Improved lipid productivity in Nannochloropsis gaditana in nitrogen-replete conditions by selection of pale green mutants. *Biotechnol. Biofuels* 13, 1–14. doi:10.1186/s13068-020-01718-8.

Chai, X., and Zhao, X. (2012). Enhanced removal of carbon dioxide and alleviation of dissolved oxygen accumulation in photobioreactor with bubble tank. *Bioresour. Technol.* 116, 360–365. doi:10.1016/j.biortech.2012.03.105.

Chaturvedi, R., and Fujita, Y. (2006). Isolation of enhanced eicosapentaenoic acid producing mutants of Nannochloropsis oculata ST-6 using ethyl methane sulfonate induced mutagenesis techniques and their characterization at mRNA transcript level. *Phycol. Res.* 54, 208–219. doi:10.1111/j.1440-1835.2006.00428.x.

Chaturvedi, R., Uppalapati, S. R., Alamsjah, M. A., and Fujita, Y. (2004). Isolation of quizalofop-resistant mutants of Nannochloropsis oculata (Eustigmatophyceae) with high eicosapentaenoic acid following N-methyl-N-nitrosourea-induced random mutagenesis.

J. Appl. Phycol. 16, 135–144. doi:10.1023/B:JAPH.0000044826.70360.8e.

Chauton, M. S., Reitan, K. I., Norsker, N. H., Tveterås, R., and Kleivdal, H. T. (2015). A techno-economic analysis of industrial production of marine microalgae as a source of EPA and DHA-rich raw material for aquafeed: Research challenges and possibilities. *Aquaculture* 436, 95–103. doi:10.1016/j.aquaculture.2014.10.038.

Chen, C., Harst, A., You, W., Xu, J., Ning, K., and Poetsch, A. (2019). Proteomic study uncovers molecular principles of single-cell-level phenotypic heterogeneity in lipid storage of Nannochloropsis oceanica. *Biotechnol. Biofuels* 12, 1–14. doi:10.1186/s13068-019-1361-7.

Chen, C. Y., Chen, Y. C., Huang, H. C., Ho, S. H., and Chang, J. S. (2015). Enhancing the production of eicosapentaenoic acid (EPA) from Nannochloropsis oceanica CY2 using innovative photobioreactors with optimal light source arrangements. *Bioresour. Technol.* 191, 407–413. doi:10.1016/j.biortech.2015.03.001.

Chen, C. Y., Chen, Y. C., Huang, H. C., Huang, C. C., Lee, W. L., and Chang, J. S. (2013). Engineering strategies for enhancing the production of eicosapentaenoic acid (EPA) from an isolated microalga Nannochloropsis oceanica CY2. *Bioresour. Technol.* 147, 160–167. doi:10.1016/j.biortech.2013.08.051.

Chen, C. Y., Nagarajan, D., and Cheah, W. Y. (2018a). Eicosapentaenoic acid production from Nannochloropsis oceanica CY2 using deep sea water in outdoor plastic-bag type photobioreactors. *Bioresour. Technol.* 253, 1–7. doi:10.1016/j.biortech.2017.12.102.

Chen, C. Y., Nagarajan, D., and Cheah, W. Y. (2018b). Eicosapentaenoic acid production from Nannochloropsis oceanica CY2 using deep sea water in outdoor plastic-bag type photobioreactors. *Bioresour. Technol.* 253, 1–7. doi:10.1016/j.biortech.2017.12.102.

Chen, Y., and Vaidyanathan, S. (2013). Simultaneous assay of pigments, carbohydrates, proteins and lipids in microalgae. *Anal. Chim. Acta* 776, 31–40. doi:10.1016/j.aca.2013.03.005.

Chew, K. W., Yap, J. Y., Show, P. L., Suan, N. H., Juan, J. C., Ling, T. C., et al. (2017). Microalgae biorefinery: High value products perspectives. *Bioresour. Technol.* 229, 53–62. doi:10.1016/j.biortech.2017.01.006.

Chini Zittelli, G., Lavista, F., Bastianini, A., Rodolfi, L., Vincenzini, M., and Tredici, M. R. (1999). Production of eicosapentaenoic acid by Nannochloropsis sp. cultures in outdoor tubular photobioreactors. *J. Biotechnol.* 70, 299–312. doi:10.1016/S0168-1656(99)00082-6.

Chiu, L. Da, Ho, S. H., Shimada, R., Ren, N. Q., and Ozawa, T. (2017). Rapid in vivo lipid/carbohydrate quantification of single microalgal cell by Raman spectral imaging to reveal salinity-induced starch-to-lipid shift. *Biotechnol. Biofuels* 10, 1–9. doi:10.1186/s13068-016-0691-y.

Chiu, S. Y., Kao, C. Y., Tsai, M. T., Ong, S. C., Chen, C. H., and Lin, C. S. (2009). Lipid accumulation and CO2 utilization of Nannochloropsis oculata in response to CO2 aeration. *Bioresour. Technol.* 100, 833–838. doi:10.1016/j.biortech.2008.06.061.

Choix, F. J., Bashan, Y., Mendoza, A., and De-Bashan, L. E. (2014). Enhanced activity of ADP glucose pyrophosphorylase and formation of starch induced by Azospirillum brasilense in Chlorella vulgaris. *J. Biotechnol.* 177, 22–34. doi:10.1016/j.jbiotec.2014.02.014.

Chua, E. T., Dal'Molin, C., Thomas-Hall, S., Netzel, M. E., Netzel, G., and Schenk, P. M. (2020). Cold and dark treatments induce omega-3 fatty acid and carotenoid production in Nannochloropsis oceanica. *Algal Res.* 51, 102059. doi:10.1016/j.algal.2020.102059.

Chung, I. K., Beardall, J., Mehta, S., Sahoo, D., and Stojkovic, S. (2011). Using marine macroalgae for carbon sequestration: A critical appraisal. *J. Appl. Phycol.* 23, 877–886. doi:10.1007/s10811-010-9604-9.

Collos, Y., Mornet, F., Sciandra, A., Waser, N., Larson, A., and Harrison, P. J. (1999). An optical method for the rapid measurement of micromolar concentrations of nitrate in marine phytoplankton cultures. *J. Appl. Phycol.* 11, 179–184. doi:10.1023/A:1008046023487.

Converti, A., Casazza, A. A., Ortiz, E. Y., Perego, P., and Del Borghi, M. (2009). Effect of temperature and nitrogen concentration on the growth and lipid content of Nannochloropsis oculata and Chlorella vulgaris for biodiesel production. *Chem. Eng. Process. Process Intensif.* 48, 1146–1151. doi:10.1016/j.cep.2009.03.006.

Costache, T. A., Gabriel Acien Fernandez, F., Morales, M. M., Fernández-Sevilla, J. M., Stamatin, I., and Molina, E. (2013). Comprehensive model of microalgae photosynthesis rate as a function of culture conditions in photobioreactors. *Appl. Microbiol. Biotechnol.* 97, 7627–7637. doi:10.1007/s00253-013-5035-2.

Cunha, P., Pereira, H., Costa, M., Pereira, J., Silva, J. T., Fernandes, N., et al. (2020). Nannochloropsis oceanica cultivation in pilot-scale raceway ponds-from design to cultivation. *Appl. Sci.* 10. doi:10.3390/app10051725.

Daboussi, F., Leduc, S., Maréchal, A., Dubois, G., Guyot, V., Perez-Michaut, C., et al. (2014). Genome engineering empowers the diatom Phaeodactylum tricornutum for

biotechnology. *Nat. Commun.* 5, 1–7. doi:10.1038/ncomms4831.

Dar, A. A., Choudhury, A. R., Kancharla, P. K., and Arumugam, N. (2017). The FAD2 gene in plants: Occurrence, regulation, and role. *Front. Plant Sci.* 8, 1–16. doi:10.3389/fpls.2017.01789.

der Poel, A. F. B. va., Abdollahi, M. R., Cheng, H., Colovic, R., den Hartog, L. A., Miladinovic, D., et al. (2020). Future directions of animal feed technology research to meet the challenges of a changing world. *Anim. Feed Sci. Technol.* 270, 1–14. doi:10.1016/j.anifeedsci.2020.114692.

Devarshi, P. P., Grant, R. W., Ikonte, C. J., and Hazels Mitmesser, S. (2019). Maternal Omega-3 Nutrition , Placental Transfer and. 11, 1107.

Doan, T. T. Y., and Obbard, J. P. (2012). Enhanced intracellular lipid in Nannochloropsis sp. via random mutagenesis and flow cytometric cell sorting. *Algal Res.* 1, 17–21. doi:10.1016/j.algal.2012.03.001.

Dolch, L.-J., Rak, C., Perin, G., Tourcier, G., Broughton, R., Leterrier, M., et al. (2017). A Palmitic Acid Elongase Affects Eicosapentaenoic Acid and Plastidial Monogalactosyldiacylglycerol Levels in Nannochloropsis. *Plant Physiol.* 173, 742–759. doi:10.1104/pp.16.01420.

Dragosits, M., and Mattanovich, D. (2013). Adaptive laboratory evolution – principles and applications for biotechnology TL - 12. *Microb. Cell Fact.* 12 VN-r, 64. doi:10.1186/1475-2859-12-64.

Dunbar, B. S., Bosire, R. V., and Deckelbaum, R. J. (2014). Omega 3 and omega 6 fatty acids in human and animal health: An African perspective. *Mol. Cell. Endocrinol.* 398, 69–77. doi:10.1016/j.mce.2014.10.009.

Egbo, M. K., Okoani, A. O., and Okoh, I. E. (2018). Photobioreactors for microalgae cultivation – An Overview. *Int. J. Sci. Engeering Res.* 9, 65–74.

Fajardo, C., De Donato, M., Carrasco, R., Martínez-Rodríguez, G., Mancera, J. M., and Fernández-Acero, F. J. (2020). Advances and challenges in genetic engineering of microalgae. *Rev. Aquac.* 12, 365–381. doi:10.1111/raq.12322.

Farag, I., & Price, K. (2013). Resources Conservation in Microalgae Biodiesel Production. *Int. J. Eng. Tech. Res.*, 49–56. Available at: https://www.erpublication.org/published_paper/IJETR011833.pdf.

Fernández-Acero, F. J., Amil-Ruiz, F., Durán-Peña, M. J., Carrasco, R., Fajardo, C., Guarnizo, P., et al. (2019). Valorisation of the microalgae Nannochloropsis gaditana biomass by

proteomic approach in the context of circular economy. *J. Proteomics* 193, 239–242. doi:10.1016/j.jprot.2018.10.015.

Freire, I., Cortina-Burgueño, A., Grille, P., Arizcun Arizcun, M., Abellán, E., Segura, M., et al. (2016). Nannochloropsis limnetica: A freshwater microalga for marine aquaculture. *Aquaculture* 459, 124–130. doi:10.1016/j.aquaculture.2016.03.015.

Fu, W., Chaiboonchoe, A., Khraiwesh, B., Nelson, D. R., Al-Khairy, D., Mystikou, A., et al. (2016). Algal cell factories: Approaches, applications, and potentials. *Mar. Drugs* 14, 225–244. doi:10.3390/md14120225.

Fu, W., Guomundsson, ??lafur, Paglia, G., Herj??lfsson, G., Andr??sson, ??lafur S., Palsson, B. O., et al. (2013). Enhancement of carotenoid biosynthesis in the green microalga Dunaliella salina with light-emitting diodes and adaptive laboratory evolution. *Appl. Microbiol. Biotechnol.* 97, 2395–2403. doi:10.1007/s00253-012-4502-5.

Fukuyama, K. (2004). Structure and function of plant-type ferredoxins. *Photosynth. Res.* 81, 289–301. doi:10.1023/B:PRES.0000036882.19322.0a.

Garibay-Hernández, A., Barkla, B. J., Vera-Estrella, R., Martinez, A., and Pantoja, O. (2017). Membrane proteomic insights into the physiology and taxonomy of an oleaginous green microalga. *Plant Physiol.* 173, 390–416. doi:10.1104/pp.16.01240.

Gimpel, J. A., Henríquez, V., and Mayfield, S. P. (2015). In metabolic engineering of eukaryotic microalgae: Potential and challenges come with great diversity. *Front. Microbiol.* 6, 1–14. doi:10.3389/fmicb.2015.01376.

Gong, Y., Guo, X., Wan, X., Liang, Z., and Jiang, M. (2013). Triacylglycerol accumulation and change in fatty acid content of four marine oleaginous microalgae under nutrient limitation and at different culture ages. *J. Basic Microbiol.* 53, 29–36. doi:10.1002/jobm.201100487.

Grant, M. A. A., Kazamia, E., Cicuta, P., and Smith, A. G. (2014). Direct exchange of vitamin B 12 is demonstrated by modelling the growth dynamics of algal – bacterial cocultures. 8, 1418–1427. doi:10.1038/ismej.2014.9.

Griffiths, M. J., Garcin, C., van Hille, R. P., and Harrison, S. T. L. (2011). Interference by pigment in the estimation of microalgal biomass concentration by optical density. *J. Microbiol. Methods* 85, 119–123. doi:10.1016/j.mimet.2011.02.005.

Gu, N., Lin, Q., Li, G., Tan, Y., Huang, L., and Lin, J. (2012). Effect of salinity on growth, biochemical composition, and lipid productivity of Nannochloropsis oculata CS 179. *Eng.*

Life Sci. 12, 631–637. doi:10.1002/elsc.201100204.

Guarnieri, M. T., and Pienkos, P. T. (2015). Algal omics: unlocking bioproduct diversity in algae cell factories. *Photosynth. Res.* 123, 255–263. doi:10.1007/s11120-014-9989-4.

Guedes, A. C., Meireles, L. A., Amaro, H. M., and Malcata, F. X. (2010). Changes in lipid class and fatty acid composition of cultures of Pavlova lutheri, in response to light intensity. *JAOCS, J. Am. Oil Chem. Soc.* 87, 791–801. doi:10.1007/s11746-010-1559-0.

Guéguen, N., Moigne, D. Le, Amato, A., Salvaing, J., and Maréchal, E. (2021). Lipid Droplets in Unicellular Photosynthetic Stramenopiles. 12, 1–22. doi:10.3389/fpls.2021.639276.

Han, D., Jia, J., Li, J., Sommerfeld, M., Xu, J., and Hu, Q. (2017). Metabolic remodeling of membrane glycerolipids in the microalga Nannochloropsis oceanica under nitrogen deprivation. *Front. Mar. Sci.* 4, 1–15. doi:10.3389/fmars.2017.00242.

Hemaiswarya, S., Raja, R., Kumar, R. R., Ganesan, V., and Anbazhagan, C. (2011). Microalgae: A sustainable feed source for aquaculture. *World J. Microbiol. Biotechnol.* 27, 1737–1746. doi:10.1007/s11274-010-0632-z.

Henry, C. (2005). Basal metabolic rate studies in humans: measurement and development of new equations. *Public Health Nutr.* 8, 1133–1152. doi:10.1079/phn2005801.

Hlavova, M., Turoczy, Z., and Bisova, K. (2015). Improving microalgae for biotechnology - From genetics to synthetic biology. *Biotechnol. Adv.* 33, 1194–1203. doi:10.1016/j.biotechadv.2015.01.009.

Hoffmann, M., Marxen, K., Schulz, R., and Vanselow, K. H. (2010). TFA and EPA productivities of Nannochloropsis salina influenced by temperature and nitrate stimuli in turbidostatic controlled experiments. *Mar. Drugs* 8, 2526–2545. doi:10.3390/md8092526.

Hu, F., Clevenger, A. L., Zheng, P., Huang, Q., and Wang, Z. (2020). Low-temperature effects on docosahexaenoic acid biosynthesis in Schizochytrium sp. TIO01 and its proposed underlying mechanism. *Biotechnol. Biofuels* 13, 1–14. doi:10.1186/s13068-020-01811-y.

Hu, H., and Gao, K. (2003). Optimization of growth and fatty acid composition of a unicellular marine picoplankton, Nannochloropsis sp., with enriched carbon sources. *Biotechnol. Lett.* 25, 421–425. doi:10.1023/A:1022489108980.

Hu, H., and Gao, K. (2006). Response of growth and fatty acid compositions of Nannochloropsis sp. to environmental factors under elevated CO2 concentration. *Biotechnol. Lett.* 28, 987–992. doi:10.1007/s10529-006-9026-6.

Huang, J., Li, Y., Wan, M., Yan, Y., Feng, F., Qu, X., et al. (2014). Novel flat-plate

photobioreactors for microalgae cultivation with special mixers to promote mixing along the light gradient. *Bioresour. Technol.* 159, 8–16. doi:10.1016/j.biortech.2014.01.134.

Huang, Q., Jiang, F., Wang, L., and Yang, C. (2017). Design of Photobioreactors for Mass Cultivation of Photosynthetic Organisms. *Engineering* 3, 318–329. doi:10.1016/J.ENG.2017.03.020.

Hulatt, C. J., Smolina, I., Dowle, A., Kopp, M., Vasanth, G. K., Hoarau, G. G., et al. (2020). Proteomic and transcriptomic patterns during lipid remodeling in nannochloropsis gaditana. *Int. J. Mol. Sci.* 21, 1–23. doi:10.3390/ijms21186946.

Hulatt, C. J., Wijffels, R. H., Bolla, S., and Kiron, V. (2017). Production of fatty acids and protein by nannochloropsis in flat-plate photobioreactors. *PLoS One* 12, 1–17. doi:10.1371/journal.pone.0170440.

Itzhaki, R. F., and Gill, D. M. (1964). A micro-biuret method for estimating proteins. *Anal. Biochem.* 9, 401–410. doi:10.1016/0003-2697(64)90200-3.

Iwai, M., Hori, K., Sasaki-Sekimoto, Y., Shimojima, M., and Ohta, H. (2015). Manipulation of oil synthesis in Nannochloropsis strain NIES-2145 with a phosphorus starvation-inducible promoter from Chlamydomonas reinhardtii. *Front. Microbiol.* 6, 1–15. doi:10.3389/fmicb.2015.00912.

Jagadevan, S., Banerjee, A., Banerjee, C., Guria, C., Tiwari, R., Baweja, M., et al. (2018). Recent developments in synthetic biology and metabolic engineering in microalgae towards biofuel production. *Biotechnol. Biofuels* 11, 1–21. doi:10.1186/s13068-018-1181-1.

Jakhwal, P., Kumar Biswas, J., Tiwari, A., Kwon, E. E., and Bhatnagar, A. (2022). Genetic and non-genetic tailoring of microalgae for the enhanced production of eicosapentaenoic acid (EPA) and docosahexaenoic acid (DHA) – A review. *Bioresour. Technol.* 344, 126250. doi:10.1016/j.biortech.2021.126250.

Janssen, J. H., Lamers, P. P., de Vos, R. C. H., Wijffels, R. H., and Barbosa, M. J. (2019). Translocation and de novo synthesis of eicosapentaenoic acid (EPA) during nitrogen starvation in Nannochloropsis gaditana. *Algal Res.* 37, 138–144. doi:10.1016/j.algal.2018.11.025.

Janssen, J. H., Spoelder, J., Koehorst, J. J., Schaap, P. J., Wijffels, R. H., and Barbosa, M. J. (2020). Time-dependent transcriptome profile of genes involved in triacylglycerol (TAG) and polyunsaturated fatty acid synthesis in Nannochloropsis gaditana during nitrogen starvation. *J. Appl. Phycol.* doi:10.1007/s10811-019-02021-2.

Janssen, M., Tramper, J., Mur, L. R., and Wijffels, R. H. (2003). Enclosed outdoor photobioreactors: Light regime, photosynthetic efficiency, scale-up, and future prospects. *Biotechnol. Bioeng.* 81, 193–210. doi:10.1002/bit.10468.

Jeon, S., Koh, H. G., Cho, J. M., Kang, N. K., and Chang, Y. K. (2021). Enhancement of lipid production in Nannochloropsis salina by overexpression of endogenous NADP-dependent malic enzyme. *Algal Res.* 54, 102218. doi:10.1016/j.algal.2021.102218.

Jiang, J. Y., Zhu, S., Zhang, Y., Sun, X., Hu, X., Huang, H., et al. (2019). Integration of lipidomic and transcriptomic profiles reveals novel genes and regulatory mechanisms of Schizochytrium sp. in response to salt stress. *Bioresour. Technol.* 294, 122231. doi:10.1016/j.biortech.2019.122231.

Junpeng, J., Xupeng, C., Miao, Y., and Song, X. (2020). Monogalactosyldiacylglycerols with High PUFA Content From Microalgae for Value-Added Products. *Appl. Biochem. Biotechnol.* 190, 1212–1223. doi:10.1007/s12010-019-03159-y.

Kameda, H., Hirabayashi, K., Wada, K., and Fukuyama, K. (2011). Mapping of Protein-Protein interaction sites in the plant-type [2Fe-2S] Ferredoxin. *PLoS One* 6. doi:10.1371/journal.pone.0021947.

Kandasamy, L. C., Neves, M. A., Demura, M., and Nakajima, M. (2021). The effects of total dissolved carbon dioxide on the growth rate, biochemical composition, and biomass productivity of nonaxenic microalgal polyculture. *Sustain.* 13, 1–10. doi:10.3390/su13042267.

Kang, S., Heo, S., and Lee, J. H. (2019). Techno-economic Analysis of Microalgae-Based Lipid Production: Considering Influences of Microalgal Species. *Ind. Eng. Chem. Res.* 58, 944–955. doi:10.1021/acs.iecr.8b03999.

Kapase, V. U., Nesamma, A. A., and Jutur, P. P. (2018). Identification and characterization of candidates involved in production of OMEGAs in microalgae: a gene mining and phylogenomic approach. *Prep. Biochem. Biotechnol.* 48, 619–628. doi:10.1080/10826068.2018.1476886.

Karthikaichamy, A., Beardall, J., Coppel, R., Noronha, S., Bulach, D., Schittenhelm, R. B., et al. (2021). Data-Independent-Acquisition-Based Proteomic Approach towards Understanding the Acclimation Strategy of Oleaginous Microalga Microchloropsis gaditana CCMP526 in Hypersaline Conditions. *ACS Omega* 6, 22151–22164. doi:10.1021/acsomega.1c02786.

Kaye, Y., Grundman, O., Leu, S., Zarka, A., Zorin, B., Didi-Cohen, S., et al. (2015). Metabolic engineering toward enhanced LC-PUFA biosynthesis in Nannochloropsis oceanica: Overexpression of endogenous δ12 desaturase driven by stress-inducible promoter leads to enhanced deposition of polyunsaturated fatty acids in TAG. *Algal Res.* doi:10.1016/j.algal.2015.05.003.

Kazbar, A., Cogne, G., Urbain, B., Marec, H., Le-Gouic, B., Tallec, J., et al. (2019). Effect of dissolved oxygen concentration on microalgal culture in photobioreactors. *Algal Res.* 39, 101432. doi:10.1016/j.algal.2019.101432.

Kechasov, D., Grahl, I. De, Endries, P., Reumann, S., Biochemistry, P., Biology, I., et al. (2020). Evolutionary Maintenance of the PTS2 Protein Import Pathway in the Stramenopile Alga Nannochloropsis. 8, 1–33. doi:10.3389/fcell.2020.593922.

Khatoon, H., Abdu Rahman, N., Banerjee, S., Harun, N., Suleiman, S. S., Zakaria, N. H., et al. (2014). Effects of different salinities and pH on the growth and proximate composition of Nannochloropsis sp. and Tetraselmis sp. isolated from South China Sea cultured under control and natural condition. *Int. Biodeterior. Biodegrad.* 95, 11–18. doi:10.1016/j.ibiod.2014.06.022.

Khoeyi, Z. A., Seyfabadi, J., and Ramezanpour, Z. (2012). Effect of light intensity and photoperiod on biomass and fatty acid composition of the microalgae, Chlorella vulgaris. *Aquac. Int.* 20, 41–49. doi:10.1007/s10499-011-9440-1.

Khozin-Goldberg, I., and Cohen, Z. (2011). Unraveling algal lipid metabolism: Recent advances in gene identification. *Biochimie* 93, 91–100. doi:10.1016/j.biochi.2010.07.020.

Khozin-Goldberg, I., Iskandarov, U., and Cohen, Z. (2011). LC-PUFA from photosynthetic microalgae: Occurrence, biosynthesis, and prospects in biotechnology. *Appl. Microbiol. Biotechnol.* 91, 905–915. doi:10.1007/s00253-011-3441-x.

Khozin-Goldberg, I., Shrestha, P., and Cohen, Z. (2005). Mobilization of arachidonyl moieties from triacylglycerols into chloroplastic lipids following recovery from nitrogen starvation of the microalga Parietochloris incisa. *Biochim. Biophys. Acta - Mol. Cell Biol. Lipids* 1738, 63–71. doi:10.1016/j.bbalip.2005.09.005.

Kim, Y. K., Yoo, W. I., Lee, S. H., and Lee, M. Y. (2005). Proteomic analysis of cadmium-induced protein profile alterations from marine alga Nannochloropsis oculata. *Ecotoxicology* 14, 589–596. doi:10.1007/s10646-005-0009-5.

Kobayashi, K. (2016). Role of membrane glycerolipids in photosynthesis, thylakoid biogenesis

and chloroplast development. *J. Plant Res.* 129, 565–580. doi:10.1007/s10265-016-0827-y.

Koh, H. G., Kang, N. K., Jeon, S., Shin, S. E., Jeong, B. R., and Chang, Y. K. (2019). Heterologous synthesis of chlorophyll b in Nannochloropsis salina enhances growth and lipid production by increasing photosynthetic efficiency. *Biotechnol. Biofuels* 12, 1–15. doi:10.1186/s13068-019-1462-3.

Kong, F., Romero, I. T., Warakanont, J., and Li-Beisson, Y. (2018). Lipid catabolism in microalgae. *New Phytol.* 218, 1340–1348. doi:10.1111/nph.15047.

Kurita, T., Moroi, K., Iwai, M., Okazaki, K., Shimizu, S., Nomura, S., et al. (2020). Efficient and multiplexable genome editing using Platinum TALENs in oleaginous microalga, Nannochloropsis oceanica NIES-2145. *Genes to Cells* 25, 695–702. doi:10.1111/gtc.12805.

Kwon, M. H., and Yeom, S. H. (2017). Evaluation of closed photobioreactor types and operation variables for enhancing lipid productivity of Nannochloropsis sp. KMMCC 290 for biodiesel production. *Biotechnol. Bioprocess Eng.* 22, 604–611. doi:10.1007/s12257-017-0107-2.

Lafarga-De la Cruz, F., Valenzuela-Espinoza, E., Millán-Núñez, R., Trees, C. C., Santamaría-del-Ángel, E., and Núñez-Cebrero, F. (2006). Nutrient uptake, chlorophyll a and carbon fixation by Rhodomonas sp. (Cryptophyceae) cultured at different irradiance and nutrient concentrations. *Aquac. Eng.* 35, 51–60. doi:10.1016/j.aquaeng.2005.08.004.

Latosinska, A., Vougas, K., Makridakis, M., Klein, J., Mullen, W., Abbas, M., et al. (2015). Comparative analysis of label-free and 8-plex iTRAQ approach for quantitative tissue proteomic analysis. *PLoS One* 10, 1–25. doi:10.1371/journal.pone.0137048.

Lauritano, C., Ferrante, M. I., and Rogato, A. (2019). Marine natural products from microalgae: An -omics overview. *Mar. Drugs* 17, 1–18. doi:10.3390/md17050269.

Lee, Y. H., Yeh, Y. L., Lin, K. H., and Hsu, Y. C. (2013). Using fluorochemical as oxygen carrier to enhance the growth of marine microalga Nannochloropsis oculata. *Bioprocess Biosyst. Eng.* 36, 1071–1078. doi:10.1007/s00449-012-0860-8.

Leflay, H., Okurowska, K., Pandhal, J., and Brown, S. (2020). Pathways to economic viability: A pilot scale and techno-economic assessment for algal bioremediation of challenging waste streams. *Environ. Sci. Water Res. Technol.* 6, 3400–3414. doi:10.1039/d0ew00700e.

Legrand, J., Artu, A., and Pruvost, J. (2021). A review on photobioreactor design and modelling for microalgae production. *React. Chem. Eng.* 6, 1134–1151. doi:10.1039/d0re00450b.

Levasseur, W., Perré, P., and Pozzobon, V. (2020). A review of high value-added molecules production by microalgae in light of the classification. *Biotechnol. Adv.* 41, 107545. doi:10.1016/j.biotechadv.2020.107545.

Li-beisson, Y. N. Y. (2016). *Lipids in Plant and Algae Development*. doi:10.1007/978-3-319-25979-6.

Li, J., Han, D., Wang, D., Ning, K., Jia, J., Wei, L., et al. (2014). Choreography of transcriptomes and lipidomes of Nannochloropsis reveals the mechanisms of oil synthesis in microalgae. *Plant Cell* 26, 1645–1665. doi:10.1105/tpc.113.121418.

Li, T., Wang, W., Yuan, C., Zhang, Y., Xu, J., Zheng, H., et al. (2020). Linking lipid accumulation and photosynthetic efficiency in Nannochloropsis sp. under nutrient limitation and replenishment. *J. Appl. Phycol.* 32, 1619–1630. doi:10.1007/s10811-020-02056-w.

Li, Y., Han, D., Hu, G., Dauvillee, D., Sommerfeld, M., Ball, S., et al. (2010). Chlamydomonas starchless mutant defective in ADP-glucose pyrophosphorylase hyper-accumulates triacylglycerol. *Metab. Eng.* 12, 387–391. doi:10.1016/j.ymben.2010.02.002.

Liang, J., Wen, F., and Liu, J. (2019). Transcriptomic and lipidomic analysis of an EPA-containing Nannochloropsis sp. PJ12 in response to nitrogen deprivation. *Sci. Rep.* 9, 1–18. doi:10.1038/s41598-019-41169-2.

Liang, S., Guo, L., Lin, G., Zhang, Z., Ding, H., Wang, Y., et al. (2017). Improvement of Nannochloropsis oceanica growth performance through chemical mutation and characterization of fast growth physiology by transcriptome profiling. *Chinese J. Oceanol. Limnol.* 35, 792–802. doi:10.1007/s00343-017-6023-7.

Liang, Y., Liu, Y., Tang, J., Ma, J., Cheng, J. J., and Daroch, M. (2018). Transcriptomic profiling and gene disruption revealed that two genes related to Pufas/DHA biosynthesis may be essential for cell growth of Aurantiochytrium sp. *Mar. Drugs* 16, 1–15. doi:10.3390/md16090310.

Lim, D. K. Y., Schuhmann, H., Sharma, K., and Schenk, P. M. (2015). Isolation of High-Lipid Tetraselmis suecica Strains Following Repeated UV-C Mutagenesis, FACS, and High-Throughput Growth Selection. *Bioenergy Res.* 8, 750–759. doi:10.1007/s12155-014-9553-2.

Liu, B., and Benning, C. (2013). Lipid metabolism in microalgae distinguishes itself. *Curr. Opin.*

Biotechnol. 24, 300–309. doi:10.1016/j.copbio.2012.08.008.

Liu, J., Han, D., Yoon, K., Hu, Q., and Li, Y. (2016a). Characterization of type 2 diacylglycerol acyltransferases in Chlamydomonas reinhardtii reveals their distinct substrate specificities and functions in triacylglycerol biosynthesis. *Plant J.* 86, 3–19. doi:10.1111/tpj.13143.

Liu, J., Mao, X., Zhou, W., and Guarnieri, M. T. (2016b). Simultaneous production of triacylglycerol and high-value carotenoids by the astaxanthin-producing oleaginous green microalga Chlorella zofingiensis. *Bioresour. Technol.* 214, 319–327. doi:10.1016/j.biortech.2016.04.112.

Liu, J., Pei, G., Diao, J., Chen, Z., Liu, L., Chen, L., et al. (2017). Screening and transcriptomic analysis of Crypthecodinium cohnii mutants with high growth and lipid content using the acetyl-CoA carboxylase inhibitor sethoxydim. *Appl. Microbiol. Biotechnol.* 101, 6179–6191. doi:10.1007/s00253-017-8397-z.

Liu, J., Sun, Z., Zhong, Y., Huang, J., Hu, Q., and Chen, F. (2012). Stearoyl-acyl carrier protein desaturase gene from the oleaginous microalga Chlorella zofingiensis: Cloning, characterization and transcriptional analysis. *Planta* 236, 1665–1676. doi:10.1007/s00425-012-1718-7.

Liu, S., Zhao, Y., Liu, L., Ao, X., Ma, L., Wu, M., et al. (2015). Improving Cell Growth and Lipid Accumulation in Green Microalgae Chlorella sp. via UV Irradiation. *Appl. Biochem. Biotechnol.* 175, 3507–3518. doi:10.1007/s12010-015-1521-6.

Ma, R., Thomas-Hall, S. R., Chua, E. T., Eltanahy, E., Netzel, M. E., Netzel, G., et al. (2018). Blue light enhances astaxanthin biosynthesis metabolism and extraction efficiency in Haematococcus pluvialis by inducing haematocyst germination. *Algal Res.* 35, 215–222. doi:10.1016/j.algal.2018.08.023.

Ma, X., Liu, J., Liu, B., Chen, T., Yang, B., and Chen, F. (2016a). Physiological and biochemical changes reveal stress-associated photosynthetic carbon partitioning into triacylglycerol in the oleaginous marine alga Nannochloropsis oculata. *Algal Res.* 16, 28–35. doi:10.1016/j.algal.2016.03.005.

Ma, X. N., Chen, T. P., Yang, B., Liu, J., and Chen, F. (2016b). Lipid production from Nannochloropsis. *Mar. Drugs* 14. doi:10.3390/md14040061.

Ma, Y., Wang, Z., Yu, C., Yin, Y., and Zhou, G. (2014). Evaluation of the potential of 9 Nannochloropsis strains for biodiesel production. *Bioresour. Technol.* 167, 503–509.

doi:10.1016/j.biortech.2014.06.047.

Ma, Y., Wang, Z., Zhu, M., Yu, C., Cao, Y., Zhang, D., et al. (2013). Increased lipid productivity and TAG content in Nannochloropsis by heavy-ion irradiation mutagenesis. *Bioresour. Technol.* 136, 360–367. doi:10.1016/j.biortech.2013.03.020.

Mahat, K., Jamaluddin, H., and Nor, N. A. (2015). The effect of different phosphate concentration on growth, lipid productivity and methyl palmitate methyl ester production by Nannochloropsis oculata. *J. Teknol.* 77, 79–83. doi:10.11113/jt.v77.6915.

Mao, X., Zhang, Y., Wang, X., and Liu, J. (2020). Novel insights into salinity-induced lipogenesis and carotenogenesis in the oleaginous astaxanthin-producing alga Chromochloris zofingiensis: A multi-omics study. *Biotechnol. Biofuels* 13, 1–24. doi:10.1186/s13068-020-01714-y.

Markou, G., Angelidaki, I., and Georgakakis, D. (2012). Microalgal carbohydrates: An overview of the factors influencing carbohydrates production, and of main bioconversion technologies for production of biofuels. *Appl. Microbiol. Biotechnol.* 96, 631–645. doi:10.1007/s00253-012-4398-0.

Martínez-Roldán, A. J., Perales-Vela, H. V., Cañizares-Villanueva, R. O., and Torzillo, G. (2014). Physiological response of Nannochloropsis sp. to saline stress in laboratory batch cultures. *J. Appl. Phycol.* 26, 115–121. doi:10.1007/s10811-013-0060-1.

Martins, D. A., Custódio, L., Barreira, L., Pereira, H., Ben-Hamadou, R., Varela, J., et al. (2013). Alternative sources of n-3 long-chain polyunsaturated fatty acids in marine microalgae. *Mar. Drugs* 11, 2259–2281. doi:10.3390/md11072259.

Mazlan, A. G., Zaidi, C. C., Wan-Lotfi, W. M., and Othman, B. H. R. (2005). On the current status of coastal marine biodiversity in Malaysia. *Indian J. Mar. Sci.* 34, 76–87.

Meireles, L. A., Guedes, A. C., and Malcata, F. X. (2003a). Increase of the Yields of Eicosapentaenoic and Docosahexaenoic Acids by the Microalga Pavlova lutheri Following Random Mutagenesis. *Biotechnol. Bioeng.* 81, 50–55. doi:10.1002/bit.10451.

Meireles, L. A., Guedes, A. C., and Malcata, F. X. (2003b). Increase of the Yields of Eicosapentaenoic and Docosahexaenoic Acids by the Microalga Pavlova lutheri Following Random Mutagenesis. *Biotechnol. Bioeng.* 81, 50–55. doi:10.1002/bit.10451.

Meng, Q., Liang, H., and Gao, H. (2018). Roles of multiple KASIII homologues of Shewanella oneidensis in initiation of fatty acid synthesis and in cerulenin resistance. *Biochim. Biophys. Acta - Mol. Cell Biol. Lipids* 1863, 1153–1163. doi:10.1016/j.bbalip.2018.06.020.

Meng, Y., Cao, X., Yao, C., Xue, S., and Yang, Q. (2017). Identification of the role of polar glycerolipids in lipid metabolism and their acyl attribution for TAG accumulation in Nannochloropsis oceanica. *Algal Res.* 24, 122–129. doi:10.1016/j.algal.2017.03.004.

Meng, Y., Jiang, J., Wang, H., Cao, X., Xue, S., Yang, Q., et al. (2015). The characteristics of TAG and EPA accumulation in Nannochloropsis oceanica IMET1 under different nitrogen supply regimes. *Bioresour. Technol.* 179, 483–489. doi:10.1016/j.biortech.2014.12.012.

Metsoviti, M. N., Papapolymerou, G., Karapanagiotidis, I. T., and Katsoulas, N. (2019). Comparison of growth rate and nutrient content of five microalgae species cultivated in greenhouses. *Plants* 8, 1–13. doi:10.3390/plants8080279.

Metsoviti, M. N., Papapolymerou, G., Karapanagiotidis, I. T., and Katsoulas, N. (2020). Effect of light intensity and quality on growth rate and composition of Chlorella vulgaris. *Plants* 9, 1–17. doi:10.3390/plants9010031.

Miazek, K., Kratky, L., Sulc, R., Jirout, T., Aguedo, M., Richel, A., et al. (2017). Effect of organic solvents on microalgae growth, metabolism and industrial bioproduct extraction: A review. *Int. J. Mol. Sci.* 18. doi:10.3390/ijms18071429.

Minhas, A. K., Hodgson, P., Barrow, C. J., and Adholeya, A. (2016). A review on the assessment of stress conditions for simultaneous production of microalgal lipids and carotenoids. *Front. Microbiol.* 7, 1–19. doi:10.3389/fmicb.2016.00546.

Miranda, J., and Krishnakumar, G. (2015). Microalgal diversity in relation to the physicochemical parameters of some Industrial sites in Mangalore, South India. *Environ. Monit. Assess.* 187. doi:10.1007/s10661-015-4871-1.

Mirón, A. S., Gómez, A. C., Camacho, F. G., Grima, E. M., and Chisti, Y. (1999). Comparative evaluation of compact photobioreactors for large-scale monoculture of microalgae. *Prog. Ind. Microbiol.* 35, 249–270. doi:10.1016/S0079-6352(99)80119-2.

Mishra, A., Medhi, K., Malaviya, P., and Thakur, I. S. (2019). Omics approaches for microalgal applications: Prospects and challenges. *Bioresour. Technol.* 291, 121890. doi:10.1016/j.biortech.2019.121890.

Mitra, M., Patidar, S. K., George, B., Shah, F., and Mishra, S. (2015a). A euryhaline nannochloropsis gaditana with potential for nutraceutical (EPA) and biodiesel production. *Algal Res.* 8, 161–167. doi:10.1016/j.algal.2015.02.006.

Mitra, M., Patidar, S. K., and Mishra, S. (2015b). Integrated process of two stage cultivation of Nannochloropsis sp. for nutraceutically valuable eicosapentaenoic acid along with

biodiesel. *Bioresour. Technol.* 193, 363–369. doi:10.1016/j.biortech.2015.06.033.

Moha-León, J. D., Pérez-Legaspi, I. A., Ortega-Clemente, L. A., Rubio-Franchini, I., and Ríos-Leal, E. (2019). Improving the lipid content of Nannochloropsis oculata by a mutation-selection program using UV radiation and quizalofop. *J. Appl. Phycol.* 31, 191–199. doi:10.1007/s10811-018-1568-1.

Mohammady, N. G. E., El-Khatib, K. M., El-Galad, M. I., Abo El-Enin, S. A., Attia, N. K., El-Araby, R., et al. (2020). Preliminary study on the economic assessment of culturing Nannochloropsis sp. in Egypt for the production of biodiesel and high-value biochemicals. *Biomass Convers. Biorefinery*. doi:10.1007/s13399-020-00878-9.

Mokashi, K., Shetty, V., George, S. A., and Sibi, G. (2016). Sodium Bicarbonate as Inorganic Carbon Source for Higher Biomass and Lipid Production Integrated Carbon Capture in Chlorella vulgaris. *Achiev. Life Sci.* 10, 111–117. doi:10.1016/j.als.2016.05.011.

Moraes, L., Rosa, G. M., Morillas España, A., Santos, L. O., Morais, M. G., Molina Grima, E., et al. (2019). Engineering strategies for the enhancement of Nannochloropsis gaditana outdoor production: Influence of the CO2 flow rate on the culture performance in tubular photobioreactors. *Process Biochem.* 76, 171–177. doi:10.1016/j.procbio.2018.10.010.

Morales-Sánchez, D., Kyndt, J., Ogden, K., and Martinez, A. (2016). Toward an understanding of lipid and starch accumulation in microalgae: A proteomic study of Neochloris oleoabundans cultivated under N-limited heterotrophic conditions. *Algal Res.* 20, 22–34. doi:10.1016/j.algal.2016.09.006.

Moreira, D., and Pires, J. C. M. (2016). Atmospheric CO2 capture by algae: Negative carbon dioxide emission path. *Bioresour. Technol.* 215, 371–379. doi:10.1016/j.biortech.2016.03.060.

Mühlroth, A., Li, K., Røkke, G., Winge, P., Olsen, Y., Hohmann-Marriott, M. F., et al. (2013). Pathways of lipid metabolism in marine algae, co-expression network, bottlenecks and candidate genes for enhanced production of EPA and DHA in species of chromista. *Mar. Drugs* 11, 4662–4697. doi:10.3390/md11114662.

Murakami, H., Kakutani, N., Kuroyanagi, Y., Iwai, M., Hori, K., Shimojima, M., et al. (2020). MYB-like transcription factor NoPSR1 is crucial for membrane lipid remodeling under phosphate starvation in the oleaginous microalga Nannochloropsis oceanica. *FEBS Lett.* 594, 3384–3394. doi:10.1002/1873-3468.13902.

Murakami, H., Nobusawa, T., Hori, K., Shimojima, M., and Ohta, H. (2018). Betaine lipid is crucial for adapting to low temperature and phosphate deficiency in nannochloropsis. *Plant Physiol.* 177, 181–193. doi:10.1104/pp.17.01573.

Naduthodi, M. I. S., Claassens, N. J., D'Adamo, S., van der Oost, J., and Barbosa, M. J. (2021). Synthetic Biology Approaches To Enhance Microalgal Productivity. *Trends Biotechnol.* 39, 1019–1036. doi:10.1016/j.tibtech.2020.12.010.

Napier, J. A., Usher, S., Haslam, R. P., Ruiz-Lopez, N., and Sayanova, O. (2015). Transgenic plants as a sustainable, terrestrial source of fish oils. *Eur. J. Lipid Sci. Technol.* 117, 1317–1324. doi:10.1002/ejlt.201400452.

Ng, I. S., Keskin, B. B., and Tan, S. I. (2020). A Critical Review of Genome Editing and Synthetic Biology Applications in Metabolic Engineering of Microalgae and Cyanobacteria. *Biotechnol. J.* 15, 1–17. doi:10.1002/biot.201900228.

Nichols, P. D., McManus, A., Krail, K., Sinclair, A. J., and Miller, M. (2014). Recent advances in omega-3: Health benefits, Sources, Products and bioavailability. *Nutrients* 6, 3727–3733. doi:10.3390/nu6093727.

Nielsen, S. L., and Hansen, B. W. (2019). Evaluation of the robustness of optical density as a tool for estimation of biomass in microalgal cultivation: The effects of growth conditions and physiological state. *Aquac. Res.* 50, 2698–2706. doi:10.1111/are.14227.

Nogueira, N., Nascimento, F. J. A., Cunha, C., and Cordeiro, N. (2020). Nannochloropsis gaditana grown outdoors in annular photobioreactors: Operation strategies. *Algal Res.* 48, 101913. doi:10.1016/j.algal.2020.101913.

Norambuena, F., Hermon, K., Skrzypczyk, V., Emery, J. A., Sharon, Y., Beard, A., et al. (2015). Algae in fish feed: Performances and fatty acid metabolism in juvenile Atlantic Salmon. *PLoS One* 10, 1–17. doi:10.1371/journal.pone.0124042.

Oishi, Y., Otaki, R., Iijima, Y., Kumagai, E., Aoki, M., Tsuzuki, M., et al. (2022). Diacylglyceryl-N,N,N-trimethylhomoserine-dependent lipid remodeling in a green alga, Chlorella kessleri. *Commun. Biol.* 5. doi:10.1038/s42003-021-02927-z.

Okuda, T., Ando, A., Negoro, H., Muratsubaki, T., Kikukawa, H., Sakamoto, T., et al. (2015). Eicosapentaenoic acid (EPA) production by an oleaginous fungus Mortierella alpina expressing heterologous the Δ17-desaturase gene under ordinary temperature. *Eur. J. Lipid Sci. Technol.* 117, 1919–1927. doi:10.1002/ejlt.201400657.

Oliver, L., Dietrich, T., Marañón, I., Villarán, M. C., and Barrio, R. J. (2020). Producing omega-

3 polyunsaturated fatty acids: A review of sustainable sources and future trends for the EPA and DHA market. *Resources* 9, 1–15. doi:10.3390/resources9120148.

Osumi, T., Tsukamoto, T., and Hata, S. (1992). 済無No Title No Title No Title. *Biochem. Biophys. Res. Commun.* 186, 811–818.

Pal, D., Khozin-Goldberg, I., Cohen, Z., and Boussiba, S. (2011). The effect of light, salinity, and nitrogen availability on lipid production by Nannochloropsis sp. *Appl. Microbiol. Biotechnol.* 90, 1429–1441. doi:10.1007/s00253-011-3170-1.

Park, S. Bin, Yun, J. H., Ryu, A. J., Yun, J., Kim, J. W., Lee, S., et al. (2021). Development of a novel nannochloropsis strain with enhanced violaxanthin yield for large-scale production. *Microb. Cell Fact.* 20, 1–11. doi:10.1186/s12934-021-01535-0.

Patelou, M., Infante, C., Dardelle, F., Randewig, D., Kouri, E. D., Udvardi, M. K., et al. (2020). Transcriptomic and metabolomic adaptation of Nannochloropsis gaditana grown under different light regimes. *Algal Res.* 45, 101735. doi:10.1016/j.algal.2019.101735.

Peltomaa, E., Johnson, M. D., and Taipale, S. J. (2018). Marine cryptophytes are great sources of EPA and DHA. *Mar. Drugs* 16, 1–11. doi:10.3390/md16010003.

Pereira, H., Páramo, J., Silva, J., Marques, A., Barros, A., Maurício, D., et al. (2018). Scale-up and large-scale production of Tetraselmis sp. CTP4 (Chlorophyta) for CO2 mitigation: From an agar plate to 100-m3 industrial photobioreactors. *Sci. Rep.* 8, 1–11. doi:10.1038/s41598-018-23340-3.

Perin, G., Bellan, A., Segalla, A., Meneghesso, A., Alboresi, A., and Morosinotto, T. (2015). Generation of random mutants to improve light-use efficiency of Nannochloropsis gaditana cultures for biofuel production. *Biotechnol. Biofuels* 8, 1–13. doi:10.1186/s13068-015-0337-5.

Poliner, E., Pulman, J. A., Zienkiewicz, K., Childs, K., Benning, C., and Farré, E. M. (2018). A toolkit for Nannochloropsis oceanica CCMP1779 enables gene stacking and genetic engineering of the eicosapentaenoic acid pathway for enhanced long-chain polyunsaturated fatty acid production. *Plant Biotechnol. J.* 16, 298–309. doi:10.1111/pbi.12772.

Posch, A. (2014). Sample preparation guidelines for two-dimensional electrophoresis. *Arch. Physiol. Biochem.* 120, 192–197. doi:10.3109/13813455.2014.955031.

Qi, B., Fraser, T., Mugford, S., Dobson, G., Sayanova, O., Butler, J., et al. (2004). Production of very long chain polyunsaturated omega-3 and omega-6 fatty acids in plants. *Nat.*

Biotechnol. 22, 739–745. doi:10.1038/nbt972.

Quinn, J. C., Yates, T., Douglas, N., Weyer, K., Butler, J., Bradley, T. H., et al. (2012). Nannochloropsis production metrics in a scalable outdoor photobioreactor for commercial applications. *Bioresour. Technol.* 117, 164–171. doi:10.1016/j.biortech.2012.04.073.

Rasdi, N. W., and Qin, J. G. (2015). Effect of N:P ratio on growth and chemical composition of Nannochloropsis oculata and Tisochrysis lutea. *J. Appl. Phycol.* 27, 2221–2230. doi:10.1007/s10811-014-0495-z.

Razzak, S. A., Ilyas, M., Ali, S. A. M., and Hossain, M. M. (2015). Effects of CO2 Concentration and pH on mixotrophic growth of Nannochloropsis oculata. *Appl. Biochem. Biotechnol.* 176, 1290–1302. doi:10.1007/s12010-015-1646-7.

Remmers, I. M., Martens, D. E., Wijffels, R. H., and Lamers, P. P. (2017). Dynamics of triacylglycerol and EPA production in Phaeodactylum tricornutum under nitrogen starvation at different light intensities. *PLoS One* 12, 1–13. doi:10.1371/journal.pone.0175630.

Riccio, G., De Luca, D., and Lauritano, C. (2020). Monogalactosyldiacylglycerol and sulfolipid synthesis in microalgae. *Mar. Drugs* 18, 1–18. doi:10.3390/md18050237.

Rocha, J. M. S., Garcia, J. E. C., and Henriques, M. H. F. (2003). Growth aspects of the marine microalga Nannochloropsis gaditana. *Biomol. Eng.* 20, 237–242. doi:10.1016/S1389-0344(03)00061-3.

Rodolfi, L., Zittelli, G. C., Barsanti, L., Rosati, G., and Tredici, M. R. (2003). Growth medium recycling in Nannochloropsis sp. mass cultivation. *Biomol. Eng.* 20, 243–248. doi:10.1016/S1389-0344(03)00063-7.

Rodolfi, L., Zittelli, G. C., Bassi, N., Padovani, G., Biondi, N., Bonini, G., et al. (2009). Microalgae for oil: Strain selection, induction of lipid synthesis and outdoor mass cultivation in a low-cost photobioreactor. *Biotechnol. Bioeng.* 102, 100–112. doi:10.1002/bit.22033.

Roleda, M. Y., Slocombe, S. P., Leakey, R. J. G., Day, J. G., Bell, E. M., and Stanley, M. S. (2013). Effects of temperature and nutrient regimes on biomass and lipid production by six oleaginous microalgae in batch culture employing a two-phase cultivation strategy. *Bioresour. Technol.* 129, 439–449. doi:10.1016/j.biortech.2012.11.043.

Roncaglia, B., Papini, A., Chini Zittelli, G., Rodolfi, L., and Tredici, M. R. (2021). Cell wall and organelle modifications during nitrogen starvation in Nannochloropsis oceanica F&M-

M24. *J. Appl. Phycol.* 33, 2069–2080. doi:10.1007/s10811-021-02416-0.

Roncallo, O. P., García Freites, S., Paternina Castillo, E., Bula Silvera, A., Cortina, A., and Acuña, F. (2013). Comparison of Two Different Vertical Column Photobioreactors for the Cultivation of Nannochloropsis sp. *J. Energy Resour. Technol.* 135, 1–7. doi:10.1115/1.4007689.

Roncarati, A., Meluzzi, A., Acciarri, S., Tallarico, N., and Melotti, P. (2004). Fatty acid composition of different microalgae strains (Nannochloropsis sp., Nannochloropsis oculata (Droop) Hibberd, Nannochloris atomus Butcher and Isochrysis sp.) according to the culture phase and the carbon dioxide concentration. *J. World Aquac. Soc.* 35, 401–411. doi:10.1111/j.1749-7345.2004.tb00104.x.

Roston, R. L., Wang, K., Kuhn, L. A., and Benning, C. (2014). Structural determinants allowing transferase activity in sensitive to freezing 2, classified as a family i lycosyl hydrolase. *J. Biol. Chem.* 289, 26089–26106. doi:10.1074/jbc.M114.576694.

Ruiz-Lopez, N., Haslam, R. P., Usher, S. L., Napier, J. A., and Sayanova, O. (2013). Reconstitution of EPA and DHA biosynthesis in Arabidopsis: Iterative metabolic engineering for the synthesis of n-3 LC-PUFAs in transgenic plants. *Metab. Eng.* 17, 30–41. doi:10.1016/j.ymben.2013.03.001.

Ryu, A. J., Jeong, B. ryool, Kang, N. K., Jeon, S., Sohn, M. G., Yun, H. J., et al. (2021). Safe-Harboring based novel genetic toolkit for Nannochloropsis salina CCMP1776: Efficient overexpression of transgene via CRISPR/Cas9-Mediated Knock-in at the transcriptional hotspot. *Bioresour. Technol.* 340, 125676. doi:10.1016/j.biortech.2021.125676.

Ryu, A. J., Kang, N. K., Jeon, S., Hur, D. H., Lee, E. M., Lee, D. Y., et al. (2020). Development and characterization of a Nannochloropsis mutant with simultaneously enhanced growth and lipid production. *Biotechnol. Biofuels* 13, 1–14. doi:10.1186/s13068-020-01681-4.

Sager, J. C., and Farlane, J. C. M. (2003). Chapter 1. Radiation. *Growth Chamb. Handb.* 46, 30–33.

Santin, A., Russo, M. T., Ferrante, M. I., Balzano, S., Orefice, I., and Sardo, A. (2021). Highly Valuable Polyunsaturated Fatty Acids from Microalgae: Strategies to Improve Their Yields and Their Potential Exploitation in Aquaculture. *Molecules* 26. doi:10.3390/molecules26247697.

Santos-Sánchez, N. F., Valadez-Blanco, R., Hernández-Carlos, B., Torres-Ariño, A., Guadarrama-Mendoza, P. C., and Salas-Coronado, R. (2016). Lipids rich in ω-3

polyunsaturated fatty acids from microalgae. *Appl. Microbiol. Biotechnol.* 100, 8667–8684. doi:10.1007/s00253-016-7818-8.

Schade, S., and Meier, T. (2021). Techno-economic assessment of microalgae cultivation in a tubular photobioreactor for food in a humid continental climate. *Clean Technol. Environ. Policy* 23, 1475–1492. doi:10.1007/s10098-021-02042-x.

Schade, S., Stangl, G. I., and Meier, T. (2020). Distinct microalgae species for food—part 2: comparative life cycle assessment of microalgae and fish for eicosapentaenoic acid (EPA), docosahexaenoic acid (DHA), and protein. *J. Appl. Phycol.* 32, 2997–3013. doi:10.1007/s10811-020-02181-6.

Scholz, M. J., Weiss, T. L., Jinkerson, R. E., Jing, J., Roth, R., Goodenough, U., et al. (2014). Ultrastructure and composition of the Nannochloropsis gaditana cell wall. *Eukaryot. Cell* 13, 1450–1464. doi:10.1128/EC.00183-14.

Sforza, E., Bertucco, A., Morosinotto, T., and Giacometti, G. M. (2012). Photobioreactors for microalgal growth and oil production with Nannochloropsis salina: From lab-scale experiments to large-scale design. *Chem. Eng. Res. Des.* 90, 1151–1158. doi:10.1016/j.cherd.2011.12.002.

Sforza, E., Calvaruso, C., La Rocca, N., and Bertucco, A. (2018). Luxury uptake of phosphorus in Nannochloropsis salina: Effect of P concentration and light on P uptake in batch and continuous cultures. *Biochem. Eng. J.* 134, 69–79. doi:10.1016/j.bej.2018.03.008.

Sforza, E., Calvaruso, C., Meneghesso, A., Morosinotto, T., and Bertucco, A. (2015). Effect of specific light supply rate on photosynthetic efficiency of Nannochloropsis salina in a continuous flat plate photobioreactor. *Appl. Microbiol. Biotechnol.* 99, 8309–8318. doi:10.1007/s00253-015-6876-7.

Sharma, N., Fleurent, G., Awwad, F., Cheng, M., Meddeb-Mouelhi, F., Budge, S. M., et al. (2020). Red light variation an effective alternative to regulate biomass and lipid profiles in phaeodactylum tricornutum. *Appl. Sci.* 10, 1–18. doi:10.3390/app10072531.

Sharmila, D., Suresh, A., Indhumathi, J., Gowtham, K., and Velmurugan, N. (2018). Impact of various color filtered LED lights on microalgae growth, pigments and lipid production. *Eur. J. Biotechnol. Biosci.* 6, 1–7. Available at: www.biosciencejournals.com.

Shi, Y., Liu, M., Ding, W., and Liu, J. (2020). Novel Insights into Phosphorus Deprivation Boosted Lipid Synthesis in the Marine Alga Nannochloropsis oceanica without Compromising Biomass Production . *J. Agric. Food Chem.* 68, 11488–11502.

doi:10.1021/acs.jafc.0c04899.

Shi, Y., Liu, M., Pan, Y., Hu, H., and Liu, J. (2021). Δ6 Fatty Acid Elongase is Involved in Eicosapentaenoic Acid Biosynthesis Via the ω6 Pathway in the Marine Alga Nannochloropsis oceanica. *J. Agric. Food Chem.* 69, 9837–9848. doi:10.1021/acs.jafc.1c04192.

Shield, R. J., and Lupatsch, I. (2012). Algae for Aquaculture and Animal Feeds. *Technol. Assess. - Theory Pract.* Volume 21, 23–37.

Singh, R. N., and Sharma, S. (2012). Development of suitable photobioreactor for algae production - A review. *Renew. Sustain. Energy Rev.* 16, 2347–2353. doi:10.1016/j.rser.2012.01.026.

Sirisuk, P., Sunwoo, I. Y., Kim, S. H., Awah, C. C., Hun Ra, C., Kim, J. M., et al. (2018). Enhancement of biomass, lipids, and polyunsaturated fatty acid (PUFA) production in Nannochloropsis oceanica with a combination of single wavelength light emitting diodes (LEDs) and low temperature in a three-phase culture system. *Bioresour. Technol.* 270, 504–511. doi:10.1016/j.biortech.2018.09.025.

Solovchenko, A., Lukyanov, A., Solovchenko, O., Didi-Cohen, S., Boussiba, S., and Khozin-Goldberg, I. (2014). Interactive effects of salinity, high light, and nitrogen starvation on fatty acid and carotenoid profiles in Nannochloropsis oceanica CCALA 804. *Eur. J. Lipid Sci. Technol.* 116, 635–644. doi:10.1002/ejlt.201300456.

Soriano-Jerez, Y., López-Rosales, L., Cerón-García, M. C., Sánchez-Mirón, A., Gallardo-Rodríguez, J. J., García-Camacho, F., et al. (2021). Long-term biofouling formation mediated by extracellular proteins in Nannochloropsis gaditana microalga cultures at different medium N/P ratios. *Biotechnol. Bioeng.* 118, 1152–1165. doi:10.1002/bit.27632.

Spilling, K., Seppälä, J., Schwenk, D., Rischer, H., and Tamminen, T. (2021). Variation in the fatty acid profiles of two cold water diatoms grown under different temperature, light, and nutrient regimes. *J. Appl. Phycol.* doi:10.1007/s10811-021-02380-9.

Srinivas, R., and Ochs, C. (2012). Effect of UV-A Irradiance on Lipid Accumulation in Nannochloropsis oculata. *Photochem. Photobiol.* 88, 684–689. doi:10.1111/j.1751-1097.2012.01091.x.

Strickland, J.D.H and Parsons, T. R. (1972). Determination of Reactive Phosphorus. *A Pract. Handb. seawater Anal.* 167, 49–55. doi:10.1007/978-1-4615-5439-4_19.

Stunda-Zujeva, A., Zuteris, M., and Rugele, K. (2018). Sunlight potential for microalgae cultivation in the mid-latitude region the baltic states. *Agron. Res.* 16, 910–916. doi:10.15159/AR.18.126.

Su, C. H., Chien, L. J., Gomes, J., Lin, Y. S., Yu, Y. K., Liou, J. S., et al. (2011). Factors affecting lipid accumulation by Nannochloropsis oculata in a two-stage cultivation process. *J. Appl. Phycol.* 23, 903–908. doi:10.1007/s10811-010-9609-4.

Südfeld, C., Hub, M., Figueiredo, D., Naduthodi, M. I. S., Oost, J. Van Der, Wijffels, H., et al. (2021). High-throughput insertional mutagenesis reveals novel targets for enhancing lipid accumulation in Nannochloropsis oceanica. 66, 239–258. doi:10.1016/j.ymben.2021.04.012.

Sugihara, S., Ozaki, T., Tojo, T., Endo, H., Saito, T., and Takimura, Y. (2019). Identification of novel 3-ketoacyl-acyl carrier protein synthase involved in producing medium chain fatty acids from microalgae. *Bioresour. Technol. Reports* 7, 100184. doi:10.1016/j.biteb.2019.03.016.

Suhaimi, N., Maeda, Y., Yoshino, T., and Tanaka, T. (2022). Effects of fatty acid synthase-inhibitors on polyunsaturated fatty acid production in marine diatom Fistulifera solaris JPCC DA0580. *J. Biosci. Bioeng.* 133, 340–346. doi:10.1016/j.jbiosc.2021.12.014.

Sui, Y., Muys, M., Vermeir, P., D'Adamo, S., and Vlaeminck, S. E. (2019). Light regime and growth phase affect the microalgal production of protein quantity and quality with Dunaliella salina. *Bioresour. Technol.* 275, 145–152. doi:10.1016/j.biortech.2018.12.046.

Sun, X. M., Ren, L. J., Ji, X. J., Chen, S. L., Guo, D. S., and Huang, H. (2016). Adaptive evolution of Schizochytrium sp. by continuous high oxygen stimulations to enhance docosahexaenoic acid synthesis. *Bioresour. Technol.* 211, 374–381. doi:10.1016/j.biortech.2016.03.093.

Szabó, M., Parker, K., Guruprasad, S., Kuzhiumparambil, U., Lilley, R. M. C., Tamburic, B., et al. (2014). Photosynthetic acclimation of Nannochloropsis oculata investigated by multi-wavelength chlorophyll fluorescence analysis. *Bioresour. Technol.* 167, 521–529. doi:10.1016/j.biortech.2014.06.046.

Takahashi, T. (2018). Applicability of Automated Cell Counter with a Chlorophyll Detector in Routine Management of Microalgae. *Sci. Rep.* 8, 1–12. doi:10.1038/s41598-018-23311-8.

Tan, K. W. M., and Lee, Y. K. (2016). The dilemma for lipid productivity in green microalgae:

Importance of substrate provision in improving oil yield without sacrificing growth. *Biotechnol. Biofuels* 9, 1–14. doi:10.1186/s13068-016-0671-2.

Tan, M. L., Juneng, L., Tangang, F. T., Chung, J. X., and Radin Firdaus, R. B. (2021). Changes in temperature extremes and their relationship with ENSO in Malaysia from 1985 to 2018. *Int. J. Climatol.* 41, E2564–E2580. doi:10.1002/joc.6864.

Tang, K. H. D. (2019). Climate change in Malaysia: Trends, contributors, impacts, mitigation and adaptations. *Sci. Total Environ.* 650, 1858–1871. doi:10.1016/j.scitotenv.2018.09.316.

Tongprawhan, W., Srinuanpan, S., and Cheirsilp, B. (2014). Biocapture of CO2 from biogas by oleaginous microalgae for improving methane content and simultaneously producing lipid. *Bioresour. Technol.* 170, 90–99. doi:10.1016/j.biortech.2014.07.094.

Tonon, T., Harvey, D., Larson, T. R., and Graham, I. A. (2002). Long chain polyunsaturated fatty acid production and partitioning to triacylglycerols in four microalgae. *Phytochemistry* 61, 15–24. doi:10.1016/S0031-9422(02)00201-7.

Tran, N. T., Padula, M. P., Evenhuis, C. R., Commault, A. S., Ralph, P. J., and Tamburic, B. (2016). Proteomic and biophysical analyses reveal a metabolic shift in nitrogen deprived Nannochloropsis oculata. *ALGAL* 19, 1–11. doi:10.1016/j.algal.2016.07.009.

Üretmen Kagıalı, Z. C., Şentürk, A., Özkan Küçük, N. E., Qureshi, M. H., and Özlü, N. (2017). Proteomics in Cell Division. *Proteomics* 17. doi:10.1002/pmic.201600100.

Valdés, F. J., Hernández, M. R., Catalá, L., and Marcilla, A. (2012). Estimation of CO 2 stripping/CO 2 microalgae consumption ratios in a bubble column photobioreactor using the analysis of the pH profiles. Application to Nannochloropsis oculata microalgae culture. *Bioresour. Technol.* 119, 1–6. doi:10.1016/j.biortech.2012.05.120.

Van Wagenen, J., Miller, T. W., Hobbs, S., Hook, P., Crowe, B., and Huesemann, M. (2012). Effects of light and temperature on fatty acid production in Nannochloropsis salina. *Energies* 5, 731–740. doi:10.3390/en5030731.

Vázquez-Romero, B., Perales, J. A., Pereira, H., Barbosa, M., and Ruiz, J. (2022). Techno-economic assessment of microalgae production, harvesting and drying for food, feed, cosmetics, and agriculture. *Sci. Total Environ.* 837. doi:10.1016/j.scitotenv.2022.155742.

Verma, R., Mehan, L., Kumar, R., Kumar, A., and Srivastava, A. (2019). Computational fluid dynamic analysis of hydrodynamic shear stress generated by different impeller combinations in stirred bioreactor. *Biochem. Eng. J.* 151, 107312.

doi:10.1016/j.bej.2019.107312.

Vieler, A., Wu, G., Tsai, C. H., Bullard, B., Cornish, A. J., Harvey, C., et al. (2012). Genome, Functional Gene Annotation, and Nuclear Transformation of the Heterokont Oleaginous Alga Nannochloropsis oceanica CCMP1779. *PLoS Genet.* 8. doi:10.1371/journal.pgen.1003064.

Vogler, B. W., Ashford, A., and Posewitz, M. C. (2021). CRISPR/Cas9 disruption of glucan synthase in Nannochloropsis gaditana attenuates accumulation of β-1,3-glucose oligomers. *Algal Res.* 58, 102385. doi:10.1016/j.algal.2021.102385.

Vogler, B. W., Brannum, J., Chung, J. W., Seger, M., and Posewitz, M. C. (2018). Characterization of the Nannochloropsis gaditana storage carbohydrate: A 1,3-beta glucan with limited 1,6-branching. *Algal Res.* 36, 152–158. doi:10.1016/j.algal.2018.10.011.

Wahidin, S., Idris, A., and Shaleh, S. R. M. (2013). The influence of light intensity and photoperiod on the growth and lipid content of microalgae Nannochloropsis sp. *Bioresour. Technol.* 129, 7–11. doi:10.1016/j.biortech.2012.11.032.

Wan Razali, W. A., Evans, C. A., and Pandhal, J. (2022). Comparative Proteomics Reveals Evidence of Enhanced EPA Trafficking in a Mutant Strain of Nannochloropsis oculata. *Front. Bioeng. Biotechnol.* 10, 1–16. doi:https://doi.org/10.3389/fbioe.2022.838445.

Wang, B., and Jia, J. (2020). Photoprotection mechanisms of Nannochloropsis oceanica in response to light stress. *Algal Res.* 46, 101784. doi:10.1016/j.algal.2019.101784.

Wang, D., Ning, K., Li, J., Hu, J., Han, D., Wang, H., et al. (2014). Nannochloropsis Genomes Reveal Evolution of Microalgal Oleaginous Traits. *PLoS Genet.* 10. doi:10.1371/journal.pgen.1004094.

Wang, H. M. D., Chen, C. C., Huynh, P., and Chang, J. S. (2015). Exploring the potential of using algae in cosmetics. *Bioresour. Technol.* 184, 355–362. doi:10.1016/j.biortech.2014.12.001.

Wang, J., and Yin, Y. (2018). Fermentative hydrogen production using pretreated microalgal biomass as feedstock. *Microb. Cell Fact.* 17, 1–16. doi:10.1186/s12934-018-0871-5.

Wang, Q., Feng, Y., Lu, Y., Xin, Y., Shen, C., Wei, L., et al. (2021). Manipulating fatty-acid profile at unit chain-length resolution in the model industrial oleaginous microalgae Nannochloropsis. *Metab. Eng.* 66, 157–166. doi:10.1016/j.ymben.2021.03.015.

Wang, W., Sheng, Y., and Jiang, M. (2022). Physiological and metabolic responses of

Microcystis aeruginosa to a salinity gradient. *Environ. Sci. Pollut. Res.* 29, 13226–13237. doi:10.1007/s11356-021-16590-8.

Wei, L., El Hajjami, M., Shen, C., You, W., Lu, Y., Li, J., et al. (2019). Transcriptomic and proteomic responses to very low CO2 suggest multiple carbon concentrating mechanisms in Nannochloropsis oceanica. *Biotechnol. Biofuels* 12, 1–21. doi:10.1186/s13068-019-1506-8.

Wei, L., and Huang, X. (2017). Long-duration effect of multi-factor stresses on the cellular biochemistry, oil-yielding performance and morphology of Nannochloropsis oculata. *PLoS One* 12, 1–20. doi:10.1371/journal.pone.0174646.

Wei, L., Jiang, Z., and Liu, B. (2022). A CRISPR/dCas9-based transcription activated system developed in marine microalga Nannochloropsis oceanica. *Aquaculture* 546, 737064. doi:10.1016/j.aquaculture.2021.737064.

Wei, L., You, W., Gong, Y., El Hajjami, M., Liang, W., Xu, J., et al. (2020). Transcriptomic and proteomic choreography in response to light quality variation reveals key adaption mechanisms in marine Nannochloropsis oceanica. *Sci. Total Environ.* 720, 137667. doi:10.1016/j.scitotenv.2020.137667.

Wietrzynski, W., and Engel, B. D. (2021). Chlorophyll biogenesis sees the light. *Nat. Plants* 7, 380–381. doi:10.1038/s41477-021-00900-6.

Willette, S., Gill, S. S., Dungan, B., Schaub, T. M., Jarvis, J. M., St. Hilaire, R., et al. (2018). Alterations in lipidome and metabolome profiles of Nannochloropsis salina in response to reduced culture temperature during sinusoidal temperature and light. *Algal Res.* 32, 79–92. doi:10.1016/j.algal.2018.03.001.

Winwood, R. J. (2013). Recent developments in the commercial production of DHA and EPA rich oils from micro-algae. *Ocl* 20, D604. doi:10.1051/ocl/2013030.

Wright, J.C., Beynon, R.J., and Hubbard, S. J. (2010). *Cross Species Proteomics.* doi:10.1007/978-1-60761-444-9_18.

Xin, Y., Shen, C., She, Y., Chen, H., Wang, C., Wei, L., et al. (2019). Biosynthesis of Triacylglycerol Molecules with a Tailored PUFA Profile in Industrial Microalgae. *Mol. Plant* 12, 474–488. doi:10.1016/j.molp.2018.12.007.

Xu, L., Weathers, P. J., Xiong, X. R., and Liu, C. Z. (2009). Microalgal bioreactors: Challenges and opportunities. *Eng. Life Sci.* 9, 178–189. doi:10.1002/elsc.200800111.

Xu, Y., Li, H., Jin, Y. H., Fan, J., and Sun, F. (2014). Dimerization interface of 3-hydroxyacyl-CoA

dehydrogenase tunes the formation of its catalytic intermediate. *PLoS One* 9. doi:10.1371/journal.pone.0095965.

Yaakob, M. A., Mohamed, R. M. S. R., Al-Gheethi, A., Aswathnarayana Gokare, R., and Ambati, R. R. (2021). Influence of Nitrogen and Phosphorus on Microalgal Growth, Biomass, Lipid, and Fatty Acid Production: An Overview. *Cells* 10, 10–20. doi:10.3390/cells10020393.

Yaakob, Z., Ali, E., Zainal, A., Mohamad, M., and Takriff, M. S. (2014). An overview: Biomolecules from microalgae for animal feed and aquaculture. *J. Biol. Res.* 21, 1–10. doi:10.1186/2241-5793-21-6.

Yang, F., Yuan, W., Ma, Y., Balamurugan, S., Li, H. Y., Fu, S., et al. (2019a). Harnessing the Lipogenic Potential of Δ6-Desaturase for Simultaneous Hyperaccumulation of Lipids and Polyunsaturated Fatty Acids in Nannochloropsis oceanica. *Front. Mar. Sci.* 6, 1–8. doi:10.3389/fmars.2019.00682.

Yang, Y. F., Li, D. W., Chen, T. T., Hao, T. Bin, Balamurugan, S., Yang, W. D., et al. (2019b). Overproduction of Bioactive Algal Chrysolaminarin by the Critical Carbon Flux Regulator Phosphoglucomutase. *Biotechnol. J.* 14, 1–8. doi:10.1002/biot.201800220.

Yu, X. J., Chen, H., Huang, C. Y., Zhu, X. Y., Wang, Z. P., Wang, D. S., et al. (2019). Transcriptomic Mechanism of the Phytohormone 6-Benzylaminopurine (6-BAP) Stimulating Lipid and DHA Synthesis in Aurantiochytrium sp. *J. Agric. Food Chem.* 67, 5560–5570. doi:10.1021/acs.jafc.8b07117.

Zhang, B., Wu, J., and Meng, F. (2021). Adaptive Laboratory Evolution of Microalgae: A Review of the Regulation of Growth, Stress Resistance, Metabolic Processes, and Biodegradation of Pollutants. *Front. Microbiol.* 12, 1–8. doi:10.3389/fmicb.2021.737248.

Zienkiewicz, A., Zienkiewicz, K., Poliner, E., Pulman, J. A., Du, Z. Y., Stefano, G., et al. (2020). The Microalga Nannochloropsis during Transition from Quiescence to Autotrophy in Response to Nitrogen Availability. *Plant Physiol.* 182, 819–839. doi:10.1104/pp.19.00854.

Zienkiewicz, K., and Zienkiewicz, A. (2020). Degradation of Lipid Droplets in Plants and Algae—Right Time, Many Paths, One Goal. *Front. Plant Sci.* 11, 1–14. doi:10.3389/fpls.2020.579019.